2011

Modeling Small Molecule Elution From a Hydrogel using a Microfluidic Technique

Stephanie Evans
Bucknell University

Follow this and additional works at: https://digitalcommons.bucknell.edu/masters_theses

Part of the Chemical Engineering Commons

I, Stephanie M. Evans, do grant permission for my thesis to be copied.

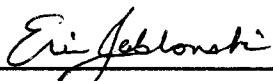# MODELING SMALL MOLECULE ELUTION FROM A HYDROGEL USING A MICROFLUIDIC TECHNIQUE
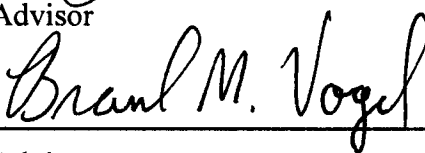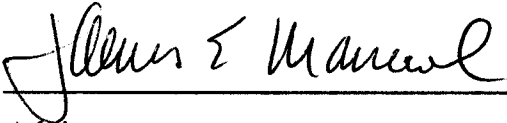
by

Stephanie M. Evans

A Thesis

Presented to the Faculty of
Bucknell University
In Partial Fulfillment of the Requirements for the Degree of
Master of Science in Chemical Engineering

Approved:

_____
Advisor

_____
Advisor

_____
Advisor

_____
Department Chairperson

May 2011

Acknowledgements

I would like to thank all three of my advisors, Dr. Erin Jablonski, Dr. James Maneval, and Dr. Brandon Vogel, for all of their help and support throughout my time as a student at Bucknell University. I would especially like to thank Professor Jablonski. Without her, I never would have begun my research or continued my education in this program. Her constant enthusiasm and encouragement kept me inspired and motivated to continue this work.

I would like to thank all of my fellow graduate students. With their friendship and support, they all helped keep me motivated and sane throughout the countless hours spent researching, writing, and studying in Dana. Additionally, I would like to thank Andrew Litzenberger, the former graduate student, for his help with MATLAB and Anne Ellenberger for her assistance with my thesis work.

Many thanks go to the Chemical Engineering Department at Bucknell University for providing me with both my Undergraduate and Graduate education. I am extremely grateful for all the challenges they have provided me during my 5 years at this school. I would also like to thank Diane Hall for all her lab assistance and Nancy for all her support and candy.

Finally I would like to thank my friends and family. I especially would like to thank my Mom and Dad for everything. I am extremely grateful for their undying belief and support they have given me and I really appreciate all the patience they had to keep me calm and sane in times when I did not think I was going to make it.

Table of Contents

List of Figures

List of Tables

List of Abbreviations

Acrylic Acid (AA)

Atomic Force Microscopy (AFM)

Bovine Serum Albumin (BSA)

Diffusion Ordered Spectroscopy (DOSY)

Differential Scanning Calorimetry (DSC)

Extracellular Matrix (ECM)

Florescence Recovery after Photobleaching (FRAP)

Fourier Transform Infrared (FTIR)

High Performance Liquid Chromatography (HPLC)

Hydroxyethyl methacrylate (HEMA)

Lower Critical Solution Temperature (LCST)

Metalloprotease 13 (MMP-13)

N-vinyl-2-pyrrolidone (NVP)

Nuclear Magnetic Resonance (NMR)

Phosphate Buffered Saline (PBS)

Poly(ethylene glycol) (PEG)

Poly(ethylene glycol) diacrylate (PEG-DA)

Poly(ethylene glycol) dimethacrylate (PEG-DM)

Poly(vinyl chloride) PVC

Radio Frequency (RF)

Self-Assembled Monolayer (SAM)

Scanning Electron Microscopy (SEM)

Thermogravimetric Analysis (TGA)

Transmission Electron Microscopy (TEM)

3-(trichlorosilyl)-propyl methacrylate (TPM)

Ultra High Vacuum (UHV)

Ultraviolet/Visible (UV/Vis)

Upper Critical Solution Temperature (UCST)

Abstract

Drug release from a fluid-contacting biomaterial is simulated using a microfluidic device with channels defined by solute-loaded hydrogel. In order to mimic a drug delivery device, a solution of poly(ethylene glycol) diacrylate (PEG-DA), solute, and photoinitiator is cured inside a microfluidic device with a channel through the center of the hydrogel. As water is pumped through the channel, solute diffuses out of the hydrogel and into the water. Channel sizes within the devices range from 300 µm to 1000 µm to simulate vessels within the body. The properties of the PEG hydrogel were characterized by the extent of crosslinking, the swelling ratio, and the mesh size of the gel. The structure of the hydrogel was related to the UV exposure dosage and the initial water and solute content in the PEG-DA solution.

A combination of three analysis techniques was used to validate the strengths and weaknesses of each method, including optical microscopy, characterization of device effluent, and NMR analyses. Diffusion coefficients for methylene blue in PEG hydrogel calculated using the three methods agree within an order of magnitude because methylene blue is capable of diffusing in the hydrogel and is not mass transfer limited into the channel. The experimental diffusion coefficients of methylene blue agree within an order of magnitude to a theoretical hydrogel diffusivity model.

Characterizing solute diffusion with a combination of the three techniques offers greater insight into molecular diffusion in hydrogels rather than employing each technique individually. All three methods are effective for determining the diffusion

coefficient of solutes that can be eluted, and each method has its own advantages. The NMR method made precise measurements for solute diffusion in all cases. The optical method was effective for visualizing the diffusion of colored solutes with the use of a stereomicroscope. The optical and effluent methods can be used to screen solutes to determine if they are capable of being eluted from the hydrogel device. Thus, designing drug delivery devices requires analysis of the effluent to establish a complete picture of elution.

1. Introduction

Hydrogels are crosslinked, water-swollen, hydrophilic polymers. One of the most important characteristics hydrogels can have is biocompatibility. Poly(ethylene glycol) (PEG) hydrogels in particular have been studied extensively for pharmaceutical and biomaterial applications, such as tissue scaffolds, because they are non-toxic and non-immugenic.[1] PEG hydrogels have been approved by the food and drug administration (FDA) for human intravenous, oral, and dermal applications.[2] This FDA approval has led to the widespread use of PEG as a component of controlled drug delivery devices, tissue scaffolds, and biological grafts.[1] The molecular diffusion of solutes between the swollen polymer chains contributes to the utility of hydrogels as drug eluting devices.

Proteins and other therapeutic drugs are easily held in the entangled network of PEG hydrogels. The hydrogel can shield entrapped molecules from enzymes and increase the circulation time above that of molecules that were injected.[3] Designing diffusion-controlled hydrogels for drug delivery involves characterizing the mesh size, polymer volume fraction, swelling, and interactions of the hydrogel network and the diffusing molecules. Once formed, the polymer network is a disordered arrangement of randomly orientated polymer chains. The appropriate design of hydrogels for the delivery of therapeutic agents in biological-fluid contacting applications requires a robust understanding of how the agent will elute from the hydrogel over time in various flow conditions.

The diffusion of molecules in a hydrogel system can be a complicated process. Obtaining data for most diffusive processes is difficult as concentration must be monitored non-invasively for long times and short distances. Many experimental processes involve transferring hydrogel slabs into fresh solutions and monitoring concentration changes with time.[4] However, previous experiments using fluorescence recovery after photo-bleaching (FRAP) are only capable of determining lateral diffusion coefficients within a hydrogel without contact from an external solvent.[56] Using these methods, the effects of a continuous process with varying flow patterns are not controlled, and the hydrogel channels are not on the scale of vasculature.

In this thesis, simulating drug elution from a biomaterial incorporates principles of microfluidics, the size scale of which is comparable to human vasculature in vitro. The area of microfluidics is concerned with fluid flow through channels on the millimeter to micrometer scale. Microfluidic devices are known as "labs on chips" for their capacity to accomplish a variety of analyses and experiments that are not feasible on a macroscale.[7] Advantages of using microfluidic devices include easy fabrication, high resolution and sensitivity, and low cost.[7] By containing PEG within a microfluidic device, the flow into the device can be controlled to produce a continuous driving force for diffusion of a solute.

With increased understanding of the diffusive behavior in hydrogels, these materials could be better tailored for specific applications, and devices could be designed to provide a desired release profile for therapeutic agents. The purpose of this thesis is to integrate a hydrogel network loaded with small molecules into a microfluidic device to

study elution. When contacted with solvent, the hydrogel will release dye through diffusion based on a concentration gradient. Three methods are used in this thesis for determining the diffusivity of the small molecules in the hydrogel, including optical digital microscopy, ultraviolet-visible spectroscopy, and nuclear magnetic resonance spectroscopy. With knowledge of the diffusion mechanism and solute-gel interactions, properties of the gel can be modified to fit the desired sustained release of molecules.

In Chapter 2 of this thesis, background information is given regarding microfluidics, properties and release systems of hydrogels, and methods for diffusion measurements. Chapter 3 contains the materials and methods used for the fabrication of hydrogels inside microfluidic devices and experimental techniques pertinent to this study. Chapter 4 provides the results and analysis of data collected. Chapter 5 details the final conclusions regarding the data analysis. Finally, chapter 6 presents future work to be conducted to continue this study.

1.1. References

(1) Ratner, B. D. In *Biomaterials science: an introduction to materials in medicine* Academic Press/Elsevier Science Pub., 2004.

(2) Greenwald, R. B.; Choe, Y. H.; McGuire, J.; Conover, C. D. Effective drug delivery by PEGylated drug conjugates. *Adv. Drug Deliv. Rev.* 2003*, 55*, 217-250.

(3) Hoare, T. R.; Kohane, D. S. Hydrogels in drug delivery: Progress and challenges. *Polymer* 2008*, 49*, 1993-2007.

(4) Weber, L. M.; Lopez, C. G.; Anseth, K. S. Effects of PEG hydrogel crosslinking density on protein diffusion and encapsulated islet survival and function *Journal of Biomedical Materials Research Part A* 2009*, 90A*, 720 - 729.

(5) Khoury, C.; Adalsteinsson, T.; Johnson, B.; Crone, W. C.; Beebe, D. J. Tunable Microfabricated Hydrogels—A Study in Protein Interaction and Diffusion. *Biomed. Microdevices* 2003*, 5*, 35 - 45.

(6) Kosto, K. B.; Deen, W. M. Hindered Convection of Macromolecules in Hydrogels. *Biophysical Journal* 2005*, 88*, 277-286.

(7) Whitesides, G. M. The origins and the future of microfluidics. *Nature* 2006*, 442*, 368-373.

2. Background

This chapter details the background information for key materials and analysis methods used in this thesis. The chapter begins with a discussion of hydrogels, their use for drug delivery, and characterization methods. Specifically, poly(ethylene glycol) diacrylate hydrogels are described and their use as the primary hydrogel of interest for this work. Finally, each of the methods used for determining diffusion coefficients is described.

2.1. Hydrogels

Hydrogels are crosslinked, water-swollen, hydrophilic polymers that form a three-dimensional network. Hydrogels can be formed into slabs, microparticles, nanoparticles, coatings or films.[1] The hydrogel network is formed either through the reaction of one or more monomers into a single polymer or through association bonds between the chains of existing polymers.[2] Polymer networks consist of multifunctional junctions, where multiple chains connect, and physical entanglements of the chains, where the chains are not chemically connected.[2] After crosslinking, the matrix is a disordered arrangement of randomly orientated polymer chains.[3] Hydrogels can be prepared from synthetic monomers or derived from natural polymers. Polymerization of synthetic monomers is initiated either by copolymerization with a crosslinking agent or through irradiative methods using electron beams, gamma rays, x-rays, or ultraviolet (UV) light. The matrix

of the hydrogel swells in the presence of water or aqueous solution, yet still maintains its original shape. Entanglements and chemical linkages prevent dissolution of the polymer chains.[4]

2.1.1. Hydrogel Applications

Hydrogels fall into two different categories: natural and synthetic. Natural polymers are inherently more biocompatible than synthetic monomers but, generally, synthetic monomers are used more often. Synthetic polymers have well defined structures and can be tailored to have characteristics similar to natural polymers and specific functions without the risk of potential pathogens causing reactions within the body.[4] Many polymers are structured to have functional groups that are recognizable on a cellular level that will not cause immunogenic reactions.[4] Biocompatibility and non-immunogenity are the key properties that allow synthetic hydrogels to be used as biomaterials within the body. Several synthetic hydrogels have already been established for blood-contacting applications including poly(vinyl alcohol), poly(acrylamides), and poly(ethylene glycol) (PEG). Due to these properties, hydrogels have garnered much interest for use in tissue engineering and controlled drug delivery. Hydrogels used in tissue engineering must be modified to encapsulate cells or to resemble the extracellular matrix (ECM) as a biomimetic scaffold for tissue formation and regeneration. The ability of small hydrophilic molecules to diffuse between the swollen polymer chains contributes to the utility of drug eluting hydrogels. Extensive modification to the chemical

composition and mechanical structure of the network is necessary before hydrogels are employed in these applications.

2.1.1.1. Use in Drug Delivery

The use of hydrogels as drug delivery devices is investigated in this thesis. In the realm of drug delivery, hydrogels are capable of containing proteins and other therapeutic drugs in the entangled network as well as shielding entrapped molecules from being metabolized after injection into the body. Many treatments have already been established in recombinant protein therapy, but challenges exist in delivering the proteins. Currently, hydrogels are the most promising potential delivery method. Injecting therapeutic proteins is not a reliable method because proteins are degraded and expelled quickly, requiring an increase in dose and the number of injections.[4] Drugs are included in the hydrogel by either post-loading or *in-situ* loading. With post-loaded hydrogels, the matrix is cured before the drug is incorporated based on diffusion into the gel. *In-situ* loaded gels are prepared with the drug premixed in the hydrogel solution. The drug release mechanism of the hydrogel network must be modified for each specific molecule to increase the duration of circulation.[1]

Designing a hydrogel for controlled release is difficult to accomplish. Mathematical models and knowledge of the physical properties of the hydrogel are essential to control release. Since several factors determine the rate at which drug is eluted, the polymer type, mesh size, and extent of crosslinking of the network must be specifically tailored to extend the period of drug delivery.[1] Three delivery methods for

release are currently being studied, diffusion-controlled, swelling-controlled, and chemically-controlled mechanisms.[4] The diffusion-controlled mechanism will be investigated using small molecules in this thesis.

Diffusion in hydrogels depends on the physical properties of the hydrogel and the diffusing molecules. Crosslink density of the network and the hydrodynamic radii of the diffusing molecules are important parameters in diffusion controlled systems.[5] Diffusion in these systems fall under two categories: reservoir and matrix. In reservoir systems, the diffusing molecules are surrounded by hydrogel, such that the concentration is highest at the hydrogel/solute boundary and zero throughout the remainder of the gel. The solute moves through the gel, down the concentration gradient based on Fick's first law of diffusion. Matrix systems initially have diffusing molecules equally distributed throughout the network, and elute from the gel when contacted with a dissolving solution.[4] The development of a mathematical model of diffusion often assumes perfect sink conditions with a constant diffusivity for the release of entrapped molecules so experiments must be designed accordingly.[4, 6]

2.1.2. Hydrogel Chemistry

Structures of crosslinked, swollen hydrogels are usually simplified to a macromolecular network of linear polymer molecules joined at tetrafunctional junctions through covalent bonds in a three dimensional arrangement. Figure 2.1 illustrates the simplified model where the black lines are the polymer chains and the black dots represent the connecting carbon atoms that link four polymer chains in tetrafunctional

junctions. Thus in this model, the network mesh size, ξ, is only dependent on the polymer chain length between junctions.[2, 7] Hydrogels with greater polymer lengths between crosslinks have a low crosslinking density, whereas hydrogels with short polymer lengths have a high crosslinking density.
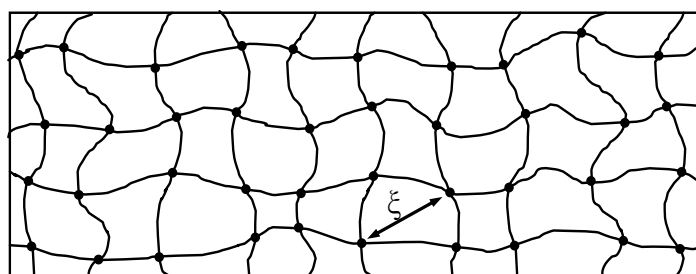
Figure 2.1. Ideal hydrogel network mesh.

However, the simple network model fails to accurately represent the complexity of hydrogel matrices. The mesh does not comprise purely linear chains and tetrafunctional junctions. Several complications in the matrix polymerization include polymer chain loops (Figure 2.2A), physical entanglements held together by weak molecular forces (Figure 2.2B), unreacted polymer end groups (Figure 2.2C), and multifunctional junctions of numerous polymer chains (Figure 2.2D). Junctions are not always connected to a single carbon atom, but are often formed by small chemical bridges or through association or aggregates of polymer chains.[2]
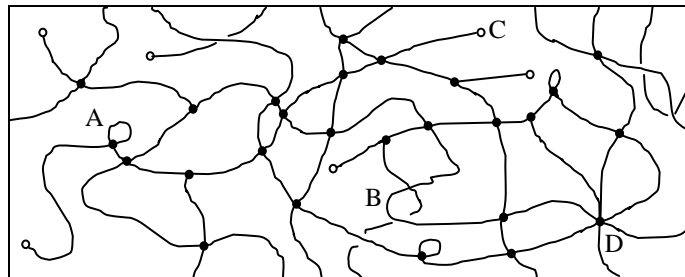
Figure 2.2. Complications within a hydrogel network including A.) Chain loops, B.)Physical entanglements, C. Unreacted end groups, and D.) Multifunctional junctions.

The importance of hydrogel mesh size is seen in solute diffusivity through the matrix. Large solutes have a rate of diffusion much smaller than that of small molecules. To move in a hydrogel large molecules require large vacancies within the gel, whereas small molecules are able to diffuse interstitially through the entangled polymer mesh. Solutes within a swollen hydrogel have a specific hydrodynamic radius. The hydrodynamic radius of a solute accounts for hydration and shape effects. Solutes with a hydrodynamic radius much smaller than the mesh size are able to diffuse freely, as shown in Figure 2.3A. Solutes with hydrodynamic radii comparable to mesh size are able to diffuse through the fluctuations of polymer chains, as shown in Figure 2.3B. However, as the mesh size decreases, the polymer chains are unable to fluctuate as easily and diffusion becomes more difficult, illustrated in Figure 2.3C.
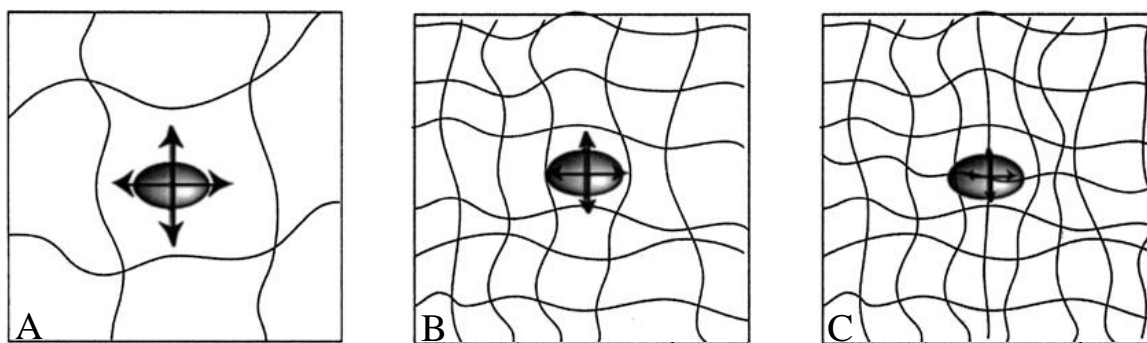
Figure 2.3. Diffusion within a hydrogel mesh of a molecule with a hydrodynamic radius A.) Smaller than the mesh size, B.) Equal to the mesh size, and C.) Larger than the mesh size.[8]

Polymer networks are crosslinked through physical methods, chemical methods, or a combination of both. Physical crosslinks do not require additional crosslinking agents because they are held together by secondary molecular forces such as hydrogen bonding, van der Waals forces, or hydrophobic interactions.[9] Due to the weak forces holding them together, these gels are referred to as "reversible" because they often degrade within the body.[9] Chemically crosslinked hydrogels are formed through chemical bonds. Chemically crosslinked hydrogels are often referred to as "irreversible," the covalent bonds are less likely to break as compared to weak interactions. Methods for the production of chemically bonded hydrogels include using aqueous solutions composed of polymers or copolymers with hydrophilic groups exposed to moderate irradiation, monomers or polymers exposed to irradiation, prepolymerized hydrogel with a second polymer exposed to irradiation (interpenetrating polymer network), monomers exposed to another group of monomers possessing the correct functional groups, and polymers exposed to macromers possessing the correct functional groups.[1, 9]

A chemically controlled mechanism can be used to model the release of immobilized drug molecules as the polymer network reacts and degrades.[6] Release could depend on molecular diffusion of the solute and polymer degradation or on degradation alone, depending on how the molecules are incorporated into the polymer.[4] When molecules are covalently linked in the hydrogel, the hydrolytic degradation depends on the rate of bond cleavage.[4] For example, in one type of biodegradable hydrogel, peptide substrates are fabricated within the gel so that enzymes catalyze the degradation.[4]

2.1.2.1. Swelling in Hydrogels

Swelling of the polymer matrix is either conducted prior to or after the polymerization of the network structure. Swelling a dry polymer network after crosslinking will occur the enthalpy of solvation and entropy of the extended chains balance.[2] Examples of highly swollen polymers include poly(vinyl alcohol), poly(N-vinyl 2-pyrrolidone), poly(hydroxyethylmethacrylate), and poly(ethylene glycol).

Swelling-controlled hydrogels used in drug release systems are known more commonly as "smart" hydrogels. Smart hydrogels respond to external signals that cause a transition from an unswollen "glassy" state to a swollen "rubbery" state.[10] In the glassy state, the molecules are entrapped tightly in the gel mesh and cannot escape. Once the hydrogel is swollen, the molecules are released. The mechanism of release is dependent on the polymer relaxation as the rate limiting step.[4] The signals used in the majority of studies are pH and temperature.

Temperature dependent hydrogels exhibit a solution-gel (sol-gel) phase transition temperature, where the solution will form a gel without an external stimulus.[11] For easier implantation it is beneficial for sol-gel polymers to solidify after injection into the body.[4] The characteristics of temperature dependent crosslinked hydrogels change based on one of two transition temperatures, the lower critical solution temperature (LCST) or the upper critical solution temperature (UCST).[9] For crosslinked hydrogels with a LCST, temperatures above the LCST trigger the gel to collapse because of hydrophobic interactions that cause the expulsion of water.[4] Below the LCST, the gel demonstrates hydrophilic properties that cause it to swell.[4, 12] One of the most commonly used polymers with a LCST is poly(n-isopropylacrylamide), which has a transition temperature at 32 °C in distilled water.[12] However, most gels have an UCST and display an opposite trend, where the gel becomes more swollen as temperature increases.[12]

pH responsive hydrogels must be ionic to exhibit swelling behavior based on the signals in an external solution. Swelling in nonionic hydrogels only depends on gel properties.[4] Anionic hydrogels have weak acidic groups incorporated into the polymer. At pH higher than the acid dissociation constant, pK_a, the weak acid deprotonates and becomes negatively ionized. When the pH of cationic gels is lower than the dissociation constant, pK_b, the weak base protonates and becomes positively ionized. As a result of ionization, the hydrogel will swell because of an increase in osmotic pressure as the gel becomes neutralized with counter-ions.[9, 13] Figure 2.4 demonstrates swelling behavior in ionic hydrogels.
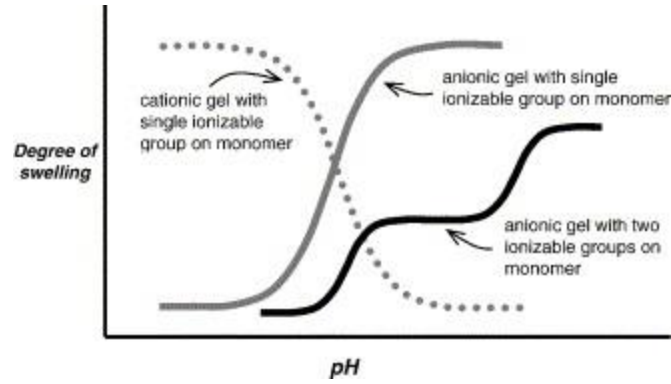
Figure 2.4. Swelling behavior in ionic hydrogels.[4]

2.1.3. Physical Models for Gel Characterization

It is important to be able to characterize the structure of the hydrogel mesh to determine how changes in the structure affect the diffusion of molecules. In previous studies, efforts have been made to calculate mesh size based on models using swelling data.[14] These models are typically derived using the Flory-Rehner model for equilibrium swelling. Equation 2,1 gives the number-average molecular weight between crosslinks, $\overline{M_c}$, for a hydrogel crosslinked before swelling.[15]

$$\frac{1}{\overline{M_c}} = \frac{2}{\overline{M_n}} - \frac{(\bar{v}/V_1)\left[\ln(1 - v_{2,s}) + v_{2,s} + \chi_1 v_{2,s}^2\right]}{\left(v_{2,s}^{1/3} - (2/\varphi)v_{2,s}\right)}$$

(2,1)

where $\overline{M_n}$ is the molecular weight of linear polymer chains without crosslinking, $\bar{v}$ is the specific volume of the polymer, V_1 is the molar volume of swelling agent, $v_{2,s}$ is the polymer volume fraction of the swollen hydrogel, χ_1 is the polymer-solute interaction parameter, and φ is functionality of the crosslinking agent. Equation 2,2 is the modified form that describes hydrogels crosslinked in water, where the volume fraction of the

polymer in the relaxed state, $v_{2,r}$, is added to account for water-induced elastic contributions.[2]

$$\frac{1}{\overline{M_c}} = \frac{2}{\overline{M_n}} - \frac{(\bar{v}/V_1)\left[\ln(1-v_{2,s})+v_{2,s}+\chi_1 v_{2,s}^2\right]}{v_{2,r}\left((v_{2,s}/v_{2,r})^{1/3}-((2/\varphi)v_{2,s}/v_{2,r})\right)} \tag{2,2}$$

The hydrogel can also be characterized using ξ, the network mesh size, as shown in Figure 2.3 of the idealized hydrogel network. Equation (2,3) gives the mathematical relationship to approximate the network mesh size.[16]

$$\xi = v_{2,s}^{-1/3}\left(\overline{r_o^2}\right)^{1/2} \tag{2,3}$$

where $\overline{r_o^2}$ is the root mean squared end to end distance of network chains between two adjacent crosslinks in the unperturbed state. $\overline{r_o^2}$ is estimated by equation (2,4), which was originally discovered by Flory.[15]

$$\left(\overline{r_o^2}\right)^{1/2} = l(C_n n)^{1/2} \tag{2,4}$$

Here, l is bond length along the polymer backbone, C_n is the Flory characteristic ratio, and n is the number of bonds between adjacent crosslinks. The mesh size can be used to estimate a diffusion coefficient using,

$$\frac{D_g}{D_0} = \left(1-\frac{r_s}{\xi}\right)exp\left(-Y\left[\frac{v_{2,s}}{1-v_{2,s}}\right]\right) \tag{2,5}$$

where D_g is the diffusion coefficient in the gel, r_s is the size of the diffusing molecule, and Y is the ratio of the critical volume required for a translation movement of the drug molecule and average free volume per molecule of solvent.[4]

2.1.4. Gel Characterization Techniques

Several mechanical and chemical characterization techniques have been used in the past to gain insight into the structural properties of hydrogels. General characterization techniques that have been used in the past are described below, as well as the specific swelling characterization techniques that were used for the experiments conducted in this thesis.

2.1.4.1. General Characterization Techniques

Mechanical techniques include tensile, compression, and rheological testing. Mechanical testing is important for development of hydrogels as replacement tissues that must be load-bearing.[17] Tensile and compression testing is conducted to determine Young's modulus, maximum load, and stress/strain behavior. Rheology studies test the viscoelastic behavior of complex materials using an applied sinusoidal stress at varying frequencies.[18] Stress and strain are measured using rheometry dynamic mechanical analysis to determine storage and loss moduli of a material.[18-20] Chemical testing has been conducted on hydrogels using Fourier transform-infrared (FT-IR) spectroscopy, X-ray diffraction, differential scanning calorimetry (DSC), and thermogravimetric analysis

(TGA). The chemical composition and degree of photopolymerization of a hydrogel can be verified using FTIR.[21, 22] X-ray diffraction is used to determine the crystalline structure of the hydrogel.[18] Differential scanning calorimetry is used to establish the phase transitions of hydrogels by heating a sample against a reference to determine how chemical structure changes with different amounts of gel and solution.[12, 20] The thermal stability of gels is found based on the weight loss at a given heating rate using TGA.[18] Additionally, the interior morphology of a hydrogel can be visualized using scanning electron microscopy (SEM), atomic force microscopy (AFM), and transmission electron microscopy (TEM).[19, 21, 23]

2.1.4.2. Swelling Characterization Techniques

The main method of characterization for hydrogels used in this thesis was conducted through swelling experiments. Swelling behavior in hydrogels is determined using the mass of dry and swollen polymer.[17] Swelling can be measured based on deswelling or reswelling. In deswelling tests, hydrogels are measured swollen, dried, and weighed again. For reswelling experiments, swollen hydrogels are dried, measured, and then placed in solution to reach an equilibrium swelling and weighed again.[17] The equation to calculate swelling percent is given by

$$Swelling\ \% = \frac{W_{swollen}}{W_{dry}} \times 100\% \tag{2,6}$$

Additional information can be obtained from swelling experiments, such as the polymer volume fraction, $v_{2,s}$.. The polymer volume fraction characterizes the amount of water the gel can retain after swelling. The polymer volume fraction can be estimated using

(2,7)

$$v_{2,s} = \frac{{}^1/_{\rho_{polymer}}}{{}^{Q_m}/_{\rho_{solvent}} + {}^1/_{\rho_{polymer}}}$$

where ρ is density and Q_m is the mass swollen ratio of the swollen mass to dry mass of the hydrogel. Gels can be dried using a fan drier or lyophilizer.[20, 22, 24, 25] Lyophilized samples are frozen in liquid nitrogen and placed under vacuum to freeze-dry water from the gel.[20] Lyophilization of the hydrogel samples was used for the experiments performed in this thesis.

2.2. Poly(ethylene glycol) diacrylate

Poly(ethylene glycol) diacrylate hydrogels have many advantages for use in drug delivery and tissue engineering that have consequently led to great interest in study. PEG-DA is a commonly used synthetic polymer for biomaterials and drug delivery.[26] PEG-DA is an amphigel that is soluble in polar and non-polar solvents.[27] It is biocompatible, has low toxicity, and can be readily excreted from the body by the kidney and liver.[22, 28] PEG-DA has been incorporated in many products that have been approved by the FDA for intravenous, oral, and dermal uses.[22] PEG-DA gels have been combined with other polymers and molecules to modify release behavior.[28] PEG-DA, shown in Figure 2.5,

makes a good candidate for tissue engineering and drug delivery because of its capacity for entrapping molecules within the crosslinked network.
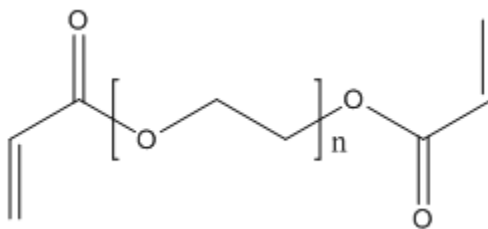
Figure 2.5. Structure of poly(ethylene glycol) diacrylate (PEG-DA)

2.2.1. Device Construction

To measure diffusion of small molecules within PEG-DA hydrogels in this thesis, hydrogels were contained within a microfluidic device. Previous diffusion coefficients have been measured for hydrogels, but a continuous flow pattern was not used. By containing hydrogel within a microfludic device, the flow into the device can be controlled to produce a continuous driving force for diffusion. Devices consist of PEG-DA photopolymerized between two glass slides. To simulate a biological-fluid contacting hydrogel, a channel, which represents a vessel in the circulatory system, spans the length of the device. Needles are connected to both ends of the channel to allow fluid to be pumped through the device. Figure 2.6 shows the schematic of devices used in the study.
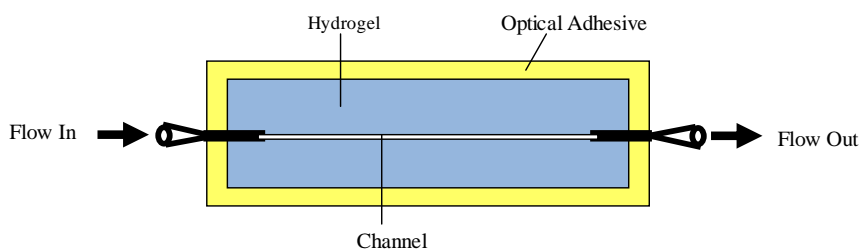
Figure 2.6. Top view of microfluidic device schematic to study small molecule diffusion in hydrogels

Facilitating PEG-DA adhesion to glass requires use of a self-assembled monolayer (SAM). Self-assembled monolayers are two-dimensional arrangements of active surfactants that create a new interface on a given surface. The surfactant molecules have head and tail ends that adsorb on a surface based on the affinity of the head group for the surface. The tail ends contain functional groups tailored to change the surface chemistry that allow the surface to have specific interactions with other molecules.[29] By changing the active surfactant, the control of growth, wetting, adhesion, lubrication, and corrosion can be increased at the interface.[29] Monolayers are formed from solution deposition or gas phase deposition. Depending on the surface, solution deposition requires cleaning or a treatment that provides the surface with the specific end groups to which the surfactant can attach.[30] Once the surface is prepared, the monolayer will spontaneously form after immersion in a solution of the active surfactant.[29] In gas phase deposition, the monolayer is created using an ultra high vacuum (UHV) chamber and controlling the flux of surfactants into the chamber.[30] Advantages of solution deposition include the simplicity of the method and low cost. Gas phase deposition is more sophisticated and costly, but it has many advantages over solution deposition. For example, with gas phase deposition the formation of the monolayer is more effective and is less likely to be contaminated.

The devices used in this thesis were soaked in a 3-(trichlorosilyl)-propyl methacrylate (TPM) solution to create a self assembled monolayer on the glass slides. Glass slides were initially prepared by depositing OH groups on the surface with ethanol and plasma cleaning to remove additional residue. The OH groups on the surface of the

glass were reacted with TPM to create the SAM, as depicted in Figure 2.7A to 2.7C. The

head molecule of TPM facilitates the bonding of PEG-DA to the glass because the PEG-

DA is able to react with the methacrylate group on the TPM, as shown in Figure 2.7.D.
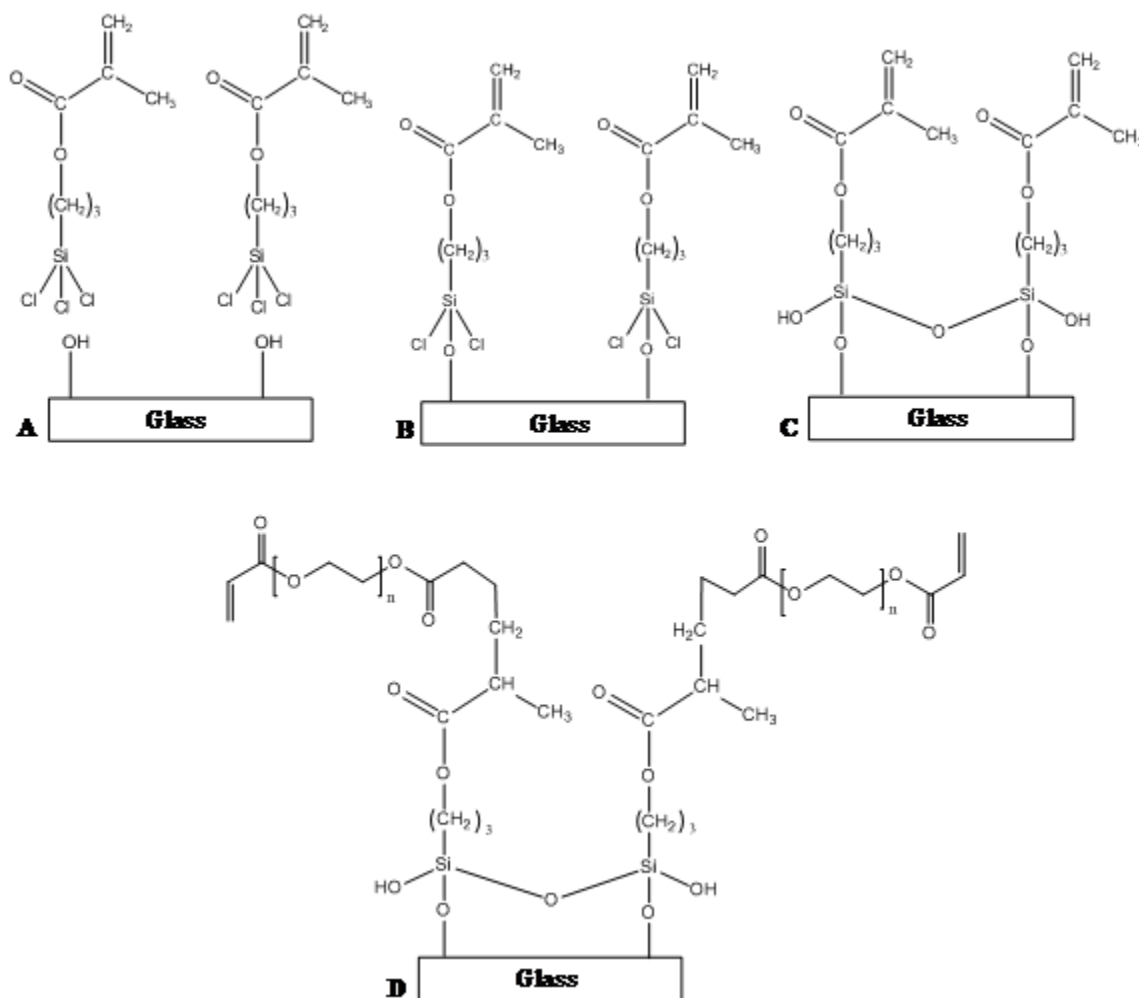
Figure 2.7. Formation of a self-assembled monolayer to bond with PEG-DA on a glass surface. A.) Structure of TPM and glass surface with OH groups. B.) Formation of SAM through reaction of TPM with OH groups on glass. C.) Condensation of water to bond TPM molecules. D.) Reaction of PEG-DA with TPM to bond to glass.

The PEG-DA hydrogel used in this work was crosslinked using irradiation with UV light. Irradiation with UV light is commonly used to crosslink hydrogels. This method activates chain growth polymerization in low molecular weight monomers and polymers using a free radical species induced by UV light. The process relies on the photoreactivity of crosslinking agents known as a photoinitiators. Two types of photoinitiators are capable of forming the free radical species, Type I and Type II. During the photocuring process for hydrogels Type I photoinitiators utilize direct photofragmentation by absorbing light to create a benzoyl or alkyl free radical.[31] 4-(2-hydroxyethoxy)-phenyl-(2-hydroxy2-methylpropyl) ketone (Irgacure 2959), shown in Figure 2.2A, is the most common Type I photoinitiator. Type II photoinitiators utilize hydrogen atom abstraction, in which an intermediate excited electron transfer complex is formed to transfer and produce an amino radical. 4-hydroxybenzophenone, shown in Figure 2.2B, with an amine co-synergist is the most common Type II photoinitiator. The free radicals produced from both types of photoinitiators cause reactions that initiate the crosslinking of the polymer chains.
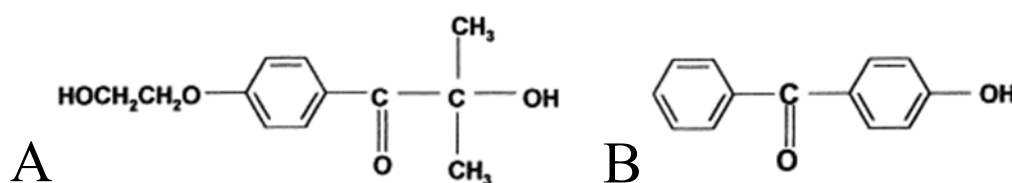
Figure 2.8. Structure of photoinitiators A.) Type I photoinitiator Irgacure 2959 B.) Type 2 photoinitiator 4-hydroxybenzophenone

PEG-DA can be UV photopolymerized to form a poly(ethylene glycol) (PEG) matrix using the Type I photoinitiator, Irgacure 2959. Irgacure 2959, is commonly used for crosslinking for PEG-DA because it was shown to have a low toxicity to human and bovine cells.[20] Crosslinks between PEG-DA chains are easily modified through use of various amounts of a photoinitiator.[6] Using photopolymerization as the polymerization technique allows for more spatial and temporal control over crosslinking and the entrapment of molecules.[20] Cells have high survival rates using photopolymerization because of rapid curing rates.[20] The mechanism for the photopolymerization of PEG-DA with Irgacure 2959 is shown in Figures 2.9 to 2.12. The photoinitiator speeds up the process of polymerization by absorbing UV light and creating free radicals.[22] Figure 2.9 displays the radical formation from Irgacure 2959.
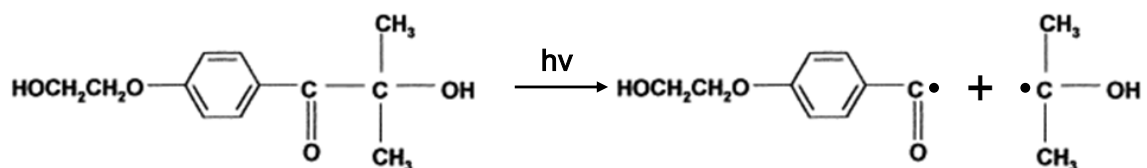
Figure 2.9. Radical formation from Irgacure 2959 being exposed to ultraviolet light

Once free radicals are generated, initiation is begun by generating an active center on the monomer, which propagates through the C=C double bond.[22] Figure 2.10 shows the generation of the active center on PEG-DA through free radical generation.
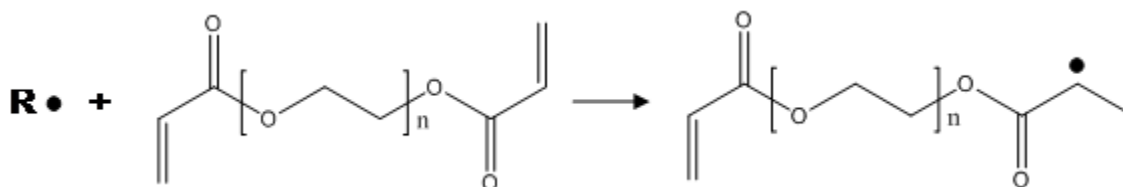
Figure 2.10. Radical reacting with PEG-DA to generate active center

After the active center is generated, it interacts with other PEG-DA species to form bonds and eventually the entire network is formed. Figure 2.11 demonstrates how the active center reacts with another PEG-DA molecule to bond. Figure 2.12 represents an ideal formation of reacting PEG-DA molecules to form a crosslinked mesh.
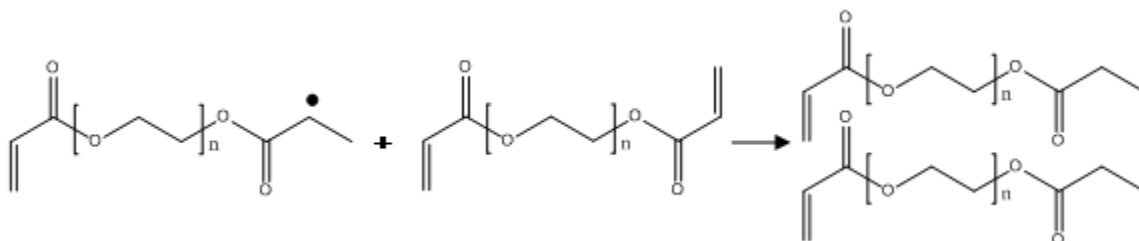
Figure 2.11. Photopolymerization process of PEG-DA
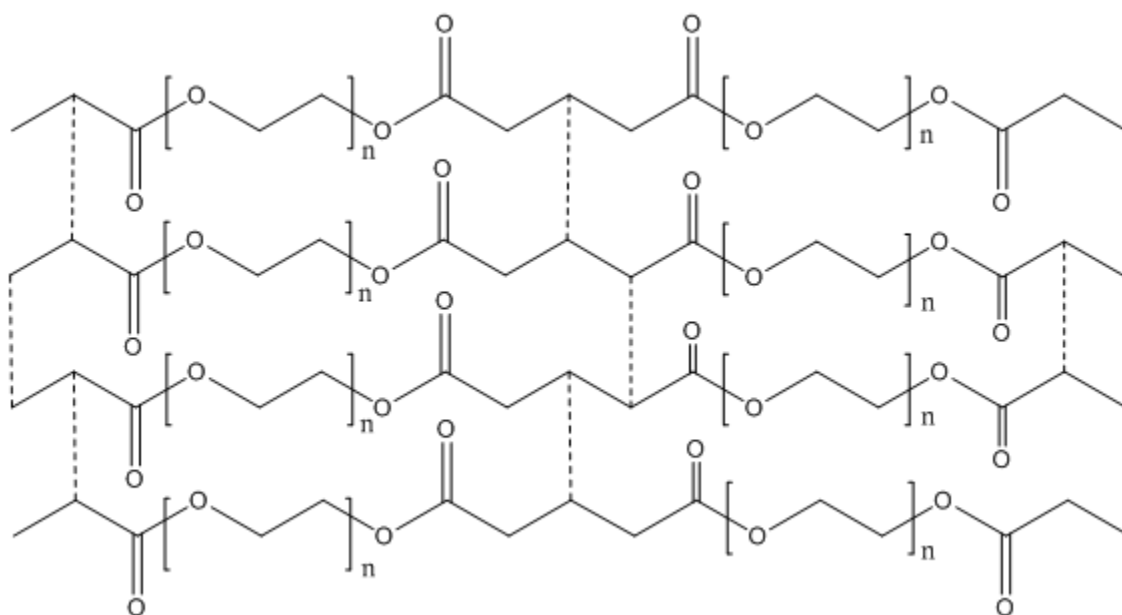
Figure 2.12. Ideal PEG network created by free radical polymerization

2.3. Microfluidics

A microfluidic characterization technique was adopted for the work conducted for this thesis. Typical microfluidic devices have a rectangular cross-section, at least one dimension less than a millimeter, and fluid flow normally contained within a microchannel.[32] Due to the small scale, microfluidic devices have a large surface area to volume ratio. Microfluidics originated from the concept of scaling down integrated circuits to miniaturize the components and increase the capacity of chips.[33] Similarly to these electronic circuits, many laboratory experiments have been scaled down and performed on a microscopic scale to increase control over highly sensitive analyses. Microfluidic devices have become known as "labs on chips" because of their ability to complete separations, reactions, and experiments unfeasible on a macroscopic scale.[34]

Poly(ethylene glycol) diacrylate can easily be applied to a microfluidic system. The photopolymerization method of crosslinking allows the fabrication of the microfluidic device to be easy and relatively inexpensive. By containing the hydrogel in a device with a microfluidic channel, the flow and transport can be controlled. To measure the release of molecules from a hydrogel mesh, the transport of the molecules should only occur through diffusion and not convection.[35]

2.3.1. Fluid Mechanics

In a microfluidic device, fluid flow can be controlled through externally applied driving forces and device fabrication techniques. Driving forces that physically move the fluid include pressure gradients, capillary effects, electronic fields, magnetic fields,

centrifugal forces, and acoustic streaming.[32] Several mechanical, chemical, and geometric properties of the device are modifiable to obtain control over the flow in the microchannel. These properties include material strength and elasticity, wettablity, chemical affinity, network connectivity and surface topography.[32] Any combination of these properties can be used to modify features of the fluid flow of the system.

Although changing the conditions of the device helps facilitate control of the fluid flow and modify the flow, fluid dynamics at the microscopic scale are much different than those at the macroscopic scale. The Reynolds number is very important in analyzing the fluid flow occurring in microfluidic devices, and is defined by

$$Re = \frac{\rho V L}{\mu} \tag{2,8}$$

The Reynolds number characterizes the flow regime as a ratio of the inertial forces to viscous forces, where ρ is the density of the fluid, V is the velocity, L is the length scale, and μ is the viscosity of the fluid. The flow regime in microfluidic devices is almost always laminar both due to the slow flow rate of fluid and the small size of the microchannel.[33] Therefore, fluid flow in microfluidic devices can be approximated by Stokes' equations for incompressible fluids and no-slip boundary conditions.[32]

2.3.2. Mass Transfer

A second dimensionless number, the Péclet number, is important for the mass transport phenomena that occur in microfluidic devices. The Péclet number is defined by

$$(2,9)$$

$$Pe = \frac{VL}{D}$$

where D is the diffusivity, V is the velocity, and L is the length scale. The Péclet number describes the mixing conditions of a solute in a fluid as a ratio of convective and diffusive transport. When the Péclet number is large, convective transport in the fluid dominates diffusion transport. In microfluidic devices the flow is laminar, convective mixing between linear streams rarely occurs, and diffusion predominantly causes mixing throughout the fluid.[36] Although complete mixing by diffusion alone would require long times at the macroscale, the small size of microfluidic devices allows diffusion to cause complete mixing in less time and become more important for establishing profiles for the concentration gradients.[36]

Diffusion coefficient measurements have previously been conducted in microfluidic devices. Culbertson, et al.[47] measured the diffusion of rhodamine 6G into a buffer stream in devices with channel widths of approximately 30 μm to 46 μm. Heeren, et al.[35] conducted diffusion experiments of fluorescein molecules in water within a microfluidic channel of 500 μm. The microfluidic device was constructed with SU-8 photoresist to contain the samples between glass slides.[35] Experiments have shown that diffusion coefficients without the effects of convection can be obtained using microfluidic devices. However, measurements of diffusion from a hydrogel using a microfluidic technique have not previously been conducted.

2.4. Diffusion Coefficient Measurement Methods

The purpose of this work is to model drug diffusion from hydrogel. Understanding diffusion in a hydrogel is an important first step for designing a robust release mechanism for a variety of molecules. Measuring the diffusion coefficient of a solute in a hydrogel provides an effective approach to quantify the movement of the solute and offer insight into the structure and performance of hydrogel materials. Differences in diffusion coefficients can be related to the hydrodynamic radii of solutes, interactions between the solute and hydrogel, and the polymer fraction of the hydrogel. This section gives background information on diffusion, summarizes previous diffusion coefficient measurement methods, and justifies the diffusion coefficient measurement methods used in this thesis.

Diffusion is the transport of matter through random molecular motion. The net transport of molecules proceeds from an area of high concentration to one of low concentration, or down a concentration gradient. The concentration gradient is a change in concentration with respect to position, and provides the driving force for diffusion to occur. The most basic expression for diffusion is given in Fick's first law of diffusion,

$$(2,10)$$

$$J = -D\frac{dC}{dx}$$

which states the mass flux is proportional to the concentration gradient. This equation is applicable for steady-state diffusion in one direction, where J is the mass flux per unit area, D is the diffusion coefficient, C is concentration, and x is distance. The material balance at a point is given by

$$\frac{\partial C}{\partial t} = -\frac{\partial J}{\partial x} \qquad (2,11)$$

Using Fick's Law, we have Equation (2,12).

$$\frac{\partial c}{\partial t} = \frac{\partial}{\partial x}\left(D\frac{\partial c}{\partial x}\right) \qquad (2,12)$$

If the diffusion coefficient is not dependent on concentration, Equation (2,12) simplifies to Equation (2,13).

$$\frac{\partial c}{\partial t} = D\frac{\partial^2 c}{\partial x^2} \qquad (2,13)$$

Equation (2,13) provides an easier method for developing an analytical solution. A solution can be derived using a variety of mathematical techniques given initial and boundary conditions.[37]

2.4.1. Previous Diffusion Measurements in Hydrogels

The diffusion of molecules in a hydrogel system is often a transient process, and so C changes with position and time. Obtaining data for most diffusive processes is difficult because concentration must be monitored non-invasively for long times and short distances. Several methods of analysis have been used previously to determine diffusion coefficients in hydrogel systems. The most notable of these being classic release experiments, fluorescence recovery after photo-bleaching (FRAP), confocal laser scanning microscopy, and Nuclear Magnetic Resonance (NMR) spectroscopy. In classic release measurement methods, the experimental process involves transferring hydrogel

slabs into fresh solutions and measuring concentrations. In FRAP experiments, a thin film hydrogel is photobleached using Ronchi ruling of constant bar and space line patterning.[8] After photobleaching, the bleached and unbleached molecules diffuse into the opposing areas. Based on the movement of the molecules and the time, a lateral diffusion coefficient can be derived. For NMR, diffusion ordered spectroscopy (DOSY) experiments have been conducted to extract diffusion coefficients from the attenuation of NMR signals.[38]

Weber, et al.[7] measured diffusion coefficients of various proteins in disc-shaped poly(ethylene glycol) dimethacrylate (PEGDM) (M_n = 2000 g/mol to 10000 g/mol) hydrogels by fitting release data to a Fickian diffusion model. Release data was measured by transferring gels into high glucose solutions at time intervals over the span of an hour, and the protein content of the solution was measured by enzyme-linked immunosorbent assay (ELISA). Diffusion coefficients were on the order of 10^{-6} cm^2/s to 10^{-7} cm^2/s.[7].

Another study by Khoury, et al.[8] was conducted by injecting protein solution (lysozyme, monoclonal antibodies, and bovine serum albumin (BSA)) into 2-hydroxyethyl methacrylate (HEMA) hydrogel and allowing the system to reach steady state. FRAP was then used to determine the lateral diffusion coefficients, which ranged from 10^{-6} cm^2/s to 10^{-10} cm^2/s.[8]

Kosto, et al.[3] performed FRAP experiments using hydrogels of agarose and small fractions of dextran with ovalbumin (MW = 45000 g/mol), BSA (MW = 68000 g/mol), and Ficoll (MW = 21300, 60700, and 105000 g/mol) as the diffusing molecules. Diffusion coefficients were found to be on the order of 10^{-6} to 10^{-8} cm^2/s.[3]

Similar experiments were conducted by Henke, et al.,[6] who used PEG prepolymers (3 and 10 kDa) to crosslink with fumaryl chloride in toluene with a water soluble crosslinking initiator and catalyst into oligo(poly(ethylene glycol)fumarate) (OPF) hydrogel. Fluoresceinisothiocyanato-dextran (FITC-dextran) (4kDA to 40kDa) and fluorescent nanoparticulate probes (100 nm diameter) were incorporated in the hydrogels after crosslinking. Release experiments were performed by placing gel slabs in vials of phosphate buffered saline (PBS) and measuring the time and percent of protein released. The lateral diffusion coefficients from the FRAP experiments were found to be on the order of 10^{-7} to 10^{-8} cm^2/s.[6] Additionally, Henke, et al.[6] used confocal laser scanning to look at the distribution of FITC-dextran in swollen and non-swollen gels.

Watkins and Anseth[25] fabricated PEG-DA (MW = 700 and 1000 g/mol) loaded with Texas red (MW = 625 g/mol) and CI-NERF (MW = 452 g/mol) in disk shapes. The disks were soaked in DI-H2O and changed every few hours. At varying time points, confocal laser scanning microscopy was used to determine the concentration profile of the disk. Concentration profiles were fit to a Fickian diffusion model to calculate a diffusion coefficient on the order of 10^{-8} cm^2/s.[25]

Diffusion coefficients were also obtained by Brandl, et al.[38] using four-armed poly(ethylene glycol) polymer (10 kDa) with FITC dextran as the diffusing molecule. Cylinders of loaded gel were immersed in PBS, where the solution was sampled at various time points to calculate the mass fraction of FITC-dextran released with time. A least squares fit was performed and diffusion coefficients were found to be 10^{-7} cm^2/s to 10^{-9} cm^2/s. From FRAP experiments, lateral diffusion coefficients were 10^{-7} cm^2/s to

10^{-9} cm^2/s. A NMR DOSY experiment was performed as well, which measured a diffusion coefficient on the order of 10^{-7} cm^2/s.[38] Diffusion coefficients are obtainable for molecules diffusing through hydrogels. Using these methods, a continuous process and perfect sink conditions are not utilized. However, by containing hydrogel within a microfluidic device, the flow into the device can be controlled to produce a continuous driving force for diffusion.

2.4.2. Short Time Release Model

The short time release model is applicable when a hydrogel slab is initially full of diffusing molecules.[39] The solution was derived considering three conditions. At time zero, the entire hydrogel has a uniform initial concentration. At all times, the concentration at the hydrogel edge in contact with the water stream is zero. Since the water is continuously flowing through the hydrogel channel and constantly sweeping away diffusing molecules, the water is assumed to be a perfect sink that always provides a driving force for the molecules to diffuse down the concentration gradient. The final condition assumes that the hydrogel is a semi-infinite slab, and states that as the distance from the hydrogel channel approaches infinity, the concentration is not changing. The release of molecules through elution in hydrogels can be approximated with a short time release model for diffusion as

$$\frac{M_t}{M_o} = \sqrt{\frac{4Dt}{\pi L^2}} \tag{2,14}$$

where M_t is the mass eluted, M_o is the initial mass, t is time, and L is the length where diffusion occurs. The derivation of this solution is shown in Appendix A. This solution can be used for short times with a constant diffusion coefficient. Although in most cases diffusion coefficients are assumed to be constant, this is only strictly accurate for dilute solutions. Diffusion coefficients are generally dependent on solute concentration, particularly for systems where there are specific interactions between the solute and diffusion medium.[40]

The short time release approximation is also used for conditions where release is diffusion limited. Mass transfer into the fluid is neglected because it occurs much faster than diffusion. The short time release approximation can be used to determine a diffusion coefficient for the experiments conducted for this thesis. The hydrogel device was constructed to fit the boundary conditions. It can be verified that mass transfer at the channel wall occurs mush faster than diffusion using the Nusselt and Biot numbers in Equations (2,15) and (2,16). The Nusselt number can be estimated for laminar flow along a flat plate using[40]

$$Nu = \frac{kL_c}{D_c} = 0.646 \left(\frac{Lv_0}{v}\right)^{1/2} \left(\frac{v}{D}\right)^{1/3}$$

(2,15)

where k is the mass transfer coefficient, L_c is the length of the channel, D_c is the free diffusion coefficient in water, v_0 is the bulk velocity, and v is the kinematic viscosity. Using the k value found in the laminar flow along a flat plate expression, the Biot number can be estimated using

$$Bi = \frac{kL_G}{D_G}$$

(2,16)

where k is the mass transfer coefficinet, L_G is the length of the hydrogel slab, and D_g is the diffusion coefficient in the hydrogel. A biot number greater than one indicates that any mass transfer limitation from a PEG hydrogel can be neglected.

2.4.2.1. Concentration Measurement

The concentration of the solute in the effluent was determined from one of two methods, ultraviolet/visible spectroscopy and high performance liquid chromatography (HPLC). Ultraviolet spectroscopy was used for the effluent of hydrogels loaded with molecules that had an absorbance peak greater than 400 nm. For effluent with molecules that do not have peaks in the ultraviolet spectrum or have peaks at wavelengths lower than 400 nm, HPLC was used to determine the concentration.

2.4.2.1.1. Ultraviolet/Visible Spectroscopy

Ultraviolet/visible spectroscopy is used to measure the intensity of light that passes through a sample as compared to a reference sample. The absorbance of molecules in a solution is proportional to the concentration of the molecules. Beer's Law, which gives the relationship between concentration and absorbance as

$$A = \varepsilon \ell c \tag{2,17}$$

where ε is the molar absorptivity, ℓ is the path length through the sample, and c is concentration.

2.4.2.1.2. High Performance Liquid Chromatography

High performance liquid chromatography is a method used to separate components based on retention time within the column. Movement of solution components through a HPLC column is dependent on interactions of the components with the stationary phase. Components with high retention times interact strongly with the stationary phase, whereas components with low retention times do not interact strongly with the stationary phase and pass through the column quickly. Concentration of a component in a solution can be determined by finding the area under the curve of the peak at the component's characteristic retention time.

2.4.2.2. Generation of Diffusion Coefficient using Short Time Release Model

Once concentration is determined from the samples, the mass released from the hydrogel can be calculated according to Equation (2,14). The fraction of dye diffused can be plotted against the square root of time to provide a linear relationship for short time data from which the diffusion coefficient can be extracted for systems with constant diffusion coefficients. The slope of the data can be determined using a best fit line to calculate the diffusion coefficient.

2.4.3. Optical Image Analysis Method

Recently, an optical method of determining the binary diffusion coefficient of corn syrup and water was conducted by monitoring the interface between the two liquids with a digital camera.[41] This provides evidence that optical images can be correlated to

diffusion coefficients. A customized MATLAB script written by Andrew Litzenberger correlates image intensity to an error function solution.[42] Error function solutions are common solutions to the continuity equation for mass with a constant diffusion coefficient and early stages of diffusion.[37]

$$\frac{C}{C_o} = erfc\left(\frac{\eta}{\sqrt{D}}\right) \tag{2,18}$$

where C is concentration at a given position and time, C_o is the initial concentration in the slab, η is the similarity variable, t is time, x is position, and D is the diffusion coefficient. The similarity variable, η, is defined as

$$\eta = \frac{x}{\sqrt{t}} \tag{2,19}$$

where x is position and t is time. Applying this optical method with a digital microscope, the diffusion coefficient of optically active molecules in a hydrogel can be determined by fitting the data extracted from device images.

2.4.3.1. Concentration Measurement

Concentration information from images of the dye loaded gel can be correlated to image intensity. A customized MATLAB script written by Andrew Litzenberger extracts concentration, position, and time data. Files are converted from RGB (red, blue, green) to grayscale with the conversion

$$GS = 0.299 * R + 0.587 * G + 0.114 * B \tag{2,20}$$

Using grayscale, the intensity of the images is normalized between 0 and 1 with respect to a relative intensity. Using the known initial dye concentration in the gel, the normalized intensity can be used to calculate the concentration of the gel.

2.4.3.2. Diffusion Coefficients from Optical Analysis

Concentration data plotted against the similarity variable, η, can be used to solve for the diffusion coefficient. Diffusion coefficients can be found by regressing the extracted image data against the analytical penetration solution to the diffusion equation, which was shown previously in Equation (2,17).

2.4.4. Nuclear Magnetic Resonance Self-Diffusion Coefficient Method

Diffusion coefficients measured with the NMR method are not the same as those measured by the optical and short time release techniques. For those methods, the dye loaded hydrogel is contacted with a water stream that acts as a sink to establish a concentration gradient. For the NMR method the measurement of diffusion has no concentration gradient. Instead, NMR measures a self diffusion coefficient. To measure a size diffusion coefficient using NMR, the length of diffusion examined must be much smaller than the size of the mesh ($L_D << \xi$). L_D is defined as

$$L_D = \sqrt{4D\Delta} \tag{2,21}$$

where D is the diffusion coefficient and Δ is the delay between gradient pulses. A larger delay between gradient pulses increases the motion of the molecules and thus the length that is travelled.

2.4.4.1. Signal Measurement

Nuclear magnetic resonance (NMR) spectroscopy is a method for studying the interaction between electromagnetic radiation and nuclei in a static magnetic field when exposed to another oscillating magnetic field.[43] Not all atomic nuclei produce a signal in NMR, however those that do resonate at different radio frequencies (RF). One of the most commonly studied nuclei is [1]H. The signal seen in NMR is caused by the spin of protons, electrons, and neutrons in a given atom that produce a net magnetization vector. In a NMR spectrometer, a coil of wire provides magnetic resonance with an alternating current at the Larmor frequency of the atomic nuclei. When pulsed with current, the spin and thus the net magnetization vector change and produce a signal. The signal is given as a free induction decay (FID), which stores all the frequencies of the protons in the measured sample that correspond to particular functional groups.[44] The spectrum of the signal from the raw data is reconstructed using Fourier transforms.

The maximum response of nuclei is seen with a 90° or $\pi/2$ pulse which rotates the magnetization vector 90°.[43] A standard two-pulse (s2pul) sequence, displayed in Figure 2.13, can be used to identify the 90° pulse or generate a sample spectrum. Using a single observed pulse time (pw) will generate a single spectrum.
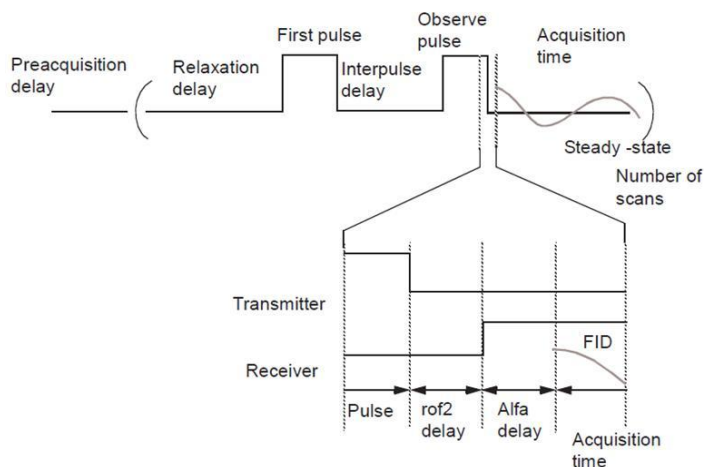
Figure 2.13. A standard two pulse sequence (s2pul)

If the observe pulse is arrayed, the signal spectrum will be generated for each observe pulse time in the array. After arraying pw, the resulting signals for each pulse time at a particular resonance are compiled, as shown in Figure 2.14. By analyzing all the signals, the 90° pulse time can be found by determining the π or 180° pulse and dividing it by two. The 180° pulse is easier to find than the 90° pulse, as it corresponds to a null point without signal.[45]
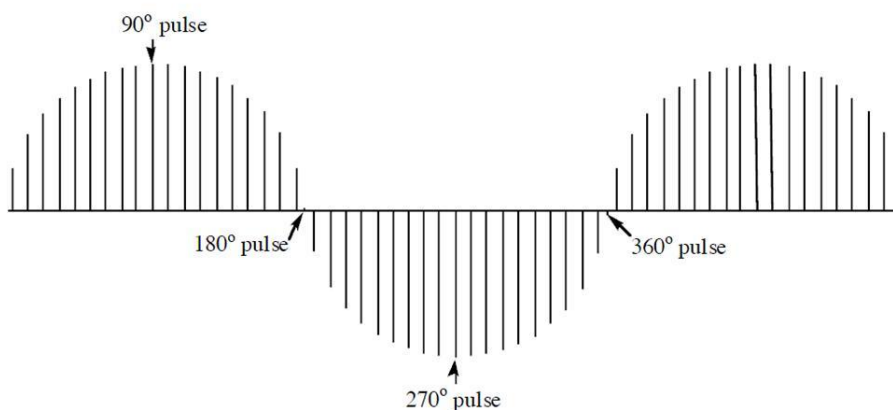
Figure 2.14. Array of NMR signals used to determine the 90° pulse.[45]

Once the 90° pulse is found, self-diffusion coefficients can be determined using several pulse sequences. The RF pulses are combined with gradient pulse spin echoes for time dependent diffusion measurement.[46]

2.4.4.2. Generation of Diffusion Coefficient using the NMR Analysis

Gradients can be used to measure diffusion because they sensitize the NMR signal to molecular motion. As the gradient strength increases, the signal becomes more attenuated. The diffusion coefficient can be determined by fitting the attenuation of the signal to a model. Samples with more attenuation have higher diffusion coefficients than samples with less attenuation for the same change in gradient strength. Diffusion coefficients can be calculated based on the expression

$$\frac{E(g)}{E(g_0)} = exp\left(\gamma^2 g^2 \delta^2 D\left(\Delta - \frac{\delta}{3}\right)\right) \tag{2,22}$$

where $E(g)/E(g_0)$ is the ratio of the signal of the gradient strength to the signal at zero gradient strength, γ is the gyromagnetic ratio, Δ is the delay between gradient pulses, δ is the duration of the gradient pulses, and D is the diffusion coefficient. The ratio of the gradient strengths for molecule being tested, R_{mb}, is shown in equation (2,23).

$$R_{mb} = \frac{E(g)}{E(g_0)} \tag{2,23}$$

From equation (2,22), a new parameter X can be established as

$$X = \gamma^2 g^2 \delta^2 \left(\Delta - \frac{\delta}{3}\right) \tag{2,24}$$

Thus Equation (2,22) can be rearranged into

$$(2,25)$$

$$D = \frac{ln(R_{mb})}{X}$$

to provide a linear relationship between X and the natural log of R_{mb}. Using this relationship, X can be plotted against $ln(R_{mb})$ to give a linear fit and a best fit line can be applied to the data, where the negative slope of the line can be used to determine the self-diffusion coefficient of the solute in the hydrogel.

2.4. References

(1) Hoare, T. R.; Kohane, D. S. Hydrogels in drug delivery: Progress and challenges. Polymer 2008, 49, 1993-2007.

(2) Peppas, N. A. In Hydrogels; Ratner, B. D., Hoffman, A. S., Schoen, F. J. and Lemons, J. E., Eds.; Biomaterials Science An Introduction to Materials in Medicine; Academic Press: San Diego, 1996.

(3) Kosto, K. B.; Deen, W. M. Hindered Convection of Macromolecules in Hydrogels. Biophysical Journal 2005, 88, 277-286.

(4) Lin, C.; Metters, A. T. Hydrogels in controlled release formulations: Network design and mathematical modeling. Adv. Drug Deliv. Rev. 2006, 58, 1379-1408.

(5) Amsden, B. Solute Diffusion within Hydrogels. Mechanisms and Models Macromolecules 1998, 31, 8382 - 8395.

(6) Henke, M.; Brandl, F.; Goepferich, A. M.; Tessmar, J. K. Size-dependent release of fluorescent macromolecules and nanoparticles from radicaly cross-linked hydrogels. European Journal of Pharmaceutics and Biopharmaceutics 2009, 184 - 192.

(7) Weber, L. M.; Lopez, C. G.; Anseth, K. S. Effects of PEG hydrogel crosslinking density on protein diffusion and encapsulated islet survival and function Journal of Biomedical Materials Research Part A 2009, 90A, 720 - 729.

(8) Khoury, C.; Adalsteinsson, T.; Johnson, B.; Crone, W. C.; Beebe, D. J. Tunable Microfabricated Hydrogels—A Study in Protein Interaction and Diffusion. Biomed. Microdevices 2003, 5, 35 - 45.

(9) Jagur-Grodzinski, J. Polymeric gels and hydrogels for biomedical and pharmaceutical applications Polym. Adv. Technol. 2009, 27 - 47.

(10) Brazel, C. S.; Peppas, N. A. Modeling of drug release from Swellable polymers. European Journal of Pharmaceutics and Biopharmaceutics 2000, 49, 47-58.

(11) Jeong, B.; Kim, S. W.; Bae, Y. H. Thermosensitive sol-gel reversible hydrogels. Adv. Drug Deliv. Rev. 2002, 54, 37-51.

(12) Geever, L. M.; Cooney, C. C.; Lyons, J. G.; Kennedy, J. E.; Nugent, M. J. D.; Devery, S.; Higginbotham, C. L. Characterisation and controlled drug release from novel drug-loaded hydrogels. European Journal of Pharmaceutics and Biopharmaceutics 2008, 69, 1147-1159.

(13) Philippova, O. E.; Hourdet, D.; Audebert, R.; Khokhlov, A. R. pH-responsive gels of hydrophobically modified poly (acrylic acid). Macromolecules 1997, 30, 8278-8285.

(14) Beamish, J. A.; Zhu, J.; Kottke-Marchant, K.; Marchant, R. E. The effects of monoacrylated poly(ethylene glycol) on the properties of poly(ethylene glycol) diacrylate hydrogels used for tissue engineering J. Biomed. Mater. Res. A. 2010, 92, 441-450.

(15) Flory, P. J. In Principles of polymer chemistry; Cornell Univ Pr: 1953.

(16) Peppas, N. A.; Huang, Y.; Torres-Lugo, M.; Ward, J. H.; Zhang, J. Physicochemical, foundations and structural design of hydrogels in medicine and biology. Annu. Rev. Biomed. Eng. 2000, 2, 9-29.

(17) Lyons, J. G.; Geever, L. M.; Nugent, M. J. D.; Kennedy, J. E.; Higginbotham, C. L. Development and characterisation of an agar-polyvinyl alcohol blend hydrogel. Journal of the Mechanical Behavior of Biomedical Materials 2009, 2, 485-493.

(18) Teng, D.; Wu, Z.; Zhang, X.; Wang, Y.; Zheng, C.; Wang, Z.; Li, C. Synthesis and characterization of in situ cross-linked hydrogel based on self-assembly of thiol-modified chitosan with PEG diacrylate using Michael type addition. Polymer 2010, 51, 639-646.

(19) Barbucci, R.; Pasqui, D.; Favaloro, R.; Panariello, G. A thixotropic hydrogel from chemically cross-linked guar gum: synthesis, characterization and rheological behaviour. Carbohydr. Res. 2008, 343, 3058-3065.

(20) Zhong, C.; Wu, J.; Reinhart-King, C.; Chu, C. Synthesis, characterization and cytotoxicity of photo-crosslinked maleic chitosan-polyethylene glycol diacrylate hybrid hydrogels. Acta Biomaterialia. 2010, 3908 - 3918.

(21) Wu, Y.; Park, H. B.; Kai, T.; Freeman, B. D.; Kalika, D. S. Water uptake, transport and structure characterization in poly(ethylene glycol) diacrylate hydrogels. J. Membr. Sci. 2010, 347, 197-208.

(22) Tan, G.; Wang, Y.; Li, J.; Zhang, S. Synthesis and Characterization of Injectable Photocrosslinking Poly (ethylene glycol) Diacrylate based Hydrogels Polymer Bulletin 2008; 2008, 61, 91 - 98.

(23) Friedman, A. J.; Han, G.; Navati, M. S.; Chacko, M.; Gunther, L.; Alfieri, A.; Friedman, J. M. Sustained release nitric oxide releasing nanoparticles: characterization of a novel delivery platform based on nitrite containing hydrogel/glass composites. Nitric Oxide 2008, 19, 12-20.

(24) Teng, Y.; Wang, X.; Wang, Y.; Ma, D. Wnt/β-catenin signaling regulates cancer stem cells in lung cancer A549 cells. Biochem. Biophys. Res. Commun. 2010, 392, 373-379.

(25) Watkins, A. W.; Anseth, K. S. Investigation of Molecular Transport and Distributions in Poly(ethylene glycol) Hydrogels with Confocal Laser Scanning Microscopy Macromolecules 2005, 38, 1326 - 1334.

(26) Mellott, M. B.; Searcy, K.; Pishko, M. V. Release of protein from highly cross-linked hydrogels of poly(ethylene glycol) diacrylate fabricated by UV polymerization. Biomaterials 2001, 22, 929-941.

(27) Padmavathi, N. C.; Chatterji, P. Structural Characteristics and Swelling Behavior of Poly (ethylene glycol) Diacrylate Hydrogels†. Macromolecules 1996, 29, 1976-1979.

(28) Tomic, K.; Veeman, W. S.; Boerakker, M.; Litvinov, V. M.; Dias, A. A. Lateral and rotational mobility of some drug molecules in a poly(ethylene glycol) diacrylate hydrogel and the effect of drug-cyclodextrin complexation J. Pharm. Sci. 2008, 97, 3245-3256.

(29) Ulman, A. Formation and structure of self-assembled monolayers. Chem. Rev. 1996, 96, 1533-1554.

(30) Schreiber, F. Structure and growth of self-assembling monolayers. Prog Surf Sci 2000, 65, 151-257.

(31) Allen, N. S.; Marin, M. C.; Edge, M.; Davies, D. W.; Garrett, J.; Jones, F.; Navaratnam, S.; Parsons, B. J. Photochemistry and photoinduced chemical crosslinking activity of type I & II co-reactive photoinitiators in acrylated prepolymers. J. Photochem. Photobiol. A. 1999, 126, 135-149.

(32) Stone, H. A.; Stroock, A. D.; Ajdari, A. ENGINEERING FLOWS IN SMALL DEVICES. Annu. Rev. Fluid Mech. 2004, 36, 381 - 411.

(33) Squires, T.; Quake, S. Microfluidics: Fluid physics at the nanoliter scale. Reviews of Modern Physics 2005, 77, 977 - 1026.

(34) Whitesides, G. M. The origins and the future of microfluidics. Nature 2006, 442, 368-373.

(35) Heeren, A.; Luo, C. P.; Roth, G.; Ganser, A.; Brock, R.; Wiesmueller, K..; Henschel, W.; Kern, D. P. Diffusion along microfluidic channels. Microelectronic Engineering 2006, 83, 1669-1672.

(36) Beebe, D. J.; Mensing, G. A.; Walker, G. M. Physics and applications of microfluidics in biology. Annu. Rev. Biomed. Eng. 2002, 4, 261-286.

(37) Crank, J. In The Mathematics of Diffusion; Clarendon Press: Oxford, NY, 1956.

(38) Brandl, F.; Kastner, F.; Gschwind, R. M.; Blunk, T.; Teßmar, J.; Göpferich, A. Hydrogel-based drug delivery systems: Comparison of drug diffusivity and release kinetics. J. Controlled Release 2010, 142, 221-228.

(39) Hadgraft, J. Calculations of drug release rates from controlled release devices. The slab. Int. J. Pharm. 1979, 2, 177-194.

(40) Cussler, E. L. In Diffusion Mass Transfer in Fluid Systems; Cambridge University Press: Cambridge, 1984.

(41) Ray, E.; Bunton, P.; Pojman, J. A. Determination of the diffusion coefficient between corn syrup and distilled water using a digital camera. American Journal of Physics 2007, 75, 903.

(42) Litzenberger, A. A Microfluidic Method to Measure Diffusion in Hydrogels, Bucknell University, Lewisburg, PA, 2010.

(43) Hornak, J. P. Basics of NMR. *http://www.cis.rit.edu/htbooks/nmr/bnmr.htm* (accessed 3/13/2011, 2011).

(44) Jacobsen, N. NMR Data Acquistion. *http://www.chem.arizona.edu/facilities/nmr/params.pdf*.

(45) Holmes, D. 90°-Degree Pulse Width Calibration. *http://www2.chemistry.msu.edu/facilities/nmr/90pulse.html*.

(46) Mair, R. W.; Cory, D. G.; Peled, S.; Tseng, C. H.; Patz, S.; Walsworth, R. L. Pulsed-field-gradient measurements of time-dependent gas diffusion. Journal of Magnetic Resonance 1998, 135, 478-486.

(47) Culbertson, C. T.; Jacobson, S. C.; Michael Ramsey, J. Diffusion coefficient measurements in microfluidic devices. Talanta 2002, 56, 365-373.

3. Materials and Methods

3.1. Materials

3.1.1. Materials for Microfluidic Device Fabrication

Glass slides (3 in x 1 in x 1 mm, VWR International, LLC), silicon spacers (University Wafer, mechanical grade SSP Si), thiolene optical adhesive (Norland Optical Adhesive-81 resin, Norland Products Inc., Cranbury, NJ), and a line-patterned transparency were used to create the empty device. Slides were cleaned using ethanol (Pharmco-Aaper, >99.98%), acetone (Recochem Inc., >99% purity by weight), isopropyl alcohol (BDH Chemicals Ltd., >99.5%), and delicate task wipers (Kimtech Sciences), and a Radio Frequency Plasma Cleaner (Harrick Scientific Products, Inc) with oxygen (Airgas) and nitrogen (Airgas). Empty devices were fabricated using ethanol (Pharmco-Aaper, >99.98%), 3-(trichlorosilyl)-propyl methacrylate (TPM) (Sigma Aldrich), deionized water, polyethylene glycol (diacrylate) (Sigma Aldrich, M_n = 575 g/mol), 4-(2-hydroxyethoxy)phenyl-(2-hydroxy-2-propyl)ketone (Irgacure 2959) (Ciba Specialty Chemicals), syringe needles (25 G x 1½ in from Becton-Dickinson), electric tape, and thiolene optical adhesive (Norland Optical Adhesive-81resin, Norland Products Inc., Cranbury, NJ). Hydrogel solution was injected using a 10 mL Luer-Lok syringe (Becton-Dickinson and Company). An ultraviolet lamp (Blak-Ray Ultraviolet Lamp, wavelength: 365 nm) and a lightmeter (290-390 nm Lutron lightmeter) were used to cure the hydrogel solution and optical adhesive. A microliter syringe needle (Hamilton Co.) and compressed air were used to clear the channel. Small molecules tested were methylene

blue (Sigma Aldrich), acid blue 22 (Sigma Aldrich), naproxen (Sigma Aldrich), brilliant black (Sigma Aldrich), and rhodamine 6G (Fluka). Sodium hydroxide (NaOH) pellets (EM Science) were used to increase the pH of deionized water to dissolve naproxen.

3.1.2. Materials for Device Diffusion

Poly(vinyl chloride) PVC M-M and M-F luer-lock tubing 24 in. in length with inner diameters of 0.065 in. and outer diameters of 0.125 in. (Cole-Parmer), a 60 mL syringe (luer-lock plastic syringes from National Scientific Company), and a syringe pump (New Era Pump Systems, Inc.) were used to deliver deionized water through the device channel. A Wolfe Digivu Stereomicroscope and Motic Images Plus 2.0 program (Motic China Co., Ltd) were used to capture images of the device during runs. Polystyrene 3 mL cuvettes (BrandTech Scientific, Inc.) were used to capture effluent, which was measured in a SpectraMax M5 spectrophotometer (Molecular Devices) or Ultimate 3000 high performance liquid chromatography column (Dionex). Cuvette samples were transferred to 1.5 mL sample vials (Agilent).

3.1.3. Materials for Lyophilization

Hydrogels for lyophilization purposes were made using glass slides (3 in. x 1 in. x 0.0393 in., VWR International, LLC), silicon spacers (University Wafer, mechanical grade SSP Si), polyethylene glycol (diacrylate) (Sigma Aldrich, $M_n = 575$ g/mol), 4-(2-hydroxyethoxy)phenyl-(2-hydroxy-2-propyl)ketone (Irgacure 2959) (Ciba Specialty Chemicals), and 10 mL luer-lok syringe (Becton-Dickinson and
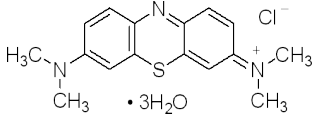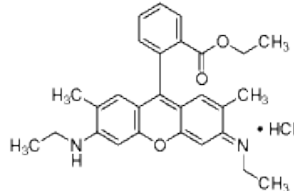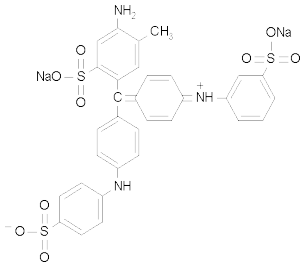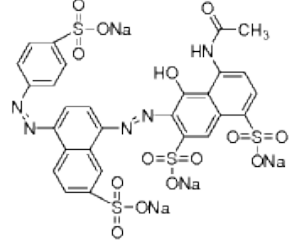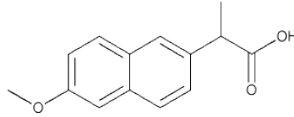
Company). Gels were cured using an ultraviolet light source (Blak-Ray Ultraviolet Lamp, wavelength = 365 nm) with a UV Lightmeter (290 nm to 390 nm Lutron lightmeter) to measure intensity. Hydrogels were removed from the glass using razors. Tools used for removing hydrogels from devices after experimentation required a tungsten-carbide scribe, chisel, and hammer. Samples were measured in a FreezMobile 12 Lyophilizer (Virtis Company, Inc.) using Liquid Nitrogen (Taylor-Wharton), 120 mL jars with rubber cap (Labconco), and filter paper (Whatman).

3.1.4. Materials for NMR

A standard NMR tube was prepared using ethanol (Pharmco-Aaper, > 99.98%), deuterium oxide (D_2O) (Norell Inc.), and a NMR tubes (5 mm, Wilmad LabGlass). Samples were made with polyethylene glycol (diacrylate) (Sigma Aldrich, M_n = 575 g/mol), 4-(2-hydroxyethoxy)phenyl-(2-hydroxy-2-propyl)ketone (Irgacure 2959) (Ciba Specialty Chemicals), and deionized water. Hydrogel solution was injected using 10 mL Luer-Lok syringe (Becton-Dickinson and Company) and cured using ultraviolet light source (Blak-Ray Ultraviolet Lamp, wavelength: 365 nm), lightmeter (290 nm to 390 nm Lutron lightmeter), and 30 rev/min axial rotator (Buehler Motor Inc.) powered by a regulated power supply machine (CSI/SPECO). Diffusion experiments were performed on the hydrogel samples using a 600 MHz DirectDrive four-channel, multinuclear NMR spectrometer (Varian). NMR experiments were controlled using the Java based VnmrJ program (Varian).

3.1.5. Small Molecules

Table 3.1. Small molecule summary table

Name	Structure	MW (g/mol)	Charge	Hydrodynamic Radius (Å)
Methylene Blue		373.9	Cation +1	4.58[1]
Rhodamine 6G		479.01	Cation +1	2.18*
Acid Blue 22		737.7	Anion -2	4.43*
Brilliant Black		871.71	Anion -4	5.11*
Naproxen		373.9	Anion -1	0.62[2]

The (*) in the table denotes hydrodynamic radii that were calculated using the polar surface area of the molecule. Using the polar surface area of the molecule underestimates the hydrodynamic radius because it does not account for the surface area of non-polar atoms or any interactions with the water in solution. Values of the hydrodynamic radii without a (*) were calculated using the known molar volume of the molecule.

3.2. Methods

All laboratory procedures are conducted in a UV sensitive area. Windows were completely covered and taped closed to shield the room from outside light. The area is lit with UV filtered light with an amber coating to minimize unwanted radiation.

3.2.1. Methods for Microfluidic Device Fabrication

The glass slides were washed with acetone and dried with KimWipes. The slides were then rinsed with isopropyl alcohol and dried with KimWipes. The cleaned slides were placed into the plasma cleaner, which was allowed to fill with oxygen for 2 minutes at 200 mTorr. Impurities from the slides were removed using plasma at the low radio frequency setting for 3 minutes. The basic empty closed-face device was created by placing two of the silicon spacers on each end of one glass slide. NOA-81 optical adhesive was poured onto the slide and covered with the second glass slide such that it rested on the silicon spacers to create a 0.12 cm space between the slides filled entirely with optical adhesive. A black photomask was placed on the slides to expose approximately 0.5 cm of the slide edge and prevent UV penetration to the rest of the

device. The slides were cured under UV light (365 nm, 5000 $\mu W/cm^2$) for approximately 3 min- 4 min. The same procedure was repeated for the other side. Spacers were removed and the excess NOA-81 resin was emptied from the center of the device using ethanol, isopropyl alcohol, and limited quantities of acetone. After cleaning the device was post cured under UV light for 20 min (365 nm, 3000 $\mu W/cm^2$) and thermally cured at 50 °C for 4 h. A finished empty device is shown in Figure 3.1.
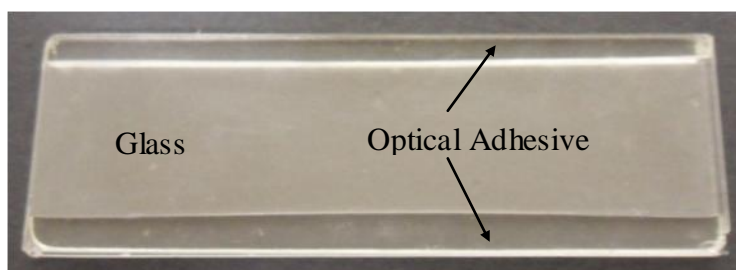
Figure 3.1. Empty device constructed using optical adhesive and glass slides

Prior to injection of the hydrogel solution, the empty device was soaked in a 1mM 3-(trichlorosilyl)propyl methacrylate (TPM) solution in ethanol. After soaking, excess TPM was washed out with ethanol and blown dry with air.

3.2.1.1. Methods for Elution Device Fabrication

For elution devices, methylene blue, acid blue 22, naproxen, brilliant black, and rhodamine 6G were investigated. For methylene blue, nine solutions of varying concentration and initial water/PEG-DA ratios were made. High, medium, and low concentrations of dye were used for each of three initial water/PEG-DA ratios. The three initial water/PEG-DA ratios used were 70/30 g H_2O/g PEG-DA, 60/40 g H_2O/g PEG-DA, and 40/60 g H_2O/g PEG-DA. Amounts of hydrogel and water were weighed and mixed.

The mass of Irgacure photoinitiator added to each solution was based on 0.25 wt% of the PEG-DA. For 70/30 solutions 0.075 g Irgacure was added, for 60/40 solutions 0.1 g Irgacure was added, and for 40/60 solutions 0.15 g Irgacure was added. Dye concentrations were based on the solubility of methylene blue in water, which is 3.55 wt%. The mass of dye added was either 0.5 %, 1 %, or 1.5 % of the 3.55 wt% of the mass of water that was in solution for 70/30 and 60/40 gels. The mass of dye added for 40/60 gels was 1 %, 1.5 %, or 2 % of the 3.55 wt% of the mass of water.

For acid blue 22 nine solutions of varying concentration and hydrogel content were made. Again, high, medium, and low concentrations of dye were used for each of three initial water/PEG-DA ratios: 70/30, 60/40, and 40/60 (g H_2O/g PEG-DA). The mass of Irgacure photoinitiator added to each solution was 0.25 wt% of the PEG-DA, where 0.075 g Irgacure was added to 70/30 solutions, 0.1 g Irgacure was added to 60/40 solutions, and 0.15 g Irgacure was added to 40/60 solutions. Dye concentrations were based on the solubility of acid blue 22 in water, which is 7 wt%. The mass of dye added was either 0.5 %, 1 %, or 1.5 % of the 7 wt% of the mass of water that was in solution for 70/30 and 60/40 gels. The mass of dye added for 40/60 gels was 1 %, 1.5 %, or 2 % of the 7 wt% of the mass of water.

Two aqueous solutions of naproxen and hydrogel were prepared of 60/40 and 40/60 initial water/PEG-DA ratios. The mass of Irgacure photoinitiator added to each solution was 0.25 wt% of the PEG-DA. Concentrations were based on the solubility of naproxen in water at a pH of 7.4, which is 6 mg/mL.[3] Naproxen is not soluble in water at low pHs but is freely soluble in high pH solutions. Naproxen was added at 1 % of the

6 mg/mL solubility of the mass of water with NaOH added to produce a solution of pH 7.4.

One solution of brilliant black in water and PEG-DA was made. The initial water/PEG-DA ratio used was 70/30 with a brilliant black concentration of 0.11 mg/g solution. One solution of rhodamine 6G was made. The initial water/PEG-DA ratio used was 40/60. The concentration of rhodamine 6G was 0.05 mg/g solution.

Hydrogel solution was injected into devices using 10 mL syringes. The filled devices were covered with a photomask, shown in Figure 3.2 and placed under the UV lamp. The photomask has a black 600 µm line across the center to pattern the channel of the device and black at the ends to leave room for the optical adhesive used to hold the needles in place; needles were used to deliver solvent through the channel during experimental trials. The UV light intensity varied among methylene blue devices from 1600 to 3000 µW/cm^2. Cure times ranged from 12 min to 70 min. For acid blue 22, UV intensity varied from 1700 µW/cm^2 to 3000 µW/cm^2, with cure times ranging from 20 min to 3 h. Intensity and cure time differed based on the amount of light that could penetrate through the dye solution and the volume of water in the device. Solutions with high dye concentrations had longer cure times than solutions with low dye concentrations. Solutions with larger amounts of water had less PEG-DA in solution and typically had longer cure times than those with less water and more PEG-DA. Because of the limitations of the UV lamp, the whole device could not receive equal light intensity and while curing devices were moved under the lamp to allow equal exposure. After

curing, excess hydrogel was cleared out of channel using the long needle of a microsyringe and compressed air.
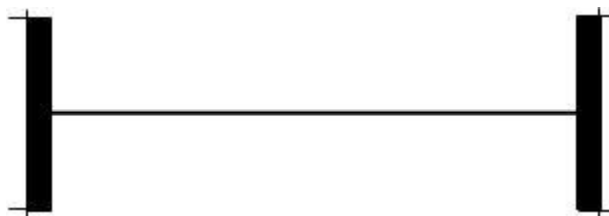
Figure 3.2. Photomask for hydrogel channel

Syringe needles were cut to approximately 1 cm with metal pliers and inserted into each end of the channel. The needles were held in place in the device against a wooden stick as NOA-81 resin was poured around the device to seal the openings and prevent the resin from dripping. The plastic connector of the needle was held closed with a finger to reduce the amount of optical adhesive that could leak into the needle point to clog it. The needles were set by holding and rotating the device under the UV light at an intensity of 5000 μW/cm^2 for approximately 2 min to cure the optical adhesive. A second coat of optical adhesive was applied to the first coat to ensure proper sealing. The needles were post-cured under UV light for 5 min on each side. Before attaching needles, devices were wrapped in black electrical tape to prevent the hydrogel from curing.

3.2.1.2. Methods for Uptake Device Fabrication

Three solutions of varying initial water/PEG-DA ratios were used for the uptake experiments, 70/30, 60/40, and 40/60. The procedure for the devices with initial

water/PEG-DA ratios of 70/30 is outlined in the previous graduate student, Andrew Litzenberger's, thesis.[4] The 60/40 devices were created using the same methodology described in Andrew Litzenberger's thesis. The 40/60 devices were prepared using the same methodology as the elution devices.

3.2.2. Methods for Optical Data Collection

3.2.2.1. Methods for Elution Optical Data Collection

For the set-up of an experiment, a device was placed under the strereomicroscope, which was controlled by Motic Images computer program. Using the Motic program, the microscope camera was programmed to have a constant exposure instead of using the auto-expose function. A white balance was performed using white paper as a reference to calibrate the camera. The device was secured underneath the microscope with tape so that the camera was focused on a smooth part of the channel. A 60 mL luer-lock syringe was filled with deionized water and locked into a syringe pump. The syringe was connected to the device using PVC luer-lock tubing. One end of a second PVC luer-lock tube was attached to the device exit needle and the opposite end was placed in a 5 mL plastic cuvette. The set up for experimental runs is shown in Figure 3.3.

Figure 3.3. Experimental setup. Water is pumped through hydrogel device and collected in cuvettes.

Prior to beginning a run, 3-4 images were manually captured of the empty device. The deionized water was pumped through the device at a flow rate of 5 mL/hr. As the water pumped through the channel, the Motic Images program was used to auto-capture images every 2 min. Each run took approximately 12 h to reach completion. Each image captured was stored as a 1024 x 768 jpeg file. Devices run for the elution study are listed in Table 3.2.

Table 3.2. Devices run for elution experiments

Initial Water/PEG-DA Ratio (g/g)	70/30			60/40			40/60		
Percent of dye solubility used in solution (%)	0.5	1.0	1.5	0.5	1.0	1.5	1.0	1.5	2.0
Methylene Blue	B13	B6	B29	B23	B18	B32	B37	B39	B44
	B14	B8	B30	B24	B20	B34	B40	B42	B45
	B19	B9	B31	B25	B22	B48	B52	B47	B46
	B56		B59				B53		B49
	B57		B60				B54		B50
	B58		B61				B55		B51
Acid Blue 22	A16	A22	A25	A13	A10	A19	A7	A4	A1
	A17	A23	A26	A14	A11	A20	A8	A5	A2
	A18	A24	A27	A15	A12	A21	A9	A6	A3
Naproxen					N10			N13	
					N11			N14	
					N12			N15	

3.2.2.2. Methods for Uptake Optical Data Collection

The procedure for the devices with initial water/PEG-DA ratios of 70/30 and 60/40 is outlined in Andrew Litzenberger's thesis.[3] The concentration of methylene blue solutions used for 70/30 and 60/40 devices were 0.0054 mg/mL and 0.0032 mg/mL respectively. For the 40/60 hydrogels of the uptake experiment, devices were placed under the strereomicroscope with the same setup as the elution devices. A methylene blue solution was pumped through the device at a flow rate of 15 mL/hr. The concentration of the methylene blue solution used for the 40/60 devices was 0.0044 mg/mL. As the water pumped through the channel, the Motic Images program was used to auto-capture images of the uptake every minute. Each run took approximately 4 h to reach completion. Each image captured was stored as a 1024 x 768 jpeg file.

3.2.3. Methods for Effluent Collection and Analysis

The UV/Vis and HPLC techniques require the analysis of the effluent released from the microfluidic devices. Because UV/Vis spectrometers measure the absorbance of a sample, a calibration curve must be used to correlate the concentration and absorbance of a given molecule. UV/Vis analysis was used for methylene blue, acid blue 22, rhodamine 6G, and brilliant black. High performance liquid chromatography was used for naproxen. A calibration curve was made to correlate the concentration and area of the peak at the specific retention time of naproxen.

3.2.3.1. Calibration Curves for Aqueous Dye Solutions

A serial dilution of methylene blue in deionized water was made with an initial concentration of 0.71 mg/mL. An initial solution of 10 mL was diluted with 10 mL of deionized H_2O, and the process was repeated for 12 samples. Using one of the more dilute samples, a spectrum run was conducted to determine the λ_{max}, which is the wavelength corresponding to the highest peak for absorbance. For methylene blue, the λ_{max} was determined to be 660 nm. Absorbance of each of the serially diluted samples was measured in the spectrophotometer at 660 nm. A plot of concentration v. absorbance was created, and the points in the linear region were kept. A line was fit to the data to determine the relationship between absorbance and concentration. The slope used for relating the absorbance v. concentration is given in Table 3.3. The calibration curve for methylene blue is given in Appendix C.

The same procedure for creating the calibration curve for methylene blue was used for acid blue 22, brilliant black, and rhodamine 6G. The λ_{max} for acid blue 22 was determined to be 580 nm, the λ_{max} for brilliant black was 571 nm, and the λ_{max} for rhodamine 6G was 530 nm. The slopes used for relating the absorbance v. concentration for all dye molecules are given in Table 3.3. The calibration curve for all of the dye molecules are given in Appendix C.

Table 3.3. The slope of absorbance v. concentration calibration curve and the λ_{max} at which the absorbance was measured for various dye molecules.

Dye Molecule	λ_{max} (nm)	Slope (mg/mL)
Methylene Blue	660	0.007755
Acid Blue 22	580	0.014533
Brilliant Black	571	0.767800
Rhodamine 6G	530	0.004368

3.2.3.2. Calibration Curve for Naproxen

A similar procedure for creating the calibration curve for methylene blue was used for naproxen. Because naproxen is only soluble in water with a high pH, the calibration curve was made using a solution of NaOH in water. A serial dilution was performed using naproxen in a solution of pH 7.4. The calibration standards were run through the HPLC with acetonitrile as a solvent. The retention time of naproxen was determined to be 10.16 min. The area under the peak at the retention time of naproxen was calculated for each standard sample. A plot of concentration v. the area under the peak at the retention time of naproxen was created. The points in the linear region were kept. A line was fit to the data to determine the relationship between area and concentration. The calibration curve for naproxen is given in Appendix C.

3.2.3.3. Effluent Analysis

For typical experiments, the effluent tubing was moved to fill a new cuvette approximately every forty minutes. At the conclusion of a run, the absorbance of the effluent was measured using a spectrophotometer. The wavelength used in the spectrophotometer was dependent on the specific dye being tested. The λ_{max} was the wavelength used to measure the absorbance for each of the dye molecules. Concentration of the effluent stream was calculated from absorbance using the calibration curve made for known concentrations of each solute using the slope of the calibration curves, which were shown in Table 3.3. For naproxen the effluent captured in cuvettes was run through the HPLC column. Concentration of the effluent stream was calculated from the area under the naproxen peak at the specific retention time. The fraction of solute diffused at each cuvette sample time was calculated using Equation (3,1).

(3,1)

$$\frac{M_t}{M_0} = \frac{\sum \dot{V} t C_t}{V_g C_0}$$

In this expression, M_t is the mass of solute diffused, M_0 is the initial mass of solute in the gel, $\dot{V}$ is the volumetric flow rate of the exiting fluid, C_t is the concentration of solute in the cuvette for any given sample, and t is the amount of time it took to fill a given cuvette. Summing the mass of solute in each cuvette gives the total amount of solute eluted at a time, t. Thus the mass fraction can be determined by dividing by the initial mass of solute in the gel, where V_g is the volume of the gel, and C_0 is the initial concentration of solute in the gel.

A burst effect had to be accounted for with the first cuvette of every run. Because the channels of devices were cleared with only air during fabrication, residual solute was left in the channel. When water is first swept through the channel during an experiment, the residual solute contributes to a burst effect of a higher concentration seen in the first cuvette. Devices that have been stored for longer than a few days also tend to dry out at the channel edge. When initially contacted with water during the experiment, the swelling contributes to an increase in the rate of solute release. To correct for the increased concentration in the first cuvette, the mass released in the first cuvette was subtracted from the total amount of solute eluted and the initial amount of solute in the gel as shown in expression (3,2), and the time the second cuvette began to fill was set to a time zero.

$$M_f = \frac{M_t - M_i}{M_0 - M_i} \tag{3,2}$$

The new fraction of solute diffused, M_f, was plotted against the average of the time the cuvette began to fill and the time the cuvette was filled.

3.2.4. Methods for NMR Analysis

3.2.4.1. Tube Preparation

NMR tubes were prepared by filling the tube with hydrogel solution to a height of approximately 1.5 in. For methylene blue, the same nine solutions of varying concentration and hydrogel content were used. High, medium, and low concentrations of solute were used for each of three initial water/PEG-DA ratios.

For acid blue 22, nine solutions of varying concentration and hydrogel content were made. Again, high, medium, and low concentrations of solute were used for each of three initial water/PEG-DA ratios.

Nuclear magnetic resonance (NMR) tubes were placed under UV light with intensities ranging from 3000 μW/cm^2 to 4500 μW/cm^2 to cure both acid blue 22 and methylene blue hydrogel solutions. Tubes were rotated axially at 30 rev/min. Cure times ranged from 10 min to 85 min for methylene blue solutions and 16 min to 150 min for acid blue 22 solutions depending on concentration of solute and water in the sample. After preparation of the NMR tubes, the cap was attached, sealed with parafilm, and stored in a refrigerator until testing. One solution of uncured methylene blue hydrogel was also prepared for comparison to cured hydrogel solutions. The solution was made with 40 wt% dI-H$_2$O and 60 wt% PEG-DA with no photoinitiator added. Methylene blue was added at 2 wt% of the water, based on the water content.

A standard NMR tube was prepared with deionized water, ethanol, and D$_2$O as a reference to calibrate the NMR. The standard solution was four parts of 90 vol% D$_2$O and 10 vol% H$_2$O and one part ethanol.

3.2.4.2. *^{1}HNMR Diffusion Analysis*

The Varian NMR spectrometer was set up using the broadband probe with the X-channel set to 4. The NMR spectrometer was used to observe ^{1}H nuclei and decouple ^{13}C. The standard ethanol and D$_2$O solution was inserted into the instrument and tuned and shimmed. After tuning, a one-pulse sequence was opened to generate and phase the

spectrum. The one-pulse sequence is shown in Figure 3.4. A relaxation delay (d1) of 5 s

was used with an observe pulse (pw) of 4 µs before the fid was acquired.

Figure 3.4. One pulse NMR sequence used to generate spectrum

Once the standard was used to calibrate the NMR, the lock was turned off, the

standard was ejected, and a hydrogel sample was inserted. The s2pul sequence was run

again to generate and phase the spectrum for the sample. The observe pulse was then

arrayed to perform a "fine" search for the π time of the sample.

Once the π time of a sample was found, a pulsed field gradient enhanced

stimulated echo (pge_ste) experiment was conducted on that hydrogel sample. The pulse

sequence for the pge_ste experiments is shown in Figure 3.5.
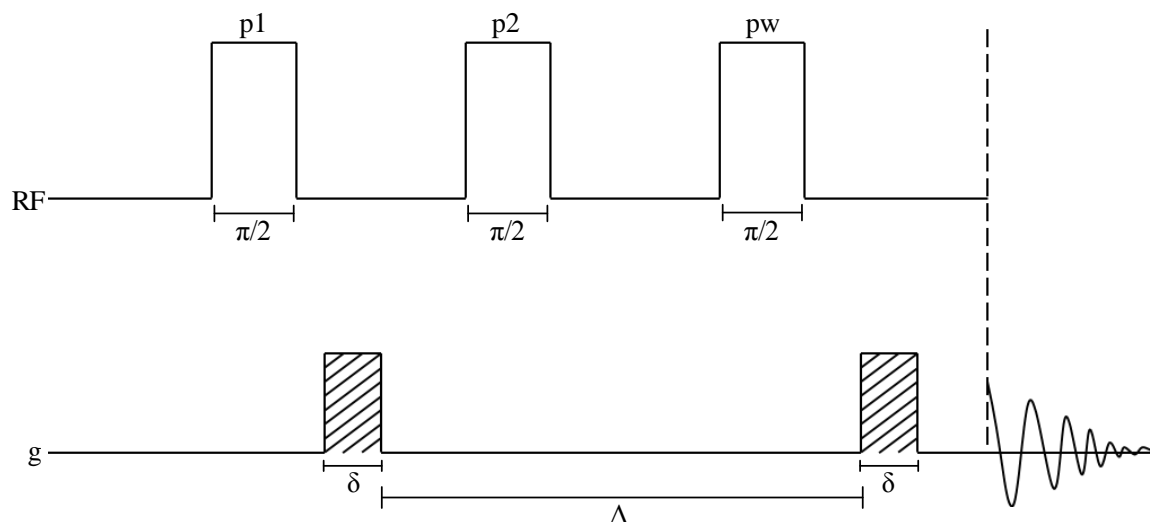
Figure 3.5. The pge_ste sequence used to generate data used to calculate diffusion coefficients.

The RF pulses, p1, p2, and pw were set to the π/2 time, which was half of the π time found from the s2pul sequence. The magnitude of the gradient pulses (g1 and g2) were varied from 0 G/cm to 30 G/cm. The duration of the gradient pulses (δ) was 0.0021 s. The delay between the gradient pulses (Δ) was 0.1 s. The sequence was run with increasing gradient strength to acquire the FID.

3.2.5. Methods for Lyophilization

Two types of gels were lyophilized: hydrogels removed from devices after elution experiments and hydrogels removed from NMR tubes. Hydrogels were removed from sealed devices by scoring the glass with a glass scribe in a rectangular shape along the optical adhesive edges. The scored lines were lightly tapped using a chisel and hammer to break the glass along the scored lines. The broken glass was removed from the device and a razor was then used to detach the hydrogel from the glass. Hydrogels were removed

from NMR tubes by breaking the ends of the tube on either side of the cured gel. The glass was scored along the tube's length with a glass scribe and slightly tapped with the chisel to crack the glass on the scored line. The cracked glass was removed to isolate the gel.

When not in use, the removed gels were placed in small weigh boats wrapped in parafilm and stored in a refrigerator at 4 °C. Prior to lyophilization, hydrogel samples were frozen in liquid nitrogen and placed into a lyophilization jar. The lyophilization jar was then attached to the lyophilizer vacuum. The lyophilizer freezer was turned on and set to -40 °C. Once the sample was attached, the vacuum was turned on and the water was removed through sublimation. Hydrogels were lyophilized for approximately 76 hours and promptly weighed. The dry gels were placed into small vials with 10 mL of water. Gels were allowed to reswell for 2 weeks at which point equilibrium was reached. The hydrogels were patted dry with filter paper and weighed.

3.3. References

(1) Pelekani, C.; Snoeyink, V. L. Competitive adsorption between atrazine and methylene blue on activated carbon: the importance of pore size distribution. *Carbon* 2000*, 38*, 1423-1436.

(2) Ting, S. S. T.; Tomasko, D. L.; Foster, N. R.; Macnaughton, S. J. Solubility of naproxen in supercritical carbon dioxide with and without cosolvents. *Ind Eng Chem Res* 1993*, 32*, 1471-1481.

(3) Amaral, M. H.; Lobo, J. M. S.; Ferreira, D. Effect of hydroxypropyl methylcellulose and hydrogenated castor oil on naproxen release from sustained-release tablets. *AAPS PharmSciTech* 2001*, 2*, 14-21.

(4) Litzenberger, A. A Microfluidic Method to Measure Diffusion in Hydrogels, Bucknell University, Lewisburg, PA, 2010.

4. Results and Discussion

This chapter contains the results and discussion for the fabrication of microfluidic devices and the diffusion of methylene blue, acid blue 22, Naproxen, brilliant black, and rhodamine 6G from hydrogel contained in microfluidic devices. Diffusion was characterized by determining the diffusivity of the molecules in gel using three methods: NMR, optical microscopy, and device effluent analyses.

Diffusion from the hydrogel was affected by the extent of crosslinking in the gel, which was dependent on the total UV exposure dose (mJ/cm^2). The total UV exposure dose depended on the solute concentration and initial water/PEG-DA ratio of the hydrogel solution. The curing conditions for uptake devices were only dependent on the initial amount of water in the hydrogel solution. As the amount of water increased, the total UV exposure dose increased due to a lower density of diacrylate groups. Evidence of gelation was not seen for 70/30 and 60/40 devices until the solution turned opaque. Overexposure to UV light past the initial opaqueness caused the gel to become brittle and crack. Overexposure leads to brittleness and rigidity because the polymer chains lose flexibility when all of the diacrylate groups of the PEG-DA react. Devices with initial water/PEG-DA ratios of 40/60 do not turn opaque when fully cured, which shows that enough PEG-DA is available to react in solution to not strain the polymer chains that could be causing the opacity. As solute concentration increases, the cure time increases because the penetration of UV light into the gel decreases. The curing conditions resulted in channel widths of 700 μm to 1000 μm.

4.1. ¹HNMR Analysis

The NMR analysis was conducted for methylene blue and acid blue 22. The gradient strength was varied to analyze the proton signals that are characteristic of the molecules. A custom MATLAB script was used to calculate the diffusivity of the dye molecules in PEG through the attenuation of the proton signal.

4.1.1. Methylene Blue NMR Analysis

The hydrogen atoms used for signal identification and peak attenuation in the methylene blue hydrogel spectrum are on the aromatic rings in Figure 4.1.
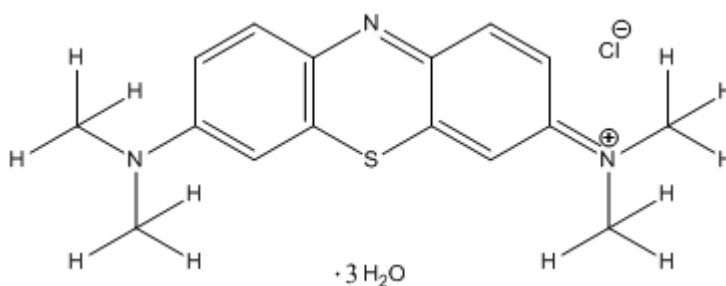
Figure 4.1. Hydrogen atoms on methylene blue for identification in ¹HNMR

Initially, the slope of the data in Figure 4.2 was used to calculate the diffusion coefficient using Equations (2,22) to (2,25). However, Equations (2,22) to (2,25) assume the data follows a straight line. From Figure 4.2 it is evident that the data is not linear, and a linear fit would overestimate the value of the diffusion coefficient. The non-linearity of the data indicates that there are possibly two components to the molecular movement seen in the NMR data, a fast component and a slow component. A model that accounts for a diffusion coefficient for the both the fast and slow component

$$R = f_1 e^{-D_1 X} + (1 - f_1) e^{-D_2 X} \qquad (4,1)$$

The values of the slow (D1) and fast (D2) diffusion coefficients could be determined by fitting the expression below to the data.
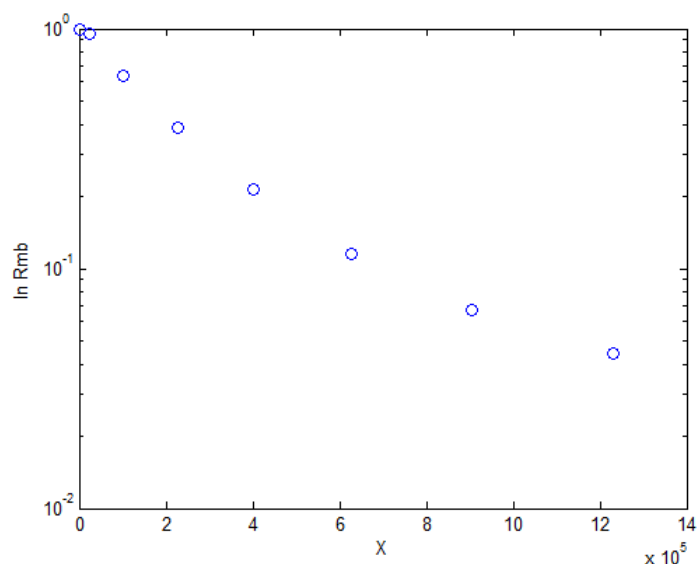
Figure 4.2. Example NMR data used to calculate fast and slow diffusion coefficient components

Diffusion coefficients calculated, assuming a single species, ranged from 10^{-6} cm^2/s to 10^{-7} cm^2/s for all gel types and dye concentrations. For a 2-species fit, the diffusion coefficients of the slow components were all on the order of 10^{-7} cm^2/s. The diffusion coefficients of the fast component ranged from 10^{-5} cm^2/s to 10^{-7} cm^2/s. A summary of the fitted results is shown in Table 4.1.

Table 4.1. Diffusion coefficients for fast, slow, and combined components of the molecular motion in PEG-DA hydrogels loaded with methylene blue dye from NMR analysis

H$_2$O/PEG-DA Ratio (g/g)	Initial Solute Concentration (mg/mL)	Combined Diffusion Coefficient (x 10^{-7} cm^2/s)	Slow Component Diffusion Coefficient (x 10^{-7} cm^2/s)	Fast Component Diffusion Coefficient (x 10^{-7} cm^2/s)
70/30	0.124	13.9 ± 3.79	6.77 ± 0.427	69.0 ± 1.56
	0.261	19.2 ± 10.1	9.38 ± 1.57	116 ± 91.3
	0.37	10.6 ± 0.636	6.86 ± 0.848	147 ± 144
60/40	0.10	7.80 ± 1.88	3.16 ± 0.769	52.3 ± 11.6
	0.213	8.25 ± 4.82	5.38 ± 1.62	57.8 ± 18.5
	0.33	6.48 ± 1.12	4.20 ± 0.263	81.9 ± 32.2
40/60	0.15	8.26 ± 8.09	4.14 ± 3.86	29.5 ± 4.87
	0.21	6.18 ± 2.19	1.89 ± 0.339	35.3 ± 0.818
	0.29	7.13 ± 3.67	2.96 ± 1.27	42.8 ± 12.3

In many of the spectra obtained for the methylene blue NMR samples, the methylene blue peaks overlap with the tail of the water peak. An example spectrum that shows the overlap is displayed in Figure 4.3 of a hydrogel sample with an initial water/PEG-DA ratio of 40/60 and dye concentration of 0.29 mg/g solution. The 3 peaks, which are characteristic of methylene blue, are expanded in Figure 4.3 to demonstrate how the tail of the water peak affects the methylene blue peaks.
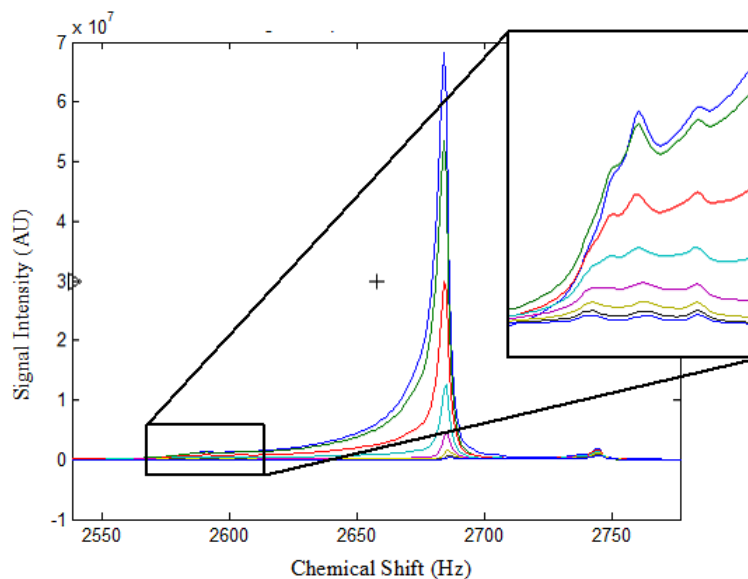
Figure 4.3. Chemical spectrum for methylene blue hydrogel overlapping with water peak tail

Since water has a much higher self-diffusion coefficient than methylene blue, the tail of the water peak could possibly be the fast component of the diffusion coefficient and thus the methylene blue is the slow component diffusion coefficient.

Not all of the hydrogel samples exhibited an overlap with the water peak. The spectrum for one hydrogel sample that does not appear to overlap with the water peak is shown in Figure 4.4 of a hydrogel with an initial water/PEG-DA ratio of 60/40 and dye concentration of 0.33 mg/g solution. The 3 characteristic methylene blue peaks are expanded in Figure 4.4 to show they are not influenced by the tail of the water peak.
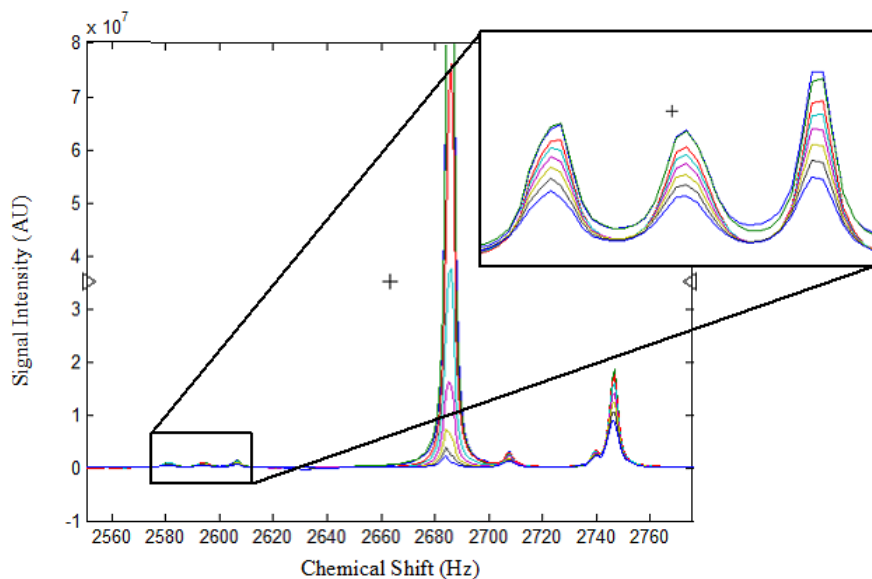
Figure 4.4. Chemical spectrum for methylene blue hydrogel without overlap with water peak tail

The resulting data trend, shown in Figure 4.5, is more linear than data resulting from spectra overlapping with the tail of the water peak shown in Figure 4.2. However, there is still evidence of slight non-linearity within the data.
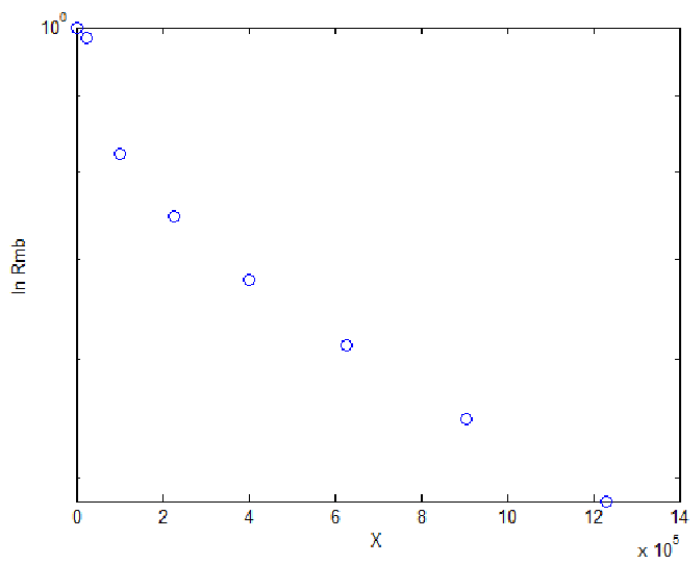
Figure 4.5. Example NMR data with greater linearity

The non-linearity could be the result of methylene blue freely diffusing through the water in the hydrogel mesh and the methylene blue encountering the polymer chains of the hydrogel mesh. Using Equation (2,21), the length of diffusion, L_D, was calculated for methylene blue.

Table 4.2. Comparison of the length of diffusion in NMR analysis and the mesh size for various initial water/PEG-DA content in methylene blue loaded hydrogels.

Initial DI-Water/PEG-DA (g/g)	L_D (Å)	Mesh Size (Å)
70/30	55000 ± 5200	22.4 ± 0.6
60/40	40500 ± 5400	21.8 ± 0.6
40/60	34000 ± 6600	21.3 ± 0.2

From the results in Table 4.2, it is clear that the length of diffusion is much greater than the mesh size. This indicates that as the methylene blue was analyzed using NMR, the diffusion of methylene blue was influenced by encounters with the polymer chains of the mesh. However, the non-linearity of the data suggests that part of the random molecular motion of the methylene blue was free diffusion in water. Litzenberger[2] measured the free diffusion of methylene blue in water to be $15.2 \times 10^{-7} \, cm^2/s$. This value is similar to the values for the fast component of diffusion in hydrogels that do not have a significant influence from the tail of the water peak. By removing the fast component of diffusion caused by the tail of the water peak and the free diffusion of methylene blue in water, the diffusion coefficient of methylene blue through the hydrogel mesh can be described as the slow diffusion component. Since the length of diffusion for NMR was much greater than the mesh size, the slow diffusion component is the movement of the methylene blue through many of the mesh spaces in the hydrogel network.

4.1.2. Acid Blue 22 NMR Analysis

The hydrogen atoms used for signal identification and peak attenuation in the acid blue 22 hydrogel spectrum are on the aromatic rings shown in Figure 4.6.
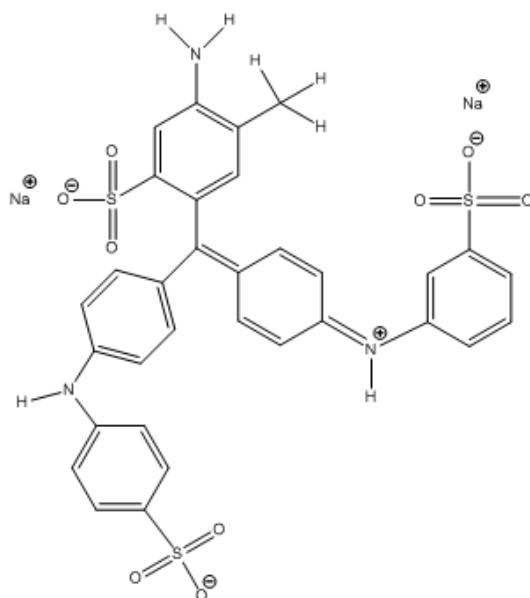
Figure 4.6. Hydrogen atoms on acid blue 22 for identification in ^{1}HNMR

The acid blue 22 diffusion coefficients calculated using the NMR analysis for the combined fast and slow component were mostly on the order of 10^{-7} cm^2/s with one on the order of 10^{-6} cm^2/s for all initial water/PEG-DA ratios and dye concentration levels. The tail of the water peak affected some of the acid blue 22 hydrogel samples, so Equation (4,1) was used to separate the slow and fast diffusion components. The slow component diffusion coefficients for all gel contents had diffusion coefficients on the order of 10^{-7} cm^2/s. The fast component diffusion coefficients for all gel contents had diffusion coefficients on that ranged from 10^{-6} cm^2/s to 10^{-7} cm^2/s. The diffusion

coefficients for all initial water/PEG-DA ratios and dye concentrations are listed in Table

4.3.

Table 4.3. Diffusion coefficients for fast, slow, and combined components of the molecular motion in PEG-DA hydrogels loaded with acid blue 22 dye seen in NMR analysis

Initial DI-H$_2$O/PEG-DA Ratio (g/g)	Initial Dye Concentration (mg/g soln)	Combined (x 10^{-7} cm^2/s)	Slow Component Diffusion Coefficient (x 10^{-7} cm^2/s)	Fast Component Diffusion Coefficient (x 10^{-7} cm^2/s)
70/30	0. 25	17.5	7.03	78.9
	0. 49	7.22	7.22	7.22
	0. 74	9.81	6.17	33.6
60/40	0. 21	7.27	5.23	40.3
	0. 42	8.41	3.86	36.5
	0. 64	6.26	2.56	18.1
40/60	0. 28	2.56	2.56	2.56
	0. 41	3.45	3.08	28.6
	0. 56	2.28	2.28	2.28

In the acid blue 22 hydrogel samples, the interaction with the tail of the water peak increased with an increase in the initial water/PEG-DA ratio of the hydrogel sample. Figure 4.7, which has an initial water/PEG-DA ratio of 70/30 with acid blue 22 concentration of 0.25 mg/g soln, shows how the acid blue 22 peaks are affected by the tail of the water peak.
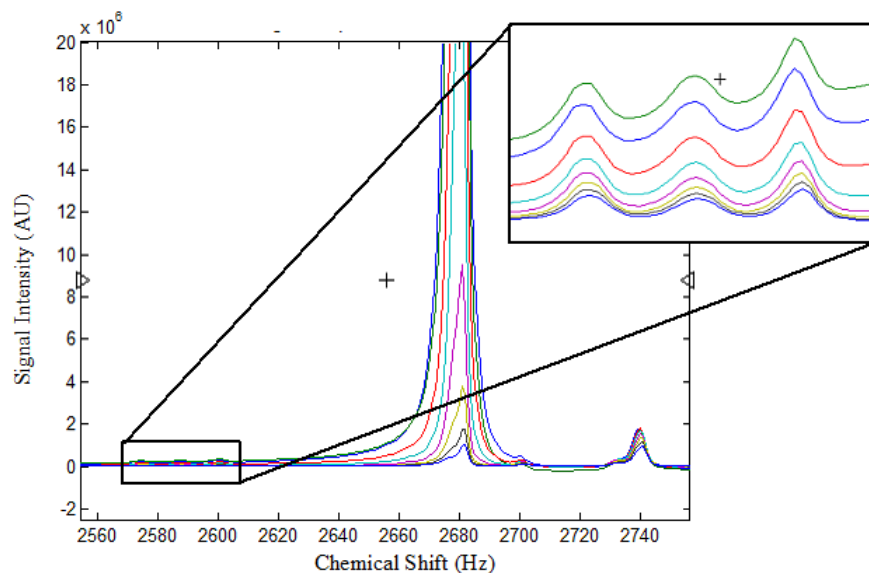
Figure 4.7. Acid blue 22 NMR spectrum with interaction with the tail of the water peak with a water/PEG-DA ratio of 70/30

As with methylene blue, when the acid blue 22 NMR data that had an overlap with the tail of the water peak was plotted, a linear trend was not observed, as shown in Figure 4.8.
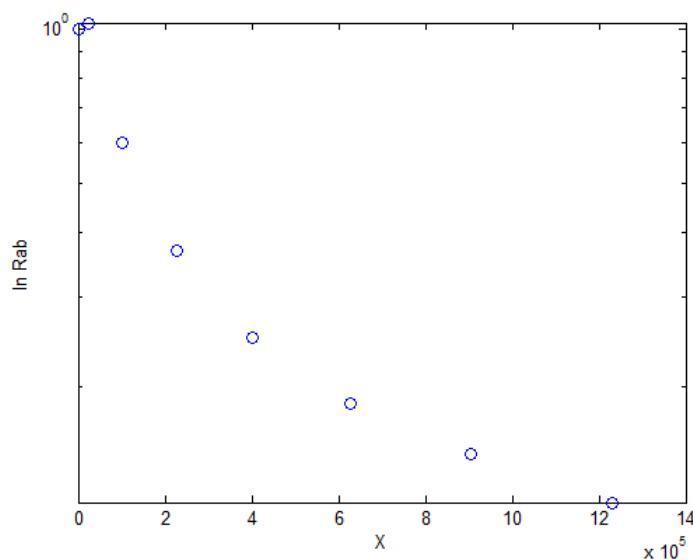
Figure 4.8. Extracted data from acid blue 22 spectrum with an initial water/PEG-DA ratio of 70/30 with interaction with the tail of the water peak.

A NMR spectrum that resulted from a 40/60 hydrogel with an acid blue concentration of

0.56 mg/g soln is shown in Figure 4.9. This sample is characteristic of hydrogels with a

low initial water content that did not have an overlap with the tail of the water peak. As

shown in Figure 4.9 the attenuation of the acid blue 22 peaks is less pronounced than in

hydrogel samples that had overlap with the tail of the water peak.
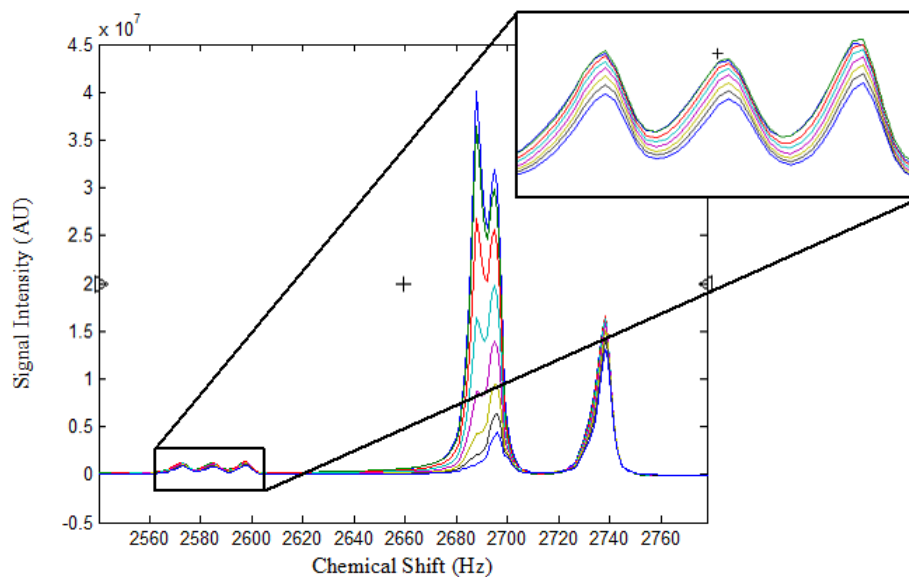
Figure 4.9. Chemical spectrum for acid blue 22 hydrogel with an initial water/PEG-DA ratio of 40/60.

The data extracted from the acid blue 22 spectrum, shown in Figure 4.10 without the

influence of the water peak, has a linear trend.

Figure 4.10. Extracted data from acid blue 22 spectrum with an initial water/PEG-DA ratio of 40/60 with no interaction with the tail of the water peak

For hydrogels, like the one shown in Figure 4.9 that had a linear data trend, the slow and fast components had the same diffusion coefficient. The length of diffusion for ac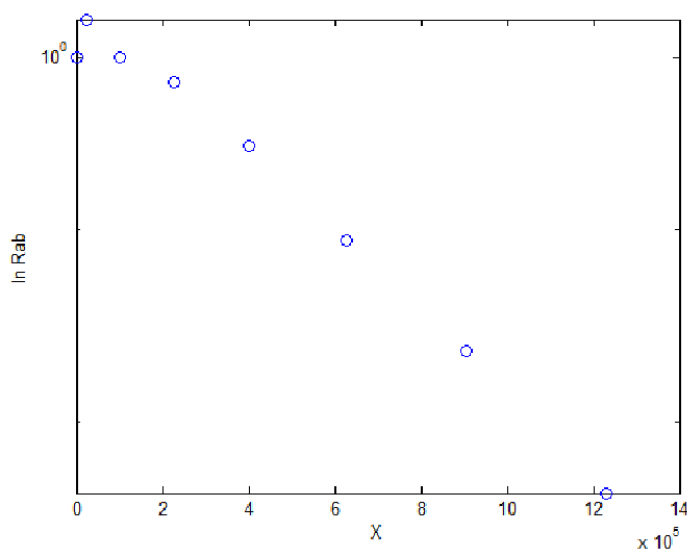id blue 22 in PEG hydrogels were calculated using Equation (2,21). Table 4.4 compares the length of diffusion for NMR to the mesh size of the hydrogels.

Table 4.4. Comparison of the length of diffusion in NMR analysis and the mesh size for various initial water/PEG-DA ratio in acid blue 22 loaded hydrogels.

Initial DI-Water/PEG-DA (g/g)	L_D (Å)	Mesh Size (Å)
70/30	47100 ± 8300	22.1 ± 0.01
60/40	39000 ± 6900	21.5 ± 0.1
40/60	39400 ± 12000	20.7 ± 0.09

The length of the mesh is much larger than the mesh size, which verifies that the acid blue 22 molecules encounter the polymer chains of the mesh during the time interval, Δ, in NMR analysis. Since the acid blue 22 molecules are significantly bigger than

methylene blue molecules, the random motion of the molecules is more likely to be inhibited by encountering the mesh than to be free diffusion in water because the molecular size of acid blue 22 is already close to the size of the mesh.

The diffusion coefficients of the slow component for both methylene blue and acid blue 22 are shown in Figure 4.11 based on the initial amount of water in the hydrogel. Concentration at each water content for acid blue 22 and methylene blue were combined because the diffusion coefficient calculated from NMR is a self-diffusion coefficient and is not driven by on a concentration gradient.
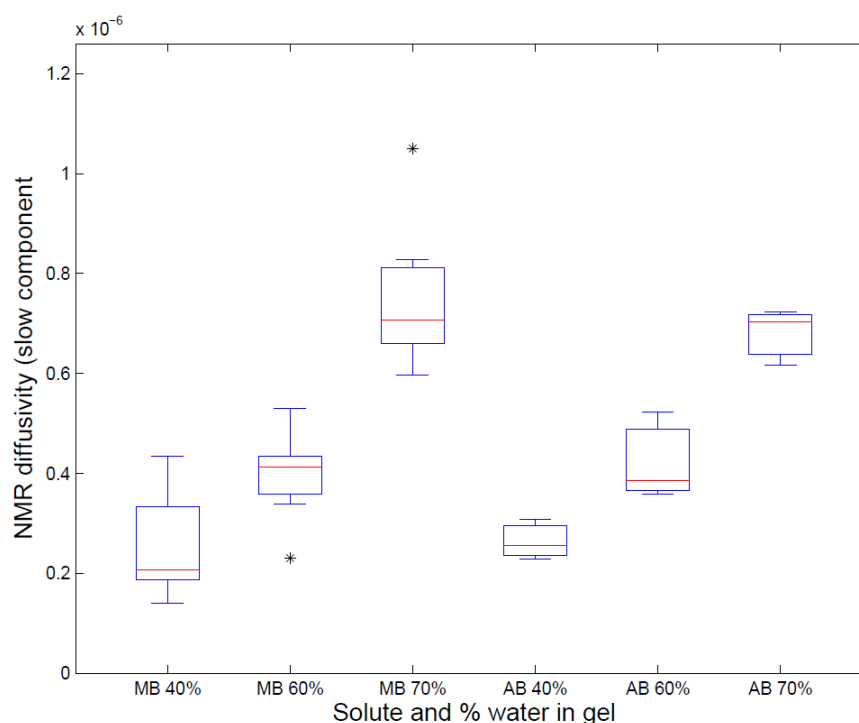
Figure 4.11. Diffusion coefficients for methylene blue and acid blue 22 measured using NMR based on initial the water/PEG-DA ratio

From Figure 4.11, it is evident that the diffusion coefficients of acid blue 22 and methylene blue increase with the initial amount of water present in the hydrogel solution.

This result is the caused by mesh size of the hydrogel. Table 4.2 and Table 4.4 show that as the initial amount of water in the hydrogel solution increases, the mesh size increases. This result is due to a decrease in the density of diacrylate groups in solution with an increase in water. The greater the density of diacrylate groups, the smaller the mesh size of the hydrogel.

4.2. Optical Microscopy Analysis

The optical microscopy analysis was conducted for methylene blue, acid blue 22, rhodamine 6G, and brilliant black. The optical microscopy method was only successful for methylene blue. Analysis of naproxen with the optical method was not attempted because the naproxen is colorless in the hydrogel. Since naproxen could not be seen within the hydrogel, images of the diffusion from the device could not be captured and analyzed. For the optical microscopy analysis to be effective when utilized, the dye molecule must be optically active, capable of diffusing through the mesh, and not limited by mass transfer at the channel.

4.2.1. Acid Blue 22 Optical Analysis

Optical analysis of acid blue 22 was not able to be conducted because the elution of the dye was limited by mass transfer from the channel. Figure 4.12 displays the elution of acid blue throughout the 12 hour trial duration of device A7.
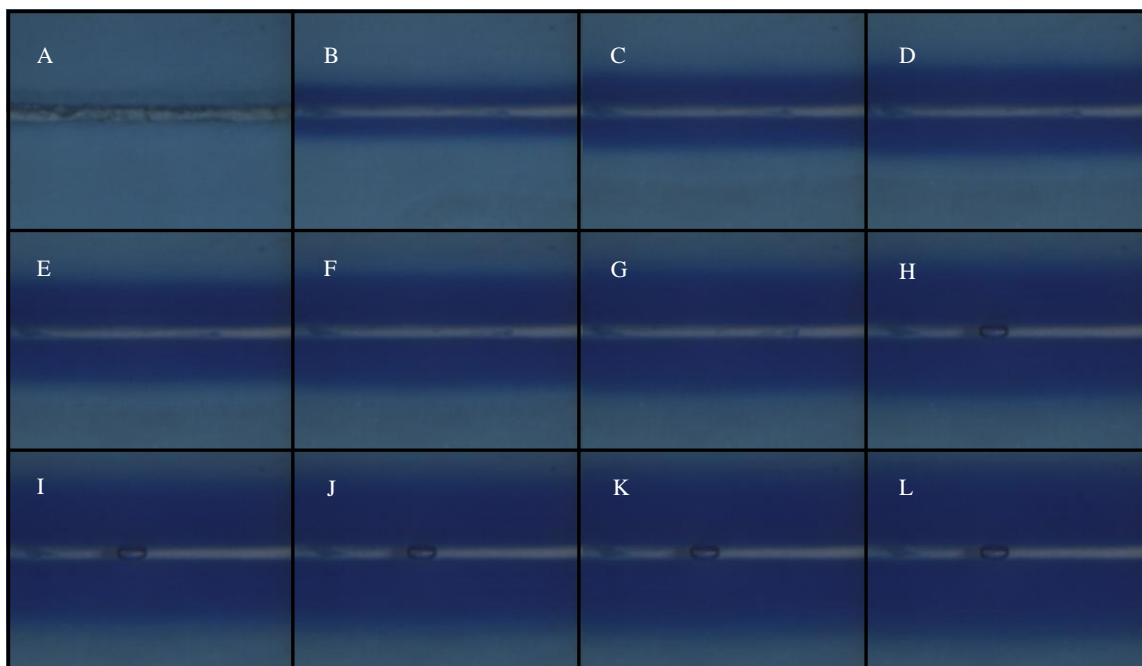
Figure 4.12. Elution of acid blue 22 in device A7 at various times. A.) Gel prior to water being pumped through the device. B.) Gel containing acid blue 22 after 1 h, C.) 2 h, D.) 3 h, E.) 4 h, F.) 5 h, G.) 6 h, H.) 7 h, I.) 8 h, J.) 9 h, K.) 10 h, and L.) 11 h.

The hydrogel started with acid blue evenly distributed throughout. As time progressed, instead of the lowest intensity occurring at the channel edge, and the highest occurring in the hydrogel edge, as would be expected for a diffusion limited system, the highest intensity was at the channel edge with dye moving from the hydrogel edge towards the channel. Figure 4.13 displays the change in apparent intensity of dye throughout the experiment using device A7, which had an initial water/PEG-DA ratio of 40/60 and a acid blue concentration of 0.28 mg dye/g soln. It was evident that dye was able to move through the gel but was not able to exit into the channel as easily. The remainder of the intensity profiles for acid blue 22, which display similar trends to device A7, are displayed in Appendix H.
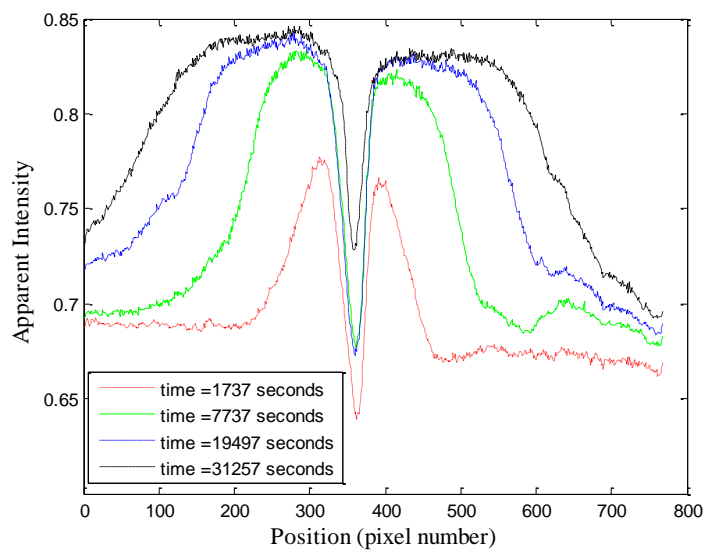
Figure 4.13. Intensity profiles for elution of acid blue 22 from loaded PEG hydrogels

The evidence for the movement of the dye through the hydrogel mesh to the channel edge is much more pronounced in gels with lower concentrations of acid blue dye than in gels with higher concentrations. As shown in Figure 4.14, images from the 60/40 device A21 with a concentration of 0.64 mg dye/g soln does not initially appear to have the same trend of dye movement. The dye level appears to remain relatively constant throughout the duration of the trial.
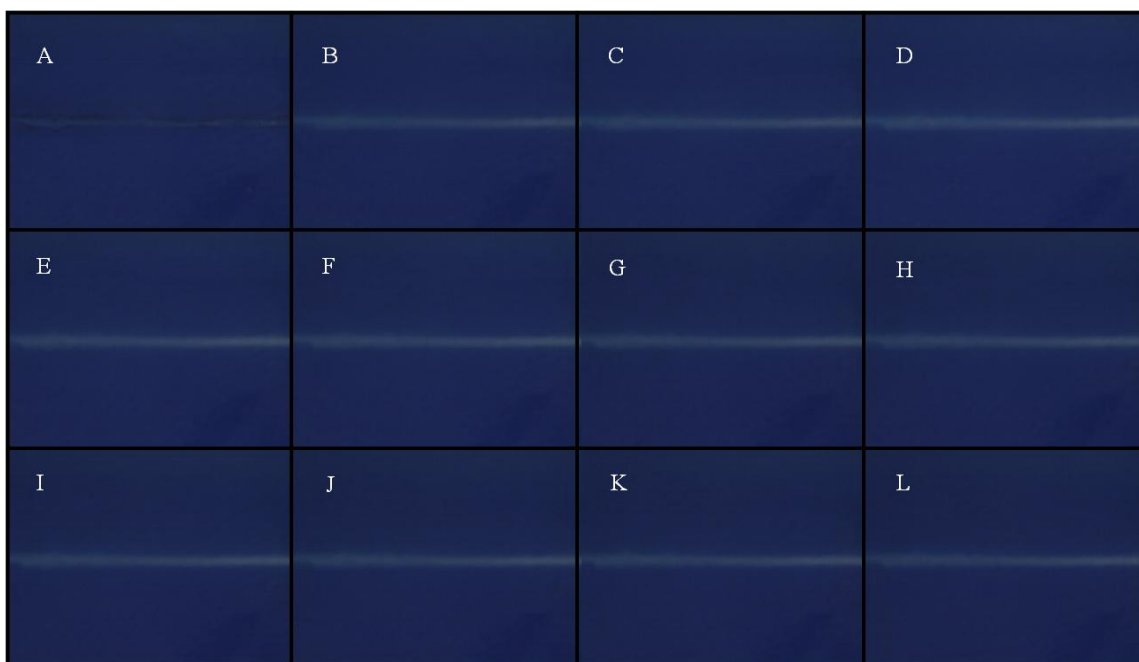
Figure 4.14. Elution of acid blue 22 in device A21 at various times. A.) Gel prior to water being pumped through the device. B.) Gel containing acid blue 22 after 1 h, C.) 2 h, D.) 3 h, E.) 4 h, F.) 5 h, G.) 6 h, H.) 7 h, I.) 8 h, J.) 9 h, K.) 10 h, and L.) 11 h.

Although the images do not appear to have a change in the intensity of dye in the hydrogel, the intensity of the dye in the hydrogel had a slight increase as time increased. Figure 4.15 illustrates the intensity profiles for the movement of acid blue 22 in device A21. The movement of dye in this device is not as drastic as was seen in the 40/60 device with a lower concentration. This could be due to limitations of the digital microscope such that it is difficult to discern between intensities once the concentration reached a specific intensity.
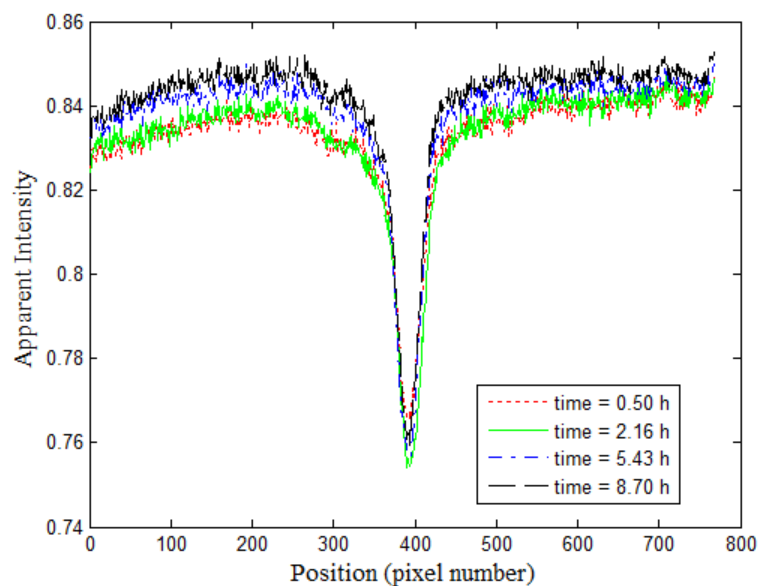
Figure 4.15. Intensity profiles for elution of acid blue 22 from loaded PEG hydrogels

Due to the non-Fickian nature of the diffusion profiles seen, the optical diffusion analysis was not applicable to the acid blue 22 system. The release of acid blue from the gel could be a result of the curing conditions and the size of the acid blue molecules, which have a molecular weight of 737.7 g/mol. By curing the hydrogel with acid blue loaded in the gel, large enough spaces were available for the molecules to move through the mesh towards the channel. The dye moves throughout the whole experiment and builds at the channel, so the driving force created by the water being pumped still exists. The limitation for release occurs at the channel, so it is likely that the release of acid blue 22 is mass transfer limited, which prevents the elution into the water stream.

4.2.2. Brilliant Black Optical Analysis

The optical diffusion analysis of brilliant black was unable to be conducted using PEG-DA with a M_n of 575 g/mol. Brilliant black has a molecular weight of 867.69 g/mol, which is much larger than acid blue 22 with a molecular weight of 737.74 g/mol. Although acid blue 22 was able to move through the hydrogel mesh toward the channel, release into the channel was limited. Being significantly larger than acid blue 22, brilliant black diffusion throughout the gel was not observed in the optical analysis nor was the brilliant black eluted. Images of brilliant black loaded into a 70/30 hydrogel with a concentration of 0.11 mg dye/g soln is shown in Figure 4.16.
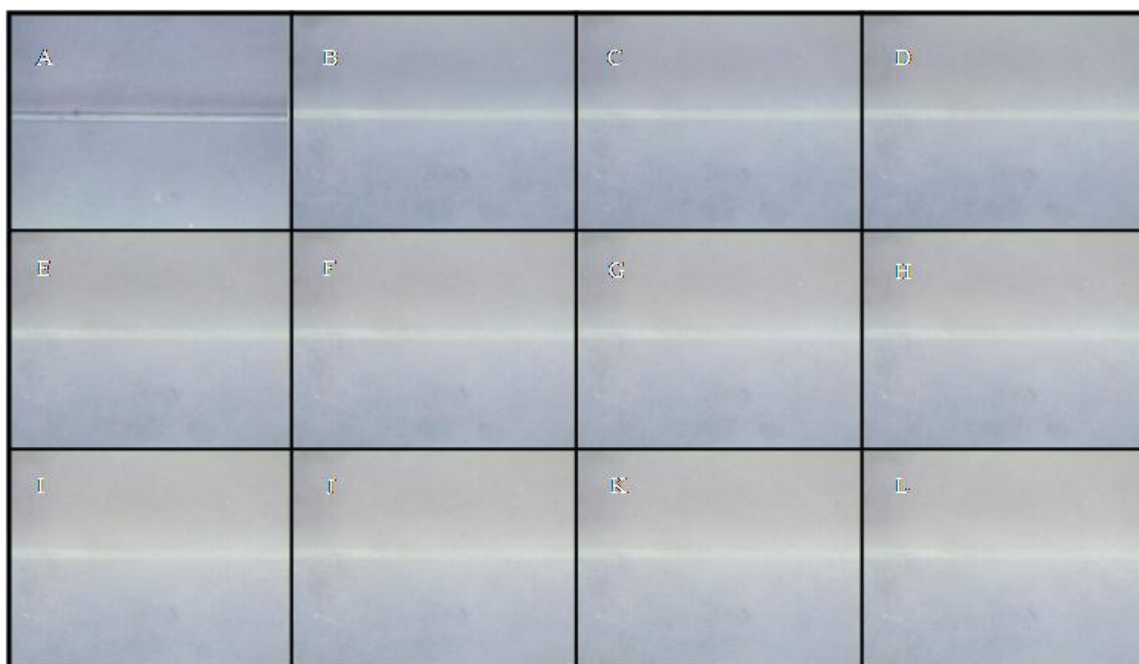
Figure 4.16. Lack of elution of brilliant black in Device BB1 at various times. A.) Gel prior to water being pumped through the device. B.) Gel containing brilliant black after 1 h, C.) 2 h, D.) 3 h, E.) 4 h, F.) 5 h, G.) 6 h, H.) 7 h, I.) 8 h, J.) 9 h, K.) 10 h, and L.) 11 h.

From the images, it appears as though there might be a slight decrease in intensity. This was not caused by the diffusion of brilliant black molecules. As the trial was conducted, the digital camera auto-exposed and prevented a constant light exposure. This result is supported by the lack of dye release in the effluent collected in cuvettes. The intensity profiles that resulted for brilliant black experiment are shown in Figure 4.17
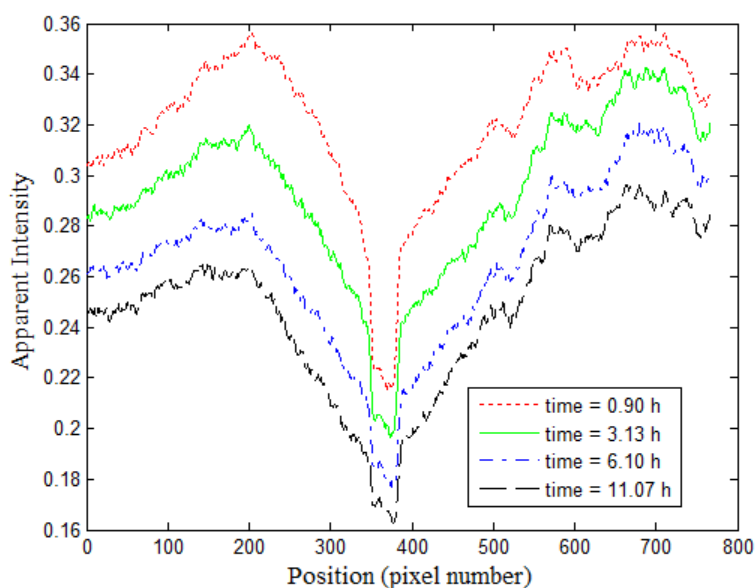
Figure 4.17. Intensity profiles for elution of brilliant black from loaded PEG hydrogels

4.2.3. Rhodamine 6G Optical Analysis

The optical diffusion analysis of rhodamine 6G was unable to be conducted using PEG-DA and water. It was determined that rhodamine 6G had a special affinity for PEG. The lack of diffusion of rhodamine 6G within the hydrogel was not dependent on size, as was the case with brilliant black. Rhodamine 6G has a molecular weight of 479.01 g/mol, which is much smaller than the molecular weight of acid blue 22. Images of rhodamine

6G loaded in a hydrogel with an initial water/PEG-DA ratio of 40/60 and dye concentration of 0.05 mg dye/g solution is shown in Figure 4.18.
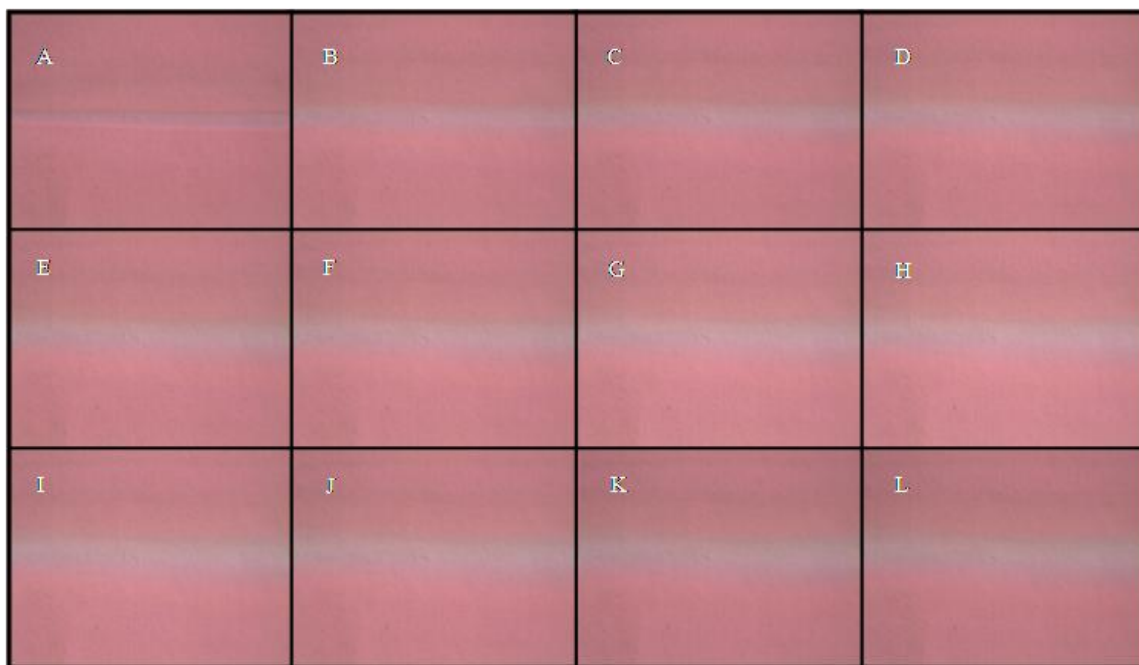
Figure 4.18. Lack of elution of rhodamine 6G in Device R3 at various times. A.) Gel prior to water being pumped through the device. B.) Gel containing rhodamine 6G after 1 h, C.) 2 h, D.) 3 h, E.) 4 h, F.) 5 h, G.) 6 h, H.) 7 h, I.) 8 h, J.) 9 h, K.) 10 h, and L.) 11 h.

From the images, it is apparent that rhodamine 6G did not diffuse from the hydrogel. The apparent intensity images, shown in Figure 4.19, support this conclusion, as it is evident that the apparent intensity profiles did not have a significant change as the trial progressed.
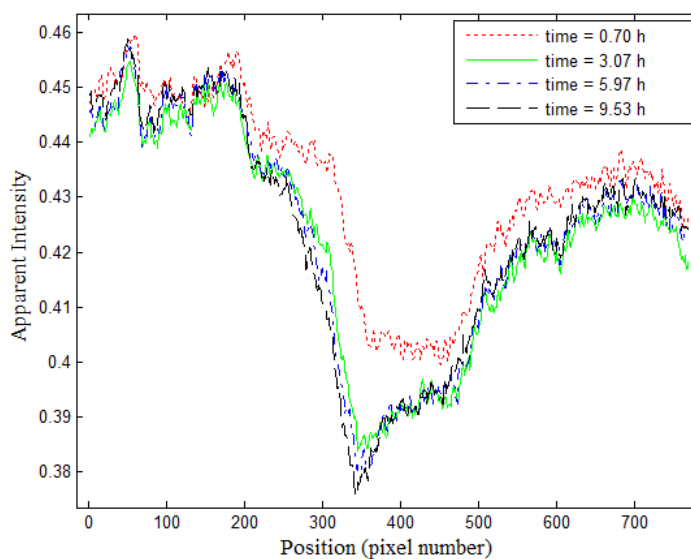
Figure 4.19. Intensity profiles for elution of rhodamine 6G from loaded PEG hydrogels

From these results, it was determined that rhodamine 6G has a special affinity for PEG. This was also shown in subsequent uptake studies, where PEG hydrogels were soaked in rhodamine 6G water solutions. The rhodamine 6G molecules had a much greater preference to interact with the PEG hydrogel than stay in the water. Since the molecular size is small enough to diffuse through the hydrogel matrix, the molecule must have a specific interaction with the PEG to inhibit the diffusion from a preloaded hydrogel matrix.

4.2.4. Methylene Blue Optical Analysis

The optical microscopy analysis was effective for methylene blue because the dye molecule was optically active, capable of diffusing through the mesh, and not limited by

mass transfer at the channel. The methylene blue diffusion analysis includes elution from a loaded PEG hydrogel and the uptake into a neat PEG hydrogel.

4.2.4.1. Methylene Blue Elution

Images of the methylene blue diffusion from the device were captured as water was pumped through the channel. Figure 4.20 displays the elution of methylene blue throughout the 12 hour trial duration of device B42, which was a 40/60 device with an initial concentration of 0.21 mg methylene blue/g soln. At time zero, the hydrogel was fully loaded with dye before water was pumped into the device. After 1 h, the concentration of dye at the channel interface decreased, but as predicted by the short time model, the dye concentration near the far edge of the device appears to have remained constant. The other elution images, which display the same trend as device B42, are displayed in Appendix D.
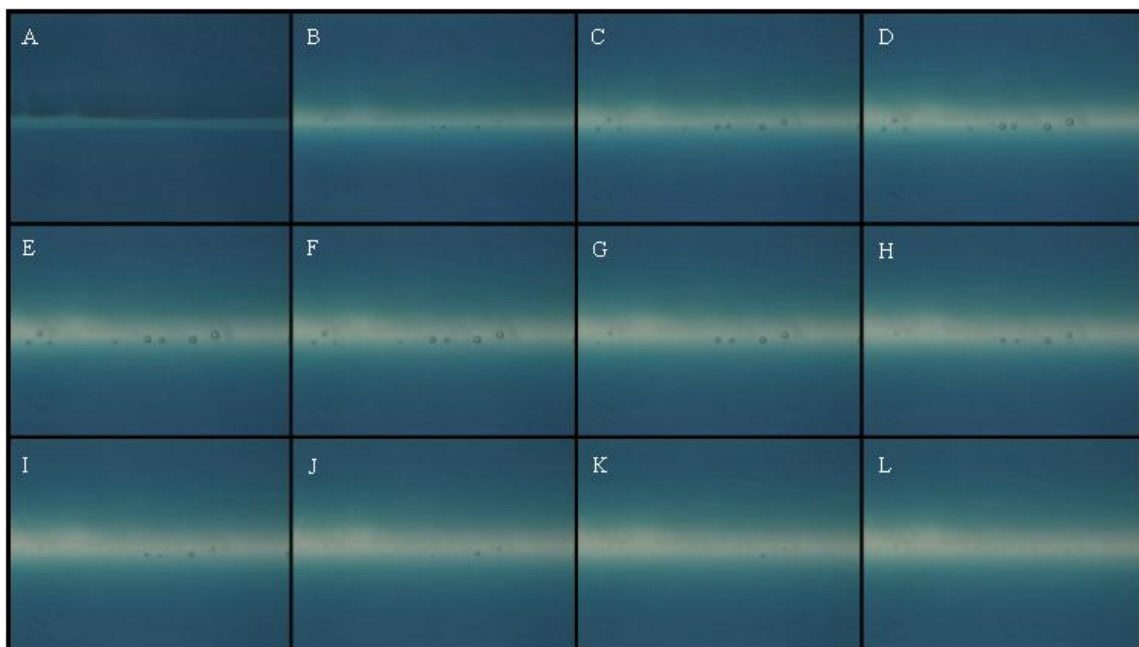
Figure 4.20. Elution of methylene blue from a PEG hydrogel cured within a microfluidic device at various times. Channel size: 900 μm. A.) Gel prior to water being pumped through the device. B.) Release of methylene blue after 1 h, C.) 2 h, D.) 3 h, E.) 4 h, F.) 5 h, G.) 6 h, H.) 7 h, I.) 8 h, J.) 9, K.) 10 h, and L.) 11 h.

Images were imported into MATLAB and analyzed using custom MATLAB scripts. The apparent intensity, without being normalized from 0 to 1, corresponding to concentration at various times for the duration of one sample run are shown in Figure 4.21.
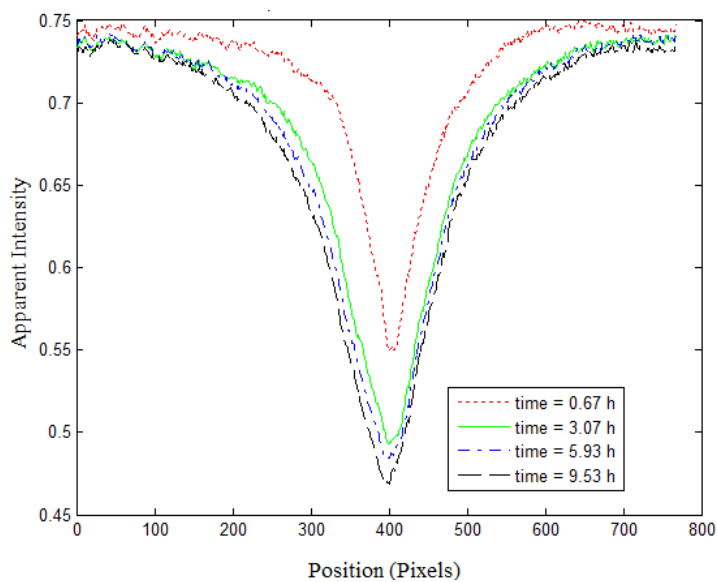
Figure 4.21. Intensity profiles for elution of methylene blue from loaded PEG hydrogels

Figure 4.22 displays the normalized intensity of dye throughout the experiment using device B42. In this case, the hydrogel slabs had the highest intensity, whereas the dI-H_2O channel had the lowest intensity. As time increased, the intensity of the hydrogel slabs near the channel decreased, but the furthest point from the channel still remained relatively constant. The intensity profiles for additional devices, which display the same trend as device B42, are displayed in Appendix H.
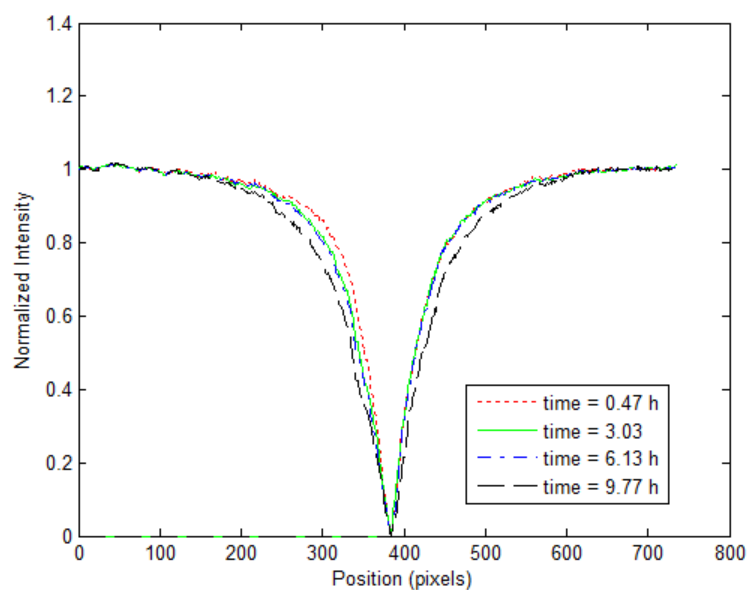
Figure 4.22. Normalized intensity profiles for the elution of methylene blue from loaded PEG hydrogels.

Each position and time from every image was collapsed to a single point using the procedure given in Appendix E that details how MATLAB m-files were used to fit the concentration distribution to a error function solution, Equation (2,18) to calculate a diffusion coefficient. The error function fit to the collapsed data points for device B42 is shown in Figure 4.23. Diffusion coefficients ranged from 10^{-7} to 10^{-8} cm^2/s with R^2 values of 0.908 to 0.997 for all samples. The fit does reasonably well except for at the curved ends of the data. This suggests that the diffusion coefficient may be dependent on concentration. The other error function fits are displayed in Appendix H.
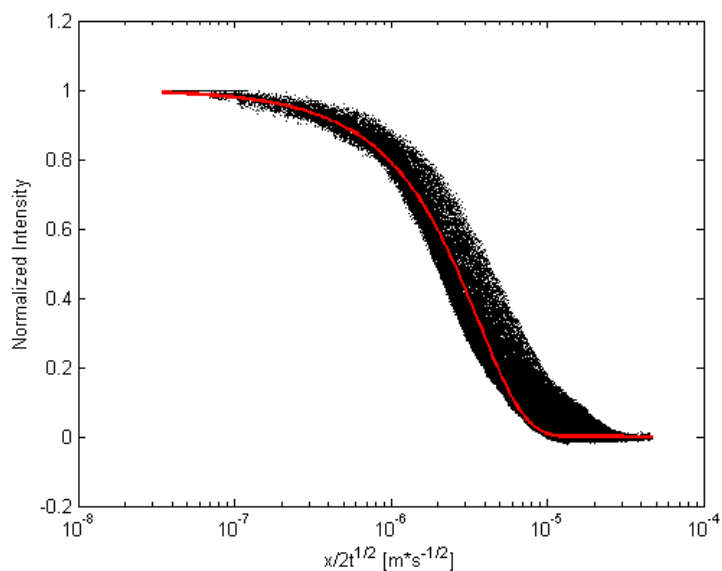
Figure 4.23. Errorfunction diffusion model fit to methylene blue elution data D = 2.83x10^{-7} cm^2/s, R^2 = 0.9986.

Table 4.5 lists average diffusion coefficients for all permutations of the initial water/PEG-DA ratios (mg/g) and concentration levels in a summary table for all experimental techniques. No apparent trend exists based on initial water/PEG-DA ratio, which indicates that during the photopolymerization process, the gels reach a similar state of crosslinking.

Table 4.5. Summary of experimentally calculated diffusion coefficients using optical method, UV/Vis spectroscopy, and NMR analysis for methylene blue dye.

DI-H_2O/PEG-DA Ratio (g/g)	Initial Dye Concentration (mg/mL)	Optical Diffusion Coefficient ($x\ 10^{-7}\ cm^2/s$)	UV/Vis Diffusion Coefficient ($x\ 10^{-7}\ cm^2/s$)	NMR Slow Component Diffusion Coefficient ($x\ 10^{-7}\ cm^2/s$)
70/30	0.124	2.71 ± 1.99	1.72 ± 1.63	6.77 ± 0.427
	0.261	0.862 ± 1.56	3.30 ± 3.77	9.38 ± 1.57
	0.37	3.46 ± 0.91	14.2 ± 7.99	6.86 ± 0.848
60/40	0.10	2.04 ± 0.92	8.74 ± 1.70	3.16 ± 0.769
	0.213	2.71 ± 3.29	7.92 ± 3.85	5.38 ± 1.62
	0.33	2.18 ± 2.27	8.51 ± 2.90	4.20 ± 0.2625
40/60	0.15	1.82 ± 1.35	2.57 ± 2.16	4.14 ± 3.86
	0.21	2.08 ± 0.86	4.64 ± 2.96	1.89 ± 0.339
	0.29	1.56 ± 0.96	10.7 ± 8.77	2.96 ± 1.27

4.2.4.2. Methylene Blue Uptake

Methylene blue dissolved in dI-H_2O was pumped through neat PEG hydrogel. Images of the dye progression into the gel were captured similarly to the elution images. Figure 4.24 shows images captured over the 4 h period of diffusion.
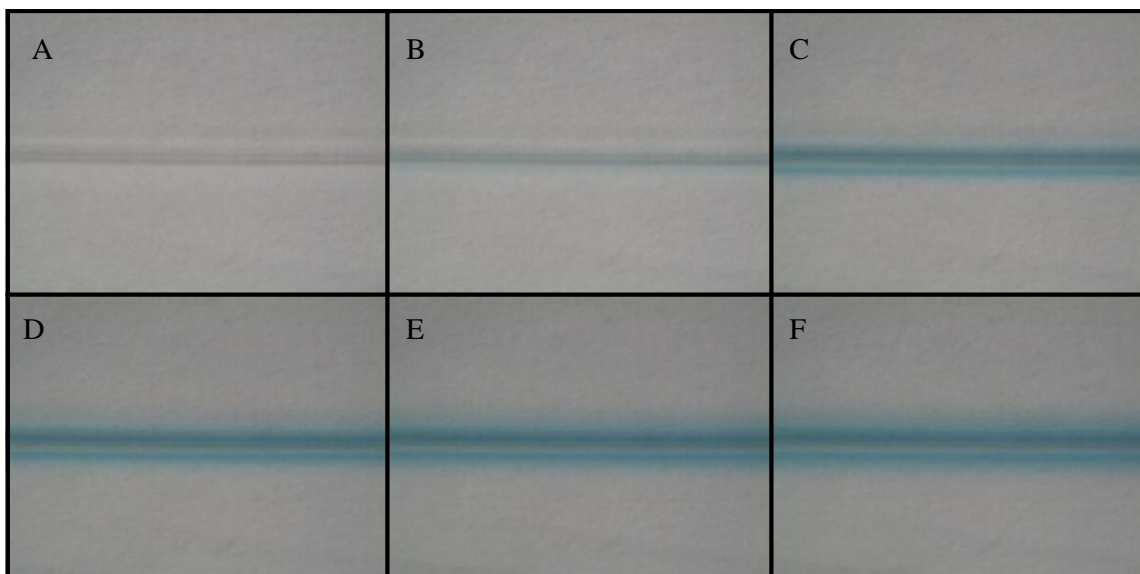
Figure 4.24. Methylene blue diffusion into PEG at various times. A.) Photocured neat PEG hydrogel before methylene blue was pumped through the channel. B.) Initial loading of methylene blue into channel. C.) Diffusion of methylene blue into the gel at 1 h. D.) 2 h. E.) 3 h. F.) 4 h.

Images were imported into MATLAB and analyzed using custom MATLAB scripts similar to those described in the elution experiments. The apparent intensity for concentration at various times for the duration of one sample device are shown in Figure 4.25. The highest intensity occurs at the channel edge, and the lowest occurs in the hydrogel edge with no dye. As time increased, methylene blue progressed further into the hydrogel slabs.
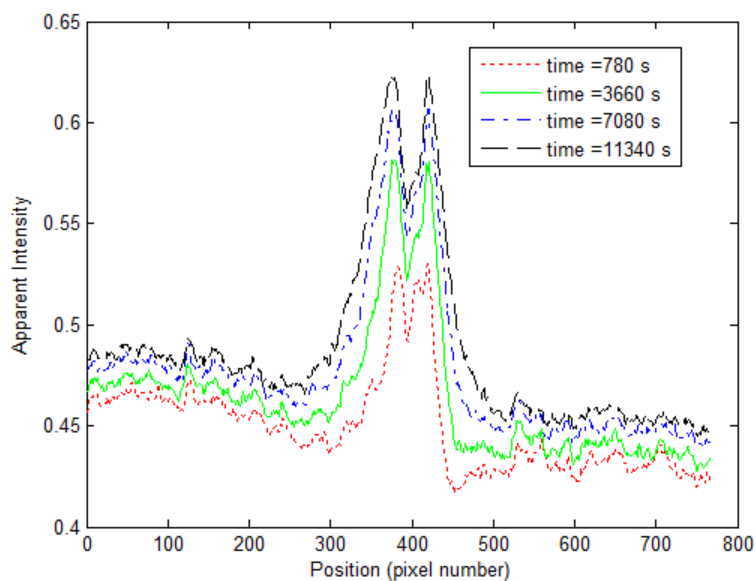
Figure 4.25. Intensity profiles of methylene blue uptake into hydrogel matrix

Similar to the elution experiments, each image at a particular time was collapsed to a single point, and the concentration distributions were fit to a error function solution to extract diffusion coefficients. Diffusion coefficients calculated from the regression were on the order 10^{-7} to 10^{-8} cm^2/s for every hydrogel analyzed. Average diffusion coefficients for 70/30, 60/40, and 40/60 initial water/PEG-DA ratio hydrogels are presented in Table 4.6. No apparent trend exists based on initial water/PEG-DA ratio, which indicates that during the photopolymerization process, all gels reach a similar state of crosslinking.

Table 4.6. Experimental diffusion coefficients for methylene blue uptake into PEG hydrogel at various initial water/PEG-DA ratios.

dI-H$_2$O/PEG-DA Ratio (g/g)	Optical Diffusion Coefficient (x 10^{-7} cm^2/s)
70/30	1.71 ± 0.15
60/40	1.81 ± 0.80
40/60	1.29 ± 0.68

Figure 4.26 displays the model fits, which matches the data very well. The R^2 values for all samples ranged from 0.920 to 0.999.
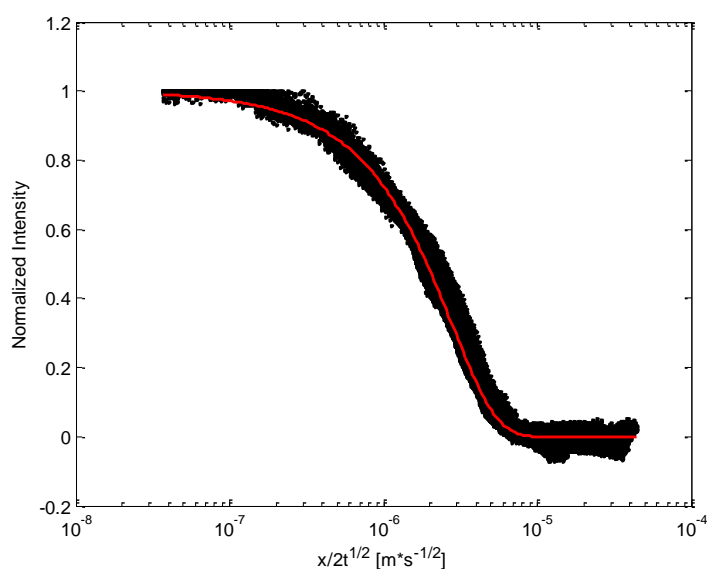
Figure 4.26. Error function model fit to data for methylene blue uptake. D = 1.61x10^{-7} cm^2/s, R^2 = 0.9992.

The diffusion coefficients of the uptake and elution gels are of the same order of magnitude. This indicates that both gel types have the same overall extent of crosslinking. Because the elution gels were polymerized with molecules present in the solution, the two gels might have differing local crosslinking, where the dye-loaded gels

have high crosslinking around the dye molecules with no crosslinking at the sites of dye molecules and the neat gels have an equal amount of crosslinking throughout. The error function model fits much better for the uptake data than the elution data. Whereas the elution data did not fit the error function at the curved ends of the model, the uptake data fits very well. This indicates that the uptake devices did not have a concentration dependent diffusion coefficient. However, much lower concentrations of dye were used in the uptake experiments than in the elution experiments. This suggests that the diffusion coefficient is constant for low concentrations of dye, but becomes variable as concentration increases.

4.3. Characterization of Device Effluent Analysis

Device effluent analysis was conducted for methylene blue, acid blue 22, rhodamine 6G, brilliant black, and naproxen. The effluent characterization method was only successful for molecules that were able to be eluted from the hydrogel. The effluent analysis of methylene blue and acid blue 22 was able to conducted using UV/Vis spectroscopy. The effluent analysis of naproxen was able to be conducted using HPLC. Brilliant black and rhodamine 6G were not able to analyzed using the effluent analysis. As discussed previously in the optical microscopy analysis discussion, brilliant black was too large to be eluted from the hydrogel and rhodamine 6G had a special affinity with PEG that prevented it from being eluted. The only quantity of brilliant black and rhodamine 6G collected in a given effluent experiment was in the first cuvette. The

release of molecules in the first cuvette is attributed to the burst effect, which swept loose PEG and dye from the channel as water was first pumped through the channel, and rehydration effects of gels that had been stored for a few days.

4.3.1. Methylene Blue Effluent Analysis

The concentration of the solution collected in each cuvette was determined by measuring the absorbance of each cuvette at 660 nm using UV/Vis spectroscopy. Figure 4.27 shows the effluent concentration for device B42 with respect to time. The effluent concentrations for the other methylene blue devices are displayed in Appendix H.
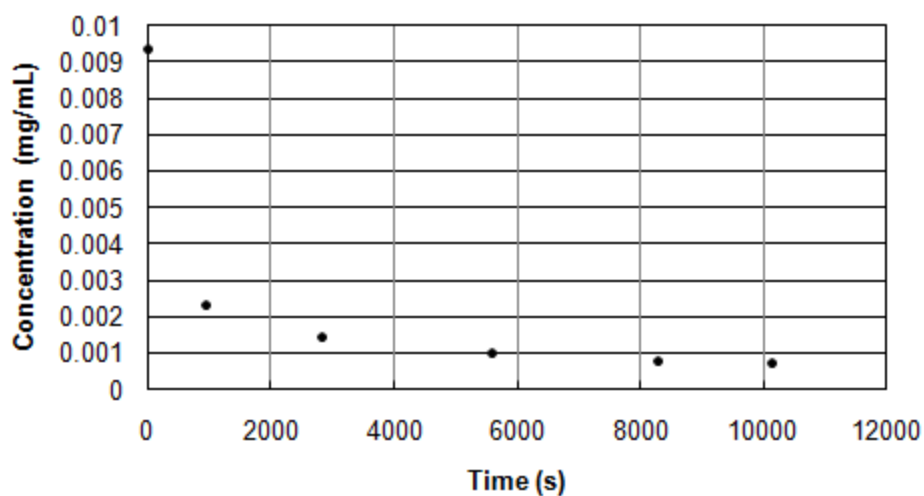

Figure 4.27. Short time elution concentration with time of methylene blue

Using the concentration of the cuvette sample and the initial concentration and volume of the hydrogel, the fraction of dye eluted from the device was calculated using Equation (3,1). As described in Equation (3,2), the mass of dye in the first cuvette was

removed from both the initial mass in the hydrogel and the mass released at every point to account for rehydration and burst effects of the gel. The linear fit correlated to the data using the short time diffusion model is shown in Figure 4.28. The slope of the data was used to calculate a diffusion coefficient with Equation (2,13).
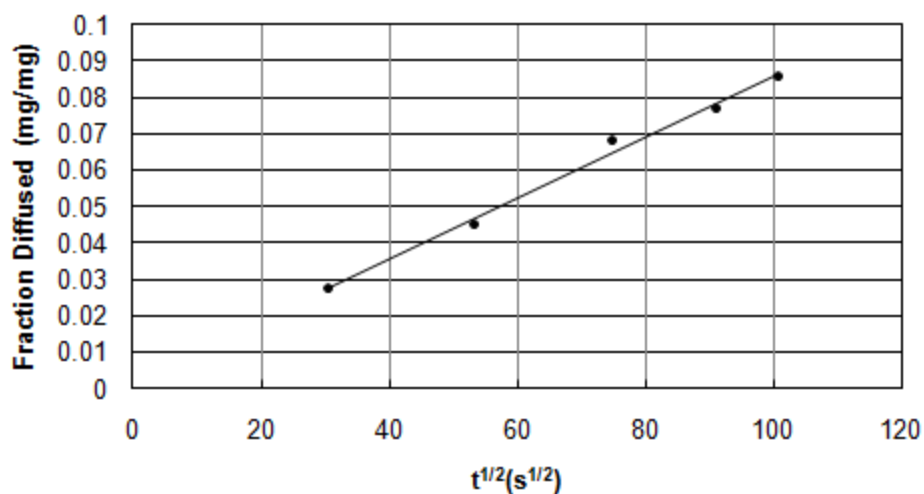
Figure 4.28. Short time diffusion model with linear fit to elution data of methylene blue

Diffusion coefficients calculated using the UV/Vis spectroscopy method ranged from 10^{-6} to 10^{-7} cm^2/s. The average diffusion coefficients for all initial water/PEG-DA ratios and dye concentrations are listed in Table 4.5.

To determine that a mass transfer limitation into the channel did not exist for methylene blue, Equations (2,15) and (2,16) were used, where k was determined to be 2.967×10^{-5} cm/s. The Biot number was calculated to be 50.4. Since the Biot number was greater than one, there was a negligible mass transfer limitation at the channel wall. Supporting calculations are shown in Appendix B.

4.3.2. Acid Blue 22 Effluent Analysis

The concentration of the solution collected in each cuvette was determined by measuring the absorbance of each cuvette at 580 nm with a UV/Vis spectrophotometer. Figure 4.29 shows the effluent concentration for device A21 with respect to time. The effluent concentrations for the other acid blue devices are displayed in Appendix H. Acid blue release from the hydrogel was not as "smooth" as it was for the methylene blue release. The concentration often fluctuated between cuvettes from high to low to high concentrations. This further demonstrates that release from the device was affected by a mass transfer limitation at the channel.
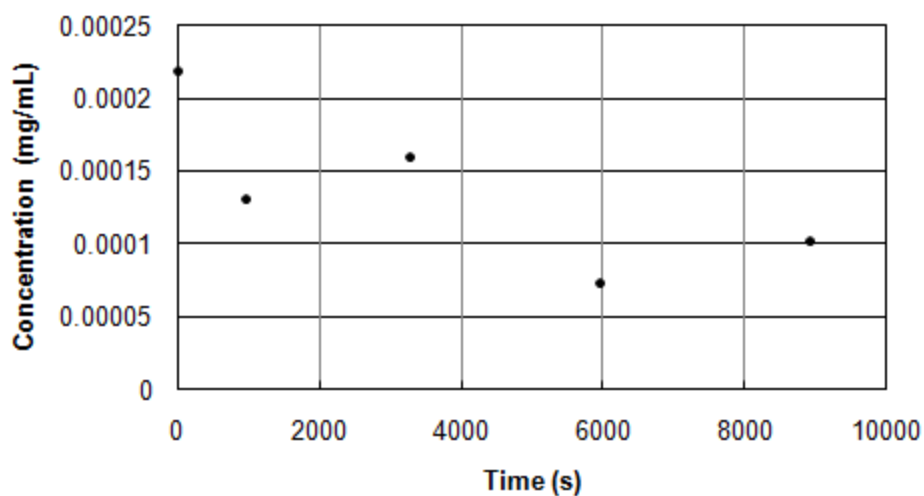

Figure 4.29. Sample short time elution concentration with time for acid blue 22 device A21

Using the concentration of the cuvette sample and the initial concentration and volume of the hydrogel, the fraction of dye eluted from the device was calculated using

Equation (3,1). A linear fit was correlated to the data using the short time diffusion model, using Equation (2,14) as shown in Figure 4.30.
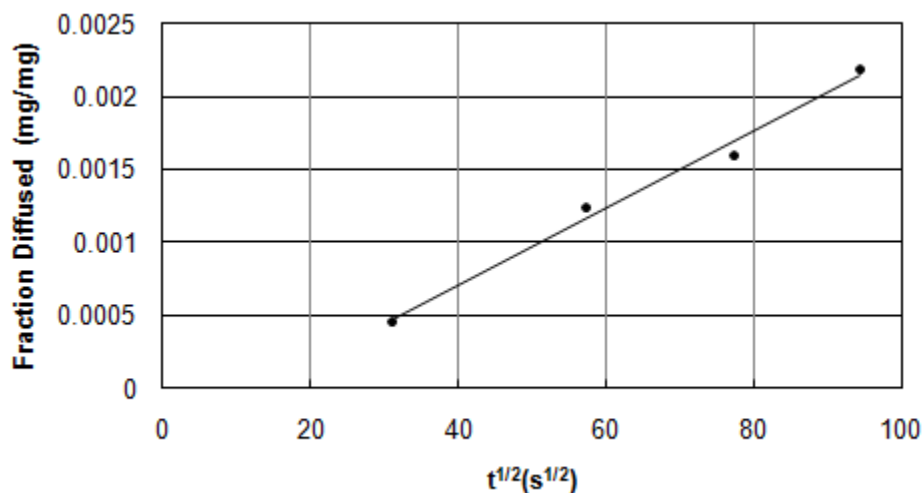
Figure 4.30. Short time diffusion model with linear fit to elution data for acid blue 22 device A21

Diffusion coefficients calculated using the UV/Vis spectroscopy method ranged from 10^{-9} cm^2/s to 10^{-10} cm^2/s. The diffusion coefficients calculated in this manner differed from the diffusion coefficients calculated using NMR. This analysis method calculated the diffusion coefficients using the concentration of the effluent captured. The short time release model assumed that the mass transfer limitation from the channel was negligible. The average diffusion coefficients for all initial water/PEG-DA ratios and dye concentrations are listed in Table 4.7. However, as with the methylene blue system, the diffusion coefficients determined using the effluent were very similar regardless of dye concentration and initial water/PEG-DA ratios.

Table 4.7. Summary of experimentally calculated diffusion coefficients for acid blue 22 using UV/Vis spectroscopy and NMR analysis.

Initial DI-H_2O/PEG-DA Ratio (g/g)	Initial Dye Concentration (mg/g soln)	UV/Vis Diffusion Coefficient (x 10^{-9} cm^2/s)	NMR Diffusion Coefficient (x 10^{-7} cm^2/s)
70/30	0. 25	1.44 ± 1.52	7.03
	0. 49	4.61 ± 1.66	7.22
	0. 74	0.86 ± 1.25	6.17
60/40	0. 21	1.11 ± 0.94	5.23
	0. 42	0.46 ± 0.40	3.86
	0. 64	0.75 ± 0.26	2.56
40/60	0. 28	3.73 ± 2.01	2.56
	0. 41	1.57 ± 2.17	3.08
	0. 56	3.57 ± 2.90	2.28

4.3.3 Naproxen Effluent Analysis

Measurement of the diffusion coefficient of naproxen by optical methods would not work. Therefore the effluent approach was attempted however the UV/Vis measurement method alone could not be conducted because the naproxen peak overlapped with the peak of unreacted PEG-DA that was eluted from the hydrogel. Because the peaks overlapped in UV/Vis, HPLC was used to separate the naproxen and PEG-DA peaks. Standard solutions of naproxen in pH 7.4 water, PEG-DA and naproxen in pH 7.4 water, and PEG-DA in pH 7.4 water were tested in the UV/Vis with glass and quartz cuvettes. Use of the quartz cuvettes revealed that uncured PEG-DA was also being eluted from the hydrogels and interfering with the naproxen peak, which is shown in Figure 4.31.
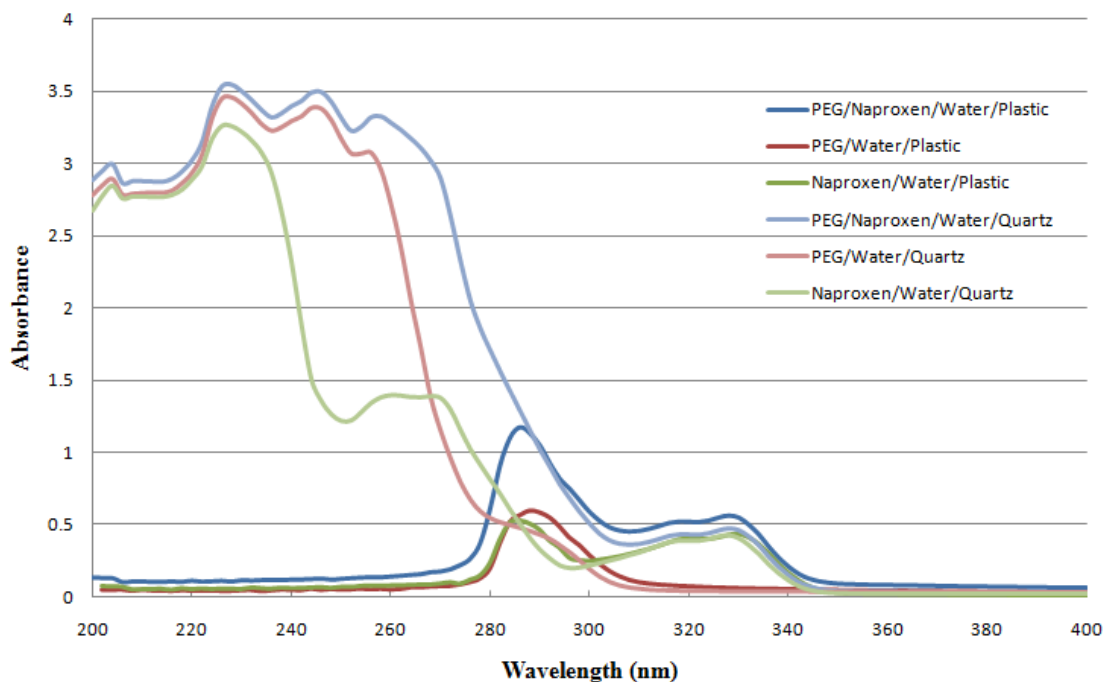
Figure 4.31. Standard solutions of PEG-DA and naproxen in pH 7.4 aqueous solution measured using UV/Vis in quartz and plastic cuvettes.

The cuvettes collected in the experiments were run through the HPLC column with a 1:1 water to acetonitrile solution at 1 mL/min. Based on the standard solutions run in the HPLC column, naproxen had a retention time of approximately 10.16 min. Tested cuvette samples from 60/40 and 40/60 initial water/PEG-DA solutions revealed two peaks at retention times that varied from 3.03 min to 3.04 min and 3.57 min to 3.63 min as shown in Figure 4.32. Neither of these peaks were found in the standard naproxen solution, as the standard solution resulted in an HPLC with a peak at 10.16 min.
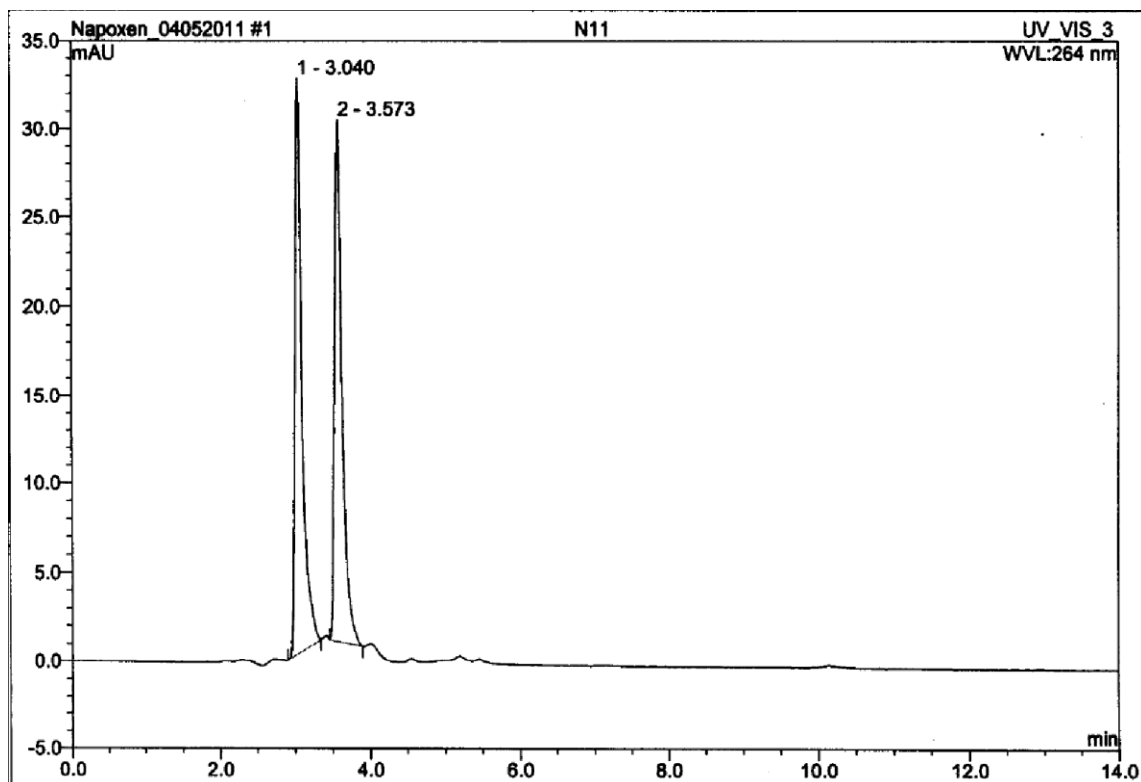
Figure 4.32. HPLC peaks measured for cuvette effluent sample of device N11

From this result, it was determined that naproxen was not being eluted or was photodegraded during UV photopolymerization of the hydrogel. Standard solutions of naproxen in pH 7.4 water were exposed to UV light for 25 min and run through the HPLC column. The UV exposed standards revealed small peaks around retention times of 3.04 min and 3.6 min, as shown in Figure 4.33. This result indicated that naproxen was being photodegraded by the UV photopolymerization method used to crosslink the hydrogels.
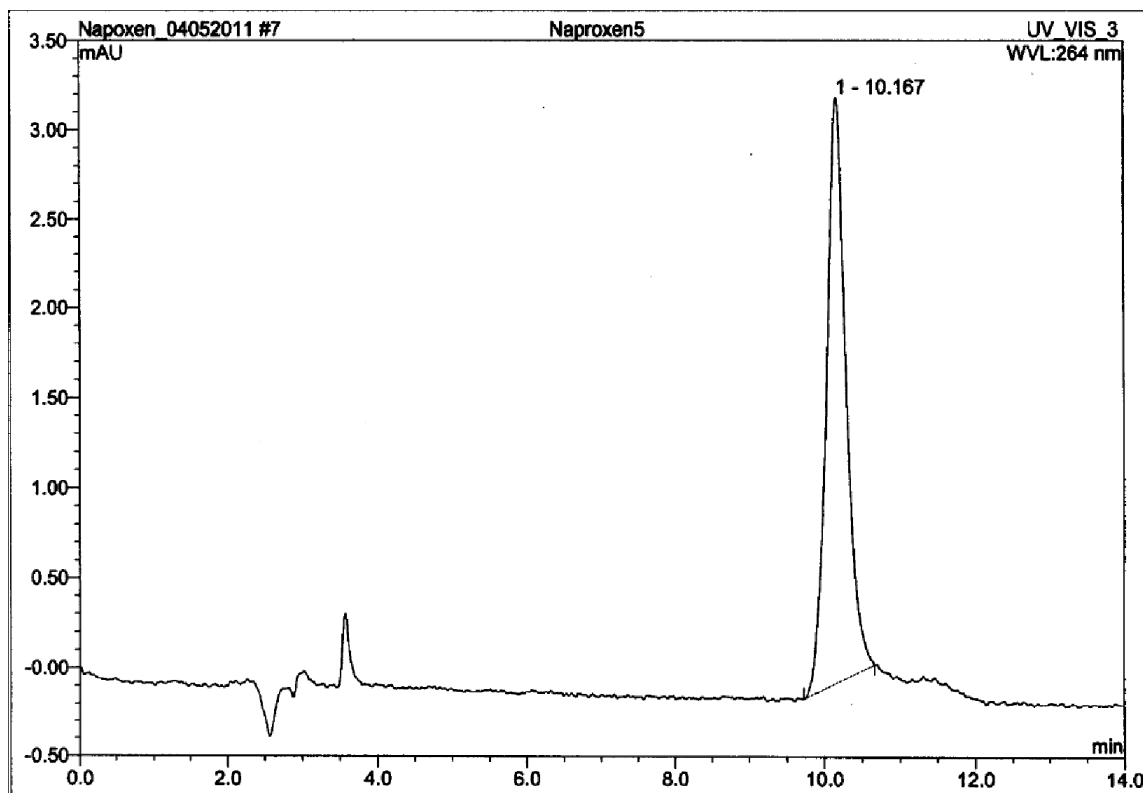
Figure 4.33. HPLC peaks measured for naproxen standard in pH 7.4 aqueous solution after 25 min of UV exposure

A standard solution of naproxen in pH 7.4 with Irgacure was also tested in the HPLC column to determine if the photoinitiator increased the effects of the UV photodegradation. From this test, it was determined that Irgacure increases the effects of photodegradation. As shown in Figure 4.34, the addition of Irgacure to the naproxen in water sample has no peak at 10.16 min and significantly increases the area under the peaks at 3.04 min and 3.6 min.
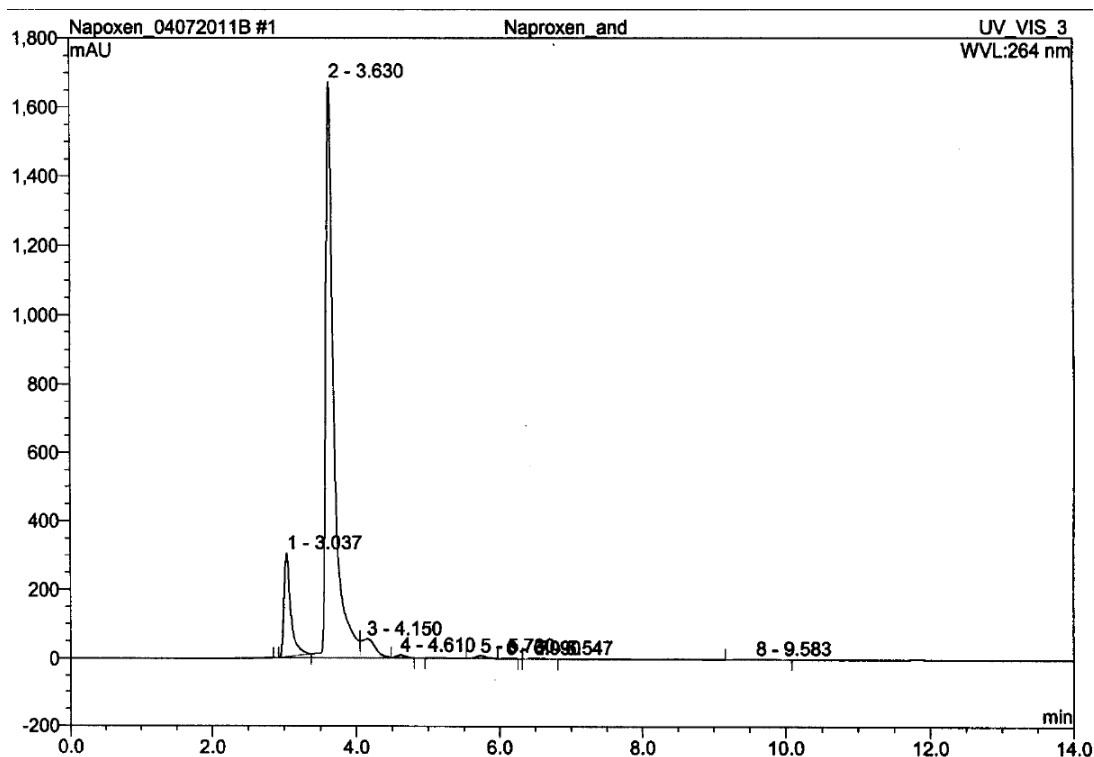
Figure 4.34. HPLC peaks measured for standard naproxen in pH 7.4 aqueous solution with the addition of Irgacure 2959 after 25 min of UV exposure.

However, it was apparent that the peak area of the naproxen degradation products for each experiment decreased with time. This indicates that the naproxen degradation products were being eluted in a similar manner to methylene blue, but a diffusion coefficient could not be calculated because the initial concentration of degradation products in the hydrogel was unknown.

4.4. Hydrogel Characterization

The polymer volume fraction, $v_{2,s}$, swelling percent, and mesh size of hydrogels were calculated using Equations (2,6), (2,7), and (2,3), respectively, to help evaluate gel

mesh properties. Methylene blue and acid blue 22 hydrogels were analyzed after running experimental trials with the microfluidic devices. The polymer volume fraction and swelling percent of methylene blue hydrogels used in the NMR analysis were calculated to confirm the hydrogels used in the NMR and effluent analyses were the same. Gels were lyophilized and subsequently swollen in water to determine the dry and swollen weights necessary to calculate the polymer volume fraction. Loss of mass from dye elution during re-swelling was assumed to be zero, due to the small initial amount of dye in each hydrogel slab combined with the loss from the elution of dye during each trial.

4.4.1. Methylene Blue Hydrogel Characterization

The polymer volume fractions for all devices were found to vary from 27.1 wt% to 35 wt%, as shown in Table 4.8. The polymer volume fractions for all NMR hydrogels were found to vary from 30.4 wt% to 36.3 wt%. The mesh size calculated for the PEG575DA used in this research ranged from 20 Å to 23 Å. Watkins and Anseth[1] used PEG700DA photopolymerized with 0.025 wt% Irgacure and determined the mesh size to be 30 Å.[1] The mesh sizes of the two molecular weights of PEG-DA are consistent because there is an increase in mesh size with an increase in the number of repeat units, which would be expected.

To ensure that a statistically significant difference did not exist between the microfluidic device hydrogel and NMR hydrogel, a two-tailed t-test ($\alpha = 0.05$) was used. Results of the t-test showed that the 70/30 device and 70/30 NMR gels were statistically the same (t = 1.963, t_{crit} = 2.776). The 60/40 device and NMR gels were statistically the

same (t = 1.834, t$_{crit}$ = 2.262) as were the 40/60 device and NMR gels (t = 1.761, t$_{crit}$ = 2.145).

Table 4.8. Swelling and polymer volume fraction in post-trial methylene blue loaded microfluidic device hydrogels and methylene blue loaded hydrogels created for NMR analysis.

Initial DI-H$_2$O/ PEG-DA Ratio (g/g)	Initial Dye Concentration (mg/g soln)	Polymer Volume (wt%)		Swelling (wt%)		Mesh Size (Å)	
		Device	NMR	Device	NMR	Device	NMR
70/30	0.124	29.1 ± 3.9	30.4	224 ± 46	206	22.4	22.1
	0.261	27.1 ± 2.6	34.2	244 ± 33	173	23.0	21.2
	0.37	32.1 ± 2.0	34.1	181 ± 16	173	21.7	21.3
60/40	0.1	29.6 ± 0.4	35.6	214 ± 5	163	22.3	21.0
	0.213	30.7 ± 1.0	33.1	203 ± 10	181	22.0	21.5
	0.33	35.0 ± 3.8	33.9	169 ± 29	175	21.1	21.3
40/60	0.15	32.8 ± 3.8	35.7	184 ± 34	162	21.5	20.9
	0.21	34.1 ± 2.1	36.3	174 ± 17	157	21.3	20.8
	0.29	35.0 ± 2.5	34.9	168 ± 20	167	21.1	21.1

The similarity of polymer volume fractions for each hydrogel indicates that the hydrogels all reached a similar state of crosslinking using the photopolymerization method. A two-tailed t-test (α = 0.05) was conducted between the polymer volume fractions to determine if the values were statistically different at varying initial water/PEG-DA ratios. Results of the t-test showed that the 70/30 gels were statistically the same as the 60/40 gels. The 60/40 gels were statistically the same as the 40/60 gels, but the 70/30 were different than the 40/60 gels. Although the compositions of the hydrogel solutions are dissimilar, the differences between the swelling ratios and mesh sizes are relatively small. This indicates that the curing conditions potentially lead to similar extent of crosslinking even though the 40/60 gels have double the amount of PEG-DA than 70/30 gels initially

have in solution. Although the NMR verified that an increase in the initial water in the hydrogel solution caused an increase in the diffusion coefficient, the diffusion coefficients were still on the same order of magnitude.

4.4.2. Acid Blue 22 Hydrogel Characterization

The polymer volume fractions for all devices were found to vary from 30.4 wt% to 36.6 wt%, as shown in Table 4.9. A two-tailed t-test ($\alpha = 0.05$) was conducted between the polymer volume fractions to determine if the values were statistically different at varying initial water/PEG-DA ratios. From the values given in Table 4.9, it appears that the polymer volume fraction increases with an increase in the amount of PEG-DA in the initial hydrogel solution. Results of the t-test showed that the 70/30 gels were statistically the same as the 60/40 gel ($t = 1.926$, $t_{crit} = 2.179$). The 60/40 were determined to be statistically different than the 40/60 gels ($t = 5.016$, $t_{crit} = 2.131$) as were the 70/30 gels ($t = 5.234$, $t_{crit} = 2.201$).

**Table 4.9. Swelling and polymer volume percent in post-trial acid blue 22 loaded microfluidic device hydrogels.**

Initial DI-H$_2$O/PEG-DA Ratio (g/g)	Initial Dye Concentration (mg/g soln)	Polymer Volume Fraction (wt%)	Swelling (wt%)	Mesh Size (Å)
70/30	0. 25	30.4 ± 5.1	224 ± 52	22.1
	0. 49	30.5 ± 4.4	222 ± 53	22.1
	0. 74	30.4 ± 0.8	218 ± 9	22.1
60/40	0. 21	33.2 ± 1.6	190 ± 14	21.5
	0. 42	32.3 ± 2.6	200 ± 26	21.7
	0. 64	33.2 ± 2.0	190 ± 18	21.4
40/60	0. 28	36.6 ± 2.1	162 ± 15	20.8
	0. 41	37.4 ± 1.6	156 ± 11	20.6
	0. 56	36.5 ± 0.1	163 ± 1	20.8

With a decrease in the initial water/PEG-DA ratio, the polymer volume fraction increases, the swelling decreases, the mesh size decreases, and the diffusion coefficient as measured by NMR decreases for methylene blue and acid blue 22. This suggests that diffusion is hindered by higher fractions of polymer in the hydrogel. With higher fractions of gel, the gel has more crosslinking, becomes more rigid, and cannot swell in water as much as hydrogels with lower fractions of hydrogel. Thus, diffusing molecules are more inhibited by the polymer chains and have a smaller mesh to diffuse through. Although the diffusion coefficients differ based on the initial water/PEG-DA ratio, the diffusion coefficients still remain on the same order of magnitude.

4.5. Comparison of Diffusion Analysis Techniques

Each of the techniques used to quantify diffusion coefficients have strengths that contribute to their usefulness. However, utilizing a combination of techniques offers greater insight into molecular diffusion in hydrogels than employing each technique individually. All diffusion coefficients calculated for methylene blue using the NMR, optical microscopy, and characterization of device effluent analyses are compared in this section, as well as those calculated for acid blue 22 using the NMR and effluent analyses. Diffusion coefficients are also compared to values calculated using the model given in Equation (2,5).

Diffusion coefficients for methylene blue using all three techniques are summarized in Figures 4.35 to 4.37 for each initial water/PEG-DA ratio.
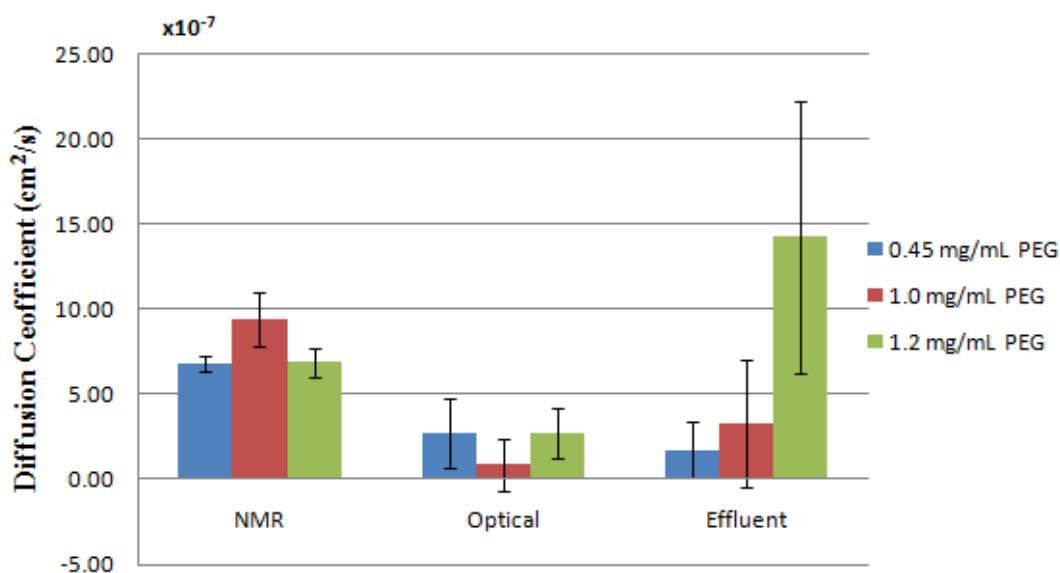
Figure 4.35. Diffusion coefficients of hydrogels with initial water/PEG-DA ratios of 70/30 for NMR, optical, and effluent analyses. Blue, red, and green columns represent low, medium, and high methylene blue concentration, respectively.
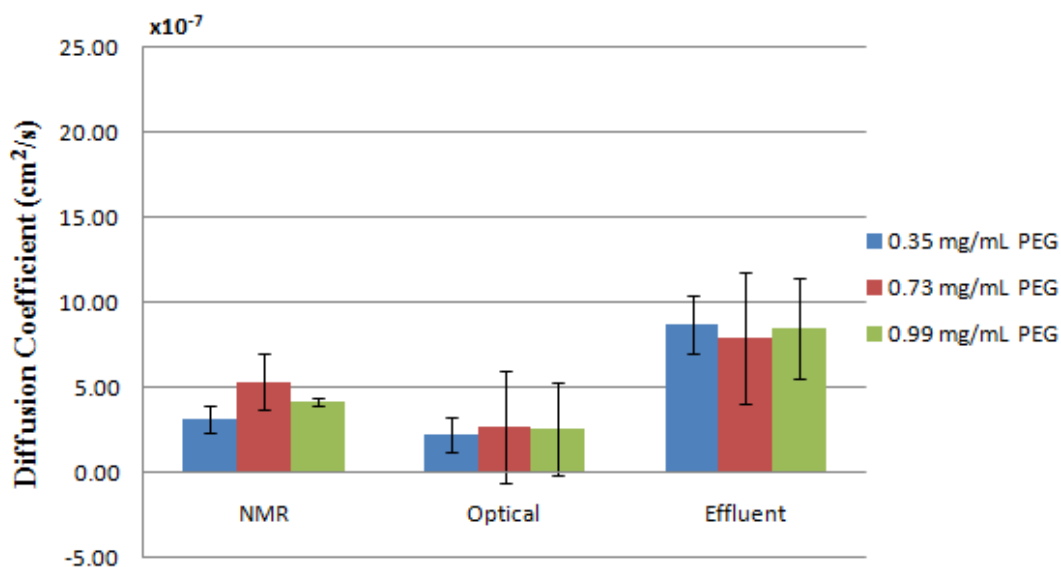
Figure 4.36. Diffusion coefficients of hydrogels with initial water/PEG-DA ratios of 60/40 gels for NMR, optical, and effluent analyses. Blue, red, and green columns represent low, medium, and high methylene blue concentration, respectively.
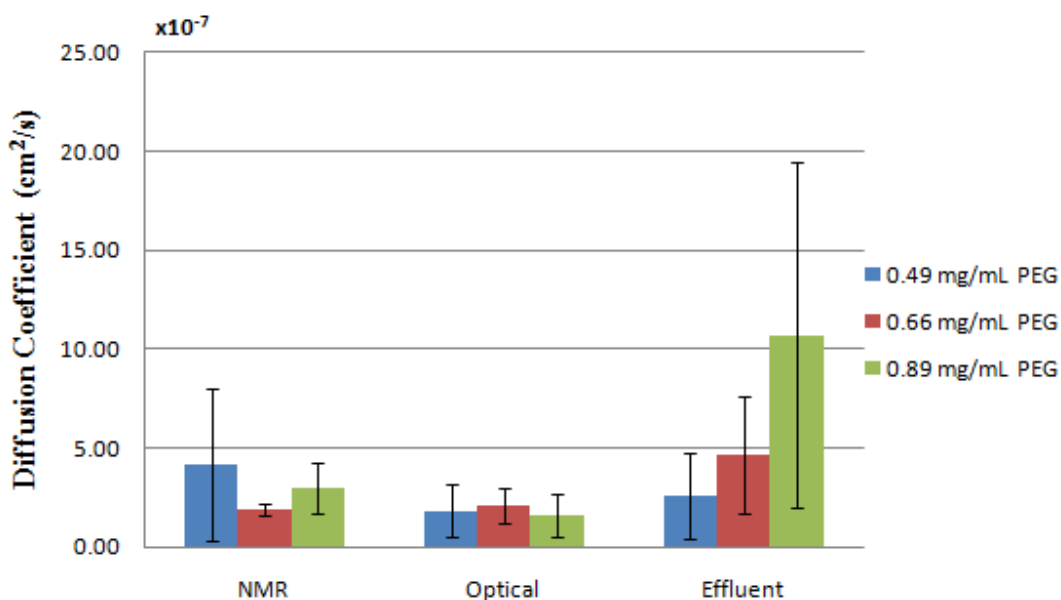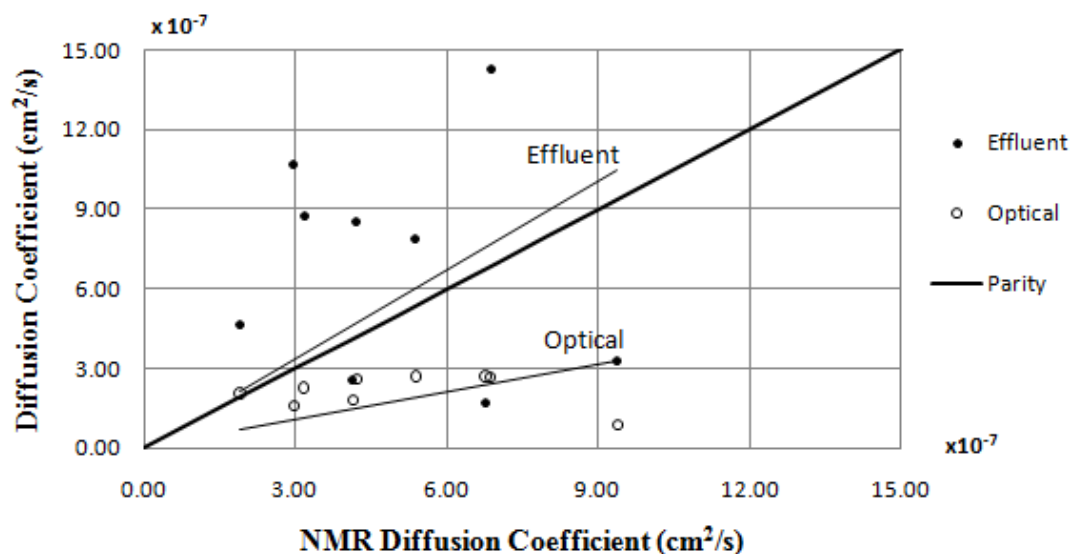

Figure 4.37. Diffusion coefficients of hydrogels with initial water/PEG-DA ratios of 40/60 gels for NMR, optical, and effluent analyses. Blue, red, and green columns represent low, medium, and high methylene blue concentration, respectively.

From these results, it is evident that the NMR measurements overall have much less variation than the optical and effluent methods. The optical and effluent methods had more variability because of differences between device curing. The effluent method in particular was dependent on the curing conditions of the device and clearing of the channel. Although a method for accounting for the burst effect was taken into consideration, variation was still seen between devices of the same dye and gel content. For 70/30 and 40/60 hydrogels, the effluent method predicted an increase in the diffusion coefficient with an increase in concentration. The optical method tended to predict diffusion coefficients that were relatively the same regardless of water content and dye concentration. The NMR method was able to distinguish an effect of the initial water/PEG-DA ratio in the hydrogel as shown by Figures 4.35 to 4.37. As the water content increased, the diffusion coefficient increased as well. The strength of the NMR analysis lies with its capability of making fine-tuned diffusion measurements that are sensitive to the movement of the dye within the hydrogel structure. Since the length of diffusion for NMR was greater than the mesh size the measurement was influenced by methylene blue encountering the polymer chains of the mesh. The other two methods are more of a "blunt" approach to calculating diffusion coefficients. Both rely on the accuracy of the mathematical model used. For the effluent method, averaging concentration over a large time interval possibly smears out differences between initial water/PEG-DA ratios that were seen with the NMR method.

Parity plots of the diffusion coefficients from NMR analysis v. diffusion coefficients of effluent and optical analyses are shown in Figures 4.38 for all dye concentrations at each initial water/PEG-DA ratio.

Figure 4.38. Parity plot between NMR diffusion coefficient for effluent and optical diffusion coefficients for all methylene blue concentrations and initial water/PEG-DA ratios.

Between the NMR and the other methods, the parity plot shows that the effluent data is generally larger than the NMR data. Between the NMR and optical methods, the optical diffusion coefficients are generally lower than the diffusion coefficients found using NMR. All the diffusion coefficients from the three analysis techniques for each concentration and initial water/PEG-DA ratio are shown in Figure 4.39.
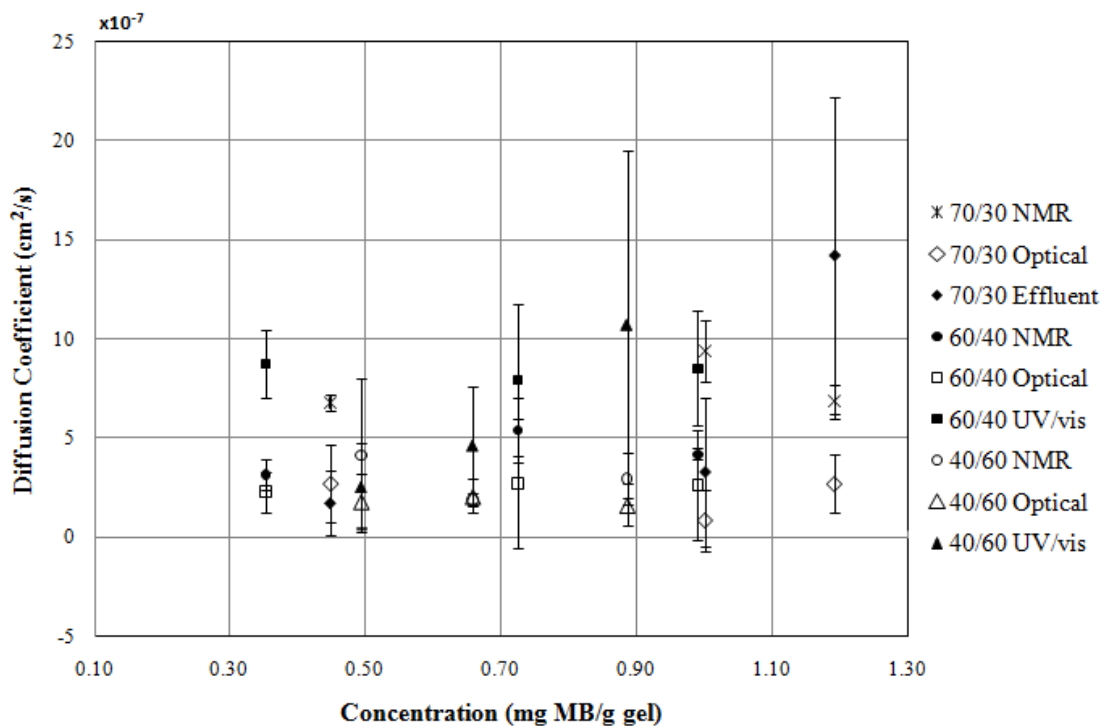
Figure 4.39. Diffusion coefficients for methylene blue elution from PEG hydrogel for all concentrations and initial water/PEG-DA ratios.

From Figure 4.39 it is evident that all the techniques used to quantify the diffusion of methylene blue from PEG hydrogel are consistent and have relatively good agreement. Methods were consistent for methylene blue because it was able to diffuse through the hydrogel and was not limited by size or mass transfer into the channel. A two tail t-test ($\alpha = 0.05$) was conducted between diffusion coefficients determined by the optical and effluent methods, optical and NMR methods, and effluent and NMR methods at each of the initial water/PEG-DA ratios. Diffusion coefficients were averaged between the three levels of concentrations at each initial water/PEG-DA ratio because the difference in concentration was too small to have a significant effect. Values determined for the t-test

are given in appendix F. The t-test demonstrated that no statistically significant difference existed between diffusion coefficients of 70/30 gels calculated by the optical and effluent methods, 70/30 gels calculated by NMR and effluent methods, 60/40 gels calculated by NMR and optical methods, 40/60 gels calculated by NMR and effluent methods, and 40/60 gels calculated by NMR and optical methods. A statistically significant difference was found between diffusion coefficients of 70/30 gels calculated by the NMR and optical methods, 60/40 gels calculated by NMR and effluent methods, 60/40 gels calculated by effluent and optical methods, and 40/60 gels calculated by effluent and optical methods. Although a statistically significant difference was found between methods for some of the gels, the diffusion coefficients are all within an order of magnitude from one another. Because monitoring diffusion is difficult for long times and short distances, diffusion coefficient measurements are often difficult to obtain. Agreement within an order of magnitude for experimental determination of diffusion coefficients is very good.

Although the NMR measurements had the least variation between samples and were capable of making fine-tuned diffusion sensitive measurements, the "blunt" methods of analysis had advantages as well. For example, the optical method provides a physical picture of the progression of the diffusion. The NMR method technique cannot provide a complete picture for elution and concentration-gradient driven diffusion. As shown in Figures 4.40 and 4.41 the diffusion coefficients calculated using the NMR analysis for acid blue were two orders of magnitude higher than those determined by the effluent method. Figure 4.40 provides a summary of all the acid blue 22 diffusion

coefficients determined using the effluent method, which range from 10^{-9} cm^2/s to 10^{-10} cm^2/s. Figure 4.41 provides a summary of all the acid blue 22 diffusion coefficients determined using the NMR method, which are all on the order of 10^{-7} cm^2/s.
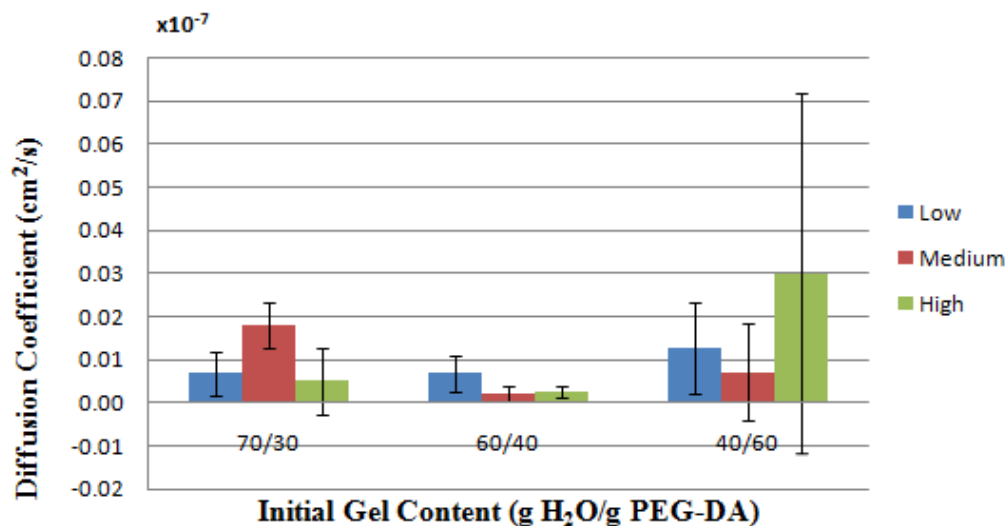
Figure 4.40. Diffusion coefficients of acid blue loaded hydrogels using the effluent analysis for all initial water/PEG-DA ratios. Low dye concentrations are 0.25 mg/g soln, 0.21 mg/g soln, and 0.28 mg/g soln for 70/30, 60/40, and 40/60 gels respectively. Medium dye concentrations are 0.49 mg/g soln, 0.42 mg/g soln, and 0.41 mg/g soln for 70/30, 60/40, and 40/60 gels respectively. High concentrations are 0.74 mg/g soln, 0.64 mg/g soln, and 0.56 mg/g soln for 70/30, 60/40, and 40/60 gels respectively.
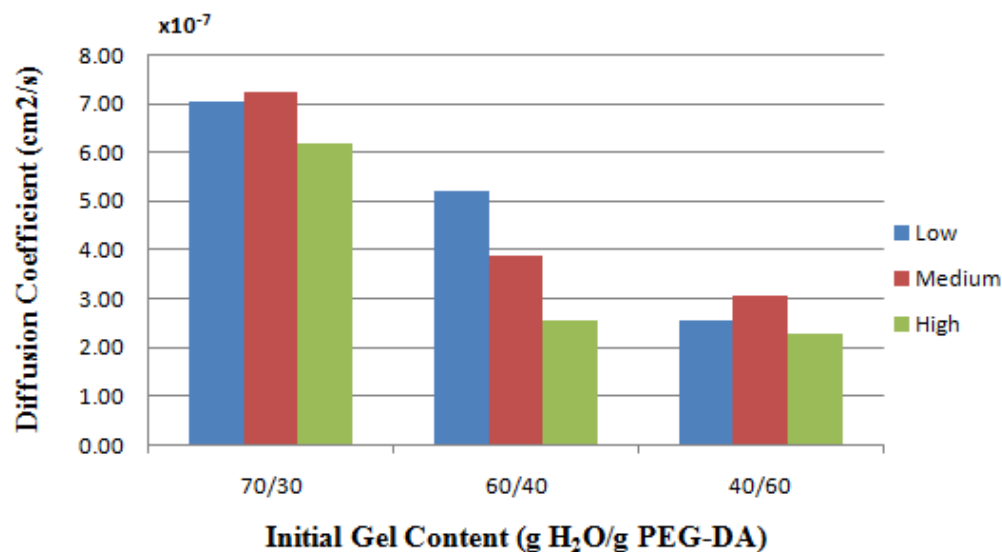
Figure 4.41. Diffusion coefficients of acid blue loaded hydrogels using the NMR analysis for all initial water/PEG-DA ratios. Low dye concentrations are 0.25 mg/g soln, 0.21 mg/g soln, and 0.28 mg/g soln for 70/30, 60/40, and 40/60 gels respectively. Medium dye concentrations are 0.49 mg/g soln, 0.42 mg/g soln, and 0.41 mg/g soln for 70/30, 60/40, and 40/60 gels respectively. High concentrations are 0.74 mg/g soln, 0.64 mg/g soln, and 0.56 mg/g soln for 70/30, 60/40, and 40/60 gels respectively.

The optical method was essential in identifying a mass transfer limitation into the hydrogel channel of acid blue 22 loaded gels because of the build-up of dye witnessed in the hydrogel at the water interface. The effluent method of analysis was useful for the verification of dye elution and provides a good start for the modeling of diffusion. The effluent analysis using high performance liquid chromatography was also useful for determining if diffusing molecules were photodegraded during UV exposure or experienced any changes when encountering the hydrogel mesh. Most eluting hydrogels are loaded in-situ as opposed to post-loaded. This is due to the long times necessary for post-loaded gels to reach equilibrium and the uncertainty of the initial concentration associated with post-loaded gels. With in-situ loaded hydrogels, it is usually assumed that

UV photopolymerization with Irgacure is safe to use because of its low toxicity and short polymerization times. Using HPLC to analyze the effluent of naproxen loaded hydrogels was instrumental in determining that naproxen photodegraded under UV light. Thus, the apparatus for flowing solvent through a hydrogel contained in a microfluidic device and collecting the effluent provides an effective method for visualizing and quantifying the diffusion of a solute. Because the NMR does make sensitive measurements, the combination of the techniques proves very useful. The optical and effluent analysis can be used as a screening tool for solutes to confirm that the solute is not just able to move within the hydrogel, but actually elute from the gel as well. This will ensure that NMR measurements are not missing any special interactions with the hydrogel or mass transfer limitations that prevent the solute from eluting from the hydrogel mesh.

Values for the diffusion coefficients of methylene blue, acid blue 22, and brilliant black were calculated using Equation (2,5), which utilizes the mesh size, size of the solute, polymer volume fraction, and diffusion in free solution to calculate the diffusion in the hydrogel. However, the theoretical model depends on values of Y, which represents the size disparity between the solute volume to the solvent molecule volume. In literature, this value is assumed to be unity. This is not an accurate assumption for this thesis because methylene blue is much larger than water. Table 4.10 provides a summary of the diffusion coefficients for the NMR analysis and the theoretical model using various Y values. A sample calculation for D_g given in Appendix G.

Table 4.10. Theoretical diffusion coefficients for methylene blue in a hydrogel mesh

Initial DI-H$_2$O/PEG-DA Ratio (g/g)	NMR Diffusion Coefficient (x 10^{-7} cm^2/s)	Theoretical Diffusion Coefficient (Y = 1) (x 10^{-7} cm^2/s)	Theoretical Diffusion Coefficient (Y = 4) (x 10^{-7} cm^2/s)	Theoretical Diffusion Coefficient (Y = 4.8) (x 10^{-7} cm^2/s)
70/30	7.67	25.2	7.29	5.25
60/40	4.25	23.8	5.99	4.16
40/60	3.00	22.6	4.83	3.21

Generally, the theoretical model shows the same trend as the experimental data. However when the *Y* value is unity, the theoretical model predicts diffusion coefficients an order of magnitude greater than those calculated experimentally. When the *Y* value is 4 or 4.8, the theoretical diffusion coefficients match the experimental diffusion coefficients. This agreement supports that the techniques are reliable for calculating the diffusion coefficients of small molecules.

4.6. References

(1) Watkins, A. W.; Anseth, K. S. Investigation of Molecular Transport and Distributions in Poly(ethylene glycol) Hydrogels with Confocal Laser Scanning Microscopy *Macromolecules* **2005***, 38*, 1326 - 1334.

(2) Litzenberger, A. A Microfluidic Method to Measure Diffusion in Hydrogels, Bucknell University, Lewisburg, PA, 2010.

5. Conclusions

This thesis has verified that an optical method for capturing images and determining the concentration profile can be used for dye uptake and elution from poly(ethylene glycol) hydrogel. The apparatus for flowing solvent through a hydrogel contained in a microfluidic device and collecting the effluent provides an effective method for visualizing and quantifying the diffusion of a solute. The three techniques used for measuring the diffusion coefficient of methylene blue dye, including the optical microscopy, characterization of device effluent, and NMR analyses all reasonably agree within an order of magnitude. The methylene blue diffusion coefficients calculated agree within an order of magnitude to a theoretical model used to predict the diffusion of a solute within a hydrogel. It was also determined that utilizing a combination of the three techniques offers greater insight into molecular diffusion in hydrogels than employing each technique individually.

The greatest strength of the NMR analysis is its capability for making fine-tuned diffusion measurements that are sensitive to movement of the dye within the hydrogel structure. NMR was used to determine that solute diffusivity increases with an increase in water content. Hydrogels with low initial water/PEG-DA ratios had greater polymer fractions and were less swollen in water. Hydrogels with greater polymer fractions and less swelling had smaller diffusion coefficients than hydrogels with low polymer fractions and were more swollen in water.

The optical and effluent analyses have more variability within measurements, but are very effective for screening solutes to confirm that the solute is not just able to move within the hydrogel, but actually elute from the gel as well. For the NMR method to produce diffusion coefficient values consistent with the optical and effluent analysis the solute molecules must not be limited by mass transfer at the channel.

Using the optical and effluent techniques, several solutes were determined not to be capable of eluting from the hydrogel mesh. Brilliant black could not be eluted from $M_n = 575$ g/mol PEG hydrogel because of size. The molecule was larger than the mesh size and thus could not move through the hydrogel. Rhodamine 6G could not be eluted from the PEG hydrogel because it had a much greater affinity for the PEG chains than it did for the contacting water stream. Acid blue 22 was able to move within the hydrogel mesh to the channel, but had a mass transfer limitation from the channel. The mass transfer limitation caused a discrepancy between the NMR and effluent analyses. Naproxen was found to photodegrade with UV exposure, which prevents the determination of a diffusion coefficient.

When designing a hydrogel for drug delivery, it is important to understand the diffusivity that is being measured. The NMR technique produces very precise measurements of solute diffusivity within hydrogels, but it is limited by its ability to provide a complete picture for elution and concentration-gradient driven diffusion at the device level. For diffusing solutes that are mass transfer limited at the channel relying only upon the NMR technique could result in the design of a hydrogel that does not elute

the required dose. A complete picture for designing drug eluting hydrogels requires analysis of the effluent.

6. Future Work

More work still can be conducted to further characterize the network and diffusion in hydrogels. Since molecular interactions with the hydrogel differ based on size, charge, and functional groups, it would be beneficial to investigate additional molecules with varying properties. It would also be valuable to entrap large therapeutic proteins inside hydrogel because many of these therapies are being developed that could benefit from a new method of release.

In addition to changing the diffusing molecules, it would also be advantageous to test PEG hydrogels with different mesh sizes because the gels studied in this investigation mostly had the same amount of crosslinking. The amount of photoinitiator added to the hydrogel solution could be changed as well as utilizing PEG-DA with varying molecular weights. In this thesis, the photoinitiator was added at 0.25 wt% of the amount of PEG-DA used in solution, with PEG-DA with a number average molecular weight of 575 g/mol between crosslinks. PEG-DA can have much larger number average molecular weight than what was used in the experiments for this thesis.

It would also be beneficial to investigate the diffusion of molecules in a microfluidic environment that more closely resembles vasculature. This includes changing the flow of the hydrogel-contacting solvent from a continuous flow pattern to a pulsating flow pattern. The solvent used could also be changed or adjusted to observe the effects how the solution in contact with the hydrogel alters the diffusion. This could include solvents with a different pH or higher solubility of the solute. Changing the

nature of the hydrogel such that it degrades in the presence of an enzyme or a particular solvent would also be a new area of investigation for this study. Degradable hydrogels have garnered much attention recently because they do not require removal from the body after releasing the drug.

More characterization of hydrogel properties would also be beneficial to conduct. Chemical tests that could be done include FT-IR spectroscopy, DSC analysis, TGA analysis, and x-ray diffraction to gain insight in the actual chemical composition and degree of photopolymerization. Mechanical tests could also be conducted to investigate the strength of the hydrogel, which would be useful knowledge to have for a biofluid contacting material. Mechanical tests that could be conducted include tensile, compression and rheological tests. Further analysis using HPLC should also be explored. The method was used to determine that naproxen photodegraded with UV exposure. The device effluent of other solute molecules could be explored to test for changes in structure resulting from incorporation into the hydrogel mesh.

The diffusion coefficient measurement techniques could also be extended. Other models could be regressed against the optical data to improve the fit for determining a diffusion coefficient. Results from the optical analysis of methylene blue indicated the diffusion coefficient had possible concentration dependence. The concentration, position, and time data could be used to determine a new model for diffusion.

Appendix A. Derivation of Short Time Release Equation

The derivation of the short time release equation began with the continuity equation of mass, shown below.

$$\frac{\partial C}{\partial t} = \frac{\partial}{\partial x}\left(D \cdot \frac{\partial C}{\partial x}\right)$$

Where C is concentration, x is position, t is time, and D is the diffusion coefficient. The diffusion coefficient was assumed to be constant, and taken out of the differential. It was also assumed that diffusion only occurs in the x-direction.
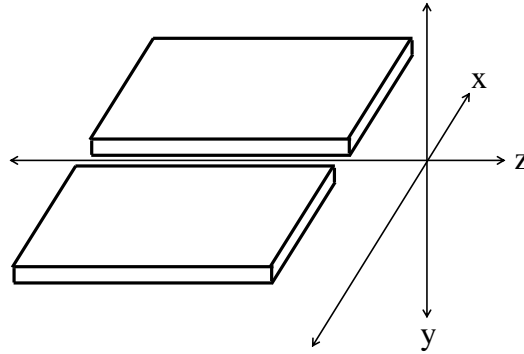
Figure A.1. Coordinate system for hydrogel slabs

The boundary conditions and initial conditions are listed for the release of molecules from a loaded hydrogel. The hydrogel was assumed to be semi-infinite, such that the concentration at the edge furthest away from the channel was not changing.

$$\frac{\partial C}{\partial t} = D\frac{\partial^2 C}{\partial x^2}$$

$$BC(1): C_A = 0 \; at \; x = 0$$

$$BC(2): \frac{dC_A}{dt} = 0 \; at \; x = \infty$$

$$IC(1): C_A = C_{A0} \ at \ t(x) = 0$$

To solve the differential equation, dimensionless conditions were established as shown below.

$$\theta = \frac{C_A}{C_{A0}}$$

$$\eta = \frac{x}{x_{ref}}$$

$$\tau = \frac{t}{t_{ref}}$$

Dimensionless concentration was defined as θ, dimensionless position was defined as η, and dimensionless time was defined as τ. Next the problem was redefined and rearranged in terms of dimensionless variables.

$$\frac{C_{A0}}{t_{ref}} \frac{\partial \theta}{\partial \tau} = \frac{D C_{A0}}{x_{ref}^2} \frac{\partial^2 \theta}{\partial x^2}$$

$$\frac{\partial \theta}{\partial \tau} = \frac{D t_{ref}}{x_{ref}^2} \frac{\partial^2 \theta}{\partial x^2}$$

In the following steps, t_{ref} and x_{ref} were defined and set such that θ was a function of the similarity variable, ξ.

$$\frac{D t_{ref}}{x_{ref}^2} = 1$$

$$x_{ref} = \sqrt{D t_{ref}}$$

$$\theta = \theta \left(\frac{x}{x_{ref}}, \frac{t}{t_{ref}} \right)$$

$$\theta = \theta \left(\frac{x}{\sqrt{D t_{ref}}}, \frac{t}{t_{ref}} \right)$$

$$\theta = \theta\left(\frac{x}{\sqrt{Dt_{ref}}}, \frac{\sqrt{t_{ref}}}{t}\right)$$

$$\theta = \theta\left(\frac{x}{\sqrt{Dt}}\right)$$

$$\xi = \frac{x}{\sqrt{4Dt}}$$

$$\theta = \theta(\xi)$$

The differential equation was rearranged in terms of ξ. To do this, the derivative of θ was taken with respect to t and x, and the second derivative of θ was taken with respect to x.

$$\frac{\partial \theta}{\partial t} = \frac{\partial \theta}{\partial \xi} \cdot \frac{\partial \xi}{\partial t} = \frac{\partial \theta}{\partial \xi}\left(-\frac{1}{2}\frac{\xi}{t}\right)$$

$$\frac{\partial \theta}{\partial x} = \frac{\partial \theta}{\partial \xi} \cdot \frac{\partial \xi}{\partial x} = \frac{\partial \theta}{\partial \xi}\left(\frac{1}{\sqrt{4Dt}}\right)$$

$$\frac{\partial^2 \theta}{\partial x^2} = \frac{\partial}{\partial x}\left(\frac{\partial \theta}{\partial \xi} \cdot \frac{\partial \xi}{\partial x}\right) = \frac{\partial}{\partial \xi}\left(\frac{\partial \theta}{\partial \xi} \cdot \frac{\partial \xi}{\partial x}\right)\frac{\partial \xi}{\partial x} = \frac{\partial}{\partial \xi}\left(\frac{\partial \theta}{\partial \xi} \cdot \frac{1}{\sqrt{4Dt}}\right)\frac{1}{\sqrt{4Dt}} = \frac{\partial^2 \theta}{\partial \xi^2} \cdot \frac{1}{4Dt}$$

The derivatives and second derivatives were substituted into the differential equation.

$$\frac{\partial \theta}{\partial t} = D\frac{\partial^2 \theta}{\partial x^2}$$

$$\frac{\partial \theta}{\partial \xi}\left(-\frac{1}{2}\frac{\xi}{t}\right) = \frac{\partial^2 \theta}{\partial \xi^2} \cdot \frac{D}{4Dt}$$

$$-2\xi\frac{\partial \theta}{\partial \xi} = \frac{\partial^2 \theta}{\partial \xi^2}$$

To put the differential in an easier form to solve, θ' was defined such that it was equal to the derivative of θ with respect to ξ.

$$\theta' = \frac{\partial\theta}{\partial\xi}$$

$$\frac{\partial\theta'}{\partial\xi} = \frac{\partial^2\theta}{\partial\xi^2}$$

$$\frac{\partial\theta'}{\partial\xi} = -2\xi\theta'$$

The resulting form of the equation was integrated.

$$\int \frac{1}{\theta'}\, d\theta' = \int -2\xi d\xi$$

$$\ln(\theta') = -\xi^2 + C_1$$

$$\theta' = C_1 e^{-\xi^2}$$

The derivative of θ with respect to ξ was substituted back in for θ'. The resulting equation was integrated again.

$$\frac{d\theta}{d\xi} = C_1 e^{-\xi^2}$$

$$\int d\theta = \int C_1 e^{-\xi^2}\, d\xi$$

$$\theta = C_1 \int_0^{\xi} e^{-\xi^2}\, d\xi + C_2$$

Next, the boundary conditions were put in terms of θ and ξ and used to find the integration constants.

$$BC(1): \theta = 0 \text{ at } \xi = 0$$

$$BC(2): \theta = 1 \text{ at } \xi = \infty$$

Using boundary condition 1, C_2 was determined to be 0.

$$\theta = C_1 \int_0^\xi e^{-\xi^2} \, d\xi$$

Using boundary condition 2, C_1 was determined.

$$1 = C_1 \int_0^\infty e^{-\xi^2} \, d\xi$$

$$C_1 = \frac{1}{\int_0^\infty e^{-\xi^2} \, d\xi}$$

$$\theta = \frac{\int_0^\xi e^{-\xi^2} \, d\xi}{\int_0^\infty e^{-\xi^2} \, d\xi}$$

$$\theta = \frac{2}{\sqrt{\pi}} \int_0^\xi e^{-\xi^2} \, d\xi$$

$$\theta = erf(\xi)$$

Concentration was substituted back in for θ.

$$C_A = C_{A0}[erf(\xi)]$$

To get the equation in terms of the mass fraction diffused, the relationship below was used.

$$(N_A)_{x=0} = D \frac{\partial C_A}{\partial x}\bigg|_{x=0}$$

The derivative of C_A with respect to x was taken, evaluated at x = 0, and substituted into the equation above. The equation was then rearranged and put in terms of mass.

$$\frac{\partial C_A}{\partial x} = C_{A0} \frac{\partial}{\partial x} erf(\xi) = C_{A0} \frac{1}{\sqrt{\pi}} e^{-\xi^2} \frac{1}{\sqrt{Dt}}$$

$$\left(\frac{\partial C_A}{\partial x}\right)_{x=0} = C_{A0}\frac{1}{\sqrt{\pi}}\frac{1}{\sqrt{Dt}}$$

$$M_t = -DA \int_0^t \left(\frac{dC}{dx}\right)_{x=0} dt$$

$$M_t = -DA \int_0^t C_{A0}\frac{1}{\sqrt{\pi}}\frac{1}{\sqrt{Dt}} dt$$

$$M_t = -\sqrt{\frac{D}{\pi}} A C_{A0} \int_0^t \frac{1}{\sqrt{t}} dt$$

$$M_t = -\sqrt{\frac{D}{\pi}} A C_{A0}\left(-2\sqrt{t}\right)$$

$$M_t = \sqrt{\frac{4Dt}{\pi}} A C_{A0} = \sqrt{\frac{4Dt}{\pi}} A \frac{M_0}{V} = \frac{M_0}{L}\sqrt{\frac{4Dt}{\pi}}$$

The final result is shown below as the short time release equation.

$$M_t = M_0 \sqrt{\frac{4Dt}{\pi L^2}}$$

Appendix B. Verification of Negligible Mass Transfer

Limitation

The verification that the mass transfer limitation at the channel is negligible using the expression for laminar flow along a flat plate to find the Nusselt number, shown in equation below.

$$Nu = \frac{kL_c}{D_c} = 0.646 \left(\frac{Lv_0}{v}\right)^{1/2} \left(\frac{v}{D}\right)^{1/3}$$

The free diffusion coefficient of methylene blue in water used in the expression for laminar flow along a flat plate to calculate k was calculated from NMR measurements of methylene blue in water to be 1.52×10^{-10} cm^2/s. The molar volume of methylene blue is known to be 2.419×10^{26} Å^3/mol. Using the molar volume, the volume of methylene blue was solved for below.

$$V = 2.419 \times 10^{26} \frac{\text{Å}^3}{mol} \cdot \frac{mol}{6.02 \times 10^{23}} = 401.8 \text{ Å}^3$$

Assuming methylene particles are spherical, the volume can be used to calculate the hydrodynamic radius. The equation for calculating the hydrodynamic radius is shown below.

$$V = \frac{4\pi}{3} R_0^3 = 401.8 \text{ Å}^3$$

The hydrodynamic radius was calculated using the volume calculated from the molar volume, and was calculated to be 4.578×10^{-10} m.

$$R_0 = 4.578 \text{ Å} = 4.578 \times 10^{-10} m$$

The area of the channel in a typical device is shown below.

$$A_{Channel} = (0.12 \text{ cm})(0.09 \text{ cm}) = 0.0108 \text{ cm}^2$$

The linear velocity of water flowing through the channel was calculated below using the volumetric flow rate of 5 cm³/h, which was used during experiments and the area or the channel.

$$v_o = \frac{5 \text{ cm}^3}{h} \cdot \frac{1}{0.0108 \text{ cm}^2} \cdot \frac{m}{100 \text{ cm}} \cdot \frac{h}{3600 \text{ s}} = 0.0013 \frac{m}{s}$$

The length of the channel in a typical device is shown below.

$$L_c = 0.05 \text{ m}$$

The length of the channel, the linear velocity of water, the kinematic viscosity of water, and the estimated diffusion coefficient were plugged into the laminar flow along a plate equation to estimate the mass transfer coefficient.

$$k = 0.646 \left(\frac{(0.05 \text{ m})\left(0.0013 \frac{m}{s}\right)}{1 \times 10^{-6} \frac{m^2}{s}} \right)^{1/2} \left(\frac{1 \times 10^{-6} \frac{m^2}{s}}{1.52 \times 10^{-10} \frac{m^2}{s}} \right)^{1/3} \cdot \frac{1.52 \times 10^{-10} \frac{m^2}{s}}{0.05 \text{ m}}$$

$$k = 2.967 \times 10^{-7} \frac{m}{s} = 2.967 \times 10^{-5} \frac{cm}{s}$$

The mass transfer coefficient was estimated to be 2.967×10^{-5} cm/s. The Biot number was used to determine that a mass transfer limitation does not exist to the water/gel boundary.

$$Bi = \frac{kL_G}{D_G}$$

The length of a gel slab in a typical device is shown below.

$$L_G = 0.85 \; cm$$

Actual measurements of the diffusion coefficients of methylene blue in PEG hydrogels were on the order of 10^{-7} cm^2/s. A typical diffusion coefficient for methylene blue in a PEG hydrogel is shown below.

$$D_G = 5 \times 10^{-7} \; \frac{cm^2}{s}$$

Thus the Biot number was calculated to be

$$Bi = \frac{(2.967 \times 10^{-5})(0.85)}{5 \times 10^{-7}} = 50.4$$

Since the Biot number is greater than one, the effect of the mass transfer limited release of methylene blue from PEG hydrogels can be neglected.

Appendix C. Calibration Curves

C.1 Methylene Blue

$y = 0.007755x$
$R^2 = 0.997551$
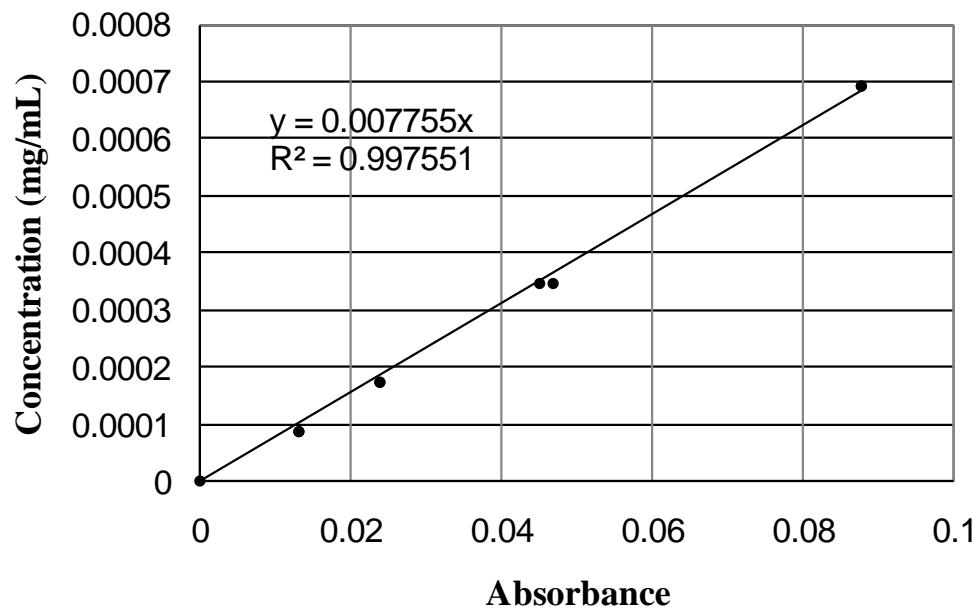
C.1. Methylene blue calibration curve

C.2 Acid Blue

y = 0.014533x
R² = 0.999609

(Y-axis: Concentration (mg/mL); X-axis: Absorbance)
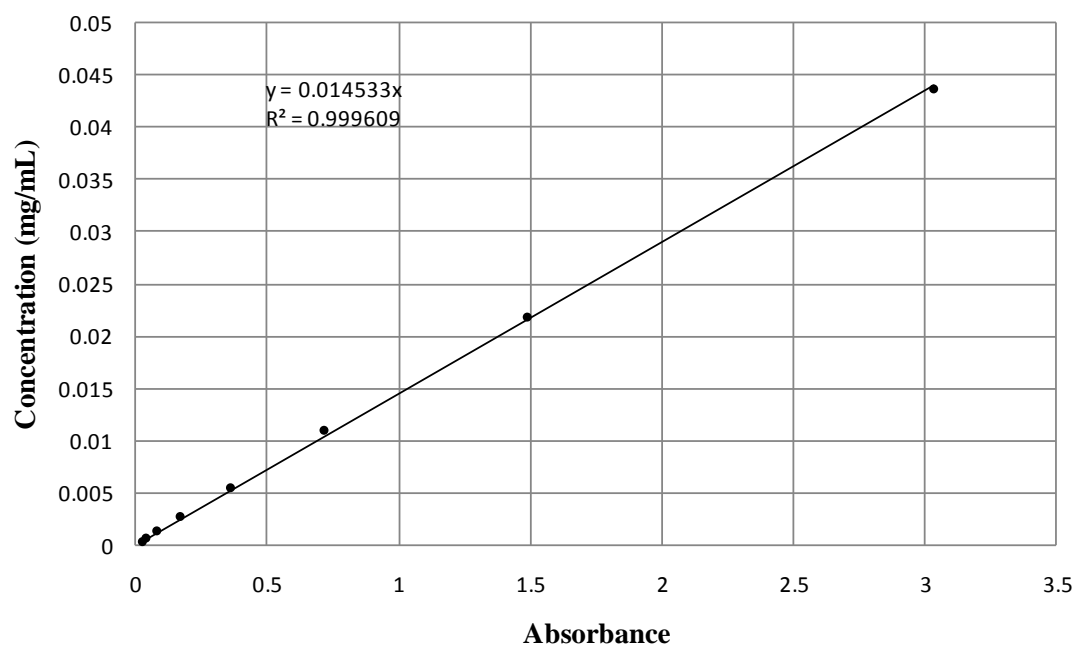
C.2. Acid blue 22 calibration curve

C.3 Brilliant Black

y = 0.767800x
R² = 0.998735

(x-axis) **Absorbance**

(y-axis) **Concentration (mg/mL)**
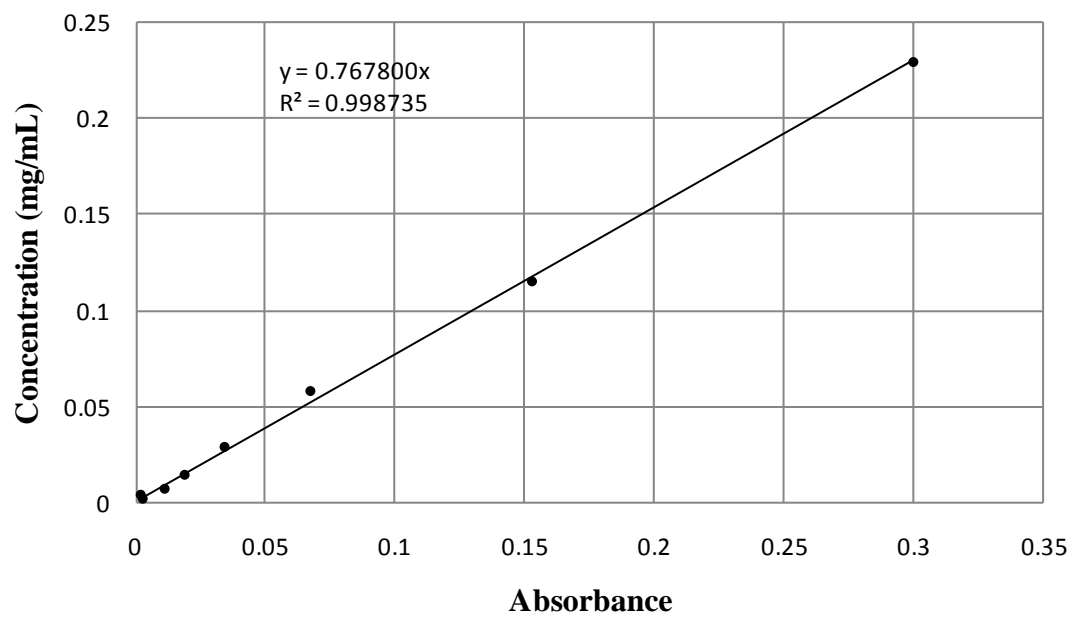
C.3. Brilliant Black calibration curve

C.4 Rhodamine 6G
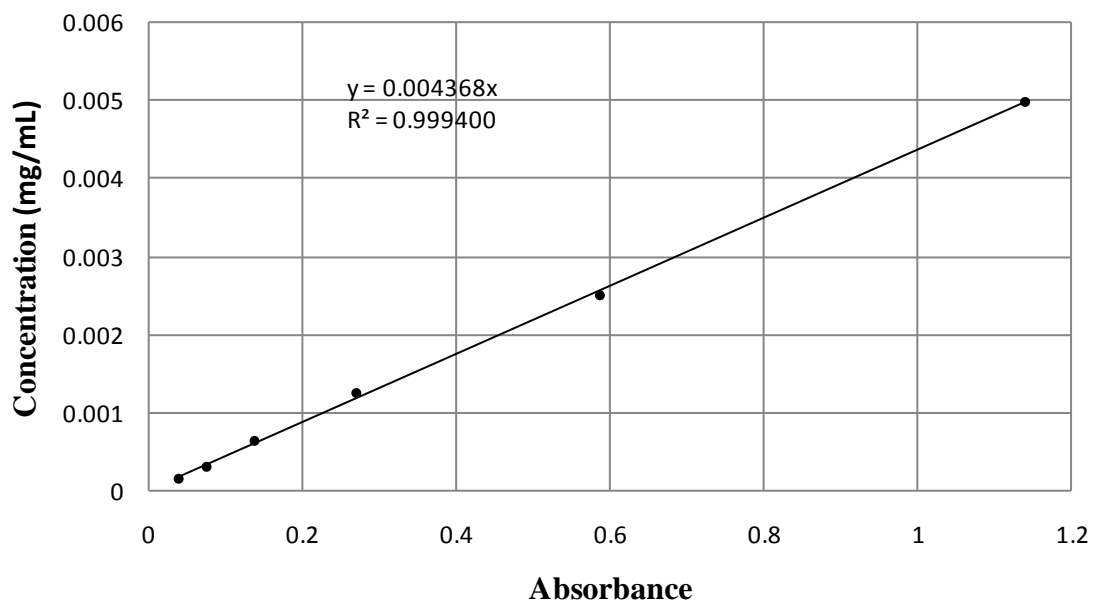
C.4. Rhodamine 6G calibration curve

C.5 Naproxen
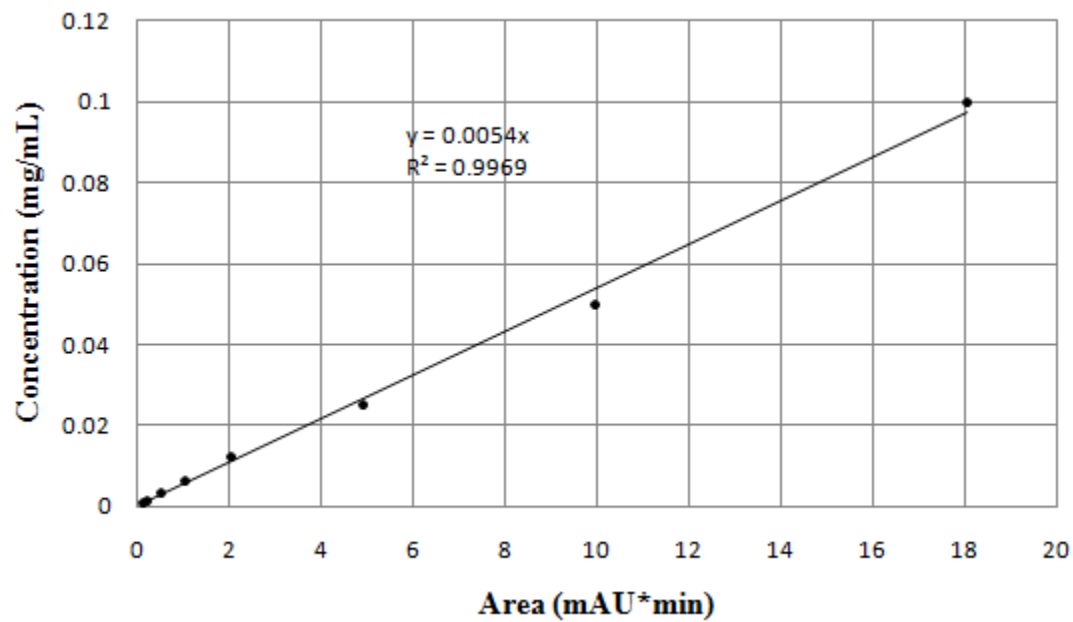
C.5. Naproxen calibration curve

Appendix D. Optical Data

D.1. 70/30 Methylene Blue 0.5 wt%
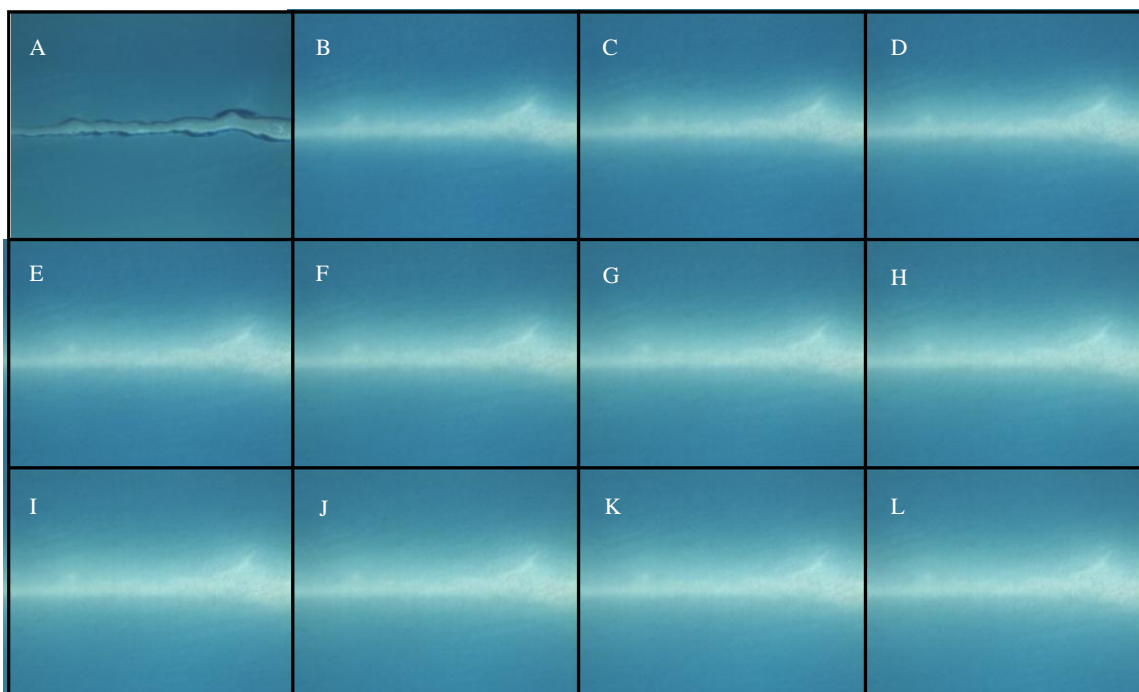
Figure D.1. Elution of methylene blue dye in Device B13 (70/30 0.000124 g/g soln) at various times. A.) Gel prior to water being pumped through the device. B.) Release of methylene blue after 1 h, C.) 2 h, D.) 3 h, E.) 4 h, F.) 5 h, G.) 6 h, H.) 7 h, I.) 8 h, J.) 9 h, K.) 10 h, and L.) 11 h.
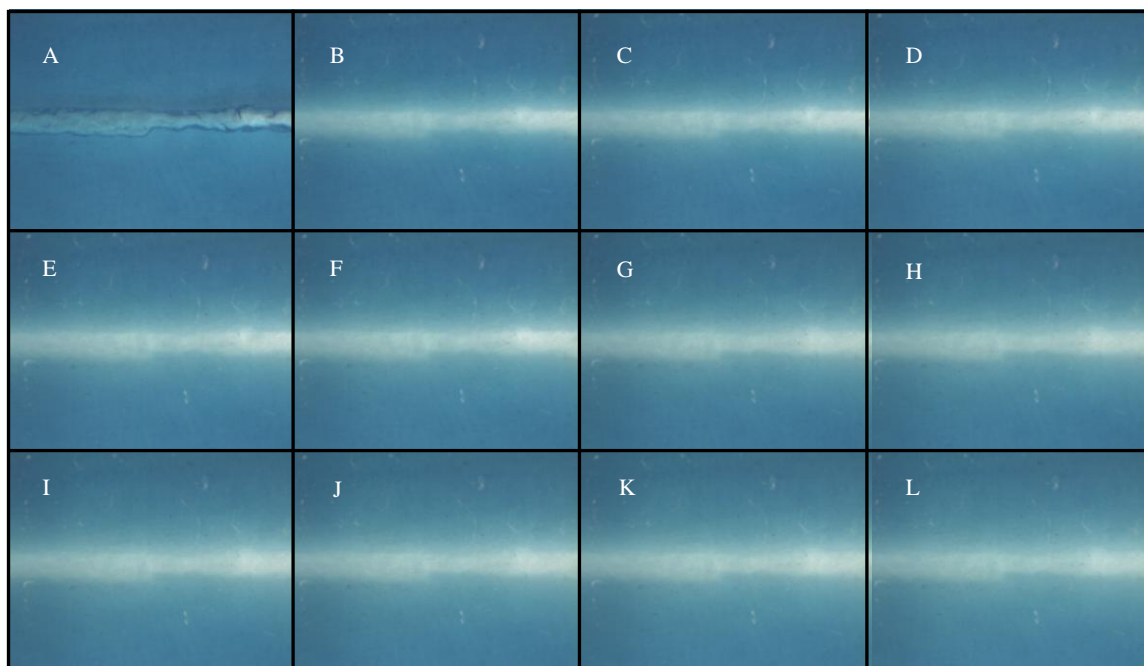
Figure D.2. Elution of methylene blue dye in Device B14 (70/30 0.000124g/g soln) at various times. A.) Gel prior to water being pumped through the device. B.) after 1 h, C.) 2 h, D.) 3 h, E.) 4 h, F.) 5 h, G.) 6 h, H.) 7 h, I.) 8 h, J.) 9 h, K.) 10 h, and L.) 11 h.
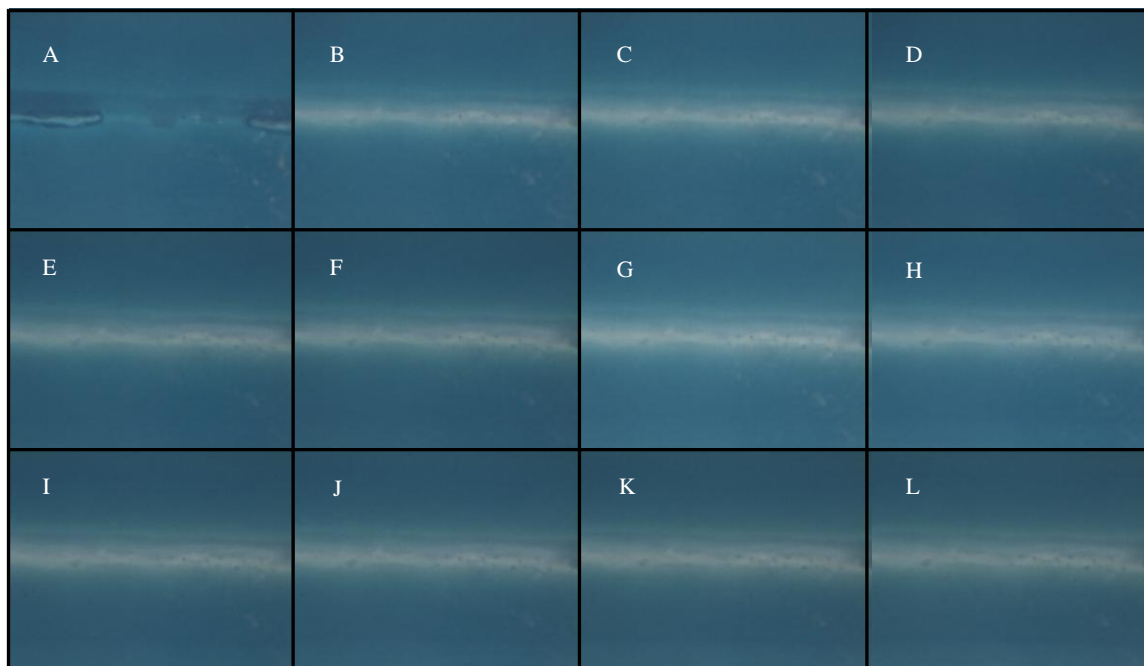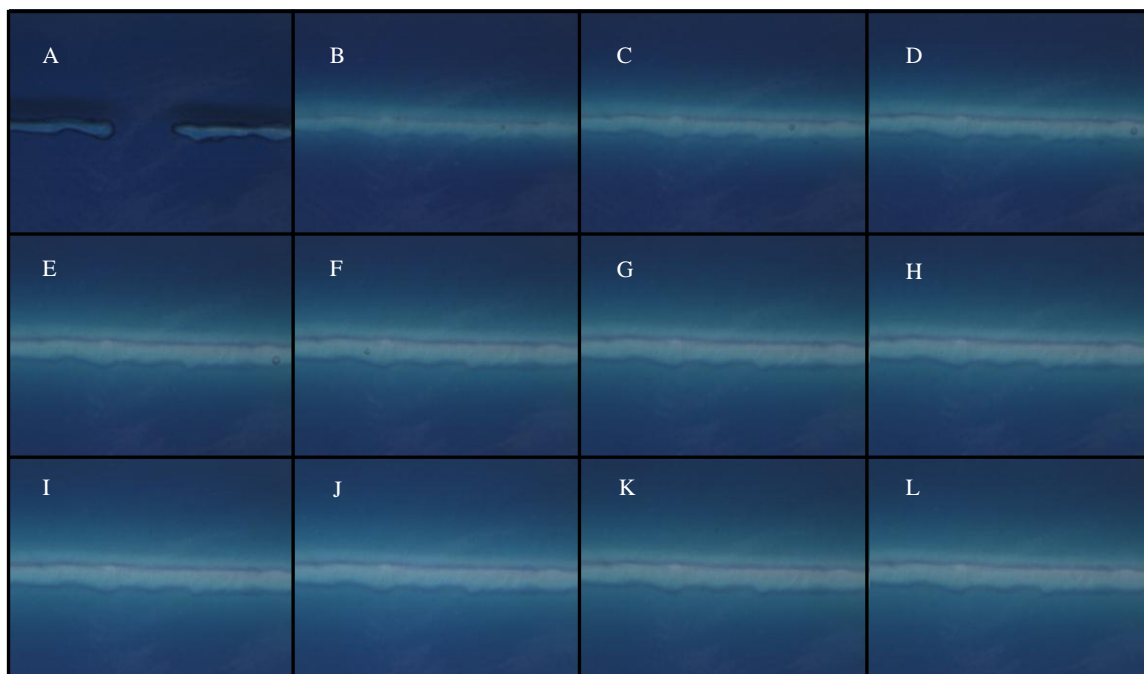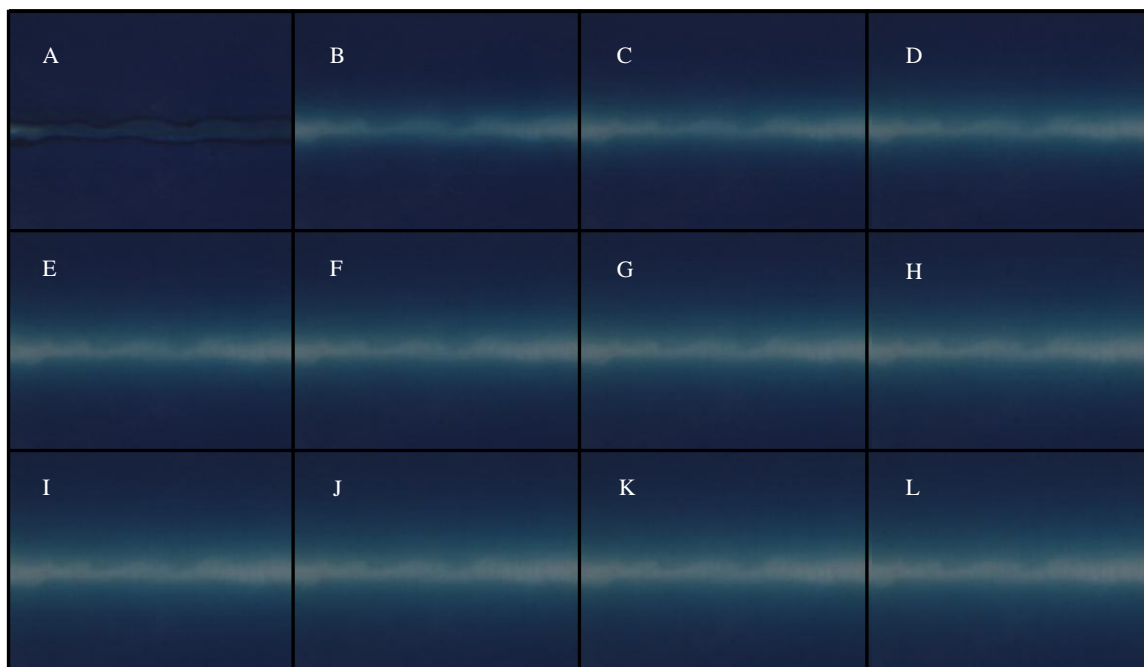

Figure D.3. Elution of methylene blue dye in Device B19 (70/30 0.000124g/g soln) at various times. A.) Gel prior to water being pumped through the device. B.) after 1 h, C.) 2 h, D.) 3 h, E.) 4 h, F.) 5 h, G.) 6 h, H.) 7 h, I.) 8 h, J.) 9 h, K.) 10 h, and L.) 11 h.
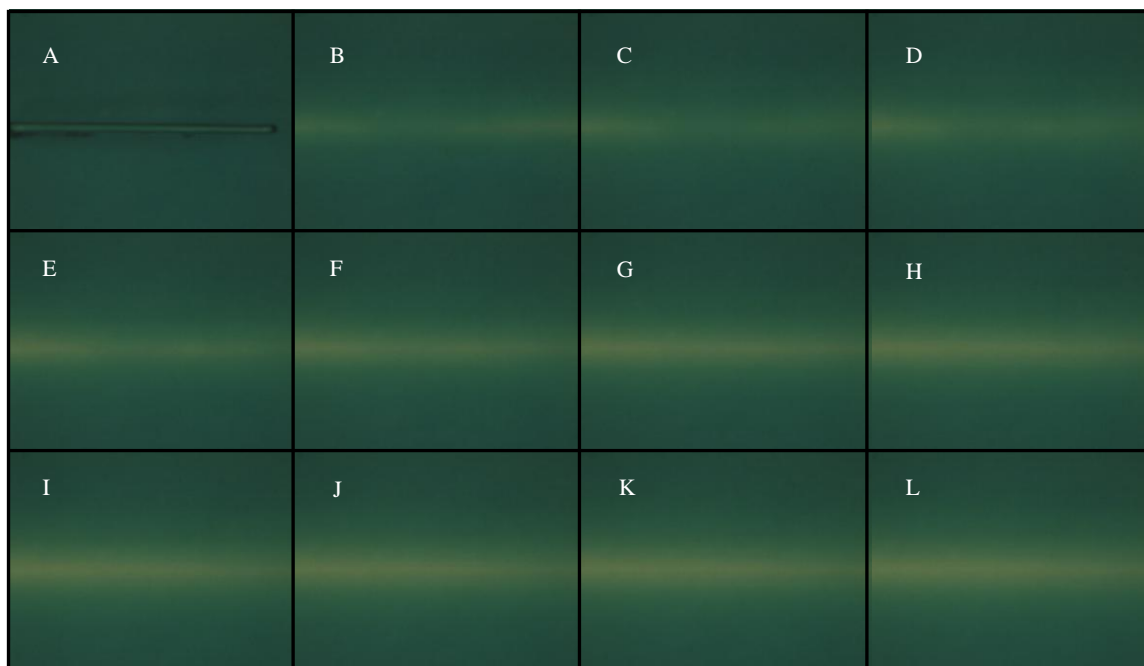
Figure D.4. Elution of methylene blue dye in Device B56 (70/30 0.000124g/g soln) at various times. A.) Gel prior to water being pumped through the device. B.) after 1 h, C.) 2 h, D.) 3 h, E.) 4 h, F.) 5 h, G.) 6 h, H.) 7 h, I.) 8 h, J.) 9 h, K.) 10 h, and L.) 11 h.
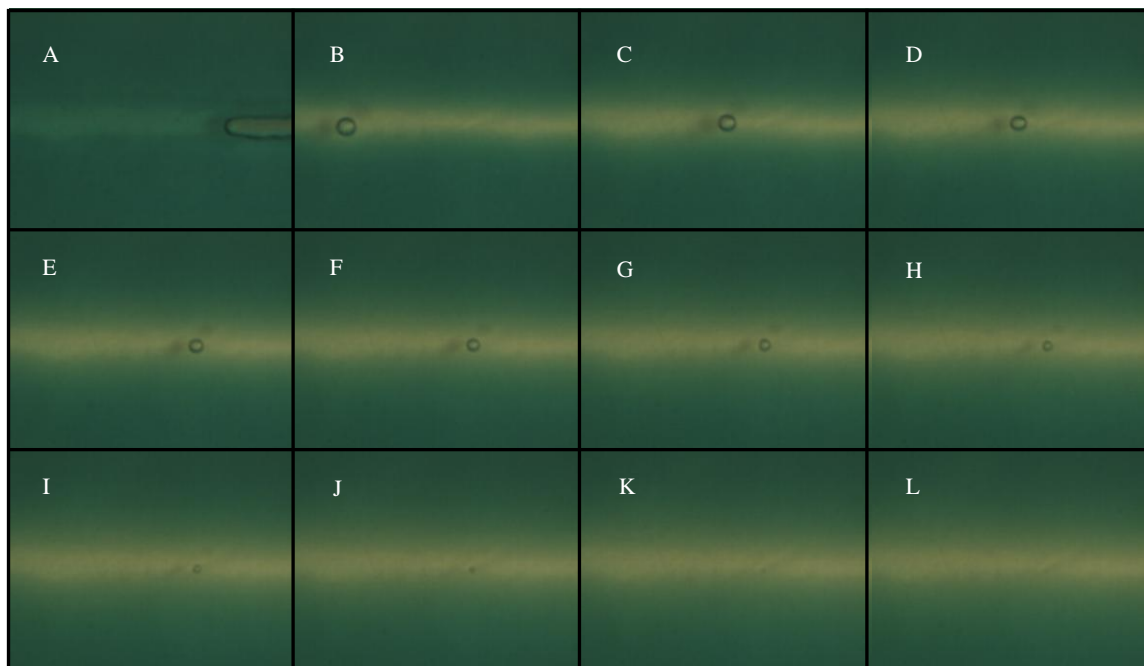
Figure D.5. Elution of methylene blue dye in Device B57 (70/30 0.000124g/g soln) at various times. A.) Gel prior to water being pumped through the device. B.) after 1 h, C.) 2 h, D.) 3 h, E.) 4 h, F.) 5 h, G.) 6 h, H.) 7 h, I.) 8 h, J.) 9 h, K.) 10 h, and L.) 11 h.
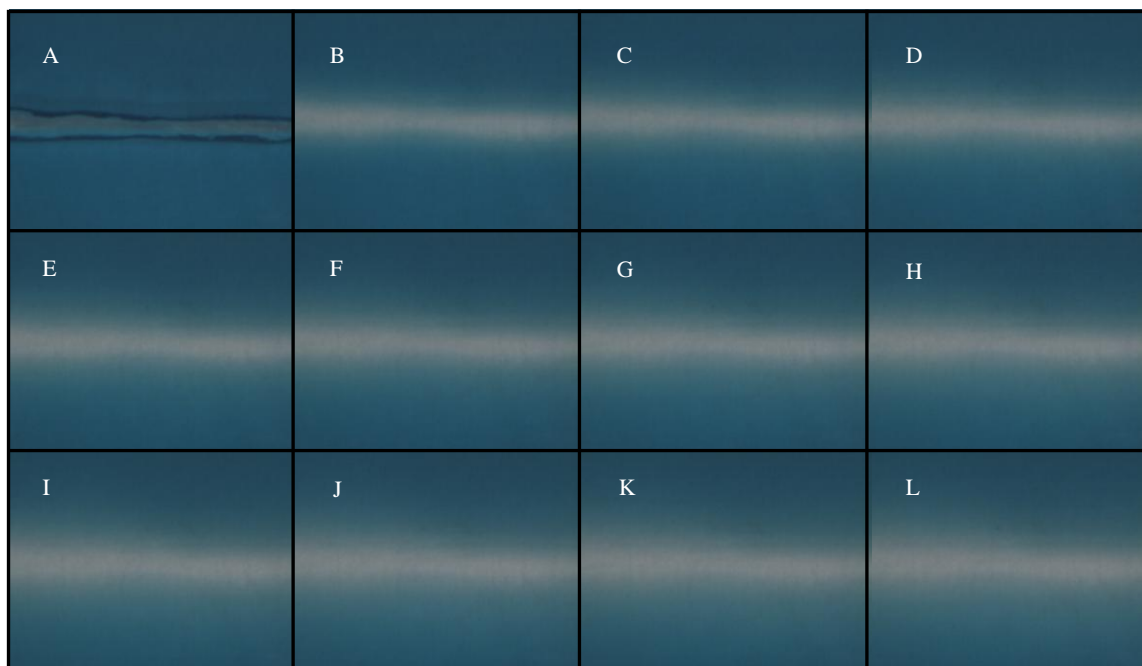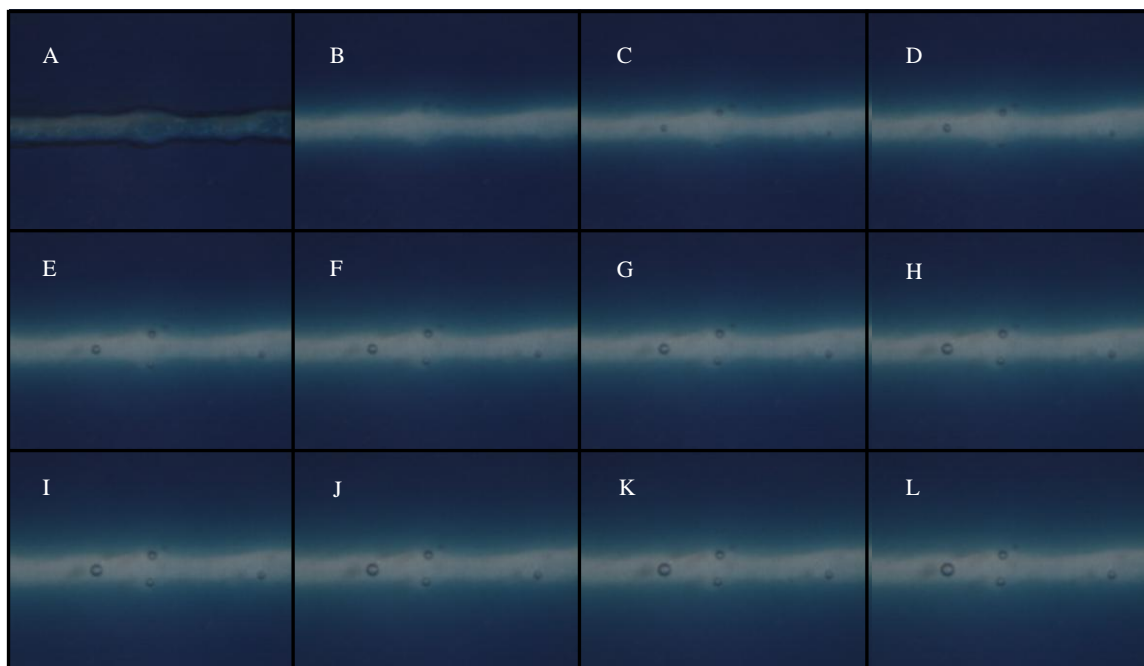
Figure D.6. Elution of methylene blue dye in Device B58 (70/30 0.000124g/g soln) at various times. A.) Gel prior to water being pumped through the device. B.) after 1 h, C.) 2 h, D.) 3 h, E.) 4 h, F.) 5 h, G.) 6 h, H.) 7 h, I.) 8 h, J.) 9 h, K.) 10 h, and L.) 11 h.
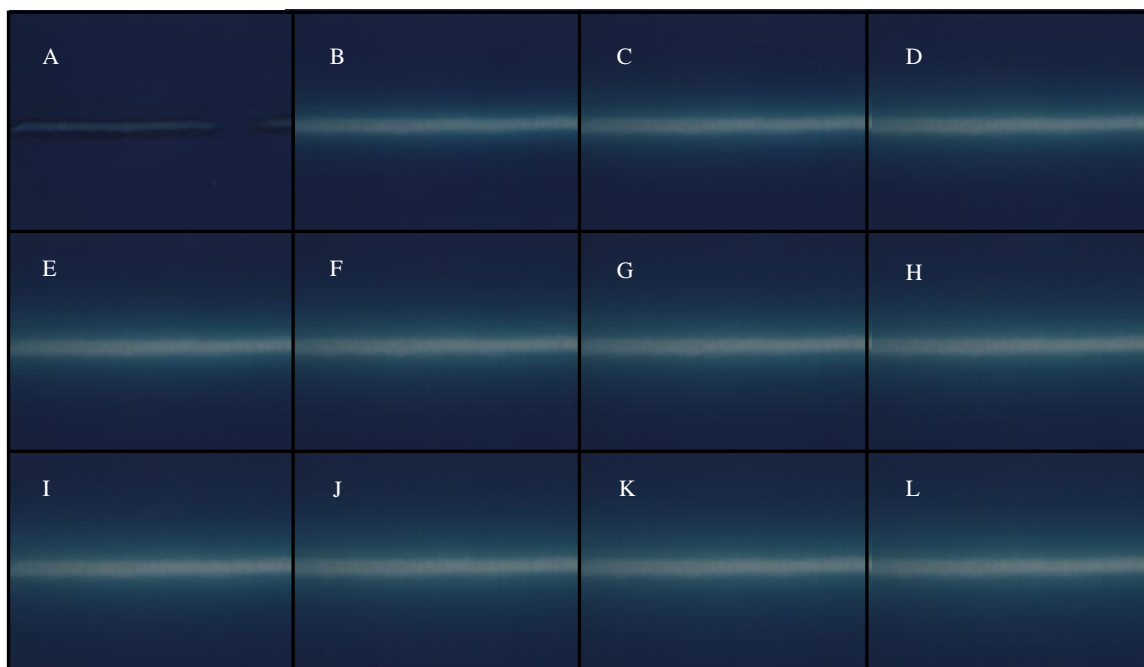
D.2. 70/30 Methylene Blue 1.0 wt%
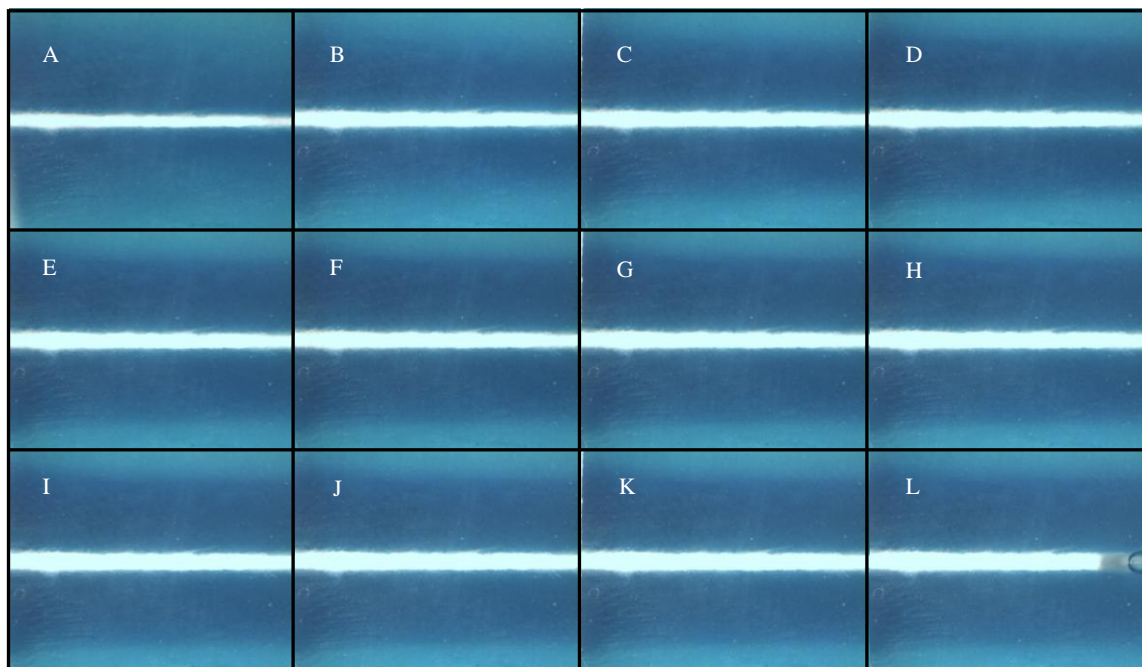
Figure D.7. Elution of methylene blue dye in Device B6 (70/30 0.000261 g/g soln) at various times. A.) Gel prior to water being pumped through the device. B.) after 1 h, C.) 2 h, D.) 3 h, E.) 4 h, F.) 5 h, G.) 6 h, H.) 7 h, I.) 8 h, J.) 9 h, K.) 10 h, and L.) 11 h.
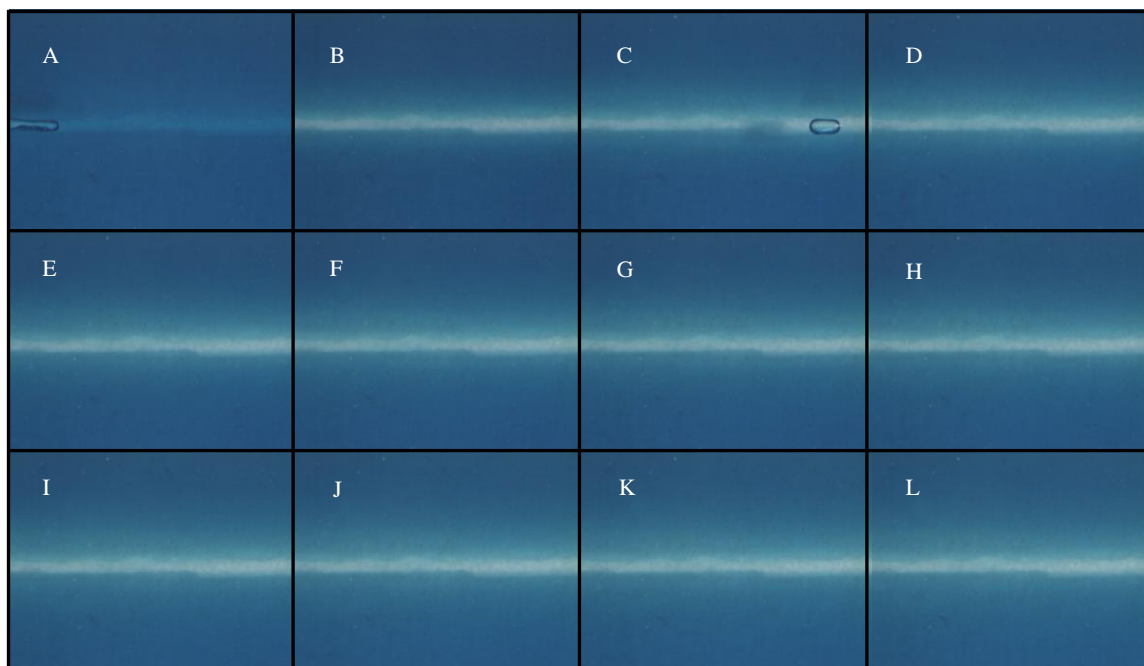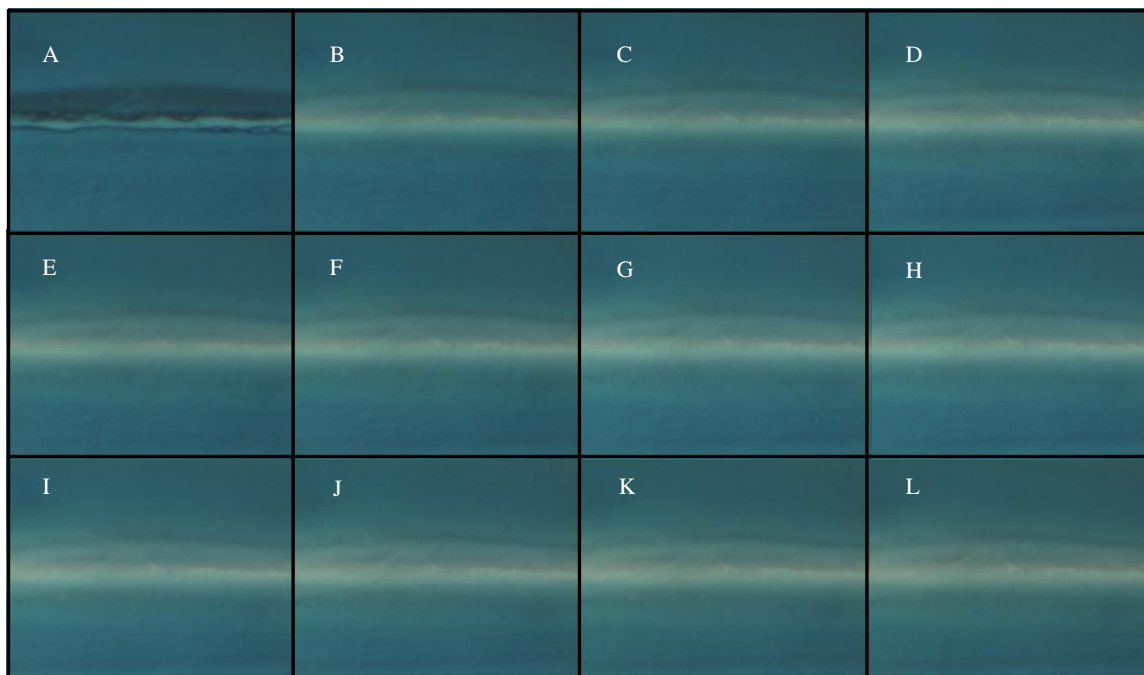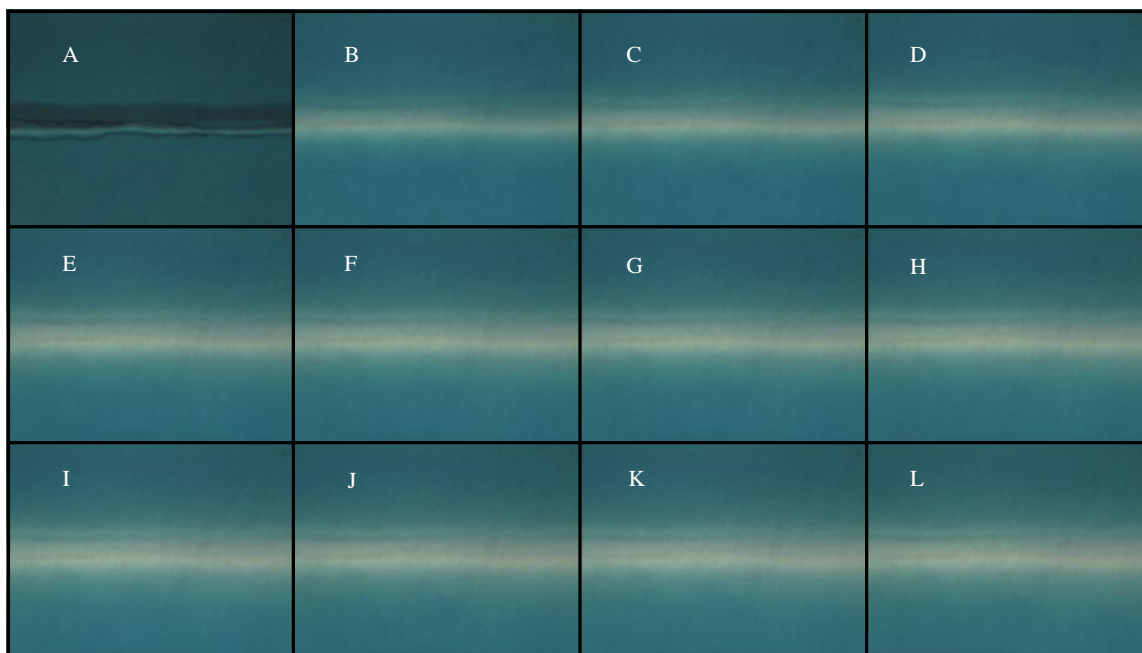
Figure D.8. Elution of methylene blue dye in Device B8 (70/30 0.000261 g/g soln) at various times. A.) Gel prior to water being pumped through the device. B.) after 1 h, C.) 2 h, D.) 3 h, E.) 4 h, F.) 5 h, G.) 6 h, H.) 7 h, I.) 8 h, J.) 9 h, K.) 10 h, and L.) 11 h.
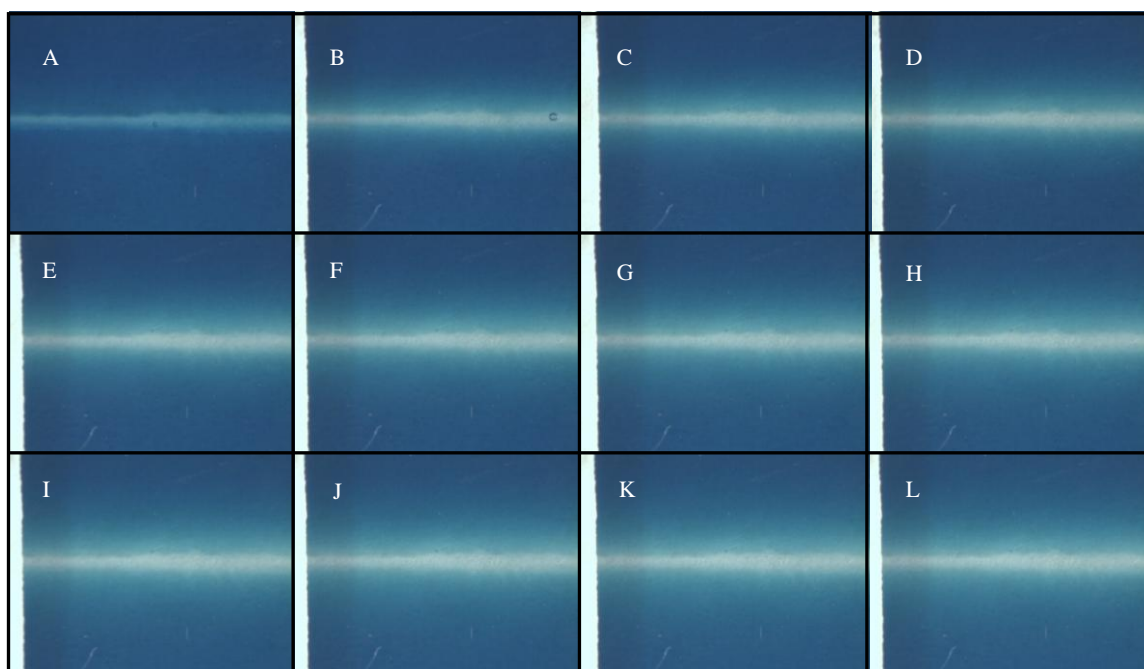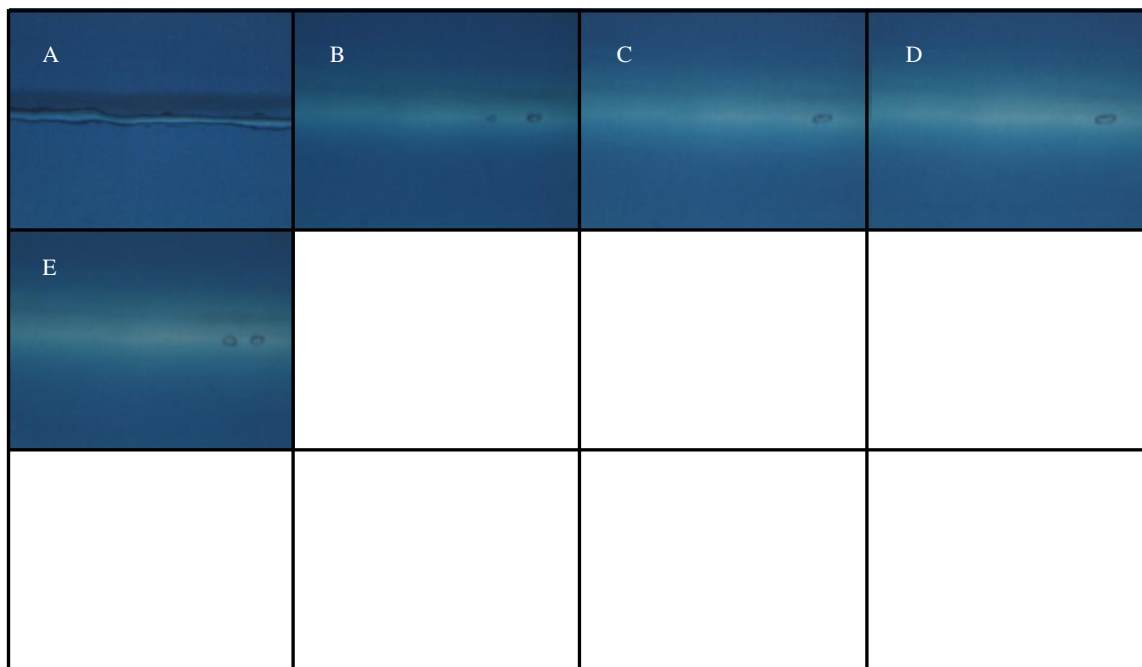

Figure D.9. Elution of methylene blue dye in Device B9 (70/30 0.000261 g/g soln) at various times. A.) Gel prior to water being pumped through the device. B.) after 1 h, C.) 2 h, D.) 3 h, E.) 4 h, F.) 5 h, G.) 6 h, H.) 7 h, I.) 8 h, J.) 9 h, K.) 10 h, and L.) 11 h.
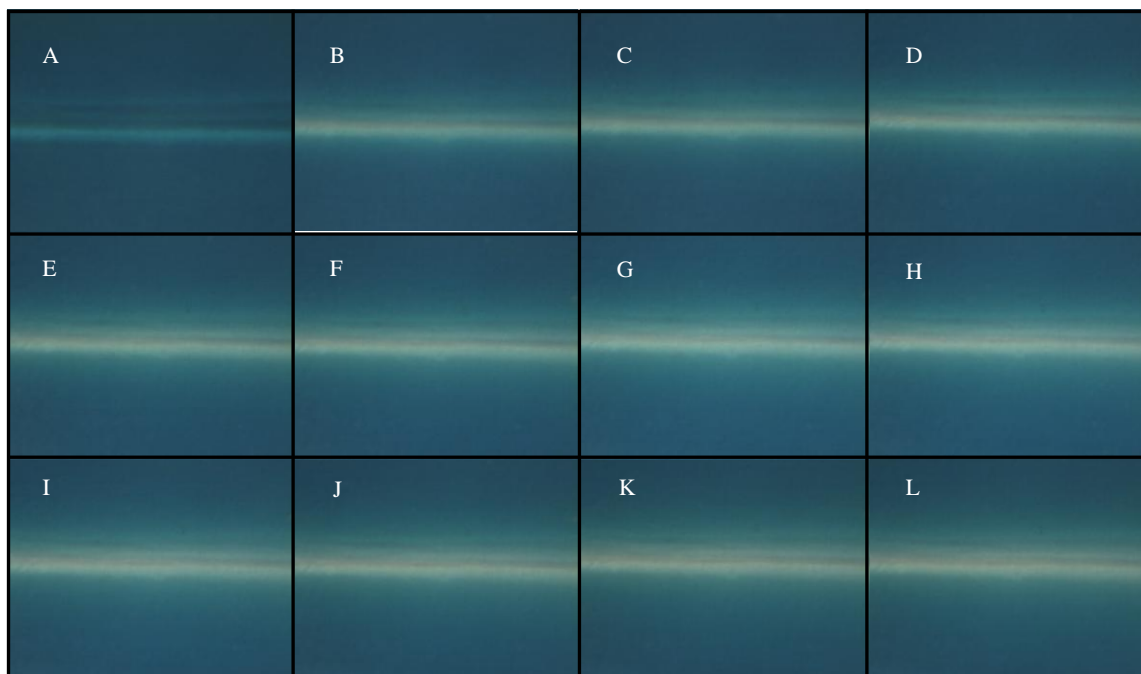
D.3 .70/30 Methylene Blue 1.5 wt%
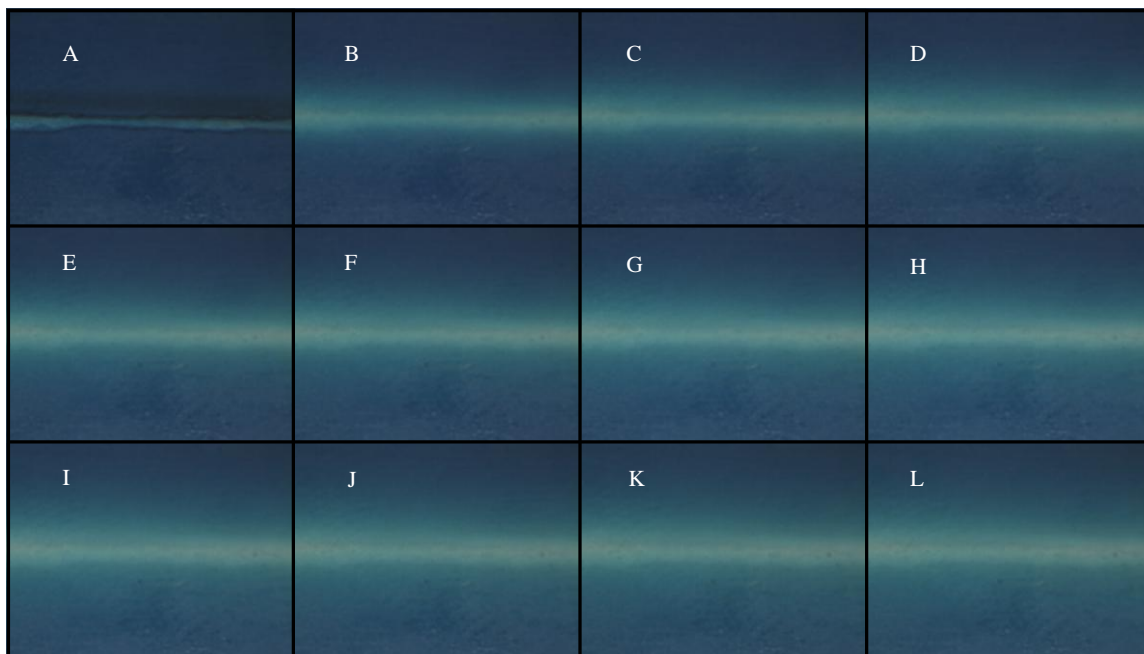
Figure D.10. Elution of methylene blue dye in Device B29 (70/30 0.00037 g/g soln) at various times. A.) Gel prior to water being pumped through the device. B.) after 1 h, C.) 2 h, D.) 3 h, E.) 4 h, F.) 5 h, G.) 6 h, H.) 7 h, I.) 8 h, J.) 9 h, K.) 10 h, and L.) 11 h.

Figure D.11. Elution of methylene blue dye in Device B30 (70/30 0.00037 g/g soln) at various times. A.) Gel prior to water being pumped through the device. B.) after 1 h, C.) 2 h, D.) 3 h, E.) 4 h, F.) 5 h, G.) 6 h, H.) 7 h, I.) 8 h, J.) 9 h, K.) 10 h, and L.) 11 h.
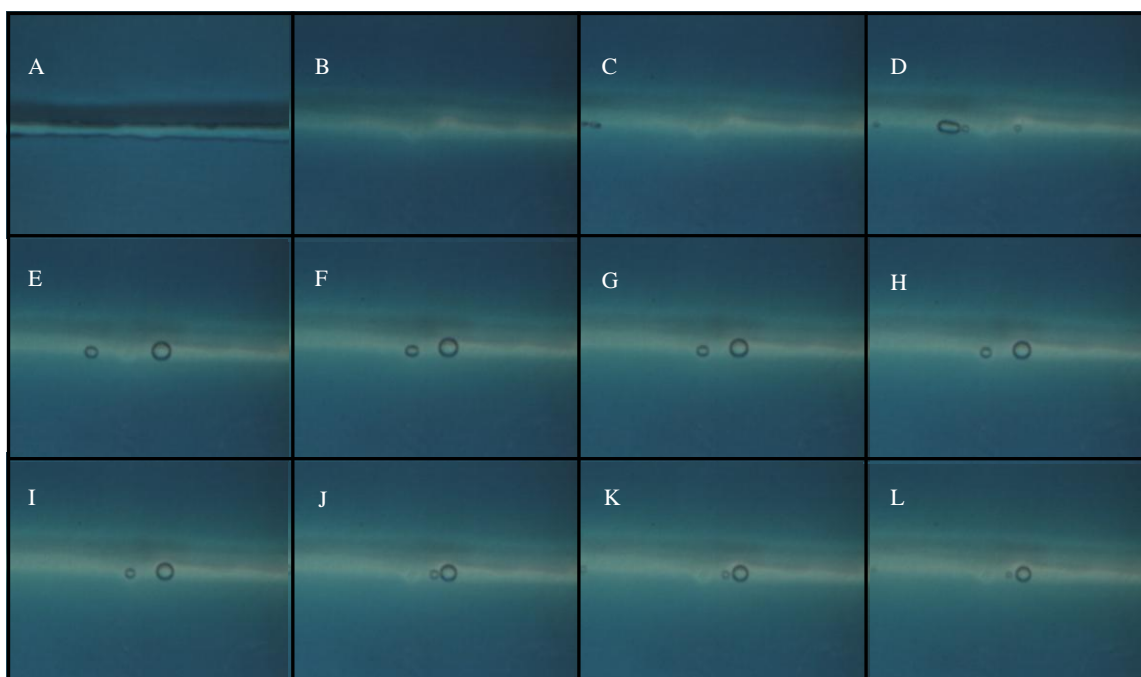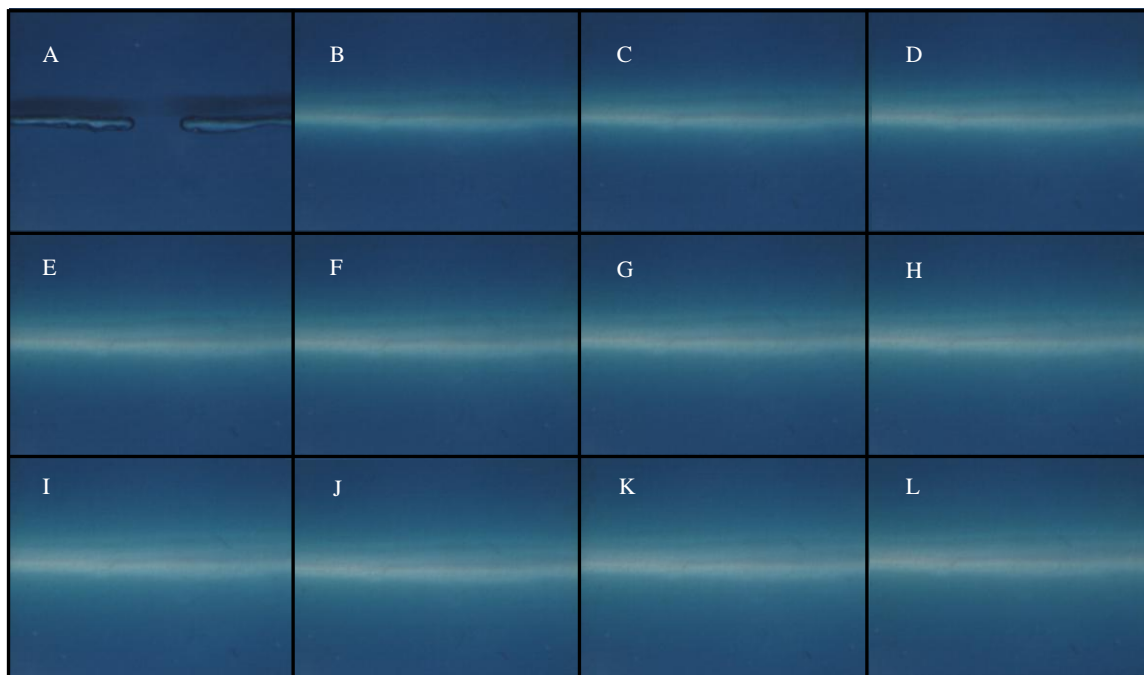

Figure D.12. Elution of methylene blue dye in Device B59 (70/30 0.00037 g/g soln) at various times. A.) Gel prior to water being pumped through the device. B.) after 1 h, C.) 2 h, D.) 3 h, E.) 4 h, F.) 5 h, G.) 6 h, H.) 7 h, I.) 8 h, J.) 9 h, K.) 10 h, and L.) 11 h.

Figure D.13. Elution of methylene blue dye in Device B60 (70/30 0.00037 g/g soln) at various times. A.) Gel prior to water being pumped through the device. B.) after 1 h, C.) 2 h, D.) 3 h, E.) 4 h, F.) 5 h, G.) 6 h, H.) 7 h, I.) 8 h, J.) 9 h, K.) 10 h, and L.) 11 h.
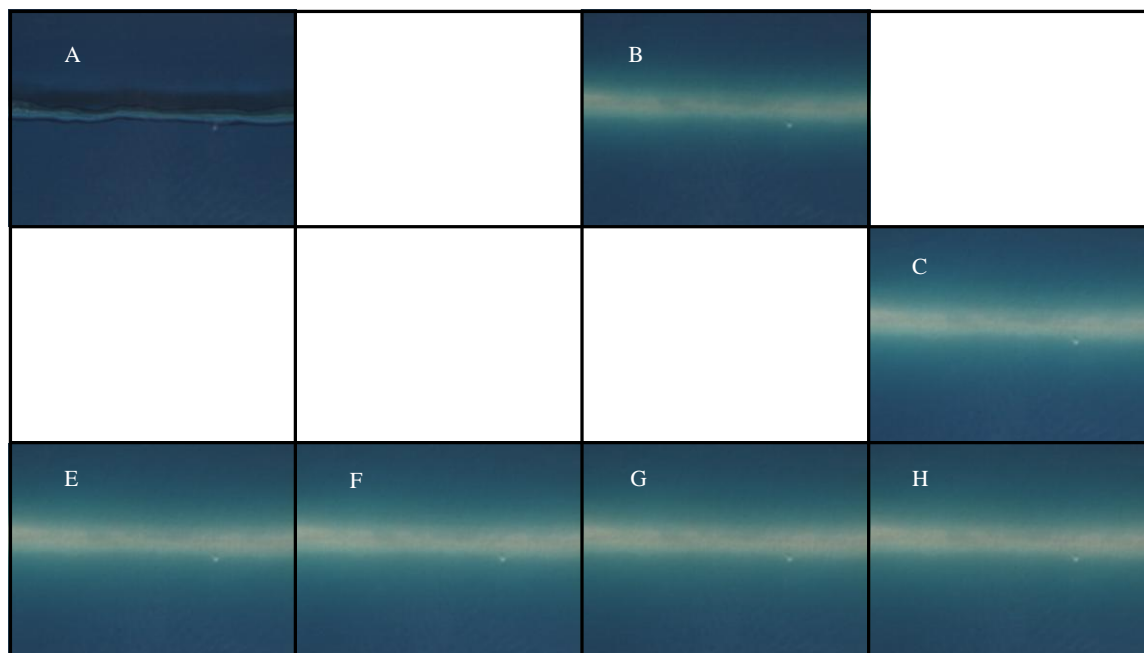

Figure D.14. Elution of methylene blue dye in Device B61 (70/30 0.00037 g/g soln) at various times. A.) Gel prior to water being pumped through the device. B.) after 1 h, C.) 2 h, D.) 3 h, E.) 4 h, F.) 5 h, G.) 6 h, H.) 7 h, I.) 8 h, J.) 9 h, K.) 10 h, and L.) 11 h.

D.4. 60/40 Methylene Blue 0.5 wt%

Figure D.15. Elution of methylene blue dye in Device B24 (60/40 0.0001 g/g soln) at various times. A.) Gel prior to water being pumped through the device. B.) after 1 h, C.) 2 h, D.) 3 h, E.) 4 h, F.) 5 h, G.) 6 h, H.) 7 h, I.) 8 h, J.) 9 h, K.) 10 h, and L.) 11 h.
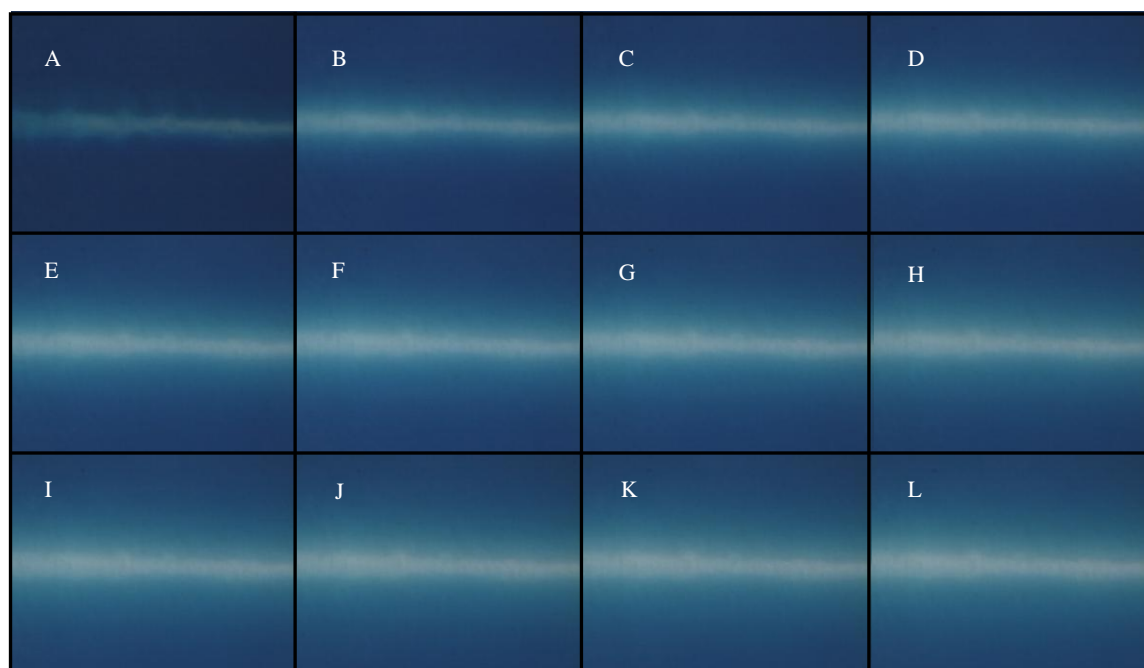
Figure D.16. Elution of methylene blue dye in Device B25 (60/40 0.0001 g/g soln) at various times. A.) Gel prior to water being pumped through the device. B.) after 1 h, C.) 2 h, D.) 3 h, E.) 4 h, F.) 5 h, G.) 6 h, H.) 7 h, I.) 8 h, J.) 9 h, K.) 10 h, and L.) 11 h.

D.5. 60/40 Methylene Blue 1.0 wt%

Figure D.17. Elution of methylene blue dye in Device B18 (60/40 0.000213 g/g soln) at various times. A.) Gel prior to water being pumped through the device. B.) after 1 h, C.) 2 h, D.) 3 h, E.) 4 h, F.) 5 h, G.) 6 h, H.) 7 h, I.) 8 h, J.) 9 h, K.) 10 h, and L.) 11 h.
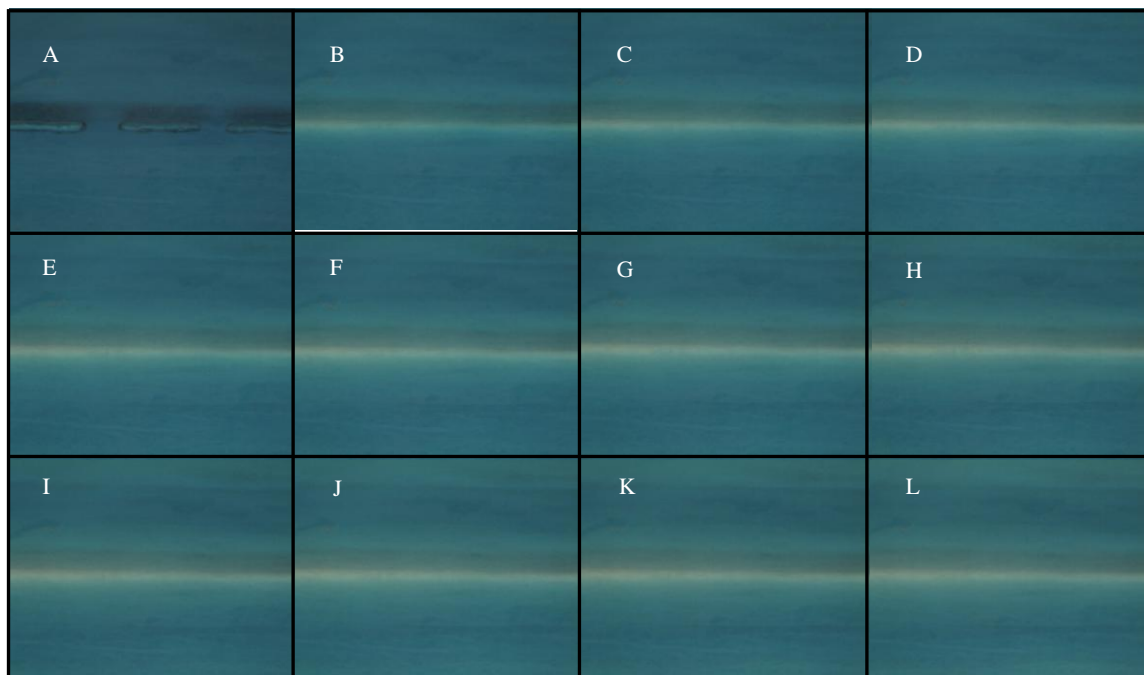
Figure D.18. Elution of methylene blue dye in Device B20 (60/40 0.000213 g/g soln) at various times. A.) Gel prior to water being pumped through the device. B.) after 1 h, C.) 2 h, D.) 3 h, E.) 4 h, F.) 5 h, G.) 6 h, H.) 7 h, I.) 8 h, J.) 9 h, K.) 10 h, and L.) 11 h.
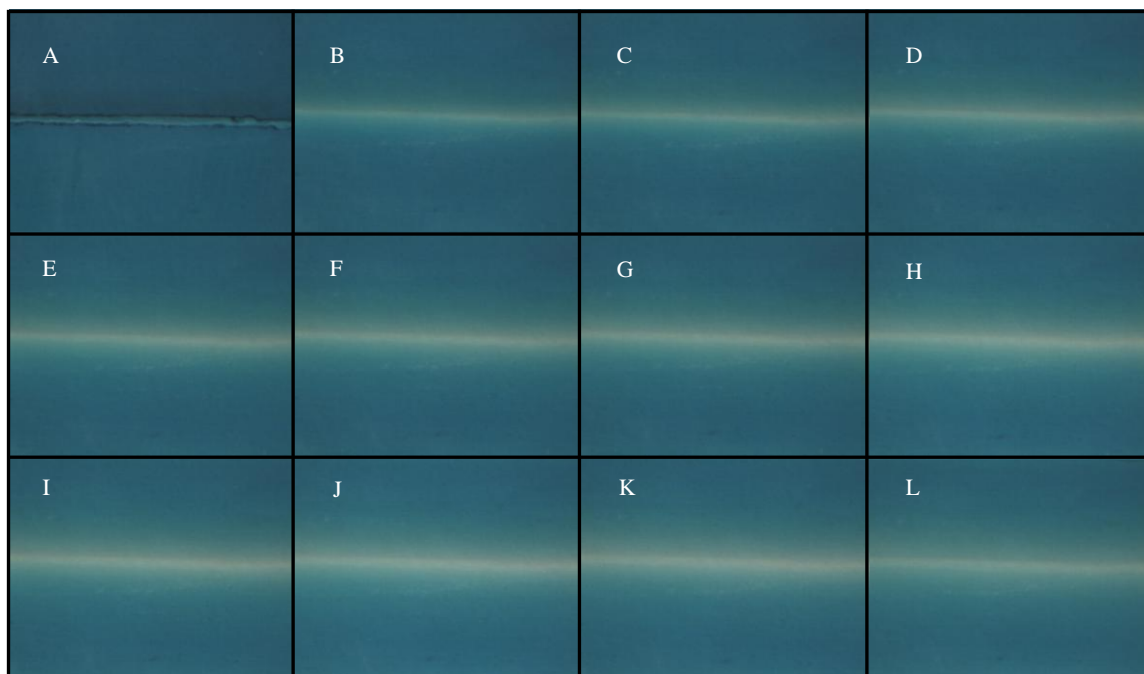

Figure D.19. Elution of methylene blue dye in Device B22 (60/40 0.000213 g/g soln) at various times. A.) Gel prior to water being pumped through the device. B.) after 1 h, C.) 2 h, D.) 3 h, E.) 4 h, F.) 5 h, G.) 6 h, H.) 7 h, I.) 8 h, J.) 9 h, K.) 10 h, and L.) 11 h.

D.6. 60/40 Methylene Blue 1.5 wt%

Figure D.20. Elution of methylene blue dye in Device B32 (60/40 0.00033 g/g soln) at various times. A.) Gel prior to water being pumped through the device. B.) after 1 h, C.) 2 h, D.) 3 h, E.) 4 h, F.) 5 h, G.) 6 h, H.) 7 h, I.) 8 h, J.) 9 h, K.) 10 h, and L.) 11 h.
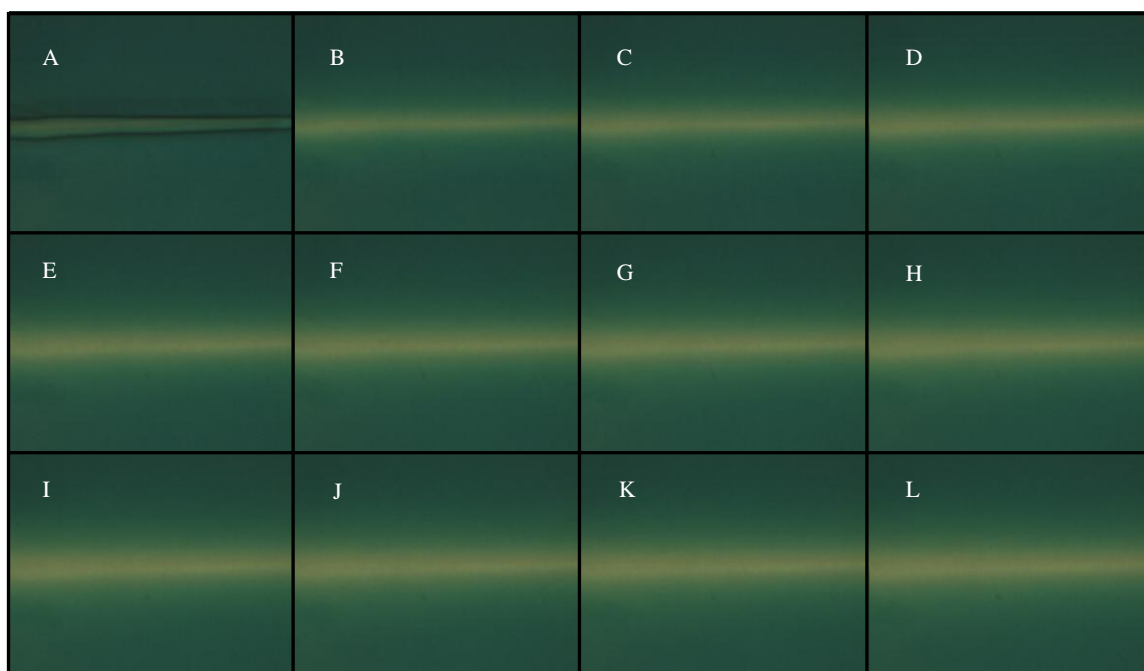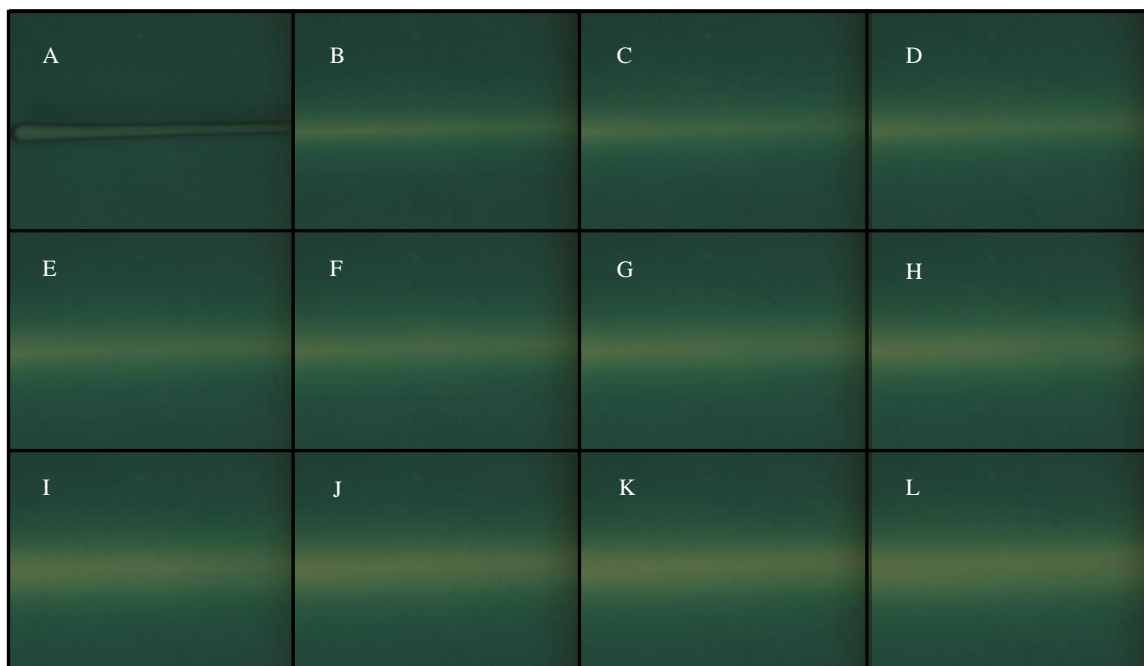
Figure D.21. Elution of methylene blue dye in Device B34 (60/40 0.00033 g/g soln) at various times. A.) Gel prior to water being pumped through the device. B.) after 1 h, C.) 2 h, D.) 3 h, E.) 4 h, F.) 5 h, G.) 6 h, H.) 7 h, I.) 8 h, J.) 9 h, K.) 10 h, and L.) 11 h.
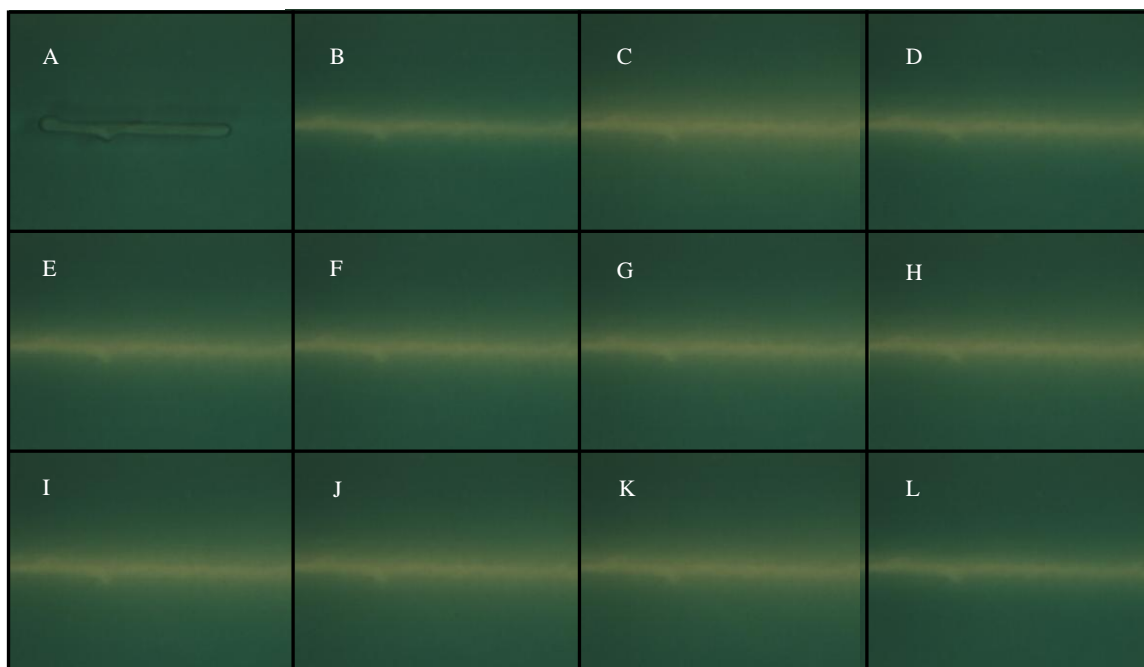

Figure D.22. Elution of methylene blue dye in Device B48 (60/40 0.00033 g/g soln) at various times. A.) Gel prior to water being pumped through the device. B.) after 1 h, C.) 2 h, D.) 3 h, E.) 4 h, F.) 5 h, G.) 6 h, H.) 7 h, I.) 8 h, J.) 9 h, K.) 10 h, and L.) 11 h.

D.7. 40/60 Methylene Blue 1.0 wt%

Figure D.23. Elution of methylene blue dye in Device B37 (40/60 0.00015 g/g soln) at various times. A.) Gel prior to water being pumped through the device. B.) after 1 h, C.) 2 h, D.) 3 h, E.) 4 h, F.) 5 h, G.) 6 h, H.) 7 h, I.) 8 h, J.) 9 h, K.) 10 h, and L.) 11 h.
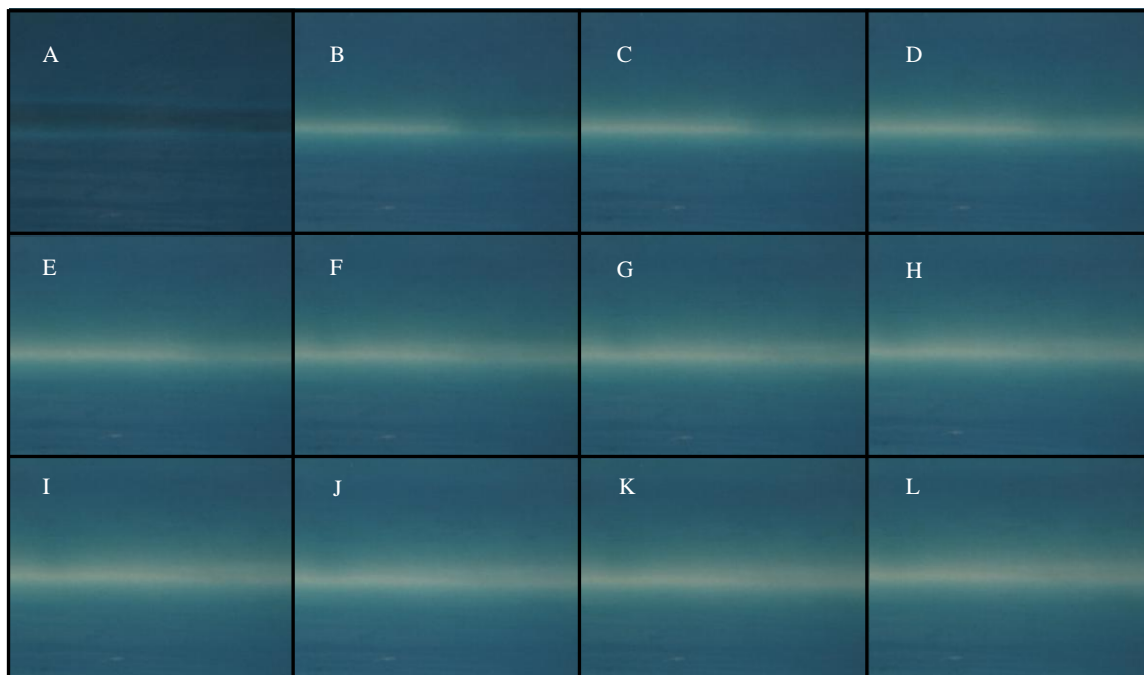
Figure D.24. Elution of methylene blue dye in Device B40 (40/60 0.00015 g/g soln) at various times. A.) Gel prior to water being pumped through the device. B.) after 1 h, C.) 2 h, D.) 3 h, E.) 4 h, F.) 5 h, G.) 6 h, H.) 7 h, I.) 8 h, J.) 9 h, K.) 10 h, and L.) 11 h.
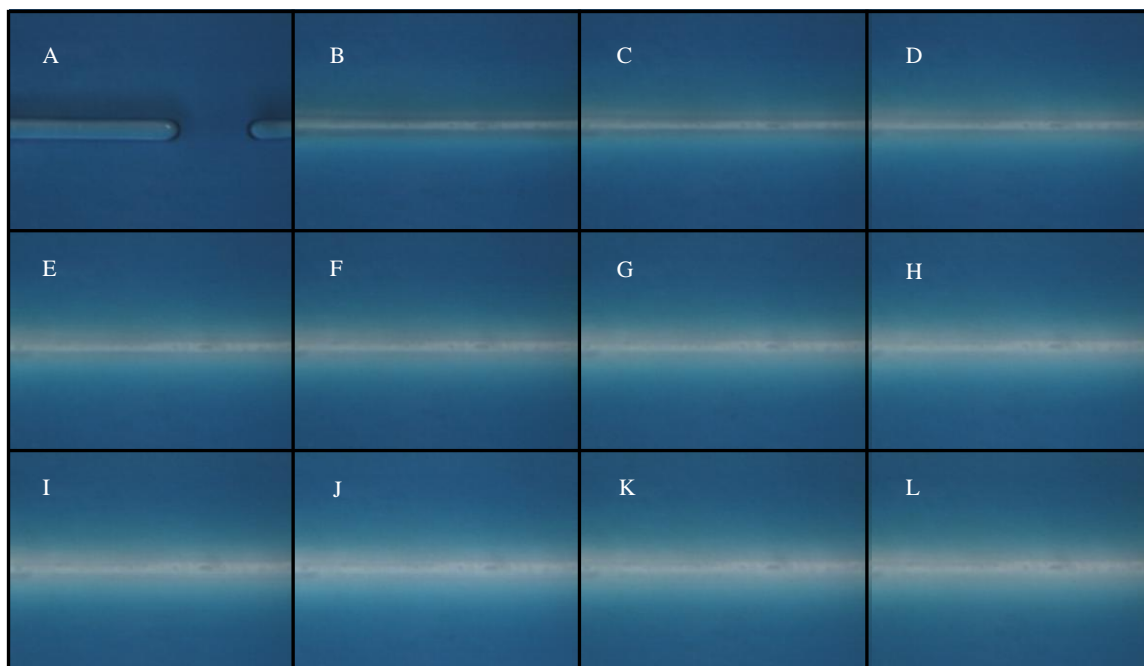

Figure D.25. Elution of methylene blue dye in Device B52 (40/60 0.00015 g/g soln) at various times. A.) Gel prior to water being pumped through the device. B.) after 1 h, C.) 2 h, D.) 3 h, E.) 4 h, F.) 5 h, G.) 6 h, H.) 7 h, I.) 8 h, J.) 9 h, K.) 10 h, and L.) 11 h.
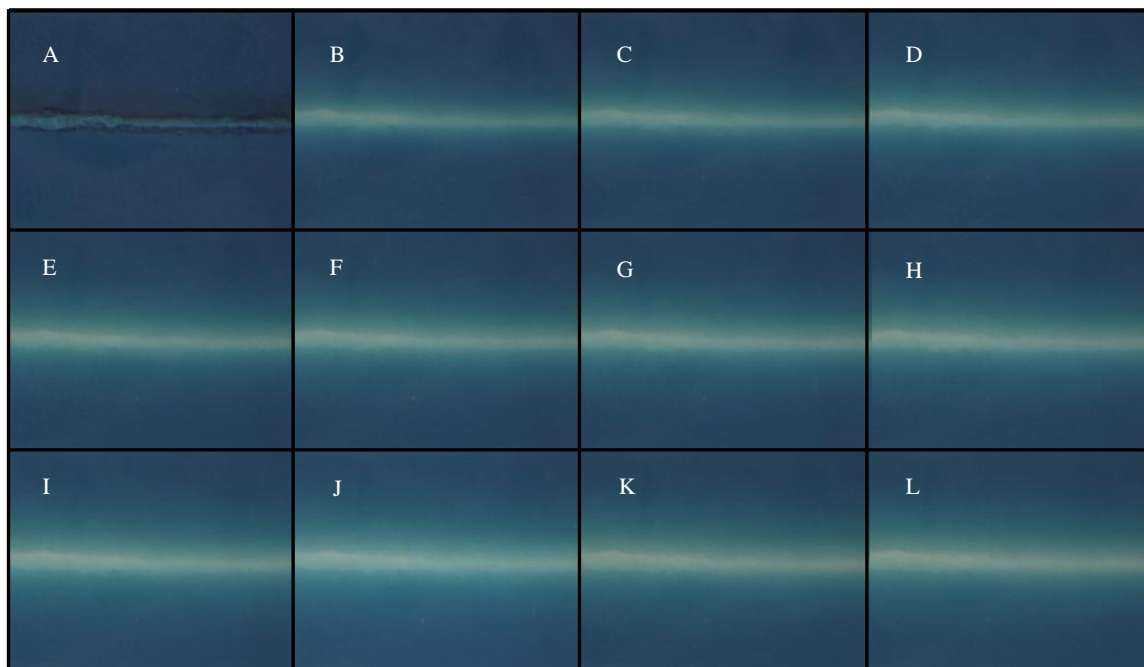
Figure D.26. Elution of methylene blue dye in Device B54 (40/60 0.00015 g/g soln) at various times. A.) Gel prior to water being pumped through the device. B.) after 1 h, C.) 2 h, D.) 3 h, E.) 4 h, F.) 5 h, G.) 6 h, H.) 7 h, I.) 8 h, J.) 9 h, K.) 10 h, and L.) 11 h.

Figure D.27. Elution of methylene blue dye in Device B55 (40/60 0.00015 g/g soln) at various times. A.) Gel prior to water being pumped through the device. B.) after 1 h, C.) 2 h, D.) 3 h, E.) 4 h, F.) 5 h, G.) 6 h, H.) 7 h, I.) 8 h, J.) 9 h, K.) 10 h, and L.) 11 h.
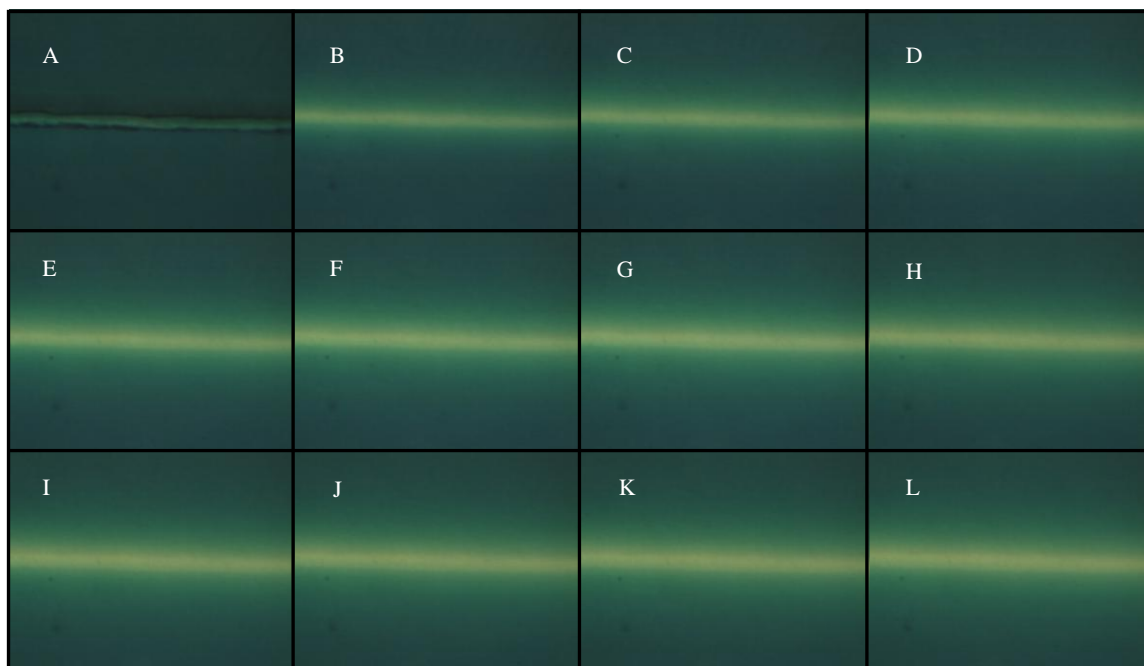
D. 8. 40/60 Methylene Blue 1.5 wt%

Figure D.28. Elution of methylene blue dye in Device B39 (40/60 0.00021 g/g soln) at various times. A.) Gel prior to water being pumped through the device. B.) after 1 h, C.) 2 h, D.) 3 h, E.) 4 h, F.) 5 h, G.) 6 h, H.) 7 h, I.) 8 h, J.) 9 h, K.) 10 h, and L.) 11 h.
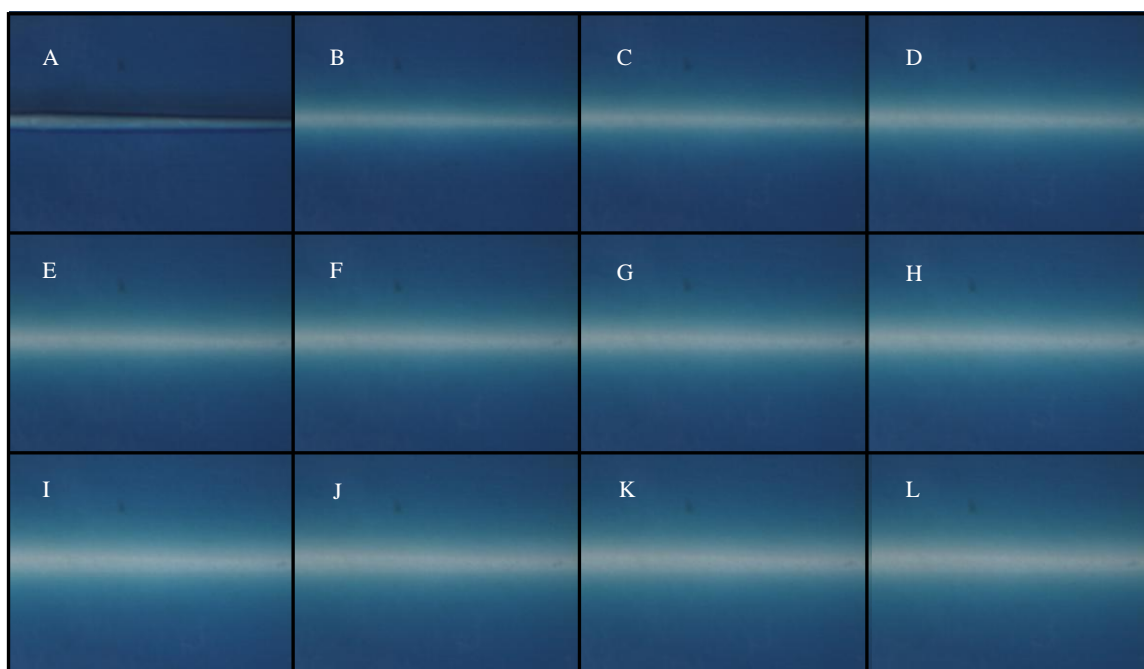
Figure D.29. Elution of methylene blue dye in Device B47 (40/60 0.00021 g/g soln) at various times. A.) Gel prior to water being pumped through the device. B.) after 1 h, C.) 2 h, D.) 3 h, E.) 4 h, F.) 5 h, G.) 6 h, H.) 7 h, I.) 8 h, J.) 9 h, K.) 10 h, and L.) 11 h.
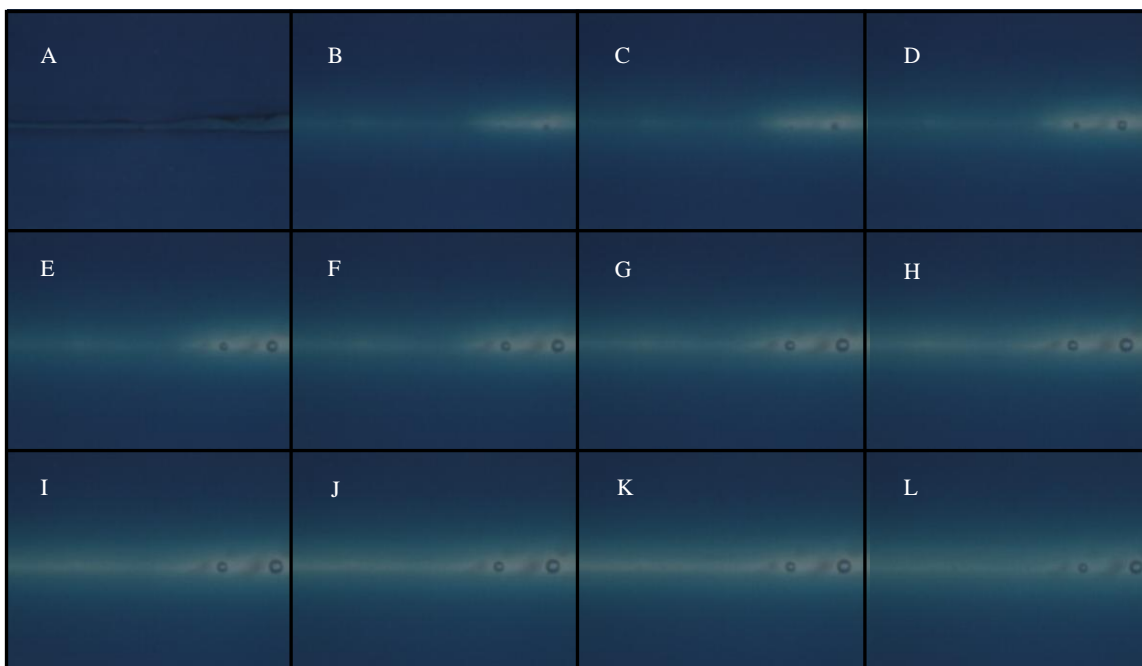
D.9 40/60 Methylene Blue 2.0 wt%

Figure D.30. Elution of methylene blue dye in Device B44 (40/60 0.00029 g/g soln) at various times. A.) Gel prior to water being pumped through the device. B.) after 1 h, C.) 2 h, D.) 3 h, E.) 4 h, F.) 5 h, G.) 6 h, H.) 7 h, I.) 8 h, J.) 9 h, K.) 10 h, and L.) 11 h.
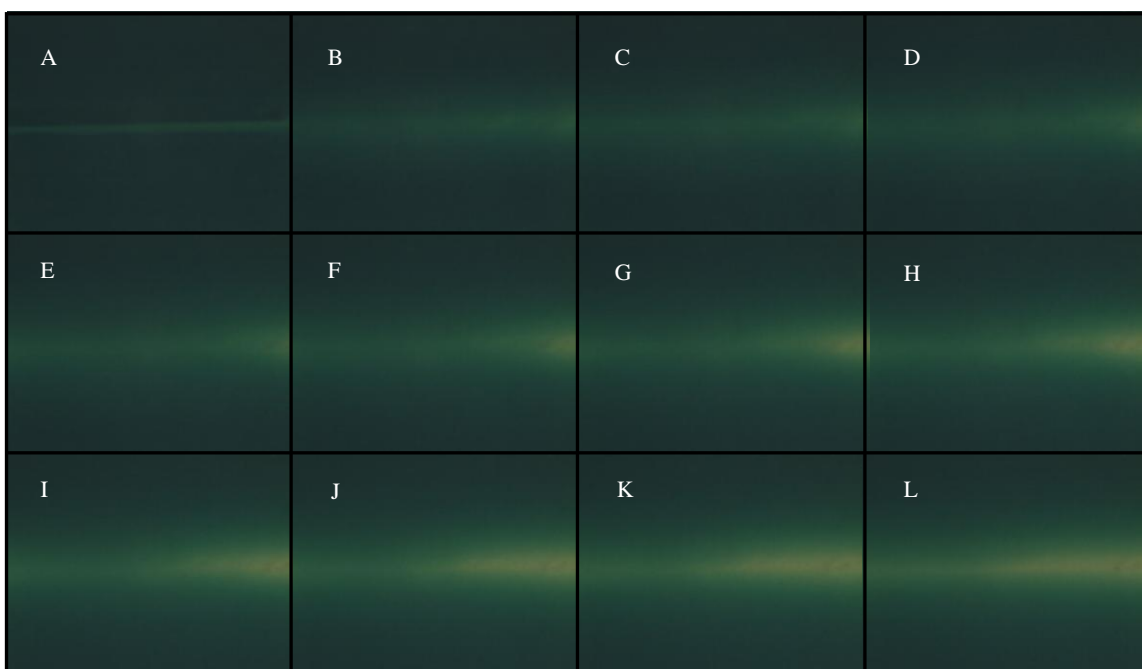
Figure D.31. Elution of methylene blue dye in Device B45 (40/60 0.00029 g/g soln) at various times. A.) Gel prior to water being pumped through the device. B.) after 1 h, C.) 2 h, D.) 3 h, E.) 4 h, F.) 5 h, G.) 6 h, H.) 7 h, I.) 8 h, J.) 9 h, K.) 10 h, and L.) 11 h.

Figure D.32. Elution of methylene blue dye in Device B46 (40/60 0.00029 g/g soln) at various times. A.) Gel prior to water being pumped through the device. B.) after 1 h, C.) 2 h, D.) 3 h, E.) 4 h, F.) 5 h, G.) 6 h, H.) 7 h, I.) 8 h, J.) 9 h, K.) 10 h, and L.) 11 h.
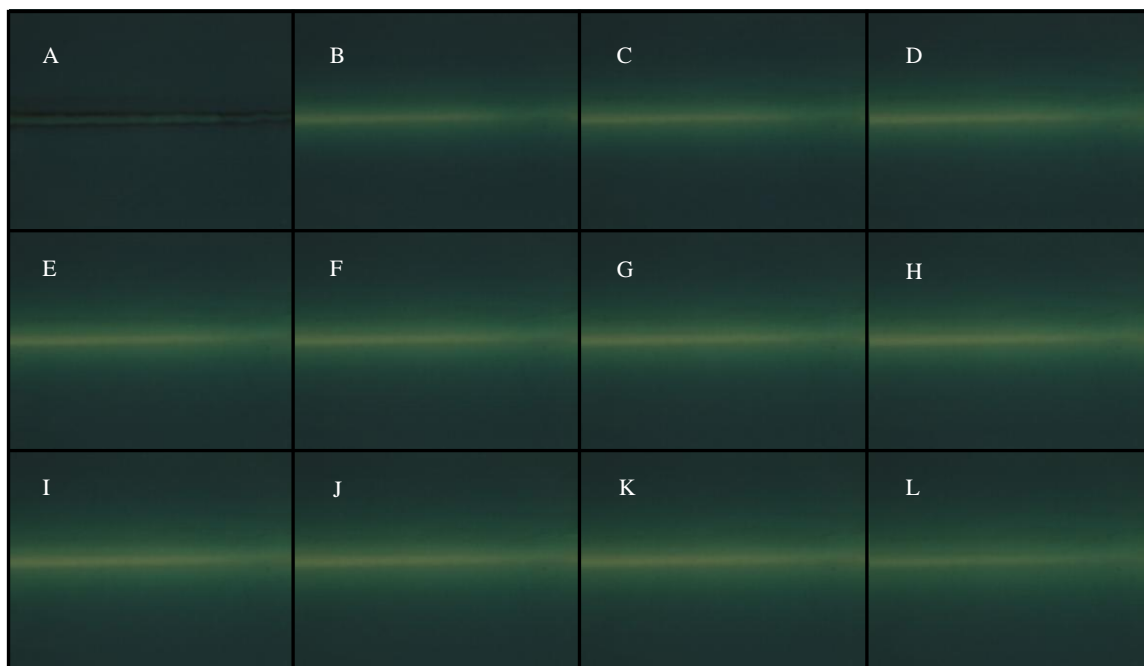
Figure D.33. Elution of methylene blue dye in Device B49 (40/60 0.00029 g/g soln) at various times. A.) Gel prior to water being pumped through the device. B.) after 1 h, C.) 2 h, D.) 3 h, E.) 4 h, F.) 5 h, G.) 6 h, H.) 7 h, I.) 8 h, J.) 9 h, K.) 10 h, and L.) 11 h.

Figure D.34. Elution of methylene blue dye in Device B50 (40/60 0.00029 g/g soln) at various times. A.) Gel prior to water being pumped through the device. B.) after 1 h, C.) 2 h, D.) 3 h, E.) 4 h, F.) 5 h, G.) 6 h, H.) 7 h, I.) 8 h, J.) 9 h, K.) 10 h, and L.) 11 h.
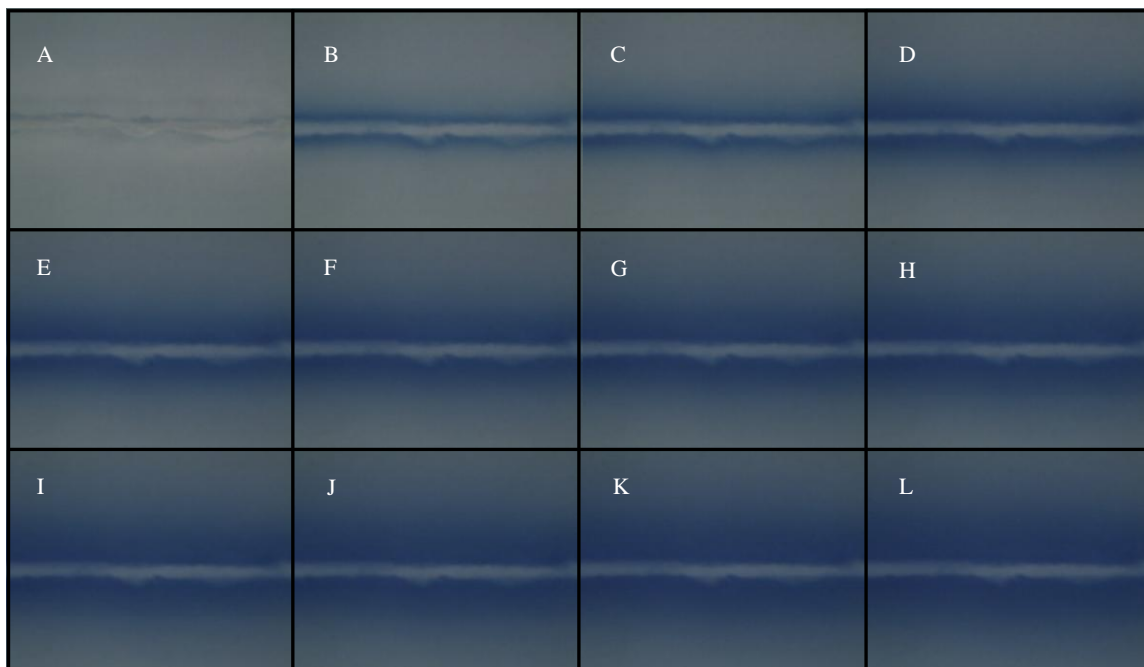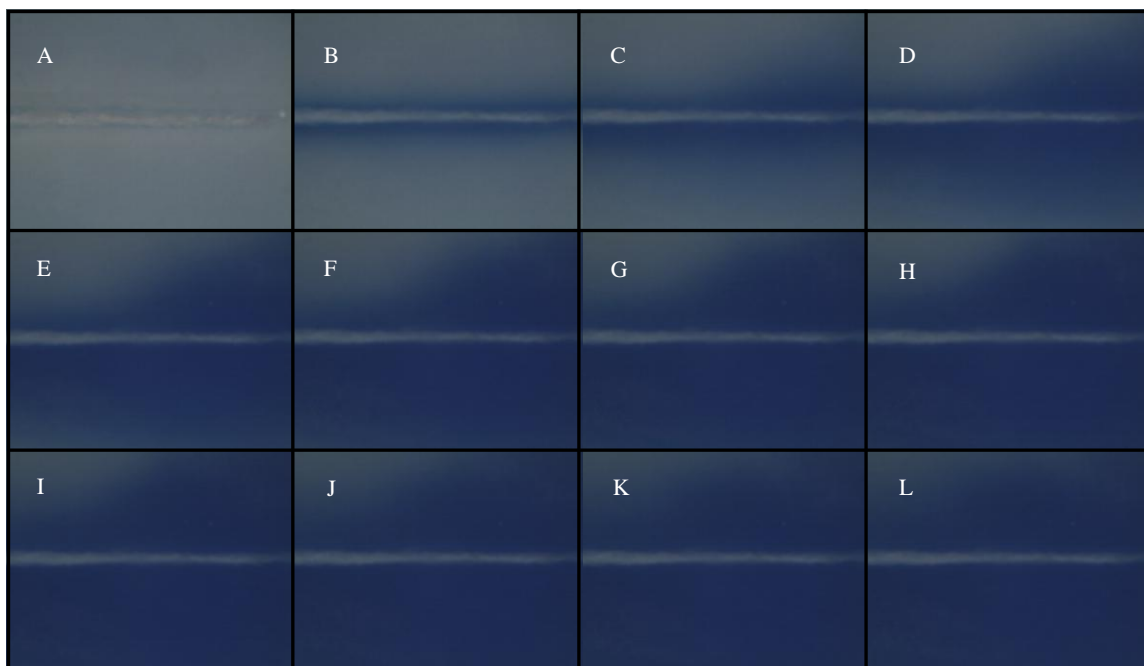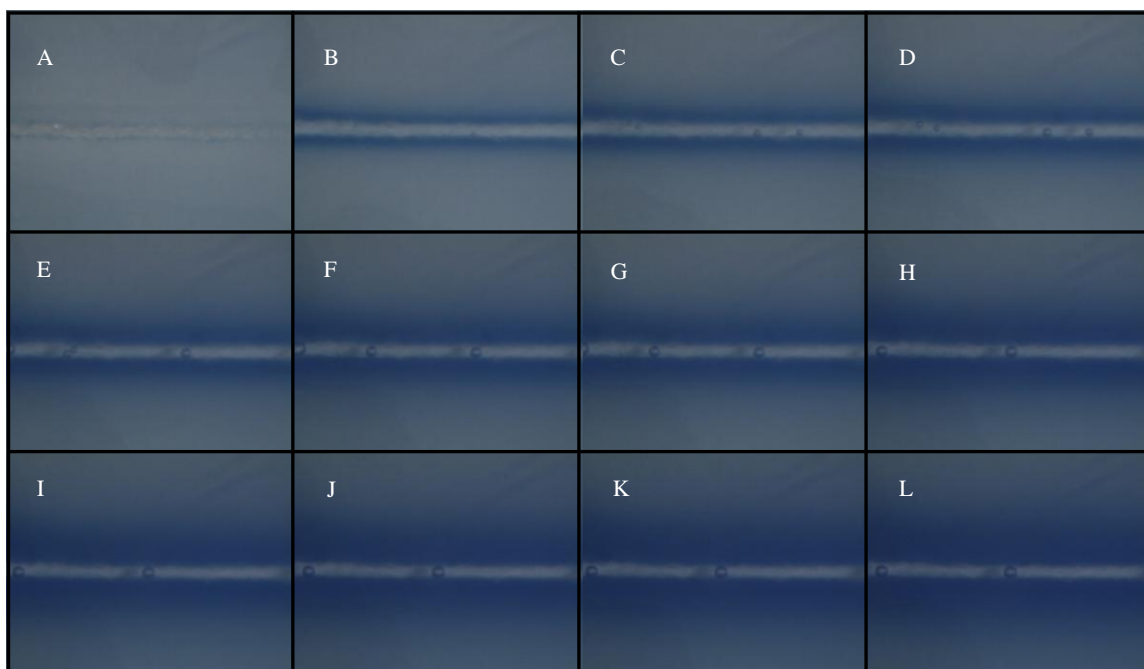
Figure D.35. Elution of methylene blue dye in Device B51 (40/60 0.00029 g/g soln) at various times. A.) Gel prior to water being pumped through the device. B.) after 1 h, C.) 2 h, D.) 3 h, E.) 4 h, F.) 5 h, G.) 6 h, H.) 7 h, I.) 8 h, J.) 9 h, K.) 10 h, and L.) 11 h.

D.10. 70/30 Acid Blue 22 0.5wt%

Figure D.36. Elution of acid blue 22 dye in Device A16 (70/30 0.00025 g/g soln) at various times. A.) Gel prior to water being pumped through the device. B.) after 1 h, C.) 2 h, D.) 3 h, E.) 4 h, F.) 5 h, G.) 6 h, H.) 7 h, I.) 8 h, J.) 9 h, K.) 10 h, and L.) 11 h.

Figure D.37. Elution of acid blue 22 dye in Device A17 (70/30 0.00025 g/g soln) at various times. A.) Gel prior to water being pumped through the device. B.) after 1 h, C.) 2 h, D.) 3 h, E.) 4 h, F.) 5 h, G.) 6 h, H.) 7 h, I.) 8 h, J.) 9 h, K.) 10 h, and L.) 11 h.
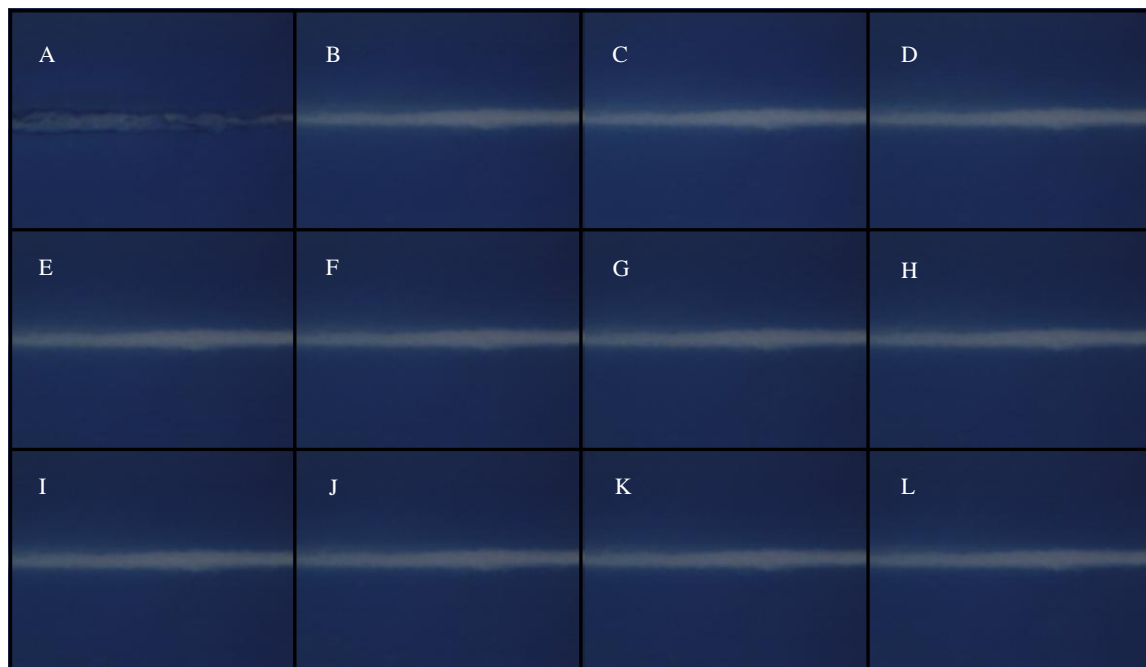

Figure D.38. Elution of acid blue 22 dye in Device A18 (70/30 0.00025 g/g soln) at various times. A.) Gel prior to water being pumped through the device. B.) after 1 h, C.) 2 h, D.) 3 h, E.) 4 h, F.) 5 h, G.) 6 h, H.) 7 h, I.) 8 h, J.) 9 h, K.) 10 h, and L.) 11 h.

D.11. 70/30 Acid Blue 22 1.0 wt%

Figure D.39. Elution of acid blue 22 dye in Device A22 (70/30 0.00049 g/g soln) at various times. A.) Gel prior to water being pumped through the device. B.) after 1 h, C.) 2 h, D.) 3 h, E.) 4 h, F.) 5 h, G.) 6 h, H.) 7 h, I.) 8 h, J.) 9 h, K.) 10 h, and L.) 11 h.

Figure D.40. Elution of acid blue 22 dye in Device A23 (70/30 0.00049 g/g soln) at various times. A.) Gel prior to water being pumped through the device. B.) after 1 h, C.) 2 h, D.) 3 h, E.) 4 h, F.) 5 h, G.) 6 h, H.) 7 h, I.) 8 h, J.) 9 h, K.) 10 h, and L.) 11 h.

Figure D.41. Elution of acid blue 22 dye in Device A24 (70/30 0.00049 g/g soln) at various times. A.) Gel prior to water being pumped through the device. B.) after 1 h, C.) 2 h, D.) 3 h, E.) 4 h, F.) 5 h, G.) 6 h, H.) 7 h, I.) 8 h, J.) 9 h, K.) 10 h, and L.) 11 h.

D.12. 70/30 Acid Blue 22 1.5 wt%

Figure D.42. Elution of acid blue 22 dye in Device A25 (70/30 0.00074 g/g soln) at various times. A.) Gel prior to water being pumped through the device. B.) after 1 h, C.) 2 h, D.) 3 h, E.) 4 h, F.) 5 h, G.) 6 h, H.) 7 h, I.) 8 h, J.) 9 h, K.) 10 h, and L.) 11 h.
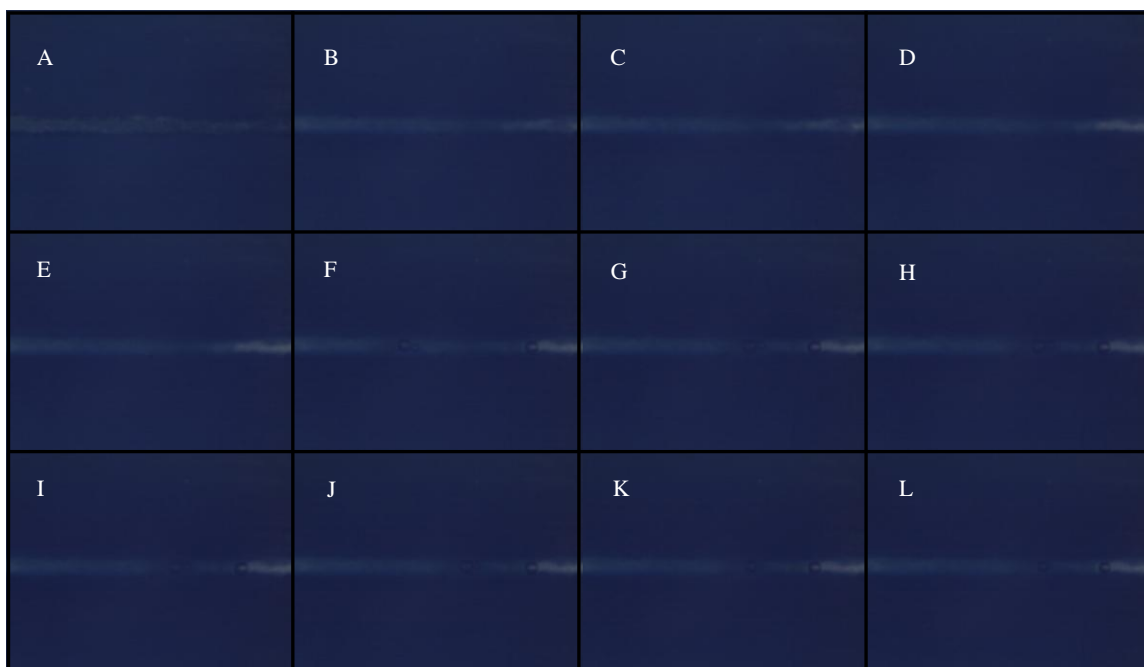
Figure D.43. Elution of acid blue 22 dye in Device A26 (70/30 0.00074 g/g soln) at various times. A.) Gel prior to water being pumped through the device. B.) after 1 h, C.) 2 h, D.) 3 h, E.) 4 h, F.) 5 h, G.) 6 h, H.) 7 h, I.) 8 h, J.) 9 h, K.) 10 h, and L.) 11 h.
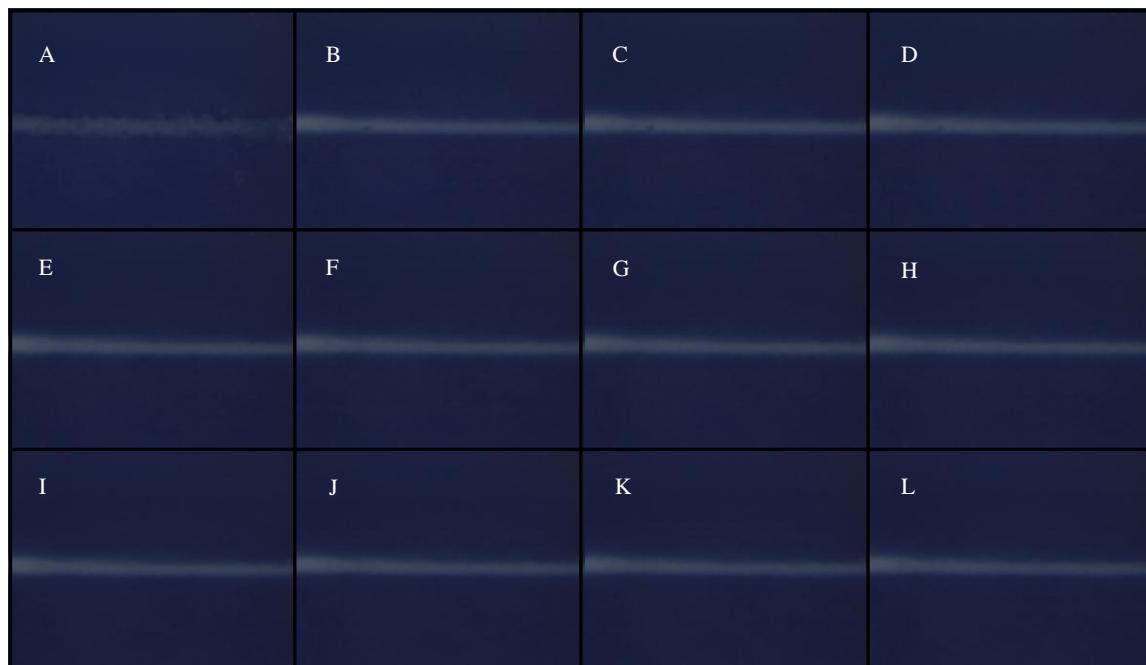

Figure D.44. Elution of acid blue 22 dye in Device A27 (70/30 0.00074 g/g soln) at various times. A.) Gel prior to water being pumped through the device. B.) after 1 h, C.) 2 h, D.) 3 h, E.) 4 h, F.) 5 h, G.) 6 h, H.) 7 h, I.) 8 h, J.) 9 h, K.) 10 h, and L.) 11 h.

D.13. 60/40 Acid Blue 22 0.5 wt%

Figure D.45. Elution of acid blue 22 dye in Device A13 (60/40 0.00021 g/g soln) at various times. A.) Gel prior to water being pumped through the device. B.) after 1 h, C.) 2 h, D.) 3 h, E.) 4 h, F.) 5 h, G.) 6 h, H.) 7 h, I.) 8 h, J.) 9 h, K.) 10 h, and L.) 11 h.
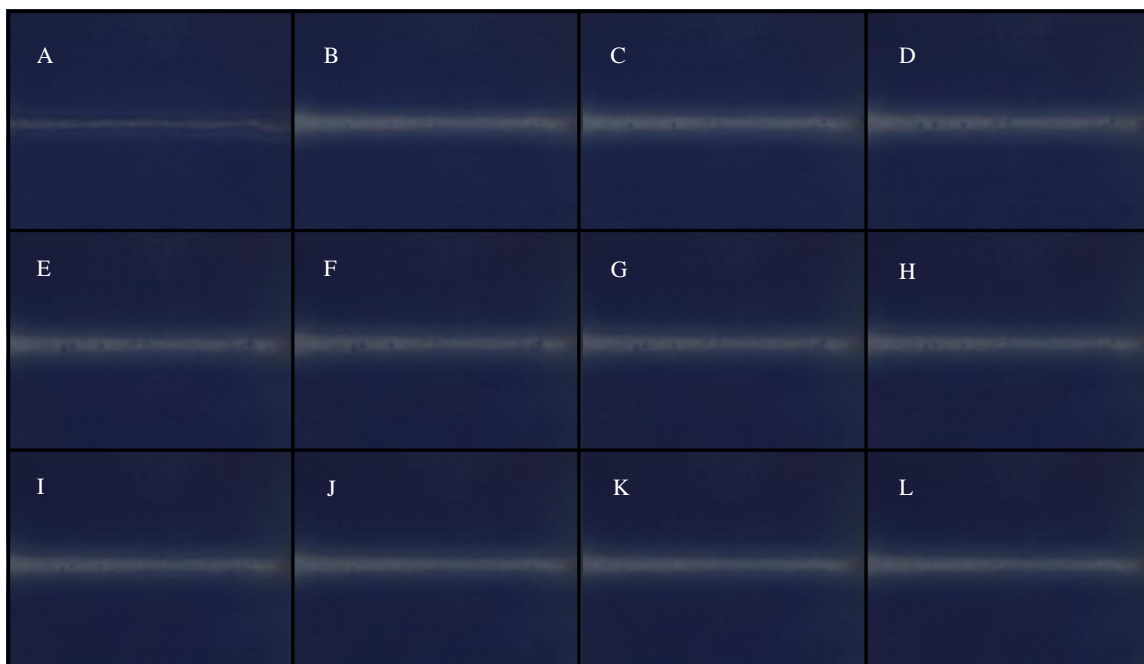
Figure D.46. Elution of acid blue 22 dye in Device A14 (60/40 0.00021 g/g soln) at various times. A.) Gel prior to water being pumped through the device. B.) after 1 h, C.) 2 h, D.) 3 h, E.) 4 h, F.) 5 h, G.) 6 h, H.) 7 h, I.) 8 h, J.) 9 h, K.) 10 h, and L.) 11 h.
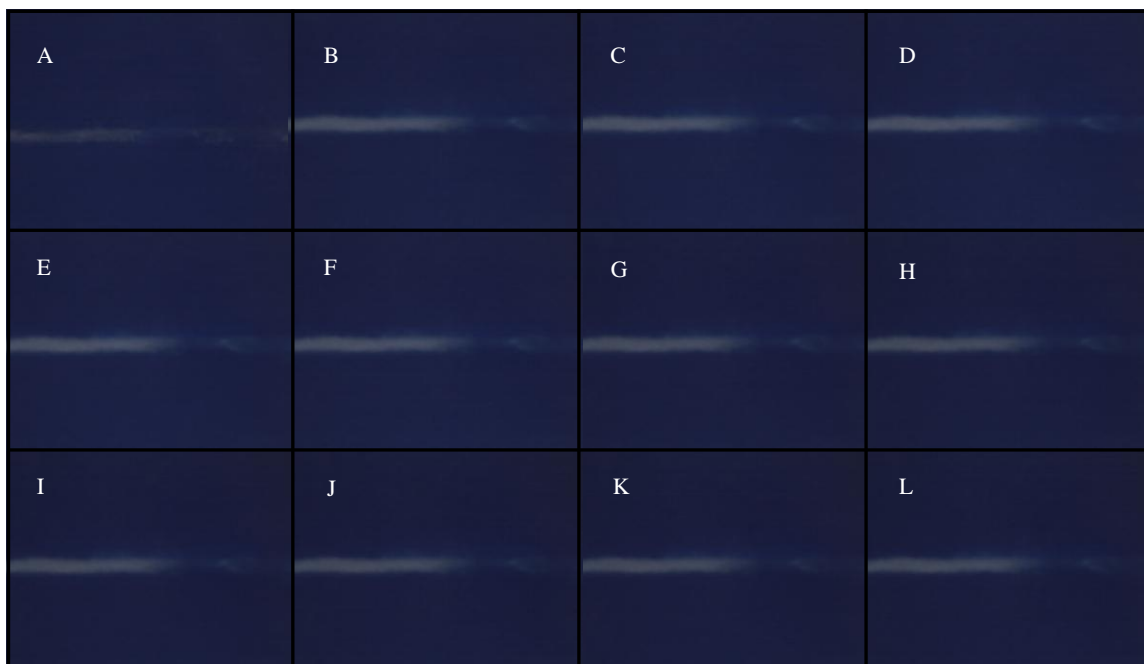

Figure D.47. Elution of acid blue 22 dye in Device A15 (60/40 0.00021 g/g soln) at various times. A.) Gel prior to water being pumped through the device. B.) after 1 h, C.) 2 h, D.) 3 h, E.) 4 h, F.) 5 h, G.) 6 h, H.) 7 h, I.) 8 h, J.) 9 h, K.) 10 h, and L.) 11 h.
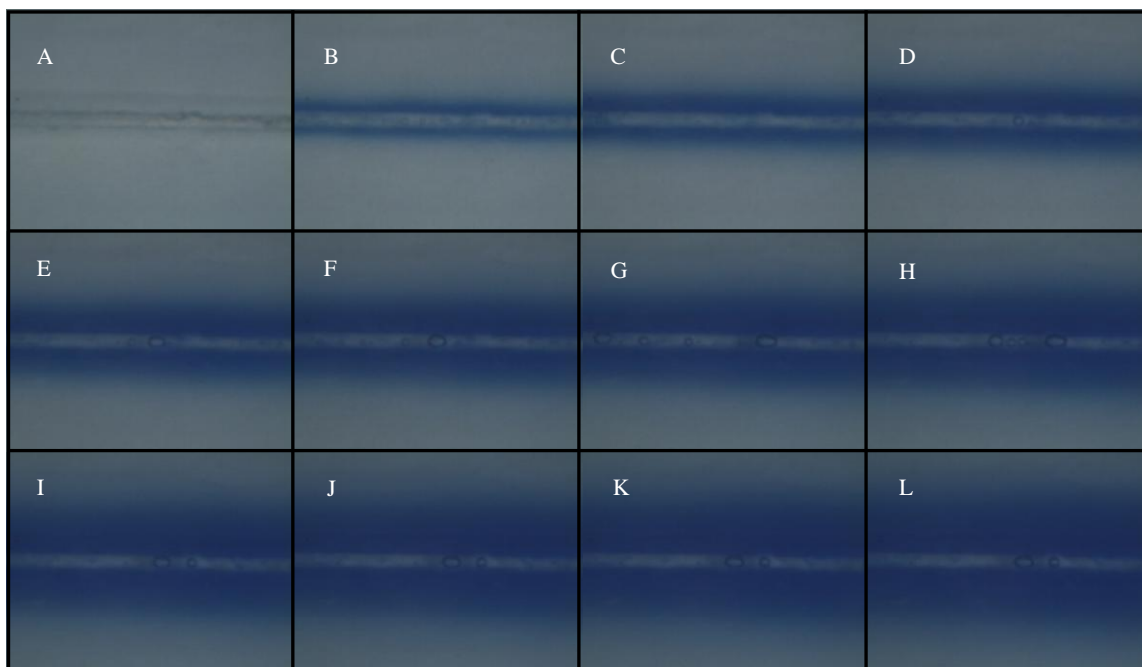
D.14. 60/40 Acid Blue 22 1.0 wt%

Figure D.48. Elution of acid blue 22 dye in Device A10 (60/40 0.00042 g/g soln) at various times. A.) Gel prior to water being pumped through the device. B.) after 1 h, C.) 2 h, D.) 3 h, E.) 4 h, F.) 5 h, G.) 6 h, H.) 7 h, I.) 8 h, J.) 9 h, K.) 10 h, and L.) 11 h.

Figure D.49. Elution of acid blue 22 dye in Device A11 (60/40 0.00042 g/g soln) at various times. A.) Gel prior to water being pumped through the device. B.) after 1 h, C.) 2 h, D.) 3 h, E.) 4 h, F.) 5 h, G.) 6 h, H.) 7 h, I.) 8 h, J.) 9 h, K.) 10 h, and L.) 11 h.
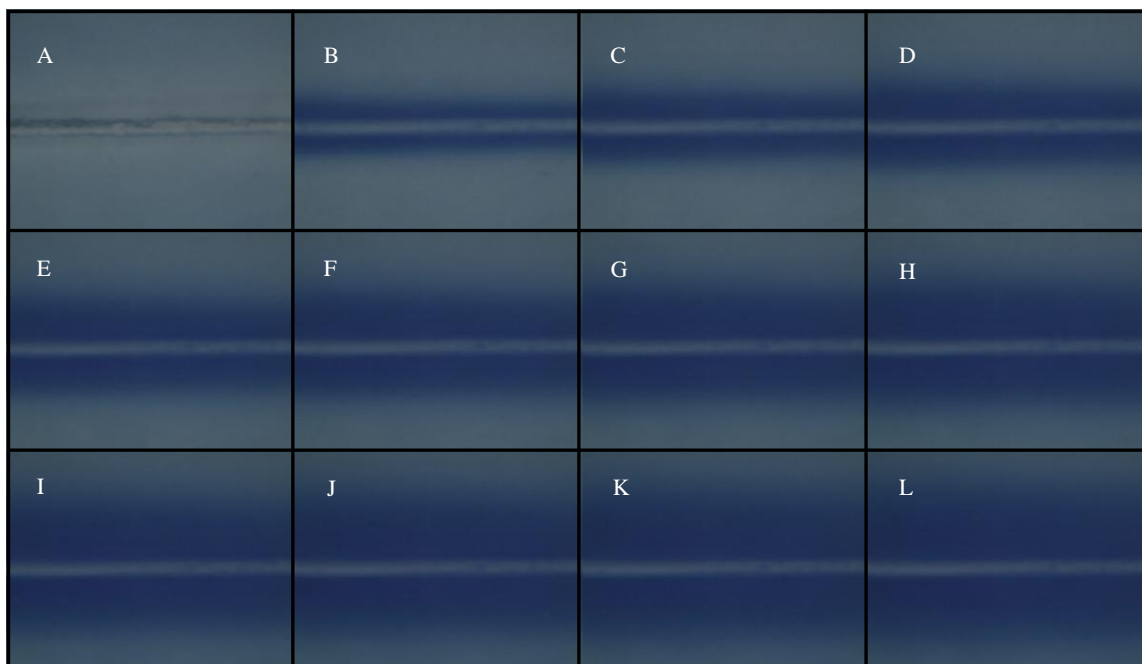

Figure D.50. Elution of acid blue 22 dye in Device A12 (60/40 0.00042 g/g soln) at various times. A.) Gel prior to water being pumped through the device. B.) after 1 h, C.) 2 h, D.) 3 h, E.) 4 h, F.) 5 h, G.) 6 h, H.) 7 h, I.) 8 h, J.) 9 h, K.) 10 h, and L.) 11 h.
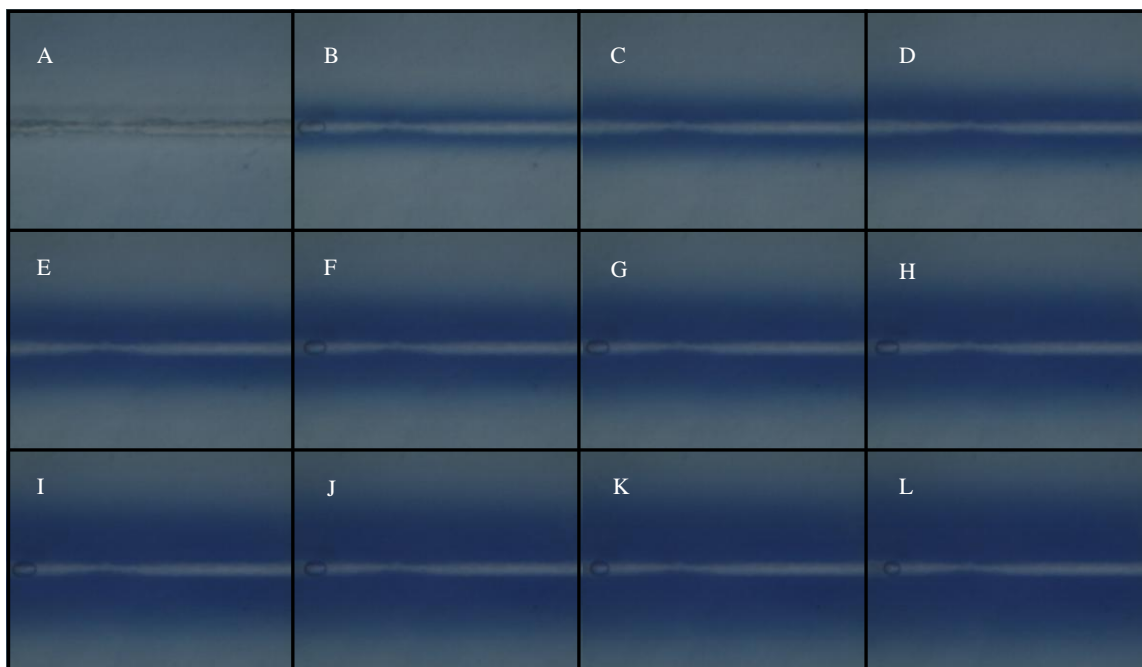
D.15. 60/40 Acid Blue 22 1.5 wt%

Figure D.51. Elution of acid blue 22 dye in Device A19 (60/40 0.00064 g/g soln) at various times. A.) Gel prior to water being pumped through the device. B.) after 1 h, C.) 2 h, D.) 3 h, E.) 4 h, F.) 5 h, G.) 6 h, H.) 7 h, I.) 8 h, J.) 9 h, K.) 10 h, and L.) 11 h.
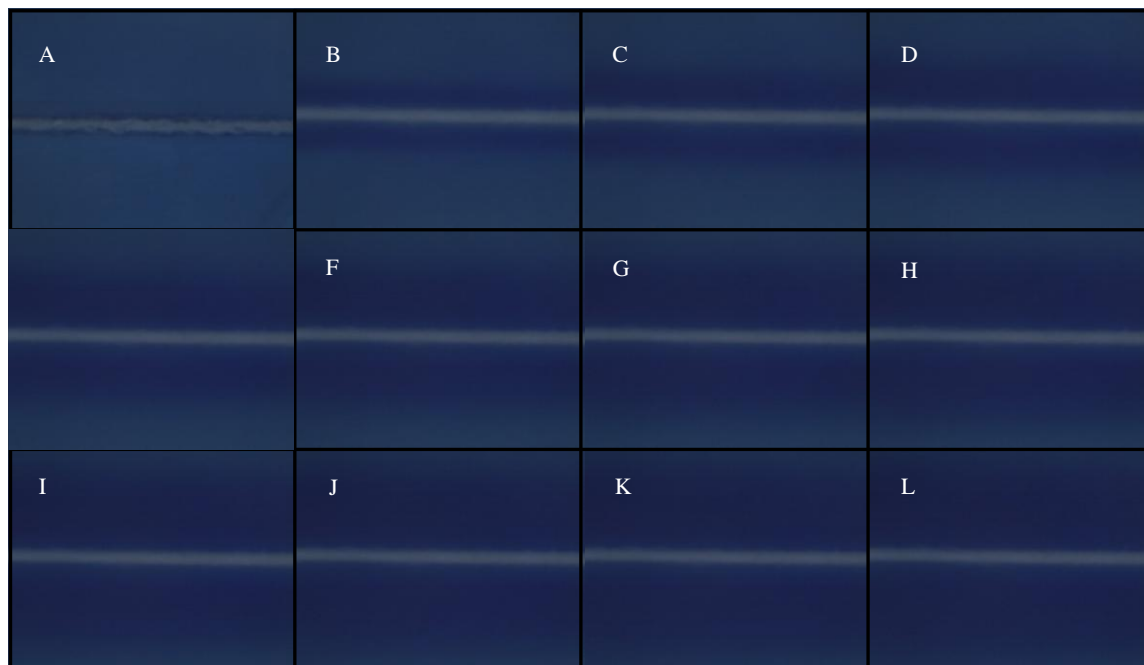
Figure D.52. Elution of acid blue 22 dye in Device A20 (60/40 0.00064 g/g soln) at various times. A.) Gel prior to water being pumped through the device. B.) after 1 h, C.) 2 h, D.) 3 h, E.) 4 h, F.) 5 h, G.) 6 h, H.) 7 h, I.) 8 h, J.) 9 h, K.) 10 h, and L.) 11 h.

Figure D.53. Elution of acid blue 22 dye in Device A21 (60/40 0.00064 g/g soln) at various times. A.) Gel prior to water being pumped through the device. B.) after 1 h, C.) 2 h, D.) 3 h, E.) 4 h, F.) 5 h, G.) 6 h, H.) 7 h, I.) 8 h, J.) 9 h, K.) 10 h, and L.) 11 h.
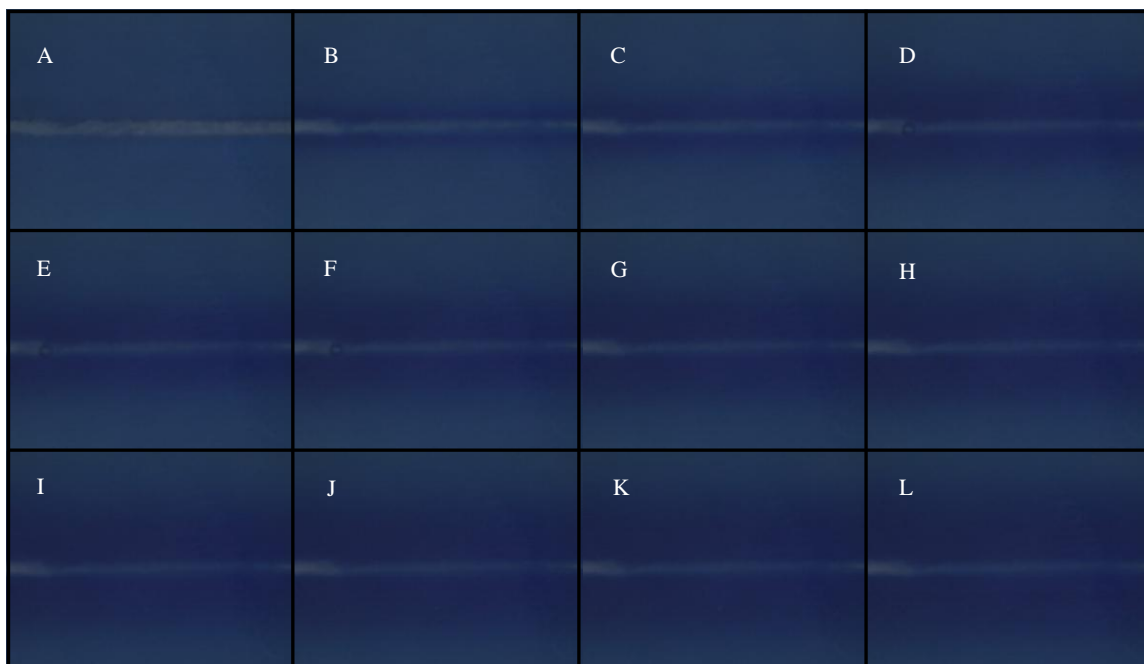
D.16. 40/60 Acid Blue 22 1.0 wt%

**Figure D.54. Elution of acid blue 22 dye in Device A7 (40/60 0.00028 g/g soln) at various times. A.)
Gel prior to water being pumped through the device. B.) after 1 h, C.) 2 h, D.) 3 h, E.) 4 h, F.) 5 h, G.)
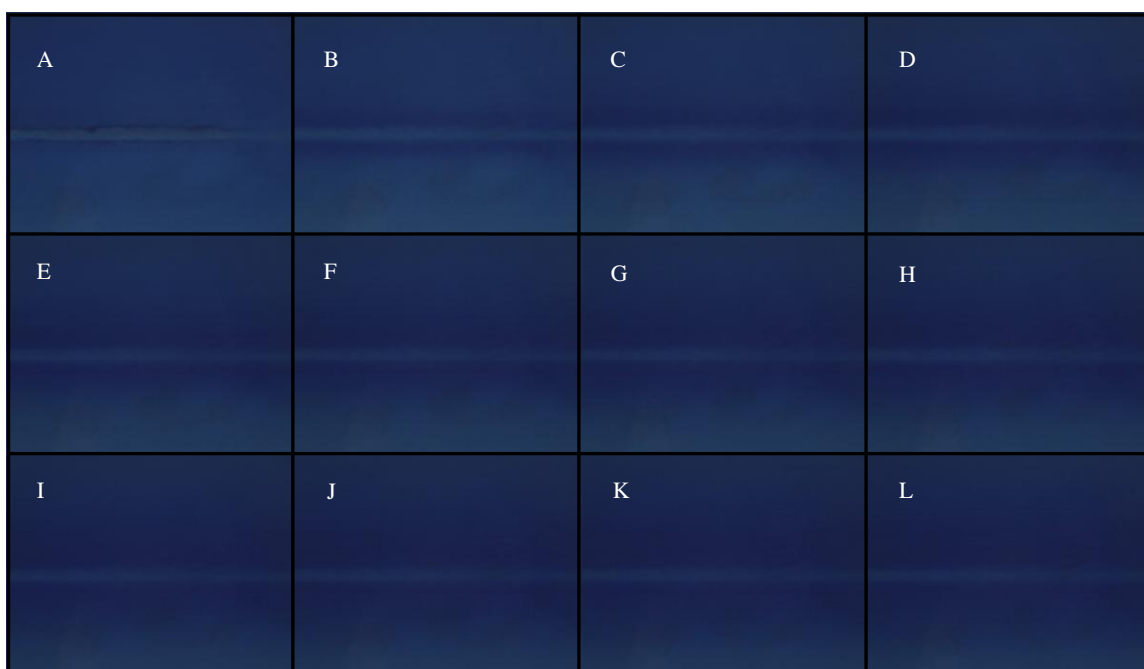6 h, H.) 7 h, I.) 8 h, J.) 9 h, K.) 10 h, and L.) 11 h.**

Figure D.55. Elution of acid blue 22 dye in Device A8 (40/60 0.00028 g/g soln) at various times. A.) Gel prior to water being pumped through the device. B.) after 1 h, C.) 2 h, D.) 3 h, E.) 4 h, F.) 5 h, G.) 6 h, H.) 7 h, I.) 8 h, J.) 9 h, K.) 10 h, and L.) 11 h.
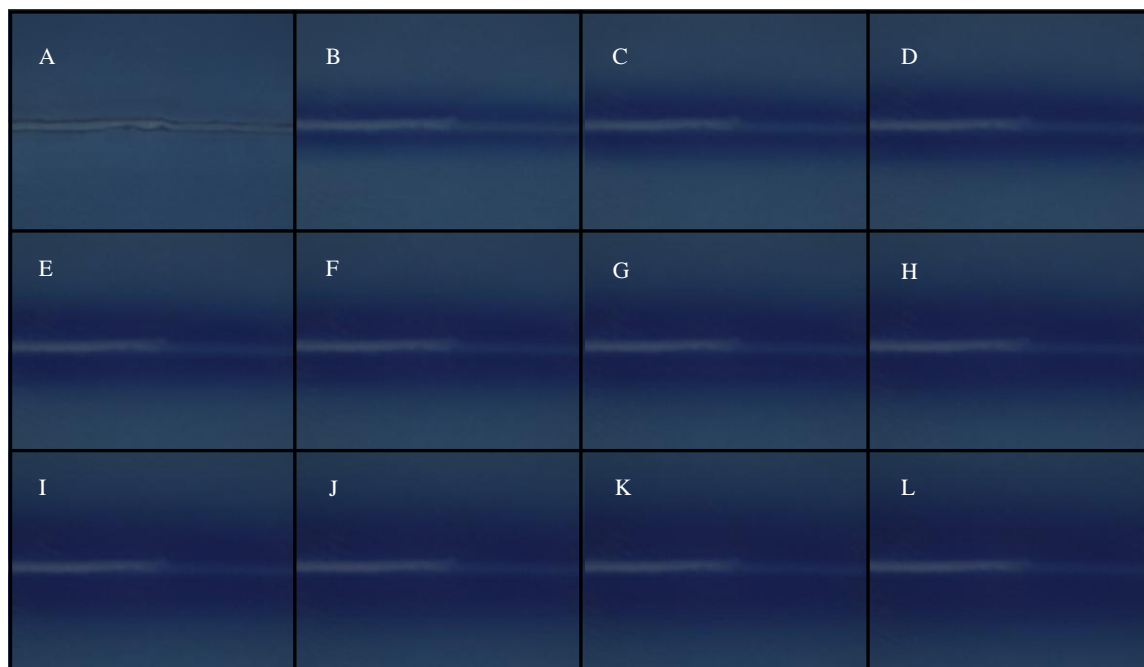

Figure D.56. Elution of acid blue 22 dye in Device A9 (40/60 0.00028 g/g soln) at various times. A.) Gel prior to water being pumped through the device. B.) after 1 h, C.) 2 h, D.) 3 h, E.) 4 h, F.) 5 h, G.) 6 h, H.) 7 h, I.) 8 h, J.) 9 h, K.) 10 h, and L.) 11 h.

D.17. 40/60 Acid Blue 22 1.5 wt%

**Figure D.57. Elution of acid blue 22 dye in Device A4 (40/60 0.00041 g/g soln) at various times. A.)
Gel prior to water being pumped through the device. B.) after 1 h, C.) 2 h, D.) 3 h, E.) 4 h, F.) 5 h, G.)
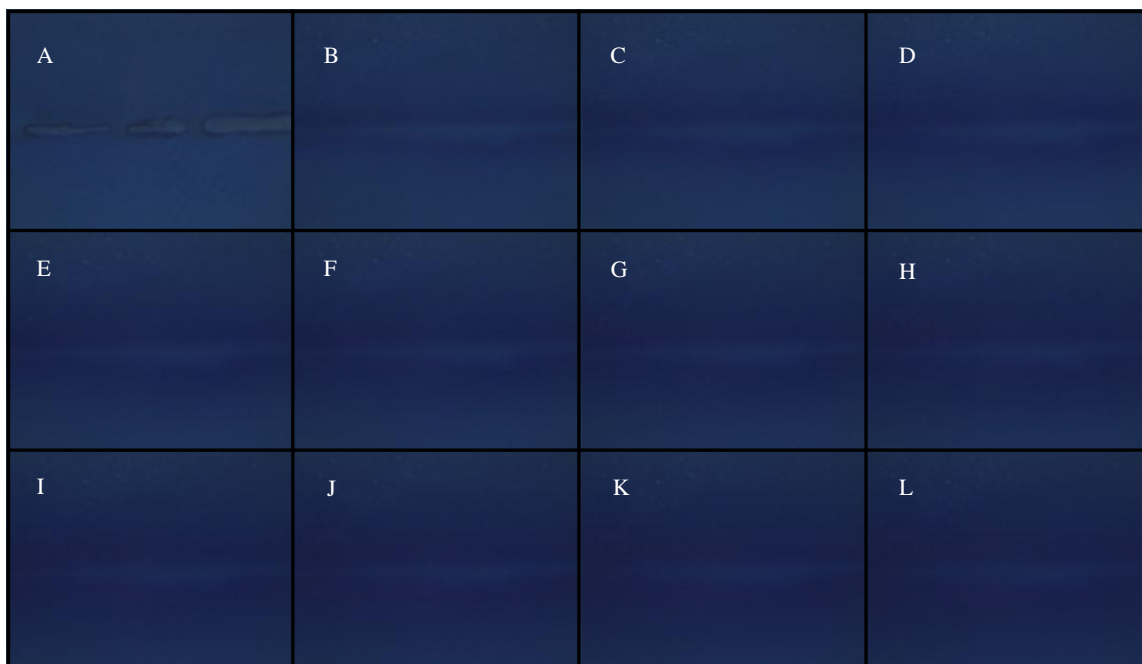6 h, H.) 7 h, I.) 8 h, J.) 9 h, K.) 10 h, and L.) 11 h.**
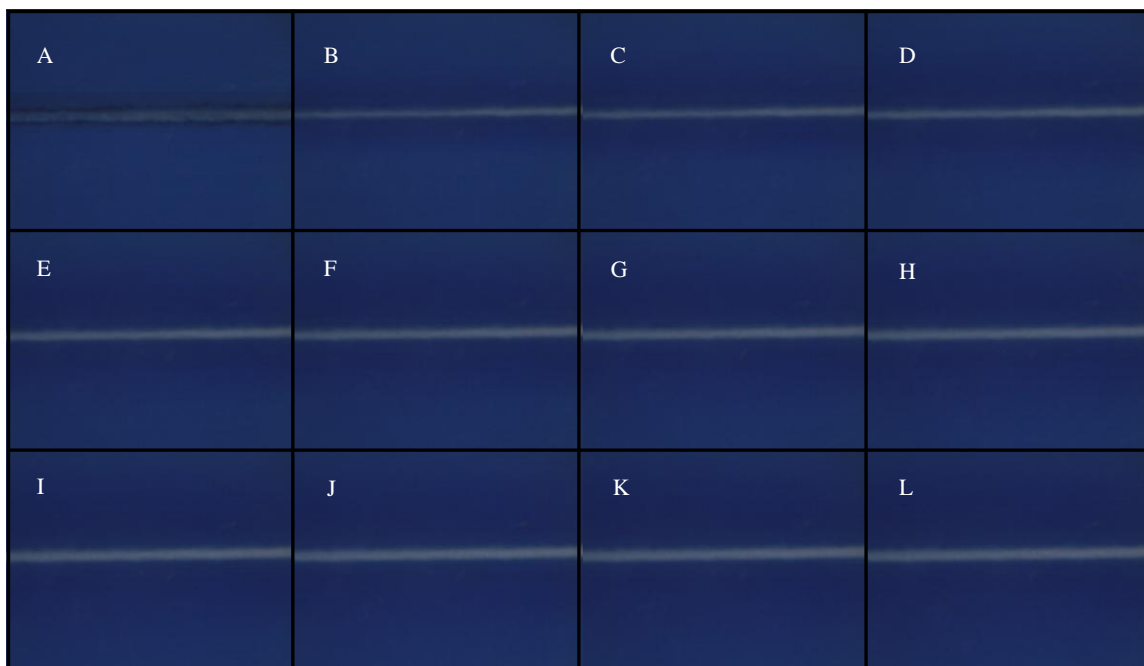
Figure D.58. Elution of acid blue 22 dye in Device A5 (40/60 0.00041 g/g soln) at various times. A.) Gel prior to water being pumped through the device. B.) after 1 h, C.) 2 h, D.) 3 h, E.) 4 h, F.) 5 h, G.) 6 h, H.) 7 h, I.) 8 h, J.) 9 h, K.) 10 h, and L.) 11 h.
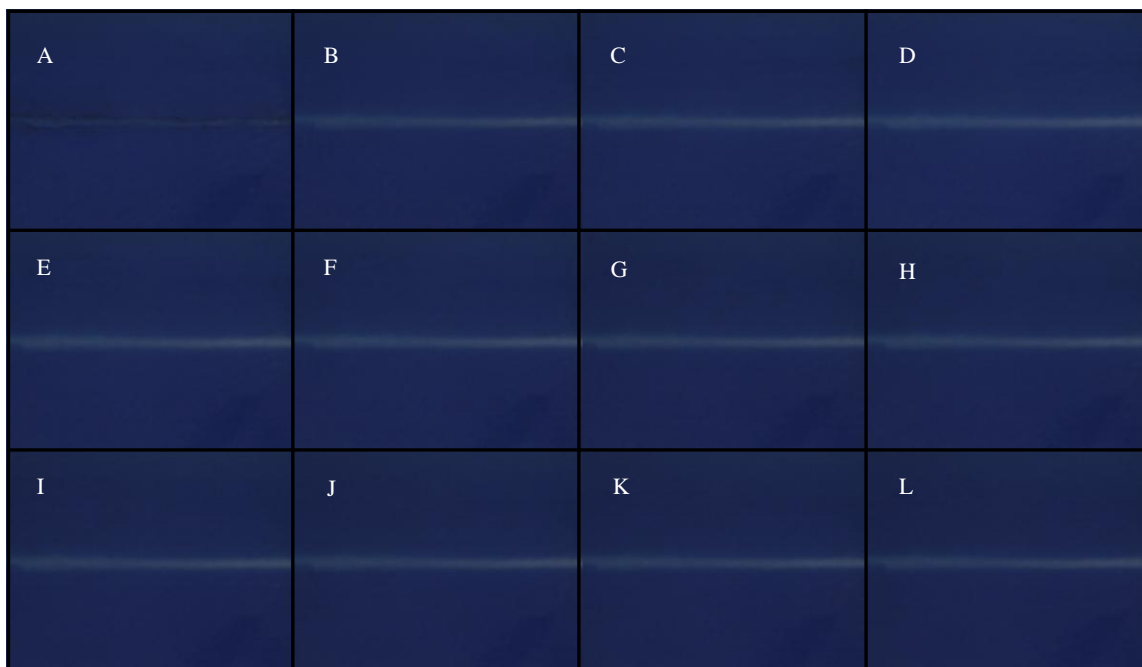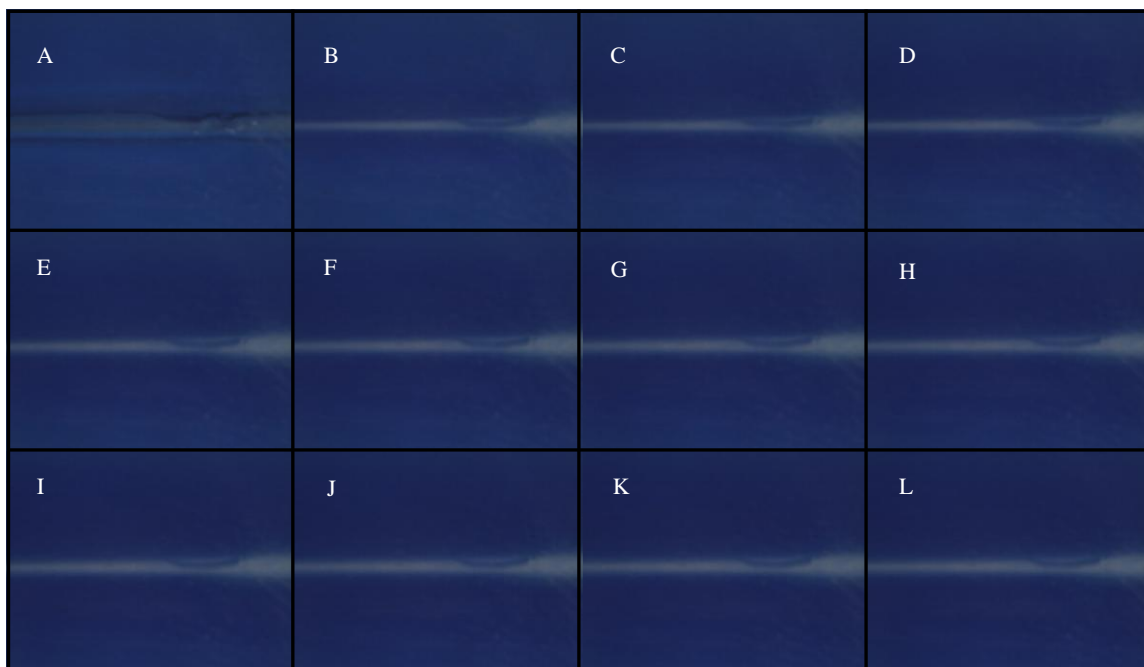

Figure D.59. Elution of acid blue 22 dye in Device A6 (40/60 0.00041 g/g soln) at various times. A.) Gel prior to water being pumped through the device. B.) after 1 h, C.) 2 h, D.) 3 h, E.) 4 h, F.) 5 h, G.) 6 h, H.) 7 h, I.) 8 h, J.) 9 h, K.) 10 h, and L.) 11 h.
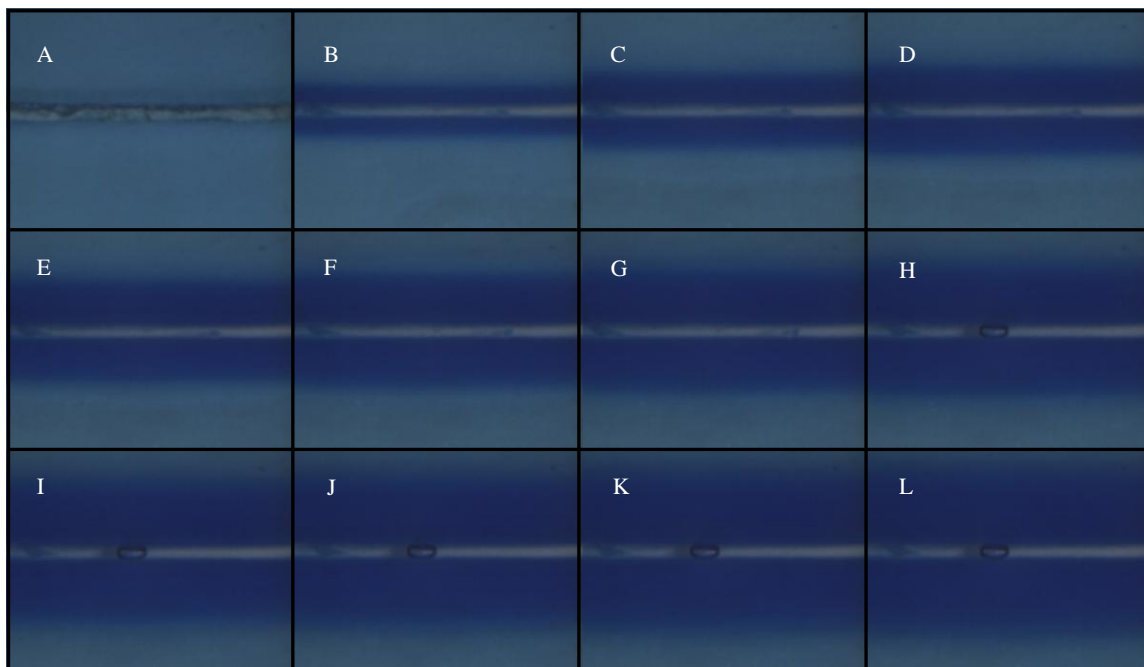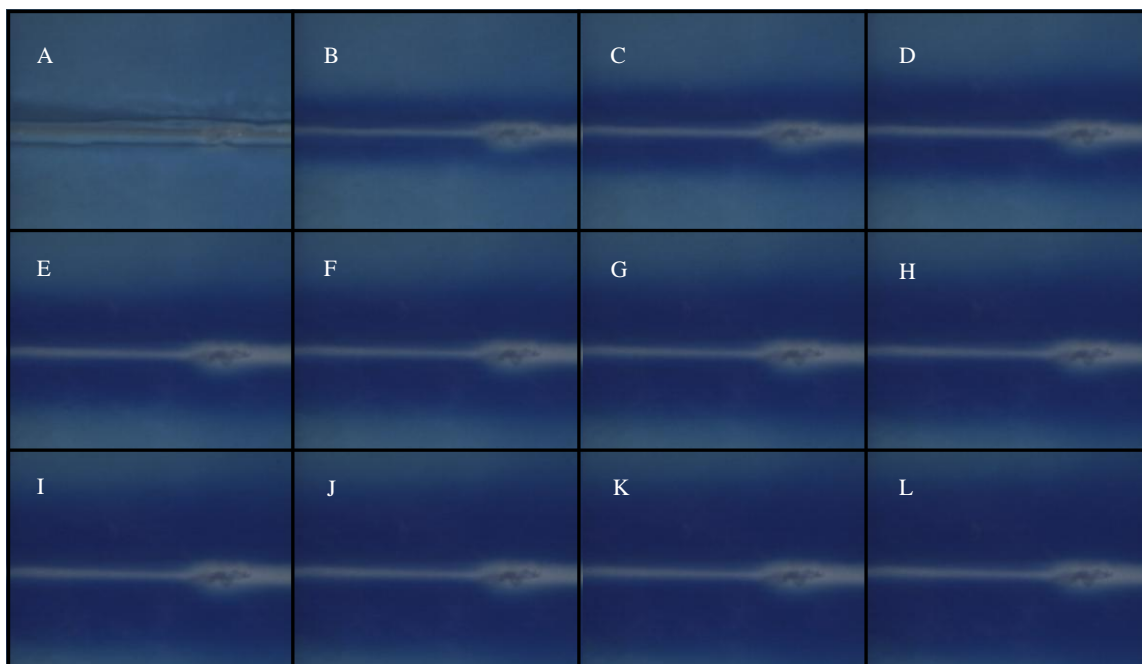
D.18. 40/60 Acid Blue 22 2.0 wt%
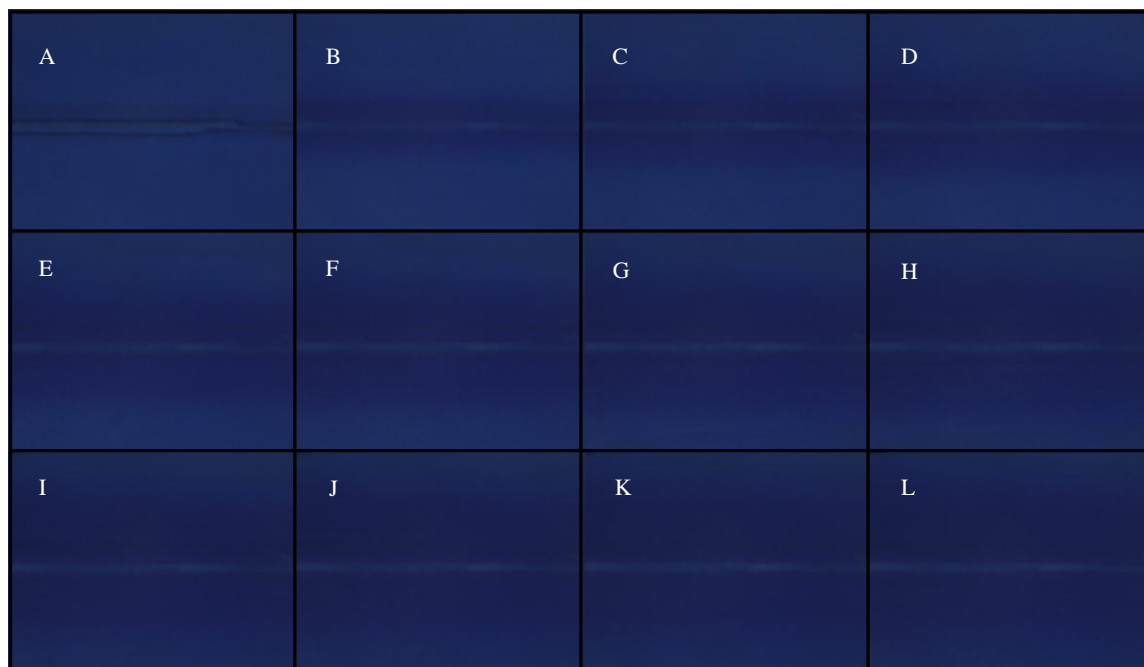
Figure D.60. Elution of acid blue 22 dye in Device A1 (40/60 0.00056 g/g soln) at various times. A.) Gel prior to water being pumped through the device. B.) after 1 h, C.) 2 h, D.) 3 h, E.) 4 h, F.) 5 h, G.) 6 h, H.) 7 h, I.) 8 h, J.) 9 h, K.) 10 h, and L.) 11 h.
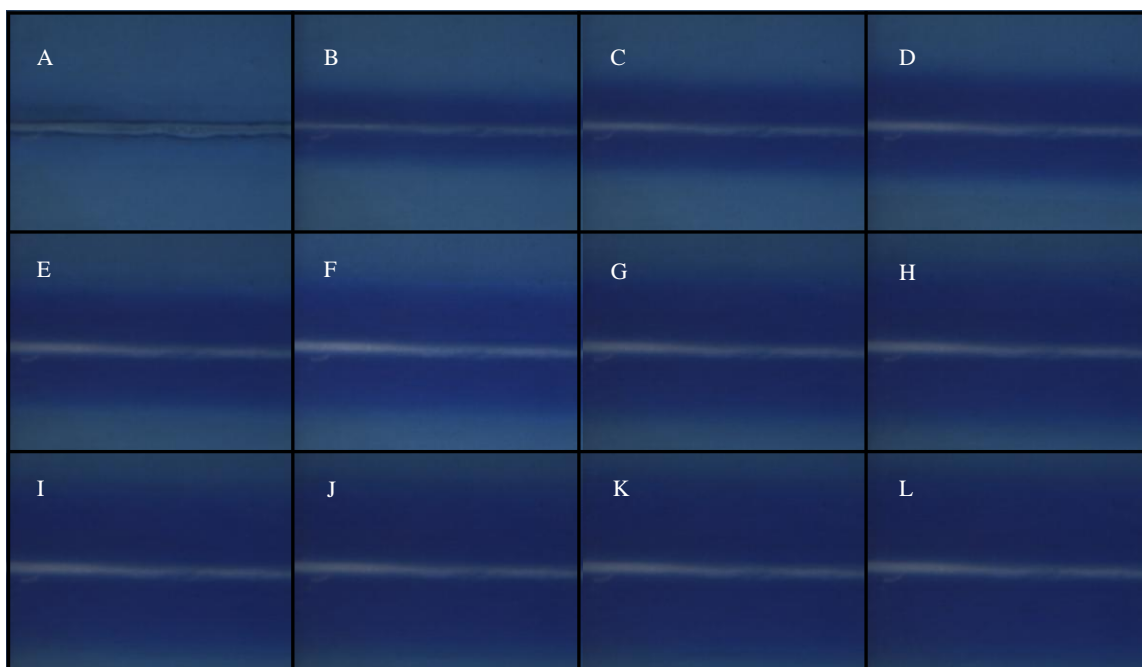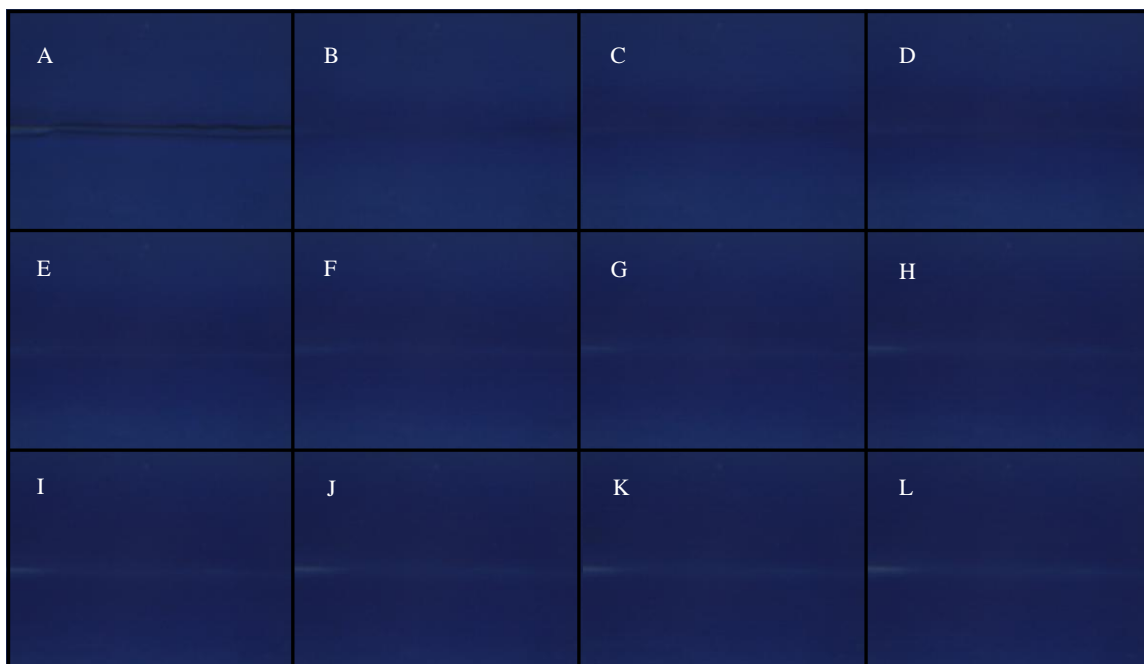
Figure D.61. Elution of acid blue 22 dye in Device A2 (40/60 0.00056 g/g soln) at various times. A.) Gel prior to water being pumped through the device. B.) after 1 h, C.) 2 h, D.) 3 h, E.) 4 h, F.) 5 h, G.) 6 h, H.) 7 h, I.) 8 h, J.) 9 h, K.) 10 h, and L.) 11 h.
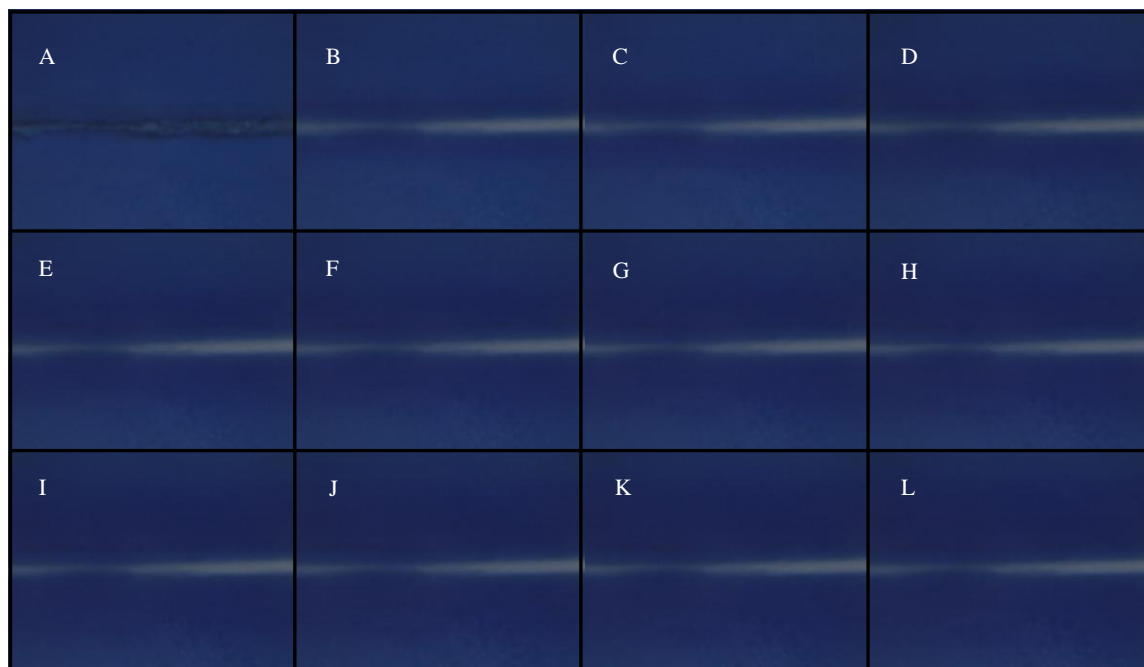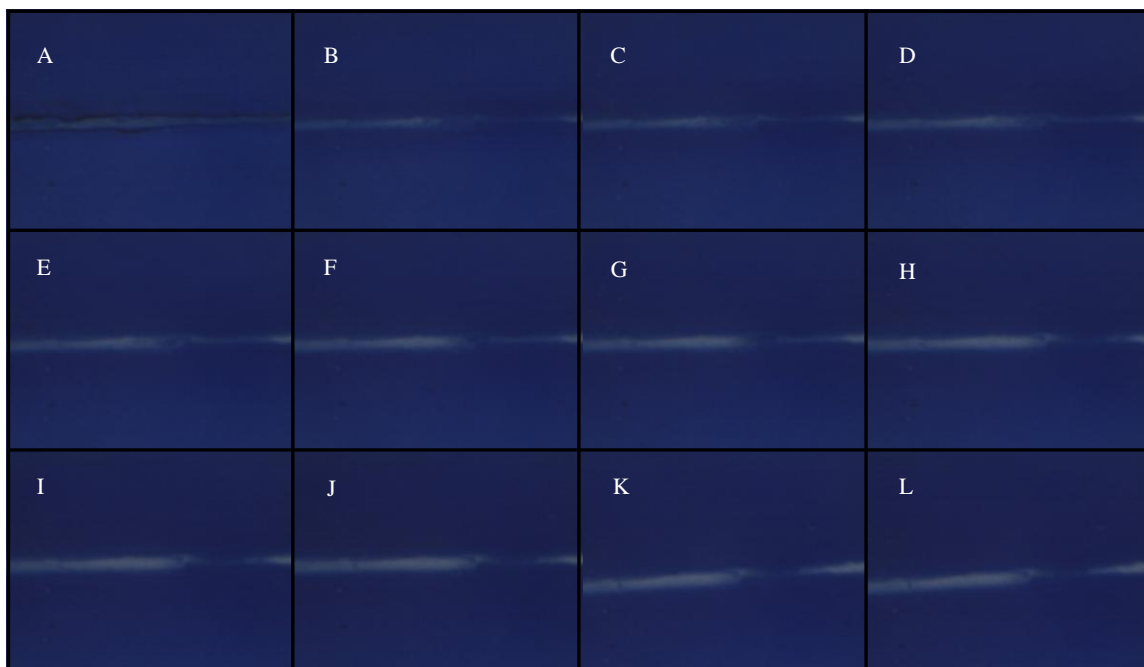

Figure D.62. Elution of acid blue 22 dye in Device A3 (40/60 0.00056 g/g soln) at various times. A.) Gel prior to water being pumped through the device. B.) after 1 h, C.) 2 h, D.) 3 h, E.) 4 h, F.) 5 h, G.) 6 h, H.) 7 h, I.) 8 h, J.) 9 h, K.) 10 h, and L.) 11 h.

Appendix E. Optical Image Analysis Procedure

The contents of this appendix describe the steps takes to use the 6 m-files in MATLAB written by Andrew Litzenberger to fit an errorfunction solution to the elution images captured for this thesis.

Before using the program, a data processing folder was created for each device and "setup" was typed into the command line to call necessary m-files specific to the m-files used to calculate the diffusion coefficient. The first step to processing the data uploads the data and saves the data into the data processing folder of your choice. Running step1.m will ask the user to specify where the pictures are located as well as where the data processing folder is located. Once input, the program will ask to choose the picture where the channel is pumped full of solution. The program will then prompt the user to select the sides of a box that will be used to analyze the pictures. This was done by clicking two spots on the picture, and the resulting box appeared in red on the picture, as shown in Figure E.1.
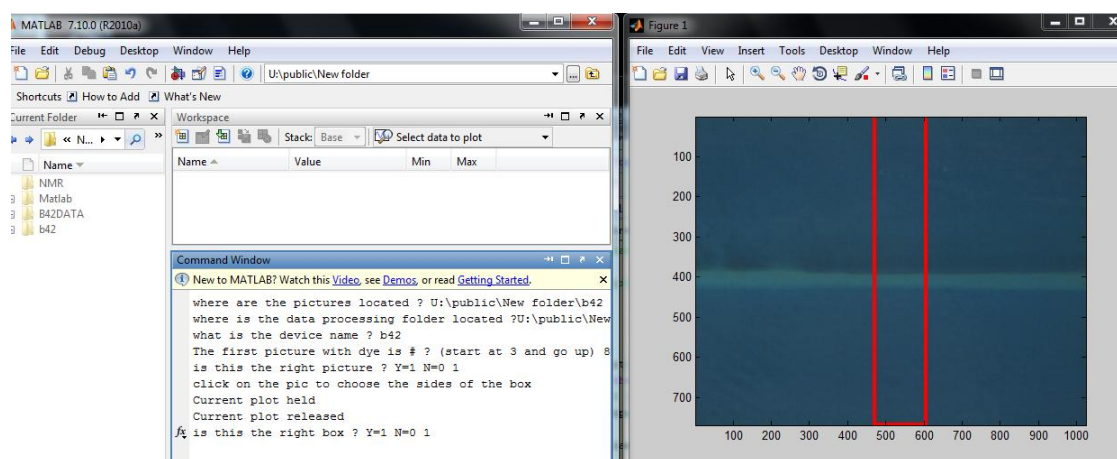
Figure E.1. Commands for the selection of data from elution images.

The program extracts time, intensity, and pixel position from the images, saves all the data, and generates a figure with the apparent intensity at each pixel position for 4 different times.

The next step in the program is to run 'step2.m'. This program asks the user if a picture with a ruler exists to create a conversion between pixel position and distance. By clicking on two points on the image with the ruler and specifying the distance between them, this conversion is calculated. Figure E.2 displays how points are specified.
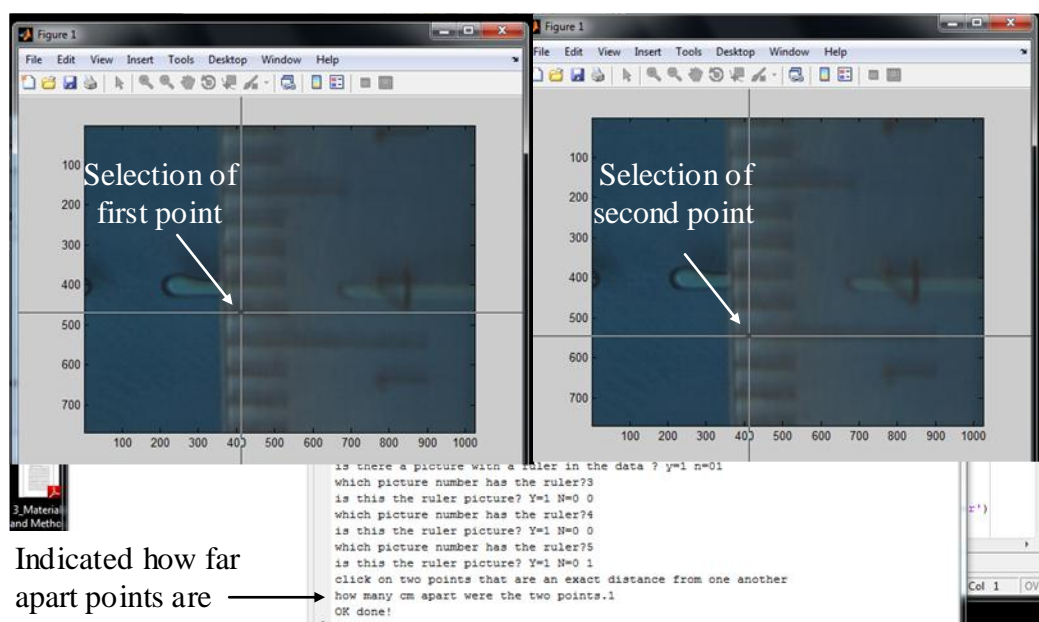
Figure E.2. Determination of the conversion between pixel position and distance using a ruler.

The 'step3.m' program was used to determine the position of the channel so that it could be subtracted from the data used to analyze the diffusion coefficient. The program asks to click on bottom, then top, then the middle of the left side of the channel. This is shown in Figure E.3. Once the bottom, top, and middle are selected, the brushing tool must be used to capture the entire portion of the channel. This process is repeated next for

the right side of the channel. Selecting the portions of the channel will fit a sigmoid function to the channel to determine the exact position.
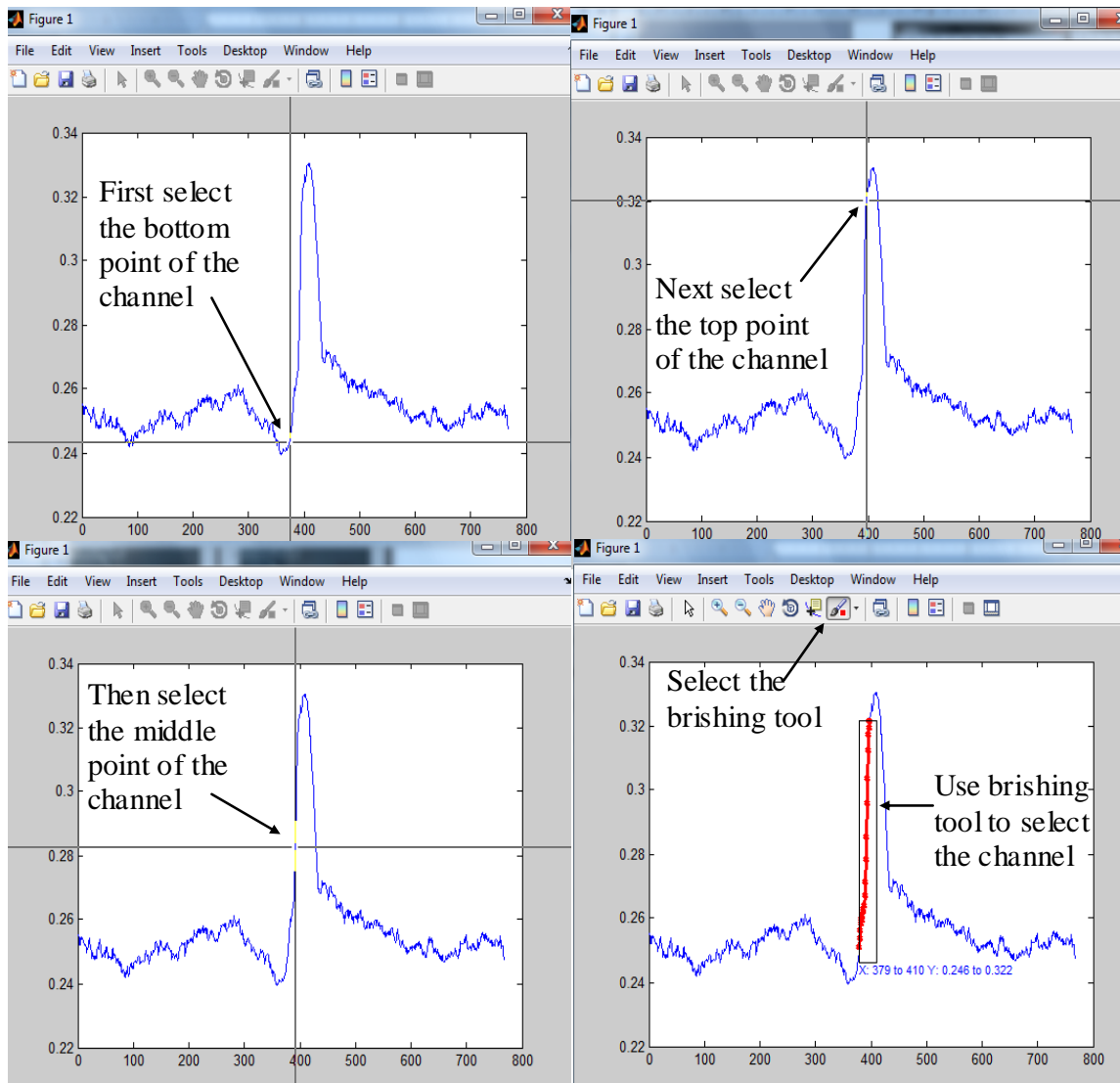
Figure E.3. Selection of the channel to remove from device data.

The location of the channel is not always perfect. It can be edited by pressing the Ctrl and C button down at the same time. This stops the script, so that the channel boundaries can be edited. By pressing the buttons, which correlate shown by the arrows in Figure E.4,

the right and left channel boundary can be moved to accurately assign the channel location.
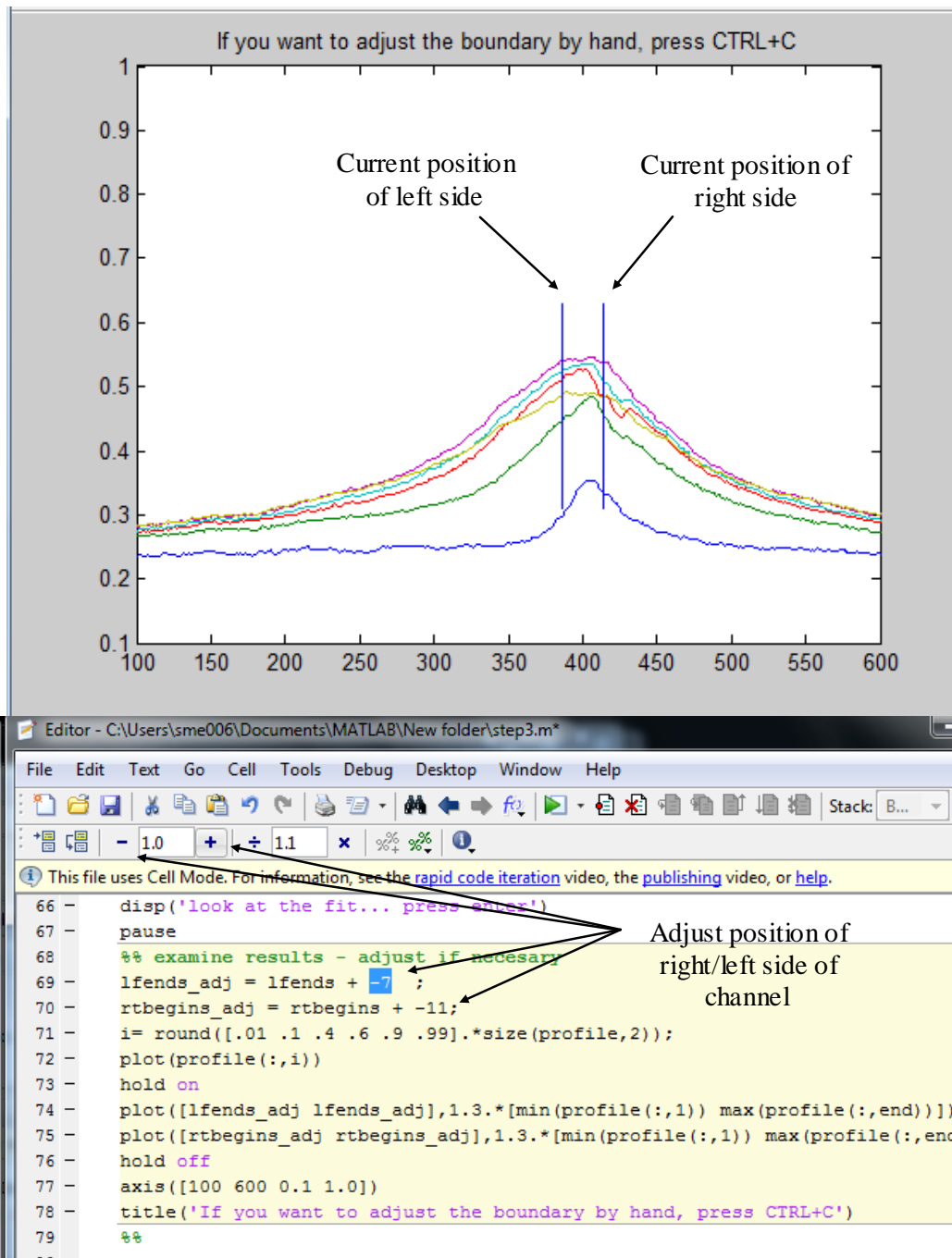
Figure E.4. Adjustment of the channel boundary position.

The step 3 script is broken up into cells. After selecting the correct channel position, the remainder of the script after the channel adjustment cell can be run by evaluating each cell individually.

The 'step4.m' file converts the intensity to concentration and plots the collapsed data at every position and time. To do this the program prompts the user to select the background and normalize the area. This is done using the brushing tool and is shown in Figure E.5.
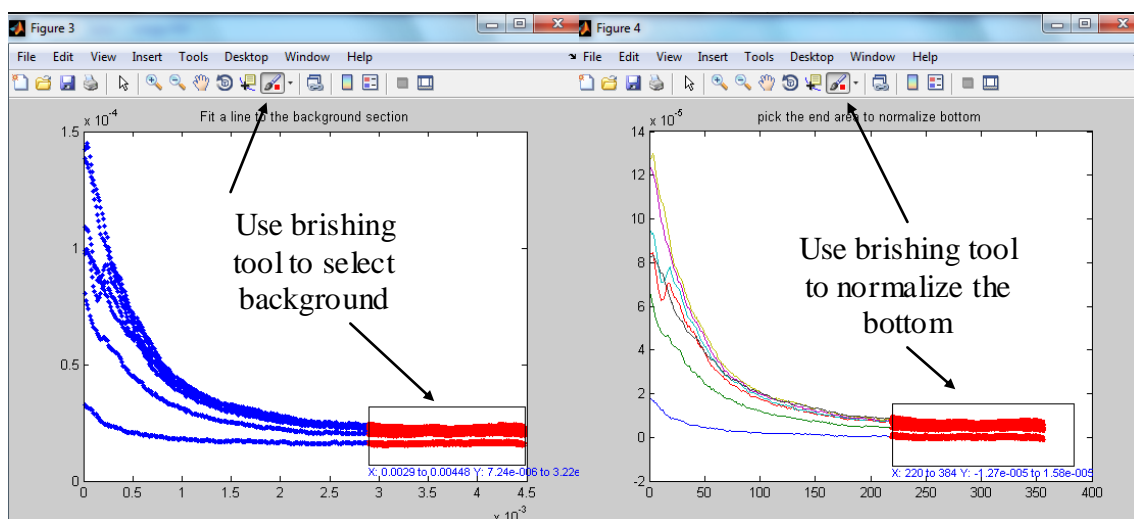
Figure E.5. Selection and normalization of the background.

Once the data is plotted, the 'step5.m' was used to fit the data to the errorfunction model. No user input is required. The 'step6.m' file was used to plot the data v. the actual fit of the errorfunction. The only action required from the user was to click on the graph to place the value of the diffusion coefficient and the r squared value on the graph.

Appendix F. Comparison of Analysis Techniques

Table F.1. Summary of all methylene blue diffusion coefficients for all devices and NMR tubes

Water/Gel Ratio (g/g)	Dye Concentration (mg/g soln)	Device	Effluent	LS Optical	RS Optical	Average Optical	NMR	Tube and Run
				Diffusion Coefficient (x 10^{-7} cm^2/s)				
70/30	0.124	B13	0.01	0.94	0.45	0.70	7.07	7_1
		b14	0.04	0.53	1.02	0.77	6.47	16_1
		b19	1.17	3.51	2.66	3.09	0.00	
		b56	1.94	6.87	5.69	6.28		
		b57	3.29	3.45	2.69	3.07		
		b58	3.88	2.53	2.18	2.36		
	0.261	B6	0.22	0.07	0.06	0.07	8.27	8_1
		B8	2.17	4.03	0.11	2.07	10.50	17_1
		B9	7.51	0.45	0.44	0.45		
	0.37	b29	7.93	2.81	Dark Image	2.81	7.65	9_1
		b30	10.15	4.10	Dark Image	4.10	6.97	13_2
		b59	25.79	Dark Image	Dark Image		5.96	18_1
		b60	13.11	Dark Image	1.18	1.18		
60/40	0.1	b23	9.94	2.95	Dark Image	2.95	3.79	4_1
		b24	7.54	1.12	Dark Image	1.12	3.38	4_2
		b25	Burst	2.80	Dark Image	2.80	2.30	13_1
	0.213	b18	9.93	8.10	5.51	6.81	4.24	5_2
		b20	3.48	0.66	0.17	0.41	4.29	5_1
		b22	10.34	1.09	0.73	0.91	5.30	14_1
							7.70	5_3
	0.33	b32	5.96	Dark Image	6.75	6.75	4.02	6_1
		b34	7.91	1.56	0.93	1.25	4.39	15_1
		b48	11.67	1.18	Dark Image	1.18		
40/60	0.15	b37	5.47	0.21	0.74	0.47	1.96	1_2
		b40	4.14	1.23	1.26	1.25	1.86	10_1
		b52	1.10	2.83	1.21	2.02	8.59	1_1
		b54	1.81	4.79	2.98	3.89		
		b55	0.31	1.68	1.27	1.48		
	0.21	b39	3.17	3.02	1.24	2.13	2.11	3_2
		b42	2.70	1.76	1.08	1.42	1.50	11_1
		b47	8.05	2.30	3.06	2.68	2.07	3_1
	0.29	b44	7.79	0.96	Dark Image	0.96	3.20	2_3
		b45	4.48	0.96	Dark Image	0.96	4.35	2_2
		b46	7.33	1.25	1.21	1.23	3.92	2_4
		b49	26.22	1.91	Dark Image	1.91	1.40	12_1
		b50	7.78	4.13	Dark Image	4.13	1.91	2_1
		b51	Burst	1.34	Dark Image	1.27		

Table F.2. Two tail t-test comparing Effluent and NMR 70/30 v. 70/30 for all concentrations

	Variable 1	*Variable 2*
Mean	5.93E-07	7.55E-07
Variance	5.30E-13	2.25E-14
Observations	13	7
Hypothesized Mean Difference	0	
df	14	
t Stat	-0.769	
P(T<=t) one-tail	0.227	
t Critical one-tail	1.761	
P(T<=t) two-tail	0.454	
t Critical two-tail	2.145	

Table F.3. Two tail t-test comparing Effluent and NMR 60/40 v. 60/40 for all concentrations

	Variable 1	*Variable 2*
Mean	8.3E-07	4.38E-07
Variance	7.17E-14	2.21E-14
Observations	8	9
Hypothesized Mean Difference	0	
df	11	
t Stat	3.710	
P(T<=t) one-tail	0.00171	
t Critical one-tail	1.795	
P(T<=t) two-tail	0.003437	
t Critical two-tail	2.201	

Table F.4. Two tail t-test comparing Effluent and NMR 40/60 v. 40/60 for all concentrations

	Variable 1	*Variable 2*
Mean	6.18E-07	2.99E-07
Variance	4.32E-13	4.4E-14
Observations	13	11
Hypothesized Mean Difference	0	
df	15	
t Stat	1.652	
P(T<=t) one-tail	0.0595	
t Critical one-tail	1.753	
P(T<=t) two-tail	0.119	
t Critical two-tail	2.131	

Table F.5. Two tail t-test comparing Optical and NMR 70/30 v. 70/30 for all concentrations

	Variable 1	*Variable 2*
Mean	2.24E-07	7.55E-07
Variance	3.19E-14	2.25E-14
Observations	12	7
Hypothesized Mean Difference	0	
df	15	
t Stat	-6.930	
P(T<=t) one-tail	2.40E-06	
t Critical one-tail	1.753	
P(T<=t) two-tail	4.81E-06	
t Critical two-tail	2.131	

Table F.6. Two tail t-test comparing Optical and NMR 60/40 v. 60/40 for all concentrations

	Variable 1	*Variable 2*
Mean	2.68E-07	4.38E-07
Variance	6.08E-14	2.21E-14
Observations	9	9
Hypothesized Mean Difference	0	
df	13	
t Stat	-1.762	
P(T<=t) one-tail	0.0507	
t Critical one-tail	1.770	
P(T<=t) two-tail	0.101	
t Critical two-tail	2.160	

Table F.7. Two tail t-test comparing Effluent and NMR 40/60 v. 40/60 for all concentrations

	Variable 1	*Variable 2*
Mean	1.84E-07	2.99E-07
Variance	1.15E-14	4.4E-14
Observations	14	11
Hypothesized Mean Difference	0	
df	14	
t Stat	-1.649	
P(T<=t) one-tail	0.0606	
t Critical one-tail	1.761	
P(T<=t) two-tail	0.121	
t Critical two-tail	2.145	

Table F.8. Two tail t-test comparing Effluent and Optical 70/30 v. 70/30 for all concentrations

	Variable 1	*Variable 2*
Mean	5.93E-07	2.24E-07
Variance	5.30E-13	3.19E-14
Observations	13	12
Hypothesized Mean Difference	0	
df	14	
t Stat	1.772	
P(T<=t) one-tail	0.0490	
t Critical one-tail	1.761	
P(T<=t) two-tail	0.098	
t Critical two-tail	2.145	

Table F.9. Two tail t-test comparing Effluent and Optical 60/40 v. 60/40 for all concentrations

	Variable 1	*Variable 2*
Mean	8.34E-07	2.69E-07
Variance	7.17E-14	6.09E-14
Observations	8	9
Hypothesized Mean Difference	0	
df	14	
t Stat	4.511	
P(T<=t) one-tail	0.000244	
t Critical one-tail	1.761	
P(T<=t) two-tail	0.000488	
t Critical two-tail	2.145	

Table F.10. Two tail t-test comparing Effluent and Optical 40/60 v.40/60 for all concentrations

	Variable 1	*Variable 2*
Mean	6.18E-07	1.84E-07
Variance	4.32E-13	1.16E-14
Observations	13	14
Hypothesized Mean Difference	0	
df	13	
t Stat	2.348	
P(T<=t) one-tail	0.0176	
t Critical one-tail	1.771	
P(T<=t) two-tail	0.0353	
t Critical two-tail	2.160	

Appendix G. Theoretical Diffusion Coefficient Calculation

The theoretical model for diffusion in a hydrogel is given below.

$$\frac{D_g}{D_0} = \left(1 - \frac{r_s}{\xi}\right) exp\left(-Y\left[\frac{v_{2,s}}{1 - v_{2,s}}\right]\right)$$

The free diffusion, D_0, was estimated using the Stoke's Einstein equation below.

$$D_0 = \frac{k_B T}{6\pi\mu R_0}$$

$$D_0 = \frac{\left(1.381 \times 10^{-23} \frac{m^2 \cdot kg}{K \cdot s^2}\right) \cdot 298K}{6\pi\left(0.001 \frac{kg}{m \cdot s}\right)(4.578 \times 10^{-10}m)} = 4.769 \times 10^{-6}\frac{cm^2}{s}$$

The size of the methylene blue molecule, r_s, is 4.58 Å. The 70/30 hydrogels were used for this sample calculation with a Y value of unity. The mesh size is 22.4 Å and the polymer volume fraction is 0.29.

$$D_g = \left(1 - \frac{4.58}{22.4}\right) exp\left(-1\left[\frac{0.29}{1 - 0.29}\right]\right) * 4.769 \times 10^{-6}\frac{cm^2}{s} = 7.67x10^{-7}\frac{cm^2}{s}$$

Appendix H. Contents of DVD

The *Effluent Analysis* folder on the DVD contains the Excel files for all of the methylene blue and acid blue 22 devices. Excel files include concentration data and plots, and the diffusion coefficients from fitting the short time release model.

The *NMR Analysis* folder on the DVD contains all of the raw data from the NMR pge_ste analysis for methylene blue and acid blue 22 and the MATLAB codes used for analysis.

The *Optical Analysis* folder on the DVD contains the concentration profiles, MATLAB code, and collapsed image data for all methylene blue devices.

The *Copy of Anne Devices Data.xlsx* file contains the diffusion coefficient values obtained by Anne Ellenberger for the 60/40 initial water/PEG-DA ratio uptake devices.

The *Device Catalog.xlsx* file contains a list of all the devices with device dimensions and diffusion coefficients for all small molecules.

The *Diffusion Coefficients and Lyophilizations.xlsx* file contains a summary of all the diffusion coefficients and lyophilization data for methylene blue and acid blue 22. The file also contains all the summary plots for methylene blue and acid blue 22.

The *NMR 2 Diffusion Coefficients.xlsx* file contains a summary of the NMR slow, fast, and combined diffusion coefficient components.

The *Parity Plots.xlsc* file contains the parity plots made for this thesis and theoretical diffusion coefficient calculations.